

Mechanistic Studies of Hydrothermal Organic Geochemistry

by

Ziming Yang

A Dissertation Presented in Partial Fulfillment  
of the Requirement for the Degree  
Doctor of Philosophy

Approved June 2014 by the  
Graduate Supervisory Committee:

Everett L. Shock, Chair  
Ian R. Gould  
George H. Wolf

ARIZONA STATE UNIVERSITY

August 2014

## ABSTRACT

The hydrothermal chemistry of organic compounds influences many critical geological processes, including the formation of oil and gas reservoirs, the degradation and transport of organic matter in sedimentary basins, metabolic cycles in the deep subsurface biosphere, and possibly prebiotic organic synthesis related to the origin of life. In most previous studies of hydrothermal organic reactions the emphasis has been mainly on determining reaction product distributions, studies that provide detailed mechanistic information or direct evidence for specific reaction intermediates are rare. To develop a better understanding, I performed hydrothermal experiments with model ketone compound dibenzylketone (DBK), which serves as a quite useful tool to probe the bond breaking and forming processes in hydrothermal geochemical transformations. A careful study of reaction kinetics and products of DBK in Chapter 2 of this dissertation reveals reversible and irreversible reaction pathways, and provides evidence for competing ionic and radical reaction mechanisms. The majority of the observed products result from homolytic carbon-carbon and carbon-hydrogen bond cleavage and secondary coupling reactions of the benzyl and related radical intermediates.

In the third chapter of the dissertation, a novel hydrothermal photochemical method is studied, which enabled *in situ* independent generation of the relevant radicals and effectively separated the radical and ionic reactions that occur simultaneously in pure thermal reactions. In the following chapter, I focus on the role of minerals on ketone hydrothermal reactions. Minerals such as quartz and corundum have no detectable effect on DBK, whereas magnetite, hematite, and troilite all increase ketone reactivity to various extents. The influence of these iron-bearing minerals can be attributed to the

mineral surface catalysis or the solution chemistry change that is presumably caused by dissolved inorganic species from minerals. In addition, some new discoveries on strong oxidizing effect of copper (II) ion under hydrothermal conditions are described in the latter chapter of the dissertation, where examples of clean and rapid reactions that converted alcohols to aldehyde and aldehydes to carboxylic acids are included.

## ACKNOWLEDGEMENTS

First of all, I would like to thank my teachers at ASU: my advisor, Everett Shock, who brought me to the world of geochemistry, introduced me into the GEOPIG family, developed me to be an independent scientific professional, and always inspiring my passion on new research challenges; my mentor, Ian Gould, who is always there to help me, provided me a unique opportunity to study at ASU, showed me how to give professional presentations, gave me useful research suggestions, and pointed me toward a successful future career; George Wolf, who provided me valuable mentoring during my qualifying exam and dissertation writing; Lynda Williams, who helped me to be equipped with the hydrothermal experimental skills and taught me how to think like a geologist in the mineral world; Hilairy Hartnett, who taught me how to become a rigorous and true analytical chemist; and Bruce Rittmann and Steven Van Ginkel, who kindled my interests and developed my skills in the field of environmental engineering.

I am very grateful to various colleagues and friends at ASU for helping me with my research and leaving me memorable graduate school experiences. People to acknowledge (without a particular order) include: Chris Glein, Jessie Shipp, Kris Fecteau, Kirt Robinson, Kristin Johnson, Peter Canovas, Grayson Boyer, Natasha Zolotova, Ariel Anbar, Panjai Prapaipong, Pierre Herckes, Jinwei Zhang, Apar Prasad, Jeff Dick, Christa Bockisch, Tamal Mukherjee, David Nutt, Mary Zhu, and Martha McDowell. In addition to my ASU colleagues, I would like to thank Dan Giammar, Young-shin Jun, Brent Williams, and Daren Chen at Washington University, who taught and mentored me during my study at the EECE Department. I am also thankful to Dimitri Sverjensky, Bob

Hazen, and George Cody at the Geophysical Lab for many insightful feedback and helpful advices on my hydrothermal research.

Staying away from home for six years and completing the graduate school would not be possible without the tremendous love and support from my family. I would like to give special thanks to my parents and my grandparents for raising me up, for always believing in me, and for always understanding and helping me through the difficulties. I can even picture a happy smile on my grandpa's face when he could see me pursue my dream this far. Their great and endless love will require a lifetime for me to repay.

## TABLE OF CONTENTS

	Page
LIST OF TABLES.....	ix
LIST OF FIGURES.....	xi
CHAPTER	
1. INTRODUCTION.....	1
1.1. Hydrothermal Chemistry of Organic Compounds.....	1
1.2. Hydrothermal Organic Functional Group Interconversions.....	4
1.3. Ketone Hydrothermal Chemistry.....	6
1.4. Dibenzylketone.....	8
1.5. Organic-Mineral Hydrothermal Interactions.....	10
1.6. Subjects of the Current Thesis.....	12
1.7. References.....	19
2. THE CENTRAL ROLE OF KETONES IN REVERSIBLE AND IRREVERSIBLE HYDROTHERMAL ORGANIC FUNCTIONAL GROUP TRANSFORMATIONS.....	27
2.1. Abstract.....	27
2.2. Introduction.....	28
2.3. Experimental.....	31
2.3.1. Reagents.....	31
2.3.2. Procedures.....	32
2.3.3. Product Analysis.....	34
2.4. Results and Discussion.....	38

CHAPTER	Page
2.4.1. Reaction Pathways for Hydrothermal Transformation of DBK.....	38
2.4.1.1. Reduction Pathway.....	41
2.4.1.2. Bond Cleavage Pathways.....	43
2.4.2. Mechanisms of the Reduction Pathway.....	43
2.4.3. Mechanisms of C-C and C-H Bond Cleavage Pathways.....	51
2.4.4. Ionic Reaction Pathways.....	55
2.4.5. Carboxylic Acids.....	57
2.5. Conclusions.....	57
2.6. References.....	76
 3. HYDROTHERMAL PHOTOCHEMISTRY AS A MECHANISTIC TOOL IN ORGANIC GEOCHEMISTRY – THE CHEMISTRY OF DIBENZYL KETONE.....	          82
3.1. Abstract.....	82
3.2. Introduction.....	83
3.3. Results and Discussion.....	87
3.3.1. Hydrothermal Reactions of DBK.....	87
3.3.2. Ambient Photochemistry of DBK.....	89
3.3.3. Hydrothermal Photochemistry of DBK.....	90
3.3.4. Hydrothermal Dehydration.....	99
3.3.5. Follow-up Ionic Reactions.....	104
3.4. Conclusions.....	106

CHAPTER	Page
3.5. Supporting Information.....	107
3.5.1. Experimental.....	107
3.5.1.1. Materials.....	107
3.5.1.2. Experimental Procedures.....	107
3.5.1.3. Electronic Structure Calculations.....	109
3.5.2. Quantum Yield Calculations.....	110
3.5.3. Product Characterization via Gas Chromatography/Mass Spectrometry.....	114
3.6. References.....	132
4. INFLUENCE OF MINERALS ON HYDROTHERMAL REACTIONS OF KETONES.....	139
4.1. Abstract.....	139
4.2. Introduction.....	140
4.3. Experimental.....	145
4.3.1. Reagents.....	145
4.3.2. Procedures.....	146
4.3.3. Product Analysis.....	148
4.4. Results and Discussion.....	150
4.4.1. Decomposition of DBK.....	150
4.4.2. Reaction Products with Hematite and Magnetite.....	153
4.4.3. Reaction Products with Troilite.....	159
4.4.4. Roles of the Minerals.....	162



CHAPTER	Page
4.5. Conclusions.....	168
4.6. References.....	189
5. OXIDATION BY COPPER (II) IN HYDROTHERMAL ORGANIC REACTIONS.....	194
5.1. Introduction.....	194
5.2. Experimental.....	197
5.3. Results and Discussion.....	200
5.3.1. Decomposition of the Carboxylic Acids, Alcohols, and Aldehydes.....	200
5.3.2. Reaction Stoichiometries.....	203
5.3.3. Ring Substituent Effects.....	205
5.3.4. Oxidation Mechanisms.....	207
5.4. Conclusions.....	214
5.5. References.....	226
6. SUMMARY OF CHAPTERS AND OUTLOOK FOR FUTURE WORK.....	230
6.1. Summary of Current Work.....	230
6.2. What We Learned from the Hydrothermal Organic Reactions.....	232
6.3. Recommendation for Future Work.....	234
6.4. References.....	239
REFERENCES.....	240

## LIST OF TABLES

Table	Page
Chapter 2	
1. Concentrations of Products from Experiments with DBK in H <sub>2</sub> O at 300°C and 700 bar.....	60
2. Concentrations of Products from Experiments with DBK, Alcohol, and Alkane in H <sub>2</sub> O at 300°C and 700 bar.....	62
Chapter 3	
S1. Fractional Chemical Yields of Products from Hydrothermal Photolysis of DBK at 300°C and 86 bar.....	127
Chapter 4	
1. Conversions, Reaction Pathways Percentages, and Estimated Mass and Hydrogen Balances from Hydrothermal Reaction of DBK in the Presence of Minerals with a Constant Mineral Surface Area at 300°C and 700 bar.....	170
2. Conversions, Reacted DBK, and Produced Hydrogen from Hydrothermal Reaction of DBK with Minerals at 300°C and 700 bar.....	172
3. Conversions, Reaction Pathways Percentages, and Estimated Mass Balances from Hydrothermal Reaction of DBK in the Presence of Minerals with Different Mineral Surface Areas at 300°C and 700 bar.....	173
Chapter 5	
1. Abundances of Organic Compounds and Cupric Ions from Experiments	

Table	Page
with Phenylacetic Acids and Sodium Phenylacetate.....	219
2. Abundances of Organic Compounds and Cupric Ions from Experiments with Benzyl Alcohols.....	221
3. Abundances of Organic Compounds and Cupric Ions from Experiments with Benzaldehydes.....	222
4. Mole Ratios and Stoichiometric Ratios between the Consumed Cupric Ions and the Consumed Starting Organic Compounds.....	223
5. Estimated Redox Potentials for Oxidation of the Carboxylate Anion, Benzyl Radical, Toluene, and Copper (I) Ion.....	225

## LIST OF FIGURES

Figure	Page
Chapter 1	
1. Calculated Metastable Equilibrium Ratios of Aliphatic Alkenes to Alcohols as a Function of Temperature at Water Saturation Pressure.....	16
2. Hydrothermal Reaction Pathways Interconvert Hydrocarbons and Carboxylic Acids by Seewald.....	17
3. Schematic Energy Diagram for Formation of a Pair of Radicals for Photochemical Excitation of Dibenzylketone.....	18
Chapter 2	
1. Scheme for Hydrothermal Organic Functional Group Interconversions.....	64
2. Schematic C-C Bond Fragmentation Reaction for DBK.....	65
3. Gas Chromatogram of Product Distribution of Hydrothermal Reaction of DBK in Water at 300°C and 700 bar after 290 h.....	66
4. Structures of Major Products Observed for Hydrothermal Reaction of DBK in Water at 300°C and 700 bar.....	67
5. Mass Spectrum and Assigned Fragments for the Four-Benzene-Ring Structure 4A.....	68
6. Schematic Representation of the Main Reaction Pathways for Hydrothermal Transformation of DBK.....	69
7. Time Dependencies of the Concentrations of DBK, Alcohol, Alkene, and Alkane at 300°C and 700 bar.....	70
8. Proposed Minimal Mechanism for Reduction of DBK to Alcohol via Hydrogen	

Figure	Page
Atom Addition to the C=O Double Bond.....	71
9. Time Dependencies of the Concentrations of DBK and Major Product Toluene in Water at 300°C and 700 bar.....	72
10. Time Dependencies of the Concentrations of DBK and Product Stilbene and Bibenzyl in Water at 300°C and 700 bar.....	73
11. Time Dependencies of the Concentrations of DBK and Three-Benzene- Ring Products in Water at 300°C and 700 bar.....	74
12. Time Dependencies of the Concentrations of DBK and Four-Benzene-Ring Products in Water at 300°C and 700 bar.....	75
 Chapter 3	
1. Gas Chromatograms of Product Distributions for DBK Thermal Reaction, Hydrothermal Photolysis, and Photolysis at Ambient.....	120
2. Comparison of Product Concentration versus Irradiation time for Photolysis of DBK.....	121
3. Concentrations of Product 4a and 4b versus time in Photolysis of DBK in Water at 300°C and 86 bar.....	122
4. Time Dependencies of Toluene Compared to Sum of 3-Ring and 4-Ring Products.....	123
5. Electronic Energy versus $\alpha$ -Hydrogen-benzylic Carbon Separation Distance for H Atom Abstraction from MBK by Benzyl Radical.....	124
6. Time Dependence of Concentration of 4a as a Function of the Sum of the 4a and 4b concentrations.....	125

Figure	Page
7. Computed Structures of Dienone 4b <sup>2</sup> and Furan 4b <sup>1</sup> .....	126
S1. Percentage Conversions of DBK as a Function of Irradiation time under Ambient and Hydrothermal Conditions.....	128
S2. Mass Spectra of Products 3a <sup>1</sup> , 3a <sup>2</sup> , and 3a <sup>3</sup> .....	129
S3. Mass Spectra of the Isomeric Products 4a.....	130
S4. Mass Spectra of the Isomeric Dehydration Product 4b.....	131
 Chapter 4	
1. Schematic Sequence of Functional Group Interconversions that Link Alkanes and Carboxylic Acids.....	175
2. Percent Conversions as a Function of Time for Hydrothermal Reaction of DBK in Water Alone and with Different Minerals at 300°C and 700 bar.....	176
3. Products from Hydrothermal Reactions of DBK with Minerals.....	177
4. Gas Chromatogram of Product Distribution of DBK Reactions with Hematite in Water at 300°C and 700 bar after 5 h.....	178
5. Gas Chromatogram of Product Distribution of DBK Reactions with Magnetite in Water at 300°C and 700 bar after 5 h.....	179
6. Proposed Reaction Scheme for Formation of Coupling Products H5 and H6 from DBK.....	180
7. Time Dependence of Concentration of Toluene.....	181
8. Time Dependence of Concentration of Bibenzyl.....	182
9. Percentage Reduction and Fragmentation Pathways for Hydrothermal	

Figure	Page
Reaction of DBK at 300°C and 700 bar.....	183
10. Time Dependencies of Concentrations of Alcohol, Alkene, and Alkane in Water Alone, with Hematite, and with Magnetite.....	184
11. Gas Chromatogram of Product Distribution of DBK Reactions with Troilite in Water at 300°C and 700 bar after 24 h.....	185
12. Time Dependencies of Concentrations of Alcohol, Alkene, and Alkane in Water Alone and with Troilite.....	186
13. DBK Conversion as a Function of Surface Area for the Added Minerals at 300°C and 700 bar after 70 h.....	187
14. Representation of a Completely Flat DBK Molecule and a Folded DBK Molecule.....	188
 Chapter 6	
1. Schematic Illustration of Organic Functional Group Interconversions under Hydrothermal Conditions.....	238

## CHAPTER 1:

### INTRODUCTION

#### **1.1. Hydrothermal chemistry of organic compounds**

Most of the Earth's organic carbon does not actively participate in the biospheric carbon cycle, but is located within the crust, mainly in the continental and marine sedimentary basins in the form of kerogen and coal (Falkowski et al., 2000; McSween et al., 2003). It is estimated that more than 15,000,000 Gt of organic matter is located beneath the surface of the Earth (McSween et al., 2003). When this organic matter is exposed to and dissolves in water at high temperatures and pressures, geological processes such as diagenesis, metamorphism, and hydrothermal alteration might take place (McSween et al., 2003). Transformations of organic compounds under hydrothermal conditions play a role in a wide range of important geochemical processes, including the degradation and transport of organic matter in marine and continental sedimentary systems (e.g., Seewald, 2003), the production of oil and gas reservoirs (Head et al., 2003; Larter et al., 2003; Jones et al., 2008), the formation of ore deposits (see Shock et al., 2013), the metabolic cycles of microorganisms in subsurface environments (Head et al., 2003; D'Hondt et al., 2004; Hinrichs et al., 2006; Horsfield et al., 2006; Mason et al., 2010; Shock and Canovas, 2010), and, possibly in prebiotic synthesis and self-assembly processes associated with the origin of life (Holm, 1992; Russell and Hall, 1997; Hazen and Deamer, 2007).



The hydrothermal chemistry of a large number of organic structures has now been studied both theoretically and experimentally. Predictive models for thermodynamic properties of various organic compounds have been developed at elevated temperatures and pressures in aqueous solutions (Shock and Helgeson, 1990; Shock, 1995; Plyasunov and Shock, 2000, 2003; Shock, 2000; LaRowe and Helgeson, 2006; Helgeson et al., 2009; Shock and Canovas, 2010; LaRowe and Dick, 2012; Sverjensky et al., 2014). Numerous hydrothermal reactions have been studied experimentally and much of this work has been reviewed and summarized by various authors (e.g., Bell and Palmer, 1994; Cody et al., 2001; Katritzky et al., 2001; McCollom and Seewald, 2003a, b; Watanabe et al., 2004; McCollom, 2013a).

At elevated temperatures and pressures, the properties of water can be very different compared to ambient conditions. The hydrogen bonds are weaker and fewer compared to ambient water (Akiya and Savage, 2002), and the dielectric constant is much lower at high temperatures and pressures (Johnson and Norton, 1991). This means that water can be an excellent solvent for many organic compounds under these conditions (Siskin and Katritzky, 2001). In addition, the dissociation constant of water ( $K_w$ ) increases dramatically with increasing temperatures (Watanabe et al., 2004), which results in high abundances of  $H^+$  and  $OH^-$  that may facilitate many acid/base-catalyzed organic reactions. Geochemically relevant hydrothermal organic reactions can have a wide temperature range, but the majority of the important processes take place between ca. 150 - 300°C, i.e., well below the critical point of water at 374°C and 221 bar (e.g., Seewald, 2003; McCollom and Seewald, 2007; Tassi et al., 2007).

Organic reactions that have now been identified in hot subcritical water (and associated confining pressures) include fragmentation into smaller structures, addition to make larger structures, and many organic functional group interconversions (see Shock et al., 2013). More importantly, these reactions occur without the addition of any external reagents or catalysts (e.g., Siskin and Katritzky, 1991; Katritzky et al., 2001; Watanabe et al., 2004). For these reasons, organic chemical reactions under conditions that mimic geochemical conditions are being studied as potential “green chemistry” systems (e.g., Avola et al., 2013; Shanab et al., 2013).

Many hydrothermal reactions are somewhat surprising when compared to the corresponding processes close to ambient conditions. Examples include the endothermic elimination of hydrogen from alcohols and alkanes to form carbonyls and alkenes, and the dehydration of alcohols to form alkenes (e.g., Antal et al., 1987; Seewald, 1994; Akiya and Savage, 2001; Katritzky et al., 2001). Alcohol dehydration is particularly surprising from the conventional organic chemistry perspective since water is the solvent. Organic chemistry textbooks teach that in the presence of water, alkenes are converted into alcohols (e.g., Bruice, 2006). Conversion of alkene plus water into alcohol is explained on the basis of the strength of the bonds that are made and broken: one carbon-carbon (C-C)  $\pi$ -bond and an oxygen-hydrogen (O-H)  $\sigma$ -bond are broken, and one carbon-hydrogen (C-H) and one carbon-oxygen (C-O)  $\sigma$ -bonds are made. Because  $\pi$ -bonds are weaker than  $\sigma$ -bonds, the addition of water to an alkene is exothermic (Bruice, 2006). This is an argument, based on that enthalpy is commonly used in textbook descriptions of conventional organic chemistry close to ambient, since enthalpic changes are usually much larger than entropic changes. Under hydrothermal conditions, however, entropic

effects are much more important, primarily due to the increased temperature, and the equilibrium can lie on the side of alkene plus water, even water is the solvent (Shock et al., 2013). The equilibrium is strongly temperature dependent, of course, and for butanol, the equilibrium is on the side of alkene plus water at temperatures above 200°C at the vapor-liquid saturation pressure of water (Figure 1). In general, hydrothermal organic reactions tend to be controlled by thermodynamics and entropy, as opposed to kinetics and enthalpy which are the primary controlling factors closer to ambient.

## **1.2. Hydrothermal organic functional group interconversions**

The most abundant organic functional groups found in geochemically relevant environments are alkanes and carboxylic acids (e.g., Seewald 2003). Seewald (2001; 2003) has proposed a reaction scheme that shows how acids and alkanes might be connected by a series of reversible and irreversible functional group interconversions (Figure 2). This model of organic compound transformations was developed mainly on the basis of hydrothermal experiments that focused on specific functional group interconversions along this pathway. Specifically, reversible hydrogenation/dehydrogenation between alkanes and alkenes under hydrothermal conditions was clearly demonstrated by Seewald (1994), who showed that ethane and ethene reached state of metastable equilibrium in H<sub>2</sub>O at 325°C and 350 bar. The hydrothermal hydration of alkenes to form alcohols has been described by Leif and Simoneit (1995), who analyzed natural hydrothermal petroleum from the Guaymas Basin and conducted hydrous pyrolysis experiments with n-C<sub>32</sub>H<sub>66</sub> at 350°C. Based on their experimental results, they

proposed an alkene to alcohol hydration step prior to formation of ketones. Similarly, Seewald (2001) reported measurable quantities of 2-butanol in hydrothermal studies of the reactions of 1-butene at 300°C with mineral buffers, and he indicated 2-butanol as the hydration product of 1-butene. The reverse reaction, dehydration of alcohols, has also reported in many hydrothermal experiments, and is perhaps the best studied hydrothermal reaction of organic compounds. Akiya and Savage (2001) studied cyclohexanol dehydration in pure water at temperatures between 250 and 380°C and found cyclohexene and other isomeric alkenes as essentially the only products. The mechanisms of hydrothermal dehydration of alcohols to form alkenes have been studied in detail (Xu et al., 1997; Antal et al., 1998; Akiya and Savage, 2001; Anikeev and Ermakova, 2003; Hunter and Savage, 2004). Kinetic studies confirm an acid catalyzed E1 or E2 elimination mechanism for alcohol dehydration where formation of oxonium ion is the necessary first step (Antal et al., 1998; Akiya and Savage, 2001). The role of water in hydrothermal alcohol dehydration has been described as a reactant, a product, and a catalyst which provides hydronium ions (Akiya and Savage, 2001). In addition, the oxidation/reduction reactions that interconvert alcohols and ketones in hydrothermal systems have also been explored (e.g., Leif and Simoneit, 1995; Seewald, 2001; Shen et al., 2010), and reversible redox schemes (e.g., hydrogen transfer reduction of ketone) were proposed.

### 1.3. Ketone hydrothermal chemistry

Compared to hydrocarbons and carboxylic acids, there are only a few reports on the hydrothermal chemistry ketones. This may be because of the low abundances of carbonyl compounds such as ketones and aldehydes in natural hydrothermal systems. Ketones have been naturally found in sedimentary organic matters, hydrous pyrolysis petroleum, and sediment extracts (Regtop et al., 1985; Leif and Simoneit, 1995). Possible transformation pathways for ketones, including reversible hydrogenation/dehydrogenation between ketones and alcohols and irreversible oxidation of ketones to form carboxylic acids, have been proposed under anoxic or mineral-buffered hydrothermal conditions (e.g., Leif and Simoneit, 1995, 2000; Seewald, 2003).

According to Figure 2, the reaction pathways expected for ketones are reduction to alcohol followed by further reduction to form an alkene and an alkane, and carbon-carbon bond breaking to form carboxylic acids. Experiments have been performed to demonstrate hydrothermal oxidation and bond-cleavage reactions of ketones. For instance, when Seewald (2001) injected propene into a hydrothermal environment buffered by hematite-magnetite-pyrite mineral assemblage, acetone was observed as a reaction product, and its follow-up decomposition reactions were found to be accompanied by the increasing concentrations of acetic acid and CO<sub>2</sub>. Similar reactions starting with 1-butene were also found to generate the corresponding ketone, 2-butanone, which decomposed via carbon-carbon bond cleavage to form acetic acid (Seewald, 2001). These production distributions suggest that ketones behave as a redox “bridge” between the alkenes/alkanes and the carboxylic acids. Reduction of ketones under hydrothermal

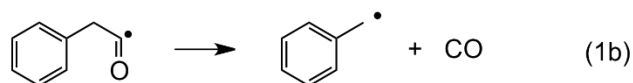
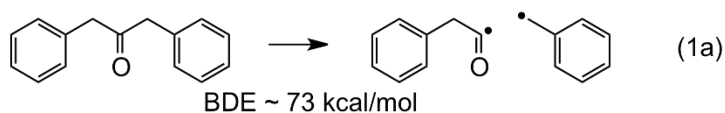
conditions has also been observed. For example, acetone, butanone, and acetophenone were observed to be reduced into the corresponding alcohols when formic acid was used as a hydrogen donor in hydrothermal water (Shen et al., 2010). Formic acid is known as a useful precursor of H<sub>2</sub> under hydrothermal conditions as a result of decarboxylation (Akiya and Savage, 1998; Yu and Savage, 1998). When Shen et al. (2010) replaced formic acid with molecular H<sub>2</sub>, however, reduction of the ketones to form alcohols was no longer observed, which prompted Shen et al. to propose a hydrogen transfer reduction mechanism for ketone reduction from formic acid rather than reaction with H<sub>2</sub>.

In addition to redox reactions, however, other reactions of ketones in high temperature water have been observed. Textbook reactions of ketones include Aldol condensation, keto-enol tautomerization, isomerization, and decarbonylation. Aldol condensation is a useful reaction for formation of carbon-carbon bonds, although a relatively high concentration of base is usually required to catalyze the reaction under conditions close to ambient (Smith and March, 2007). Under hydrothermal conditions, however, Aldol condensation products can readily be formed using only trace quantities of catalytic base. Taken as an example, 3-methylcyclopent-2-enone was prepared in over 80% yield from 2,5-hexanedione using 0.05% aqueous NaOH at 200°C, whereas a similar yield under traditional reflux conditions at atmospheric pressure can only be obtained using a 20 to 400 times more concentrated hydroxide solution (An et al., 1997). Isomerization reactions of ketones have also been reported to occur in useful yields, for example, efficient hydrothermal formation carvacrol from carvone was observed for reaction times of hours (An et al., 1997). One of the fastest hydrothermal reactions observed for ketones is hydrogen exchange via keto-enol tautomerism. A series of

ketones, including acetone, pinacolone, cyclopentanone, and acetophenone, were studied in deuterium oxide ( $D_2O$ ) as the solvent at temperatures between 200 and 280°C by Siskin and Katritzky (2001). Exhaustive H-D exchange was observed at the  $\alpha$  and  $\alpha'$  positions relative to the carbonyl groups in just an hour. This suggests that formation of enolate and enol intermediates can readily occur under hydrothermal conditions. Formation of these species are usually catalyzed by base and acid, respectively.

#### 1.4. Dibenzylketone

As discussed in more details in later Chapters, dibenzylketone (DBK) has been chosen for the majority of the experimental work in this thesis. The known chemistry of DBK is dominated by cleavage of the benzylic carbon-acyl carbon bond, Eqn. 1a, which is the bond cleavage that must occur in this ketone to form carboxylic acids according to Figure 2. This bond dissociation energy has been estimated to be 73 kcal/mol (Luo, 2007), which is lower than what is expected for a conventional carbon ( $sp^3$ )-carbon ( $sp^2$ ) bond (Smith and March, 2007). The reason is that the benzyl radical formed upon homolysis of DBK is resonance stabilized.



The majority of the work on DBK chemistry has involved photochemical excitation (e.g., Gould et al., 1984). Excitation of DBK results in formation of radicals with an overall quantum yield of ca. 0.7 (Robbins and Eastman, 1970). Excitation of DBK forms the first excited singlet state, Figure 3, which intersystem crosses to the triplet state (3DBK\*). Homolytic bond fragmentation in the triplet state is efficient and forms a benzyl radical and phenacyl radical pair in an overall triplet state. Based on orbital symmetry arguments (Michl and Bonacic-Koutecky, 1990), the excited singlet state can undergo bond fragmentation to form only a pair of ions, whereas it is the triplet state that can fragment to give a pair of radicals. The fact that the triplet state mainly undergoes bond cleavage to give the radicals is confirmed by magnetic field and isotope effects studies (Gould et al., 1984), although evidence for a small amount of cleavage from the singlet state has also been reported (Noh et al., 1993). The energy loss that accounts for radical formation being less than 100% efficient (the quantum yield is ca. 0.7) includes fluorescence and non-radiative decay from the less reactive excited singlet state (Noh et al., 1993).

The phenacyl radical formed in the initial cleavage has been shown to undergo further rapid carbon-carbon bond cleavage to generate a second benzyl radical and carbon monoxide, Eqn. 1b. At room temperature, this reaction occurs within ca. 250 ns (Turro et al., 1983). The overall product of photolysis is thus a pair of benzyl radicals.

Pyrolysis of DBK at 500 - 700°C was first reported by Hurd et al. (1933). The major product observed was toluene, together with other unidentified aromatic and polymeric products. The toluene was suggested to have been formed by addition of a hydrogen atom to a benzyl radical formed upon bond homolysis. Removal of hydrogen



from DBK itself was suggested, although the possible mechanistic pathways were not fully explored in this early work. Thus, from both the reported photochemistry and thermochemistry, DBK is anticipated to have relatively facile carbon-carbon bond fragmentation under hydrothermal conditions.

### **1.5. Organic-mineral hydrothermal interactions**

Geochemical processes involving organic compounds take place not just in an aqueous medium, but in the presence of gases and electrolytes, with variable pH, and perhaps most importantly, inorganic materials such as minerals and clay substrates. The study of hydrothermal organic-mineral interactions and mineral catalysis of organic reactivity is potentially of great interest in a wide range of scientific disciplines, including geochemistry, mineralogy, organic catalysis, petrology, and astrobiology. Suggestions that minerals can, and perhaps should, influence organic hydrothermal reactivity have been made for decades (Jurg and Eisma, 1964; Shimoyam and Johns, 1971; Espitalié et al., 1980; Simoneit, 1992; Seewald, 2001; McCollom and Seewald, 2003), and there have been some spectacular reports of the ways in which naturally occurring inorganic substrates can influence the stability of organic structures under hydrothermal laboratory conditions (Leif and Simoneit, 2000; Cody et al., 2001; Seewald, 2001; Foustoukos and Seyfried, 2004; Fu et al., 2008; Williams et al., 2010). As an example, Cody et al. (2000) showed that the presence of iron sulfide and CO enabled the production of decanoic acid and organosulfur compounds from nonanethiol, suggesting a catalytic effect of iron sulfide minerals and the possible formation of organometallic phases under hydrothermal

conditions. Carboxylation and carbonyl insertion have been well documented for alkylthiol compounds in the presence of transition metal sulfides, such as FeS, NiS and CoS, and heterogeneous catalysis on the mineral surface was proposed (Huber and Wachtershauser, 1997; Cody et al., 2001, 2004).

Several studies of hydrothermal organic reactions have been reported in the presence of mineral assemblages that have been used to control experimental variables such as oxidation state, pH, and dissolved sulfur species (Seewald, 1994, 2001; Andersson and Holm, 2000; McCollom and Seewald, 2003; McCollom 2013). For instance, pyrite-pyrrhotite-magnetite, hematite-magnetite, and hematite-magnetite-pyrite assemblages have been used to regulate the activities of dissolved H<sub>2</sub> and H<sub>2</sub>S in hydrothermal solution (e.g., Seewald 2001). These iron-containing minerals have been found playing different roles in organic hydrothermal reactions, including the promotion of bond cleavage processes on the mineral surface, and the alteration of solution properties such as ionic strength, pH, and dissolved metals and sulfur compounds. In recent work, Reeves et al. (2012) took advantage of a pyrite-pyrrhotite-magnetite assemblage to provide a redox-buffered hydrothermal environment for C<sub>1</sub>-C<sub>5</sub> n-alkanes at 323°C and 350 bar, where they observed reversible and extensive water-derived hydrogen incorporation into C<sub>2</sub>-C<sub>5</sub> n-alkanes, but comparatively little exchange for CH<sub>4</sub>, suggesting the occurrence of isotopic exchange should be within reversible equilibration between the alkane and the corresponding alkene. McCollom (2013) studied the influence of iron oxide and sulfide minerals on hydrothermal decomposition of amino acids norvaline and alanine. The observed fact that both amino acids decomposed more rapidly and with altered product distributions in the presence of minerals compared to

water alone, allows him to propose that the mineral effects were due to both surface catalysis, and changes in chemical species in the solution phase.

## **1.6. Subjects of the current thesis**

As described earlier, ketones occupy an important central location in the reaction scheme of Figure 2, since this is the functional group in the reaction scheme where carbon-carbon bond cleavage is required. Although the redox reactions that take the ketone toward the alkane are reversible according to the published data in the literature, carbon-carbon bond cleavage in the direction of carboxylic acids is unlikely to be so. It is widely observed that carboxylic acids accumulate relative to other functional groups in natural environments such as sedimentary basins and hydrothermal fluids (Pittman and Lewan, 1994; Shock, 1995; Lang et al., 2010). Carbon-carbon bond breaking in carboxylic acids (e.g., decarboxylation) has been observed under hydrothermal reactions (Bell and Palmer, 1994; McCollom and Seewald, 2003), however, bond cleavage in ketones has not been studied specifically, and the mechanisms are unknown. As discussed above, the hydrothermal reactions of ketones that have been reported often do not relate very well to the entire reaction scheme given in Figure 2. In addition, several of the previous studies were carried out in the presence of minerals buffers or other additives (e.g., Seewald, 2001; Shen et al., 2010), but understanding on ketone hydrothermal chemistry in pure H<sub>2</sub>O condition is thus lacking. Of particular interest is the way that carbon-carbon bond cleavage competes with the other redox reactions of ketones of Figure 2.

Using Figure 2 as the starting point, this work has several specific goals related to ketone hydrothermal chemistry: (1) determine whether reversible functional-group interconversions along the entire reaction scheme of Figure 2 can be observed and characterized within a single chemical system; (2) determine how irreversible C-C bond cleavage competes with reversible functional-group interconversions; (3) determine the products of the C-C bond cleavage reactions, particularly in relationship to how carboxylic acids may ultimately be formed; (4) where possible, obtain mechanistic information on the various hydrothermal reactions of ketones; and (5) perform time series experiments to give direct experimental support for the reaction sequence of Figure 2, and to obtain relative rate data for as many of the reactions of Figure 2 as possible. To address these problems, experiments have been performed using DBK as the model ketone in water at high temperatures and pressures. The details of these experiments are given in Chapter 2 of this thesis.

Although a large number of hydrothermal organic reactions have been studied, the emphasis has been mainly on product distributions, reports of mechanistic studies have been less frequent, and direct evidence for proposed intermediates is often lacking. This is partly because many hydrothermal reactions give complex product mixtures, and many reactions are reversible (Seewald, 2003; Seewald et al., 2006; Yang et al., 2012; Shipp et al., 2013). The need for high-pressure experimental apparatus can also complicate the use of many routine analytical procedures. Other than kinetic measurements (e.g., Belsky et al., 1999; McCollom and Seewald, 2003), and in some cases isotope effects (e.g., Hoering, 1984; Yamamoto et al., 2004; McCollom et al., 2010; Reeves et al., 2012), the mechanistic toolbox for hydrothermal organic reactions has been somewhat limited to

date. In addition, both ionic and radical organic reactions may occur simultaneously under hydrothermal conditions (Katritzky et al., 2001), although it is generally thought that ionic reactions are more prevalent at lower temperatures whereas radical reactions dominate at higher temperatures (Burdige, 2006; LaRowe and Van Cappellen, 2011). Obtaining evidence for reaction mechanisms and identifying primary reaction products and intermediates under hydrothermal conditions is thus challenging. A second objective of the thesis work is to develop new and effective experimental probes for hydrothermal organic reaction mechanisms. The novel approach of using hydrothermal photochemistry has been found quite useful in unraveling the complex hydrothermal reaction pathways and mechanisms for DBK. Using photochemistry the primary hydrothermal radical products can be identified, and the rapid follow-up thermal reactions can be monitored much more readily than in a pure hydrothermal experiment. The hydrothermal photolysis of DBK is described in Chapter 3 of this thesis.

Interactions between organic compounds and minerals should be a major component in natural hydrothermal geochemical processes. As mentioned above, mineral assemblages have the advantage of regulating fluid chemistry and may effectively simulate geologically relevant environments, nevertheless, an understanding of potential contribution of each individual mineral, such as among those common iron oxides and sulfides, may remain complicated. Example important issues include which specific minerals enhance, suppress, or do not influence organic hydrothermal reactivity and which minerals initiate new reaction pathways? When minerals influence reactions, which mainly promote reactions via surface catalytic effects and which mainly serve as reactants and which change the solution chemistry? Additionally, the specific effects of

minerals on the hydrothermal reactions of ketones have not been addressed. The third main goal of this thesis is to provide an entry into answering some of these questions. Using the hydrothermal chemistry of DBK in water alone as a well-defined starting point, the ways in which several common minerals including hematite ( $\text{Fe}_2\text{O}_3$ ), magnetite ( $\text{Fe}_3\text{O}_4$ ), troilite ( $\text{FeS}$ ), corundum ( $\text{Al}_2\text{O}_3$ ) and quartz ( $\text{SiO}_2$ ) influence ketone under hydrothermal conditions have been investigated, and the results of these experiments are described in Chapter 4.

Finally, there is also interest in possible ways in which geochemically relevant reactions might be useful in developing new green chemistry. Geochemically relevant reactions take place in water as the solvent and can involve common Earth abundant reagents and catalysts. Hydrothermal oxidation of several organic structures using the mild oxidizing reagent copper (II) is described in Chapter 5. Copper is an abundant metal in Earth's crust in the form of copper-ore deposits (Kesler and Wilkinson, 2008), and hydrothermal interactions between copper and organic matter presumably occur in nature. However, little is known about how aqueous copper ions behave in organic-rich hydrothermal fluids. Copper (II) is virtually not well used as an oxidizing agent in conventional organic chemistry and represents a potentially useful mild reagent compared to those commonly used in organic chemistry that are mainly based on chromium in oxidation state VI and manganese in oxidation state VII (Sheldon and Kochi, 1981).

**Figure 1.** Calculated metastable equilibrium ratios of aliphatic alkenes to alcohols as a function of temperature at water saturation pressure (by Shock et al., 2013). Numbers on the curves refer to the number of carbons in alkene and alcohol (e.g., 4 stands for the reaction between butanol and butene plus water). The increasing ratios of alkene/alcohol suggest alcohol dehydration becomes thermodynamically favorable as temperature increases.

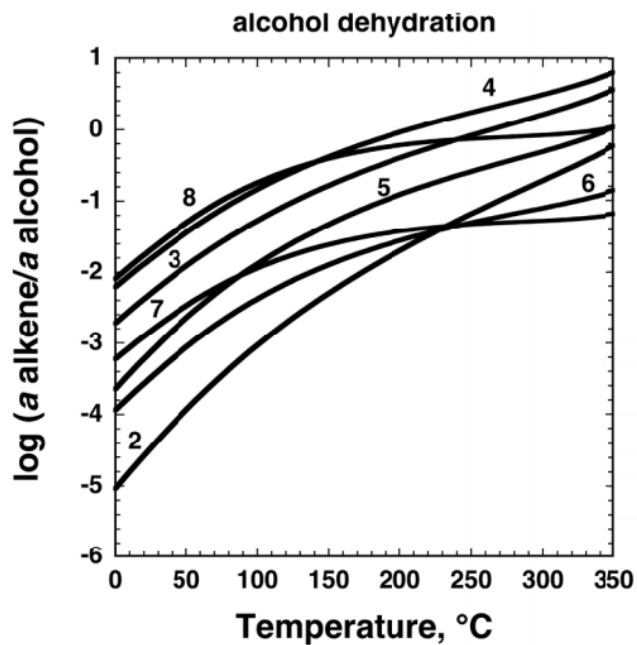


**Figure 2.** Schematic illustration of the proposed oxidation and reduction (horizontal), and hydration/dehydration (vertical) pathways that interconvert hydrocarbon and carboxylic acid functionalities under hydrothermal conditions by Seewald (2003). Note the central position of the ketone functional group. Evidence has been obtained that suggests all the reactions are reversible (see text), except the carbon-carbon cleavage reaction that forms carboxylic acids.

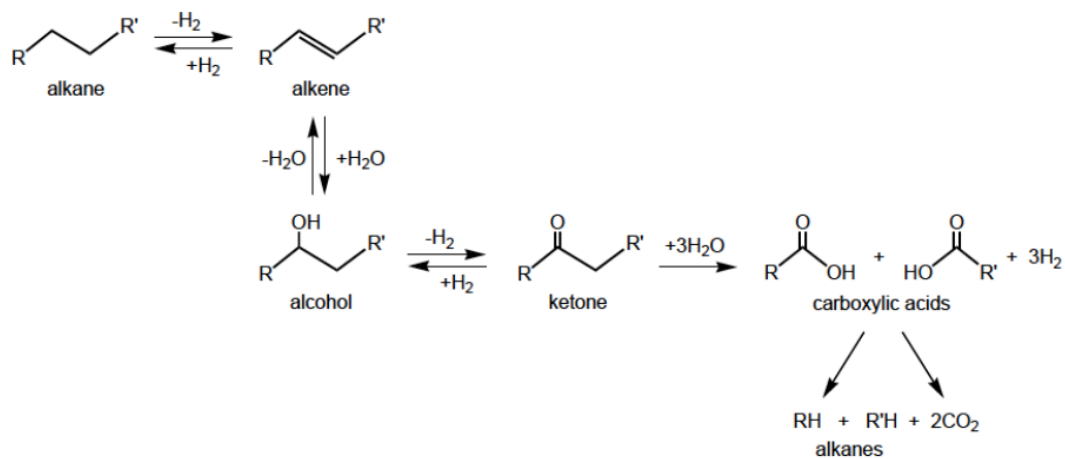
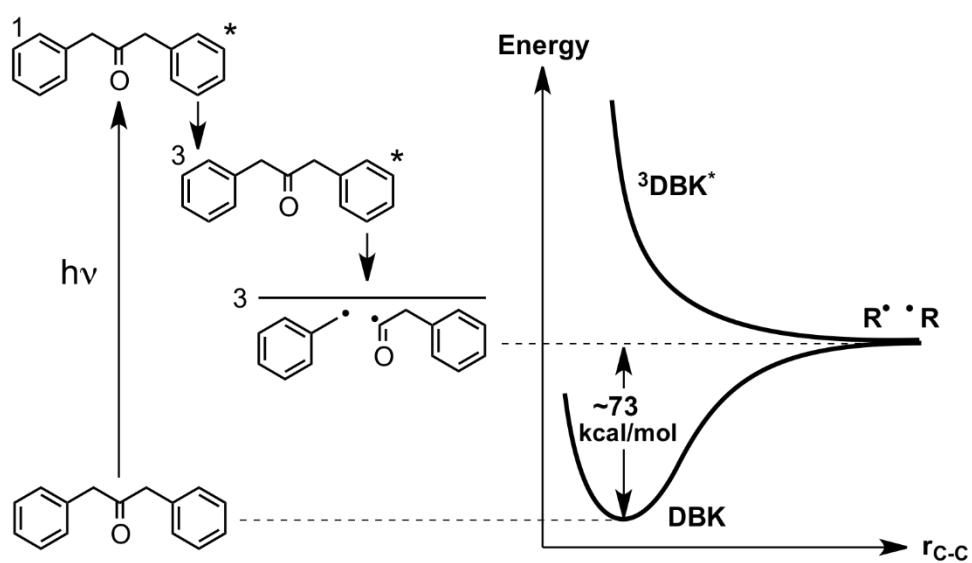




**Figure 3.** Schematic energy diagram for formation of a pair of radicals for photochemical excitation of dibenzylketone (DBK). The plot shows the energies of the ground singlet (DBK) and excited triplet ( $^3\text{DBK}^*$ ) states as a function of carbon-carbon bond separation distance ( $r_{\text{C-C}}$ ). The energies of a triplet and a singlet radical pair are essentially identical at large  $r_{\text{C-C}}$ .



## 1.7. References

- Akiya N. and Savage P. E. (1998) Role of water in formic acid decomposition. *AICHE J.* **44**, 405-415.
- Akiya N. and Savage P. E. (2001) Kinetics and mechanism of cyclohexanol dehydration in high-temperature water. *Ind. Eng. Chem. Res.* **40**, 1822-1831.
- Akiya N. and Savage P. E. (2002) Roles of water for chemical reactions in high-temperature water. *Chem. Rev.* **102**, 2725-2750.
- An J., Bagnell L., Cablewski T., Strauss C. R. and Trainor R. W. (1997) Applications of high-temperature aqueous media for synthetic organic reactions. *J. Org. Chem.* **62**, 2505-2511.
- Andersson E. and Holm N. G. (2000) The stability of some selected amino acids under attempted redox constrained hydrothermal conditions. *Origins Life Evol. Bios.* **30**, 9-23.
- Anikeev V. and Ermakova A. (2003) The influence of the density of supercritical water on the rate constant for the dehydration of isopropanol. *Russ. J. Phys. Chem.* **77**, 211-214.
- Antal M. J., Brittain A., DeAlmeida C., Ramayya S., Roy J. C. (1987) Heterolysis and hemolysis in supercritical water. *ACS Sym. Ser.* **329**, 77-86.
- Antal M. J., Carlsson M., Xu X. and Anderson D. G. M. (1998) Mechanism and kinetics of the acid-catalyzed dehydration of 1- and 2-propanol in hot compressed liquid water. *Ind. Eng. Chem. Res.* **37**, 3820-3829.
- Avola S., Guillot M., da Silva-Perez D., Pellet-Rostaing S. and Kunz W.; Goettmann F. (2013) Organic chemistry under hydrothermal conditions. *Pure Appl. Chem.* **85**, 89-103.
- Bell J. L. S. and Palmer D. A. (1994) Experimental studies of organic acid decomposition. *Organic Acids in Geological Processes* (eds. E. D. Pittman and M. D. Lewan). Springer-Verlag, New York. pp. 226-269.
- Belsky A. J., Maiella P. G. and Brill T. B. (1999) Spectroscopy of hydrothermal reactions – 13. Kinetics and mechanisms of decarboxylation of acetic acid derivatives at 100-260°C under 275 bar. *J. Phys. Chem. A* **103**, 4253-4260.

- Burdige D. J. (2006) *Geochemistry of Marine Sediments*. Princeton University Press: Princeton, NJ.
- Bruice P. Y. (2006) *Organic Chemistry* (5th Edition). Prentice Hall.
- Cody G. D., Boctor N. Z., Filley T. R., Hazen R. M., Scott J. H., Sharma A. and Yoder H. S. (2000) Primordial carbonylated iron-sulfur compounds and the synthesis of pyruvate. *Science* **289**, 1337-1340.
- Cody G. D., Boctor N. Z., Hazen R. M., Brandes J. A., Morowitz H. J., Yoder H. S. (2001) Geochemical roots of autotrophic carbon fixation: Hydrothermal experiments in the system citric acid, H<sub>2</sub>O-(±FeS)-(±NiS). *Geochim. Cosmochim. Acta* **65**, 3557-3576.
- Cody G. D. (2004) Transition metal sulfides and the origins of metabolism. *Annu. Rev. Earth Planet. Sci.* **32**, 569-599.
- D'Hondt S., Jørgensen B. B., Miller D. J., Batzke A., Blake R., Cragg B. A., Cypionka H., Dickens G. R., Ferdelman T., Hinrichs K.-U., Holm N. G., Mitterer R., Spivak A., Wang G., Bekins B., Engelen B., Ford K., Gettemy G., Rutherford W. D., Sass H., Skilbeck C. G., Aiello I. W., Guèrin G., House C. H., Inagaki F., Meister P., Naehr T., Niituma S., Parkes R. J., Schippers A., Smith D. C., Teske A., Wiegel J., Padilla C. N. and Acosta J. L. S. (2004) Distributions of microbial activities in deep seafloor sediments. *Science* **306**, 2216-2221.
- Espitalie J., Madec M. and Tissot B. (1980) Role of mineral matrix in kerogen pyrolysis – influence on petroleum generation and migration. *AAPG Bulletin-American Association of Petroleum Geologists*. **64**, 59-66.
- Falkowski P., Scholes R. J., Boyle E., Canadell J., Canfield D., Elser J., Gruber N., Hibbard K., Hogberg P., Linder S., Mackenzie F. T., Moore B., Pedersen T., Rosenthal Y., Seitzinger S., Smetacek V. and Steffen W. (2000) The global carbon cycle: A test of our knowledge of earth as a system. *Science* **290**, 291-296.
- Foustoukos D. I. and Seyfried Jr. W. E. (2004) Hydrocarbons in hydrothermal vent fluids: the role of chromium-bearing catalysts. *Science* **304**, 1002-1005.
- Fu Q., Foustoukos D. I., Seyfried Jr. W. E. (2008) Mineral catalyzed organic synthesis in hydrothermal systems: An experimental study using time-of-flight secondary ion mass spectrometry. *Geophys. Res. Lett.* **35**, L07612.

- Gould I. R., Turro N. J. and Zimmt M. B. (1984) In *Advances in Physical Organic Chemistry* (eds: Gold V. and Bethell D.). Academic Press, New York. Vol. 20, 1-51.
- Hazen R. M. and Deamer D. (2007) Hydrothermal reactions of pyruvic acid: synthesis, selection, and self-assembly of amphiphilic molecules. *Origins of Life and Evolution of Biospheres* **37**, 143-152.
- Head I. M., Jones D. M. and Larter S. R. (2003) Biological activity in the deep subsurface and the origin of heavy oil. *Nature* **426**, 344-352.
- Hinrichs K.-U., Hayes J. M., Bach W., Spivak A. J., Hmelo L. R., Holm N. G., Johnson C. G. and Sylva S. P. (2006) Biological formation of ethane and propane in the deep marine subsurface. *Proc. Natl. Acad. Sci. USA* **103**, 14684-14689.
- Hoering T. C. (1984) Thermal reactions of kerogen with added water, heavy water and pure organic substances. *Org. Geochem.* **5**, 267-278.
- Holm N. G. (ed.) (1992) *Marine Hydrothermal Systems and the Origin of Life*. Kluwer Academic Publishers, Dordrecht, Netherlands.
- Horsfield B., Schenk H. J., Zink K., Ondrak R., Dieckmann V., Kallmeyer J., Mangelsdorf K., di Primo R., Wilkes H., Parkes R. J., Fry J. and Cragg B. (2006) Living microbial ecosystems within the active zone of catagenesis: Implications for feeding the deep biosphere. *Earth Planet. Sci. Lett.* **246**, 55-69.
- Huber C. and Wächtershäuser G. (1997) Activated acetic acid by carbon fixation on (Fe,Ni) S under primordial conditions. *Science* **276**, 245-247.
- Hunter S. E. and Savage P. E. (2004) Recent advances in acid- and base-catalyzed organic synthesis in high-temperature liquid water. *Chem. Eng. Sci.* **59**, 4903-4909.
- Hurd D. D., Christ R. and Thomas R. L. (1933) Preparation and pyrolysis of dibenzyl ketone, phenylacetic anhydride and diphenylacetic anhydride. *J. Am. Chem. Soc.* **55**, 2589-2592.
- Johnson J. W. and Norton D. (1991) Critical phenomena in hydrothermal systems: State, thermodynamic, electrostatic, and transport properties of H<sub>2</sub>O in the critical region. *Am. J. Sci.* **291**, 541-648.
- Jones D. M., Head I. M., Gray N. D., Adams J. J., Rwan A. K., Aitken C. M., Bennett B., Huang H., Brown A., Bowler B. F. J., Oldenburg T., Erdmann M. and Larter S. R. (2008) Crude-oil biodegradation via methanogenesis in subsurface petroleum reservoirs. *Nature* **451**, 176-180.

- Jurg J. W. and Eisma E. (1964) Petroleum hydrocarbons: generation from fatty acid. *Science* **19**, 1451-1452.
- Katritzky A. R., Nichols D. A., Siskin M., Murugan R. and Balasubramanian M. (2001) Reactions in high-temperature aqueous media. *Chem. Rev.* **101**, 837-892.
- Kesler S. E. and Wilkinson B. H. (2008) Earth's copper resources estimated from tectonic diffusion of porphyry copper deposits. *Geology*. **36**, 255-258.
- Lang S. Q., Butterfield D. A., Schulte M. D., Kelley D. S. and Lilley M. D. (2010) Elevated concentrations of formate, acetate and dissolved organic carbon found at the Lost City hydrothermal field. *Geochim. Cosmochim. Acta* **74**, 941-952.
- LaRowe D. E. and Dick J. M. (2012) Calculation of the standard molal properties of crystalline peptides. *Geochim. Cosmochim. Acta* **80**, 70-91.
- LaRowe D. E. and Helgeson H. C. (2006) Biomolecules in hydrothermal systems: Calculation of the standard molal thermodynamic properties of nucleic-acid bases, nucleosides, and nucleotides at elevated temperatures and pressures. *Geochim. Cosmochim. Acta* **70**, 4680-4724.
- LaRowe D. E. and Van Cappellen P. (2011) Degradation of natural organic matter: A thermodynamic analysis. *Geochim. Cosmochim. Acta* **77**, 2030-2042.
- Larter S. R., Wilhelms A., Head I., Koopmans M., Aplin A., Di P. R., Zwach C., Erdmann M. and Telnaes N. (2003) The controls on the composition of biodegraded oils in the deep subsurface: Part I - Biodegradation rates in petroleum reservoirs. *Org. Geochem.* **34**, 601-613.
- Leif R. N. and Simoneit B. R. T. (1995) Ketones in hydrothermal petroleum and sediment extract from Guaymas Basins, Gulf of California. *Org. Geochem.* **23**, 889-904.
- Leif R. N. and Simoneit B. R. T. (2000) The role of alkenes produced during hydrous pyrolysis of a shale. *Org. Geochem.* **31**, 1189-1208.
- Luo Y-R. (2007) *Comprehensive Handbook of Chemical Bond Energies*. CRC Press: Boca Raton, FL.
- Mason O. U., Nakagawa T., Rosner M., Van Nostrand J. D., Zhou J., Maruyama A., Fisk M. R. and Giovannoni S. J. (2010) First investigation of the microbiology of the deepest layer of ocean crust. *PLoS ONE*. **5**, 1-11.
- McCullom T. M. (2013a) Laboratory simulations of abiotic hydrocarbon formation in Earth's deep subsurface. *Rev. Mineral. Geochem.* **75**, 467-494.

- McCollom T. M. (2013b) The influence of minerals on decomposition of the n-alkyl-alpha-amino acid norvaline under hydrothermal conditions. *Geochim. Cosmochim. Acta* **104**, 330-357.
- McCollom T. M. and Seewald J. S. (2003a) Experimental constraints on the hydrothermal reactivity of organic acids and acid anions: I. Formic acid and formate. *Geochim. Cosmochim. Acta* **67**, 3625-3644.
- McCollom T. M. and Seewald J. S. (2003b) Experimental study of the hydrothermal reactivity of organic acids and acid anions: II. Acetic acid, acetate, and valeric acid. *Geochim. Cosmochim. Acta* **67**, 3645-3664.
- McCollom T. M. and Seewald J. S. (2007) Abiotic synthesis of organic compounds in deep-sea hydrothermal environments. *Chem. Rev.* **107**, 382-401.
- McCollom T. M., Lollar B. S., Lacrampe-Couloume G. and Seewald J. S. (2010) The influence of carbon source on abiotic organic synthesis and carbon isotope fractionation under hydrothermal conditions. *Geochim. Cosmochim. Acta* **74**, 2717-2740.
- McSween H., Richardson S. and Uhle M. (2003) *Geochemistry: Pathways and Processes* (Second Edition). Columbia University Press, New York.
- Michl J. and Bonacic-Koutecky V. (1990) *Electronic Aspects of Organic Photochemistry*. Wiley-Interscience, New York.
- Noh T. H., Step E. and Turro N. J. (1993) Singlet-state photochemistry of dibenzyl ketone and its o-tolyl derivatives. *J. Photochem. Photobiol.* **72**, 133-145.
- Pittman E. D. and Lewan M. D. (1994) *Organic Acids in Geological Processes*. Springer-Verlag, Berlin.
- Plyasunov A. V. and Shock E. L. (2000) Standard state Gibbs energies of hydration of hydrocarbons at elevated temperatures as evaluated from experimental phase equilibria studies. *Geochim. Cosmochim. Acta* **64**, 2811-2833.
- Plyasunov A. V. and Shock E. L. (2003) Prediction of the vapor-liquid distribution constants for volatile nonelectrolytes in H<sub>2</sub>O up to the critical temperature of water. *Geochim. Cosmochim. Acta* **67**, 4981-5009.
- Ragtop R. A., Ellis J., Crisp. P. T., Ekstrom A. and Fookes C. J. R. (1985) Pyrolysis of model compounds on spent oil shales, minerals and charcoal – Implications for shale oil composition. *Fuel.* **64**, 1640-1646.

- Reeves E. P., Seewald J. S. and Sylva S. (2012) Hydrogen isotope exchange between n-alkanes and water under hydrothermal conditions. *Geochim. Cosmochim. Acta* **77**, 582-599.
- Robbins W. K. and Eastman R. H. (1970) Photodecarbonylation in solution. I. Quantum yields and quenching results with dibenzyl ketones. *J. Am. Chem. Soc.* **92**, 6076-6077.
- Russell M. J. and Hall A. J. (1997) The emergence of life from iron monosulfide bubbles at a submarine hydrothermal redox and pH front. *J. Geol. Soc. London* **154**, 377-402.
- Seewald J. S. (1994) Evidence for metastable equilibrium between hydrocarbons under hydrothermal conditions. *Nature* **370**, 285-287.
- Seewald J. S. (2001) Aqueous geochemistry of low molecular weight hydrocarbons at elevated temperatures and pressures: constraints from mineral buffered laboratory experiments. *Geochim. Cosmochim. Acta* **65**, 1641-1664.
- Seewald J. S. (2003) Organic-inorganic interactions in petroleum producing sedimentary basins. *Nature* **426**, 327-333.
- Seewald J. S., Zolotov M. Y. and McCollom T. (2006) Experimental investigation of single carbon compounds under hydrothermal conditions. *Geochim. Cosmochim. Acta* **70**, 446-460.
- Shanab K., Neudorfer C., Schirmer E. and Spreitzer H. (2013) Green solvents in organic synthesis: An overview. *Curr. Org. Chem.* **17**, 1179-1187.
- Sheldon R. A. and Kochi J. K. (1981) *Metal-catalysed Oxidations of Organic Compounds*, Academic Press, New York.
- Shen Z., Zhang Y., Jin F., Zhou X., Kishita A. and Tohji K. (2010) Hydrogen-transfer reduction of ketones into corresponding alcohols using formic acid as a hydrogen donor without a metal catalyst in high-temperature water. *Ind. Eng. Chem. Res.* **49**, 6255-6259.
- Shimoyam A. and Johns W. D. (1971) Catalytic conversion of fatty acids to petroleum-like paraffins and their maturation. *Nat. Phys. Sci.* **232**, 140-144.
- Shipp J., Gould I., Herckes P., Shock E., Williams L., and Hartnett H. (2013) Organic functional group transformations in water at elevated temperature and pressure:

- Reversibility, reactivity, and mechanisms. *Geochim. Cosmochim. Acta* **104**, 194-209.
- Shock E. L. (1995) Organic acids in hydrothermal solutions: Standard molal thermodynamic properties of carboxylic acids, and estimates of dissociation constants at high temperatures and pressures. *Am. J. Sci.* **295**, 496-580.
- Shock E. L. (2000) Thermodynamic response of organic compounds in geochemical processes of sedimentary basins. *Reviews in Economic Geology*, Volume **9** (eds: T. H. Giordano, R. M. Kettler, S. A. Wood). pp. 105-117.
- Shock E. L. and Helgeson H. C. (1990) Calculation of the thermodynamic and transport properties of aqueous species at high pressures and temperatures: Standard partial molal properties of organic species. *Geochim. Cosmochim. Acta* **54**, 915-945.
- Shock E. L. and Canovas P. C. (2010) The potential for abiotic organic synthesis and biosynthesis at seafloor hydrothermal systems. *Geofluids* **10**, 161-192.
- Shock E. L., Canovas P., Yang Z., Boyer G., Johnson K., Robinson K., Fecteau K., Windman T., and Cox A. (2013) Thermodynamics of organic transformations in hydrothermal fluids. *Rev. Mineral. Geochem.* **76**, 311-350.
- Simoneit, B. R. T. (1992) Aqueous organic geochemistry at high temperature/high pressure. In *Marine Hydrothermal Systems and the Origin of Life*, Holm N.G. Ed., Kluwer, Dordrecht, Netherlands, Chapter 4.
- Siskin M. and Katritzky A. R. (1991) Reactivity of organic compounds in hot water – Geochemical and technological implications. *Science* **254**, 231-237.
- Siskin M. and Katritzky A. R. (2001) Reactivity of organic compounds in superheated water: general background. *Chem. Rev.* **101**, 826-835.
- Smith M. B. and March J. (2007) *March's Advanced Organic Chemistry: Reactions, Mechanisms, and Structure*. Wiley-Interscience, Hoboken, New Jersey.
- Sverjensky D. A., Harrison B. and Azzolini D. (2014) Water in the deep Earth: The dielectric constant and the solubilities of quartz and corundum to 60 kb and 1200 degrees C. *Geochim. Cosmochim. Acta* **129**, 125-145.
- Tassi F., Vaselli O., Capaccioni B., Montegrossi G., Barahona F. and Caprai A. (2007) Scrubbing process and chemical equilibria controlling the composition of light hydrocarbons in natural gas discharges: An example from the geothermal fields of El Salvador. *Geochim. Geophys. Geosys.* **8**, doi:10.1029/2006GC001487.



- Turro N. J., Gould I. R. and Baretz B. H. (1983) Absolute rate constants for decarbonylation of phenylacetyl and related radicals. *J. Phys. Chem.* **87**, 531-532.
- Watanabe M., Sato T., Inomata H., Smith Jr. R. L., Arai K., Kruse A. and Dinjus E. (2004) Chemical reactions of C<sub>1</sub> compounds in near-critical and supercritical water. *Chem Rev.* **104**, 5803-5821.
- Williams L. B., Holloway J. R., Canfield B., Glein C., Dick J., Hartnett H. and Shock E. L. (2010) Birth of biomolecules from the warm wet sheets of clays near spreading centers. In *Earliest Life on Earth* (eds. Golding S. and Glikson M.). Springer Publishing. Chapter 4.
- Xu X., Antal M. J. and Anderson D. G. M. (1997) Mechanism and temperature-dependent kinetics of the dehydration of tert-butyl alcohol in hot compressed liquid water. *Ind. Eng. Chem. Res.* **36**, 23-41.
- Yamamoto M., Yokota Y., Oshima K. and Matsubara S. (2004) H-D exchange reaction on benzene ring of polystyrene in hydrothermal deuterium oxide with platinum (IV) oxide catalyst. *Chem. Comm.* **15**, 1714-1715.
- Yang Z., Gould I. R., Williams L., Hartnett H., and Shock E. L. (2012) The central role of ketones in reversible and irreversible hydrothermal organic functional group transformations. *Geochim. Cosmochim. Acta* **98**, 48-65.
- Yu J. and Savage P. E. (1998) Decomposition of formic acid under hydrothermal conditions. *Ind. Eng. Chem. Res.* **37**, 2-10.

## CHAPTER 2:

### THE CENTRAL ROLE OF KETONES IN REVERSIBLE AND IRREVERSIBLE HYDROTHERMAL ORGANIC FUNCTIONAL GROUP TRANSFORMATIONS

Revised with permission from Yang Z., Gould I. R., Williams L. B., Hartnett H. E., and Shock E. L. (2012) The central role of ketones in reversible and irreversible hydrothermal organic functional group transformations. *Geochim. Cosmochim. Acta* **98**, 48-65.

Copyright 2012 Elsevier Ltd.

#### **2.1. Abstract**

Studies of hydrothermal reactions involving organic compounds suggest complex, possibly reversible, reaction pathways that link functional groups from reduced alkanes all the way to oxidized carboxylic acids. Ketones represent a critical functional group because they occupy a central position in the reaction pathway, at the point where carbon-carbon (C-C) bond cleavage is required for the formation of the more oxidized carboxylic acids. The mechanisms for the critical bond cleavage reactions in ketones, and how they compete with other reactions are the focus of this experimental study. We studied a model ketone, dibenzylketone (DBK), in H<sub>2</sub>O at 300°C and 70 MPa for up to 528 h. Product analysis was performed as a function of time at low DBK conversions to reveal the primary reaction pathways. *Reversible* interconversion between ketone, alcohol, alkene and alkane functional groups is observed in addition to formation of radical coupling products derived from *irreversible* C-C and carbon-hydrogen (C-H)

homolytic bond cleavage. The product distributions are time-dependent but the bond cleavage products dominate. The major products that accumulate at longer reaction times are toluene and larger, dehydrogenated structures that are initially formed by radical coupling. The hydrogen atoms generated by dehydrogenation of the coupling products are predominantly consumed in the formation of toluene. Even though bond cleavage products dominate, no carboxylic acids were observed on the timescale of the reactions under the chosen experimental conditions.

## **2.2. Introduction**

Organic compounds react at high temperatures and pressures in the presence of minerals and aqueous solutions during diagenesis, metamorphism, and hydrothermal alteration. Maturation of organic matter occurs during burial in continental and marine sedimentary basins, which leads to production of oil and natural gas, and in hydrothermal systems driven by igneous processes (Head et al., 2003; Larter et al., 2003; Seewald, 2003; Hinrichs et al., 2006; McCollom and Seewald, 2007). In many instances, evidence from natural systems can be used to argue for metastable equilibria among organic compounds and between organic compounds and their inorganic geologic environments (Shock, 1988; 1989; 1994; Helgeson et al. 1993; 2009). Experimental tests of metastable equilibria have led to hypotheses about the reaction pathways that organic compounds follow in natural systems (Seewald, 1994; 2001; 2003; McCollom and Seewald, 2003; Seewald et al., 2006). Numerous hydrothermal organic reactions have been explored (Siskin and Katritzky, 1991; Bell and Palmer, 1994; Andersson and Holm, 2000;

Katritzky et al., 2001; McCollom and Seewald, 2007; Morooka et al., 2007, among many others), and thermodynamic properties at elevated temperature and pressures are available for many organic compounds as gases, liquids, solids and in aqueous solution (Shock and Helgeson, 1990; Shock, 1995; Amend and Helgeson, 1997; 2000; Helgeson et al., 1998; Richard and Helgeson, 1998; Plyasunov and Shock, 2000; 2003; Richard, 2001; Plyasunova et al., 2004; Dick et al., 2006; LaRowe and Helgeson, 2006a, b; LaRowe and Dick, 2012). However, kinetic, and particularly mechanistic, information related to individual hydrothermal organic reactions is scarce. Therefore, the goal of this study was to investigate hydrothermal organic reaction mechanisms with a focus on ketones, which occupy a key stage in the hypothesized production of carboxylic acids.

A series of interrelated reactions that transform functional groups from alkanes to carboxylic acids, passing through ketones, as described by Seewald (2003), is summarized in Fig. 1. Seewald (2003) developed this model of organic compound transformations based on his pioneering experimental work that allowed him to propose which steps in the overall process were reversible and which were irreversible. The kinetics and thermodynamics of the dehydrogenation/hydrogenation reactions that interconvert alkanes and alkenes were described by Seewald (1994) for hydrothermal conditions, and for catalysis by platinum in the gas phase by Adlhart and Uggerud (2007). The hydrothermal hydration of alkenes to form alcohols (Seewald, 2001), and in particular the mechanism of dehydration of alcohols to form alkenes, also has been studied in detail (Xu et. al, 1997; Antal et. al, 1998; Akiya and Savage, 2001; Anikeev and Ermakova, 2003; Hunter and Savage, 2004). The oxidation/reduction reactions that interconvert alcohols and ketones in sedimentary basins have also been studied in

previous work (Leif and Simoneit, 1995; Seewald, 2003), but the conversion extents and reaction mechanisms were not extensively described. Ketones occupy an important central location in the reaction scheme of Fig. 1, since in order to proceed to carboxylic acids, C-C bond cleavage of ketones is required. Furthermore, although the redox reactions that take the ketone toward the alkane are, at least in principle, reversible, C-C bond cleavage in the direction of carboxylic acids is unlikely to be so (Fig. 1). It is widely observed that carboxylic acids accumulate relative to other functional groups in many natural sedimentary basin and hydrothermal fluids (Pittman and Lewan, 1994; Shock, 1995; Windman et al., 2007; Lang et al., 2010). Although skeletal fragmentation can be observed in hydrothermal reactions (Bell et al., 1994; McCollom and Seewald, 2003), the mechanism of bond cleavage for ketones is unknown, and the extent to which C-C bond cleavage competes with the other reactions shown in Fig. 1 has also not been studied.

Using Fig 1 as the starting point, the project reported here had several specific goals: (1) determine whether reversible functional-group interconversions along the entire reaction scheme of Fig. 1 can be observed and characterized within a single chemical system; (2) determine how irreversible C-C bond cleavage competes with reversible functional-group interconversions; (3) determine the products of the C-C bond cleavage reactions, particularly in relationship to how carboxylic acids may ultimately be formed; (4) where possible, obtain mechanistic information on the various hydrothermal reactions of ketones; and (5) perform time-series experiments to give direct experimental support for the reaction sequence of Fig. 1, and to obtain relative rate data for as many of the reactions of Fig. 1 as possible.

Our experimental approach uses a model ketone, dibenzylketone (DBK) (Fig. 2) that was selected to give mechanistic insight. The experiments rely on extraction of all organic products from the aqueous phase after reaction, and the benzene rings in DBK ensure that the majority of the products have low volatility and are easily extractable into organic solvents. Importantly, the benzene rings should stabilize both ionic and/or radical intermediates involved in C-C bond cleavage at the carbonyl carbon by resonance (Fig. 2), which will facilitate this reaction pathway. Hydrothermal experiments were conducted in time-series at low extents of conversion in order to provide relative rate information and evidence for the reaction sequence of Fig. 1.

## 2.3. Experimental

### 2.3.1. Reagents

Dibenzylketone was purchased from Sigma-Aldrich, and was recrystallized three times from diethyl ether (5%)/hexanes (95%) to reach a purity of >99.9%, as determined by gas chromatography. 1, 3-Diphenylpropane (99%) was purchased from Frinton Laboratories Inc. and was purified (>99.6%) using preparative thin layer chromatography. Dichloromethane (DCM, 99.9%) and deuterium oxide (99.9% D<sub>2</sub>O) were purchased from Fisher Chemical and Cambridge Isotope Laboratories Inc., respectively. Deionized (DI) water was obtained using a Diamond Ultrapure Water System (18.2 MΩ·cm resistivity). Decane (99%) and dodecane (99%), both from Sigma-Aldrich, were used as internal standards for quantitative analysis using gas

chromatography. 1,3-diphenyl-2-propanol and *p*-methyldibenzylketone, and a mixture of *cis*- and *trans*-1,3-diphenylpropene, were synthesized as described by Coan and Becker (1954; 1963). The alcohol and the ketone were purified using chromatography to reach >99% and >98% purity, respectively.

### 2.3.2. Procedures

Previous laboratory studies of organic reactions in water at elevated temperatures and pressures used fixed volume reactors constructed from gold, titanium, stainless steel and quartz (Palmer and Drummond, 1986; Bell et al., 1994; McCollom et al., 1999). Because hydrothermal reactions may be influenced by the reactor, gold capsules were used in this work as gold was shown by Bell et al. (1994) to exhibit the weakest catalytic effect. Gold is also flexible allowing the pressure inside the sample to be controlled externally, using water as a pressurizing medium, to avoid generating a vapor phase at temperatures below the critical point of H<sub>2</sub>O. The capsules were made from gold tubing with a 5 mm outer diameter, 4 mm inner diameter and a length of ~37.5 mm. The internal volumes of the capsules were ~1.75 mL. The capsules were cleaned by rinsing with 12 M HCl, followed by boiling in deionized water, and were then annealed at 580°C for 12 h before use. The capsules were first arc-welded at one end using a precision welder. The water and ketone were added and removal of oxygen was accomplished by purging with low-pressure ultra-high purity argon for one minute. Dibenzylketone concentrations of one molal in H<sub>2</sub>O were used to minimize errors associated with loading sub-milligram quantities of the ketone into the gold capsules. 42 mg of purified DBK

and 200  $\mu\text{L}$  of argon-purged deionized water or deuterium oxide were added to the capsules before a second purging of the headspace using argon. Capsules were then cooled using liquid nitrogen to solidify the contents, quickly pinched closed and carefully sealed by welding while submerged in a methanol:ice (1:1) cold bath to minimize evaporative losses.

The solubility of DBK under the reaction conditions was confirmed as follows. Around 42 mg of DBK and 200  $\mu\text{L}$  of water were added to a fused silica glass tube of 6 mm OD and 2 mm ID. The sample was evacuated at liquid nitrogen temperature and sealed to a length of ca. 13 cm. The sample occupied ca. 8 cm of the tube length, the rest being evacuated headspace. The silica glass tube was placed into a large brass block that was equipped with viewing ports and was heated using cartridge heaters. The sample was observed visually as it was heated, using the ports, or by briefly removing the tube from the block. Undissolved DBK was readily observed as liquid droplets in the water. The DBK was visually observed to start dissolving as the temperature was slowly increased above 200°C, and complete dissolution occurred at ca. 295°C, although it was found that an equilibration period of ca. 1 h was required to achieve complete dissolution, which is presumably a consequence of restricted mass transport in the narrow silica glass tubing. In this way, a homogeneous phase was confirmed visually at the experimental temperature of 300°C for three independently prepared samples.

The gold capsules were placed into a 51 cm stainless-steel cylindrical pressure vessel (Williams et al., 2001) that was filled with DI water and pressurized to 70 MPa (10,150 psi) at room temperature. The reaction vessel was then inserted into a preheated



clamshell furnace and allowed to reach 300°C, while maintaining a constant pressure of 70 MPa. A thermocouple inside the pressure vessel was used to monitor the temperature in the vicinity of the reacting capsules. Owing to its large heat capacity, the pressure vessel typically required 3-4 h for the furnace to heat the sample up to 300°C. The zero time point for each experiment was taken to be the time at which the temperature reached 298°C, after which the rate of temperature increase to 300°C was about 1.5°C per hour. This means that some conversion to products may have occurred during the ramp-up heating. Time-series experiments were performed for up to a maximum time of 528 h after the time zero point, under constant temperature and pressure conditions. The maximum uncertainty in the temperature and pressure is estimated to be 5°C in temperature and 5 MPa in pressure for the experiments (Williams et al., 2001). After the desired experimental duration, the pressure vessel was quenched quickly in an ice bath and the temperature dropped to room temperature within one minute. Then the gold capsules were removed from the vessel. The weights of the gold capsules were measured both before and after each experiment using a 0.01 mg-scale balance to ensure no loss of mass.

### *2.3.3. Product analysis*

The concentrations used in the Tables and Figures in this work are in millimolal, which refer to the samples at the experimental high temperature and pressure, where they are solutions with the organic compounds dissolved in the water. At room temperature, the organic compounds will not be completely dissolved in the water. Before extracting

the reaction products, the capsules were first rinsed in dichloromethane and then frozen in liquid nitrogen to avoid evaporation of any volatile products upon opening. The extraction solvent dichloromethane (DCM, 99.9%) contained 1.3 mM decane and 11.1 mM dodecane as gas chromatography internal standards. The organic products in the opened capsules were extracted using 3.0 mL of DCM in a 4 mL silanized glass vial (Supelco, Inc.) by shaking using a Vortex Genie 2 for 2 minutes. The products were analyzed using a Varian CP-3800 gas chromatograph (GC) equipped with a polycapillary column (5% diphenyl/95% dimethylsiloxane, Supelco, Inc.) and a flame-ionization detector. The GC oven was programmed to start at 80°C, increase in temperature at 10°C min<sup>-1</sup> to 220°C, at 20°C min<sup>-1</sup> to 300°C, and held at 300°C for 15 mins. The injector temperature was set to 275°C. The reproducibility of GC analyses was found to be ±5% by comparing peak area ratios for triplicate autosampler injections (Varian CP-8400) of each sample. Where possible, the reaction products were identified by co-injecting authentic samples in the gas chromatograph. The dodecane and decane internal standards were used to quantify concentrations by comparison to calibration curves that were generated by plotting the ratio of the peak area of the analyte to that of the internal standard vs. concentration of the analyte. The higher-concentration dodecane was chosen as a reference for DBK and the lower concentration decane was used as the reference for the lower concentration products. When authentic samples were not available to identify the products, high-resolution gas chromatography-mass spectrometry (GC-MS) in the High Resolution-MS Laboratory at Arizona State University was used to determine molecular ion masses and to deduce plausible structures by fragmentation pattern analysis.

Mass balance at the various reaction times was estimated based on the numbers of benzene rings in the products and in the reacted DBK. Products were identified that contained one, two, three and four benzene rings. The total number of benzene rings in the consumed DBK was compared to the total number of benzene rings in the products. Because many products were formed at very small yields, not all of them were included in the mass balance calculations. The products that were included in the mass balance calculations are those summarized in Table 1. To be included in Table 1, the minimum concentration needed to exceed reliably detectible concentrations at any of the reaction times, which were taken to be 0.003, 0.003, 0.002 or 0.002 mM in the 3 mL DCM extracts for products that contained one, two, three or four benzene rings, respectively. The cutoff concentrations vary because products with different numbers of benzene rings had differing response factors by gas chromatography. Experiments at each point in the time-series were run in duplicate, and comparison of peak areas in the gas chromatograms of the various products revealed  $\pm 10\%$  uncertainty based on triplicate analyses. There is additional uncertainty associated with conversion of peak areas into concentrations owing to the need to assume gas chromatogram response factors for some of the peaks. The response factors (RF) were measured relatively to a constant internal standard. The RF for structures with the same number of benzene rings were found to be similar. In addition, the RF for structures that contained two benzene rings were essentially twice as large as those that contained one benzene ring. As an example,  $RF(\text{toluene}) = 0.394$  and  $RF(\text{ethylbenzene}) = 0.448$ , compared to  $RF(\text{bibenzyl}) = 0.889$  and  $RF(1,3\text{-diphenylpropane}) = 0.934$ . The concentrations of the known products were determined using their individual response factors, and the concentrations of the

unknown two-benzene-ring products were determined using an RF value of 0.934. The concentrations of the three- and four-benzene-ring products were estimated by assuming that RF of the various structures are proportional to the number of benzene rings that they contain. Specifically, RF values of 1.401 and 1.868 were assumed for the three-benzene-ring and four-benzene-ring structures, which are 1.5 and 2.0 times larger, respectively, than the average RF value for the two-benzene-ring structures. Given these several sources of uncertainty, mass balance calculations were only attempted for DBK conversions greater than 5%, which correspond to reaction times of at least 168 h. Errors in the mass balance calculations based on benzene rings vary from  $\pm 10\%$  to  $\pm 15\%$  depending on the duration of the experiment. We took the average uncertainty to be  $\pm 12\%$ .

The hydrogen balance was estimated by comparing the total number of hydrogen atoms in the products to the total number of hydrogen atoms in the consumed DBK. The hydrogen inventory did not include the five hydrogens that are included in the benzene rings in the DBK or the products, in order to maximize any differences. Hydrogen balance calculations depend on the mass balance calculations described above, the errors are estimated to be  $\pm 15\%$ .

## 2.4. Results and discussion

### 2.4.1. Reaction pathways for hydrothermal transformation of DBK

The hydrothermal transformation of DBK was studied for reaction times of 0, 12, 24, 46, 70, 168, 290 and 528 h. The conversion of DBK was low (by design) for all reaction times, and reached only 14.5% conversion after 528 h. Even at these low conversions, the number of products observed by gas chromatography was large as demonstrated by the sample chromatogram shown in Fig. 3. All of the products that attained minimum concentrations, as defined in the Experimental section, are summarized in Table 1. To make characterization of the various products tractable, they were categorized based on the number of benzene rings they contain.

Most of the lower-retention-time products that contained one and two benzene rings could be identified using purchased standards. These include benzene (1A), toluene (1B), ethylbenzene (1C), bibenzyl (2B) and stilbene (2D). The alphanumerical assignments for the various compounds are based on the number of benzene rings they possess, 1, 2, 3 etc., and the order in which they elute under the GC conditions, A, B, C, etc. (Table 1). These assignments (Table 1) are also included in the major product structure summary shown in Fig. 4, which includes the alcohol 2F, alkene 2E and alkane 2C products expected for the reaction pathways that is shown in Fig. 1. The alkene 2E formed mainly (>90%) as the *trans*-stereoisomer. The identities 2F, 2E, and 2C were all confirmed by comparison to standards.

The majority of the higher-retention-time products could not be identified using purchased standards. High-resolution mass spectrometry was used to obtain molecular masses, and this information was used to determine the number of benzene rings in each structure. Products with GC retention times between 15 and 20 mins contain three benzene rings, and those with retention times between 21 and 25 mins contain four benzene rings (Fig. 3).

The mass spectrometry data show that, although there are a large number of products, many have similar masses and thus probably represent structural and/or stereoisomers. We have been able to assign likely, but tentative structures to many of the larger products on the basis of the fragmentation patterns observed in their mass spectra. An example is shown in Fig. 5 for the four-benzene-ring structure 4A. The stereochemistry with respect to the C=C double bonds in 4A cannot be determined using mass spectrometry, therefore the structure in Fig. 5 is chosen because we expect it to be one of the more stable isomers owing to the *trans*-configuration of the upper double bond. In cases where more than one isomer was detected (i.e., more than one peak with the same molecular ion), a single representative structure is included in Fig. 4. The various possible structural and stereoisomers for each molecular mass are not shown.

An estimate of the mass balance for the various reaction times can be obtained by comparing the number of moles of benzene rings in the consumed DBK to the number of moles of benzene rings in all of the products. As mentioned in the Experimental section, this was only attempted for DBK conversions of at least 5%, corresponding to reaction times of  $\geq 168$  h. The mass balance values for the 168-, 290-, and 528-h experiments are 88%, 96% and 116%, respectively (see Table 1). Although the average of these values is

almost exactly 100%, the mass balance values increase slightly but systematically with increasing reaction time, and beyond the experimental uncertainty. We have yet to establish the reason for the increasing trend in the mass balance determined in this way, but it may be a consequence of the requirement to estimate the gas chromatography response factors for the three- and four-benzene-ring products, and the fact that the product distribution is time-dependent. At later reaction times the three- and four-benzene-ring product concentrations tend to increase compared to many of the smaller products, with the exception of toluene (discussed below). An estimate of the hydrogen balance was also performed for the later reaction times, considering only the non-benzene ring hydrogens in products comparing to the ones in consumed DBK molecules. The hydrogen balance values for the 168-, 290-, and 528-h experiments are 89%, 93% and 119%, respectively (Table 1). The average is again near 100%, and there is again a slight trend of increasing hydrogen balance with increased reaction time that is outside of the estimated experimental uncertainty of  $\pm 15\%$ . As in the case of the benzene-ring mass balance, we suspect that the observed trend reflects uncertainties in determining the time-dependent concentrations of the three- and four-ring compounds.

Despite the variations in relative product concentrations with time, two major reaction pathways can be identified. One corresponds to the reversible functional-group interconversions shown in Fig. 1. The other is associated with C-C bond fragmentation reactions. The reversible reaction pathways are shown in the lower left corner of Fig. 6, and the primary bond-breaking reactions in the lower right corner. Additional reaction products from interaction of the products of C-C bond breaking with other reaction products abetted by C-H bond breaking are shown in the upper panel of Fig. 6. For the

purpose of discussing reaction mechanisms, the products are distributed among reaction pathways as shown in Fig. 6.

#### 2.4.1.1. Reduction pathway

Starting with DBK, the formation of alkane 2C involves reduction, and so we have called the part of the reaction path that links DBK with 2C in Fig. 6 the *reduction pathway* (even though formation of alkene 2E from alcohol 2F is neither an oxidation nor a reduction). Indeed, starting with DBK we observed formation of the alcohol 2F, alkene 2E and alkane 2C, with strongly time-dependent product distributions (see below). In addition to the products involved in the reduction pathway, many other products were formed as a result of bond cleavage reactions. The extent to which the DBK reactions follow the reduction pathway versus bond cleavage pathways can be estimated from the ratio of the sum of the concentrations of the reduction pathway products, i.e., alcohol 2F, alkene 2E and alkane 2C to the concentration of the consumed DBK. This ratio (expressed as a percentage) is given in Table 2 for two of the reaction times, and is found to be time-dependent (ca. 22% for the 24-h reaction and ca. 10% for the 70-h reaction). Nevertheless, all of the structures along the reduction pathway were observed at most reaction times, and, importantly, the alkane 2C was a major product at all reaction times.

We performed experiments that started with the alcohol 2F, which is one reduction step down the pathway from DBK. The alcohol is much more reactive than DBK and after 24 h essentially all of the alcohol had been consumed. The major product in this case was the alkane 2C, but the alkene 2E was also observed, and, importantly, so



was DBK (see Table 2). Other bond cleavage products were observed that contain one and two benzene rings, similar to those formed when starting with DBK. In addition, coupling products similar to those formed from DBK that contain three and four benzene rings were also found, although no attempts were made to characterize these in detail. The extent to which the alcohol reaction gave reduction pathway products was estimated in a similar manner to that for DBK described above, and was found to be ca. 21% for a 24-h reaction. The fact that this is very close to the extent of reduction for DBK in the same time frame is probably coincidental, since the product distributions differ, especially among the coupling products.

Experiments were performed starting with the alkane 2C. In this case the product distribution was quite complex, and again, many bond cleavage and coupling products with three and four benzene rings were observed but were not characterized. After 70 hours, the major products were toluene (1B) and ethylbenzene (1C). Products that had two benzene rings include bibenzyl and stilbene, as well as the alkene 2E, and DBK (Table 2). An extremely small amount of the alcohol 2F was found, consistent with the rapid reactivity of the alcohol under the experimental conditions. The extent to which the alkane reaction products partition along the reduction pathway in the opposite direction was estimated as described above, yielding ca. 6% for the 70-h experiment. These experiments support interpretation of the reduction pathway in terms of the reaction scheme of Fig. 1, and demonstrate conclusively that interconversion occurs among *all of the structures* in the reduction pathway, from DBK to alkane 2C.

#### 2.4.1.2. Bond cleavage pathways

Ketones are key functional groups in the reaction sequence shown in Fig. 1 since they represent the point at which C-C bond cleavage must occur in order to form carboxylic acids. Under the hydrothermal experimental conditions (300°C, 70 MPa), many products were observed that are associated with C-C bond cleavage. These include benzene (1A), toluene (1B), ethylbenzene (1C) and diphenylmethane (2A) (Table 1). Significantly, bibenzyl (2B) and trans-stilbene (2D) were also observed, in addition to other larger structures such as 3A-3F, 4A, and 4B. Note that most of the larger products require both C-C and C-H bond cleavage. The formation of the larger products is readily explained in terms of radical coupling reactions (see further below), which strongly suggests that C-C and C-H bond cleavage reactions occur mainly *via* homolysis to form radicals under the conditions of the experiment.

#### 2.4.2. Mechanisms of the reduction pathway

To form alkane 2C from DBK, the ketone must first undergo reduction to form alcohol 2F followed by dehydration to form alkene 2E followed by further reduction. The time dependencies of the concentrations of these four compounds, starting with DBK, are shown in Fig. 7, and can be seen to be consistent with this reaction pathway. The concentration of the alcohol 2F initially rises quickly, and then decreases to essentially zero by ca. 70 h. The alkene 2E concentration increases on a timescale that

corresponds to that for decomposition of the alcohol, and then decreases on a slower timescale after the alcohol has mostly reacted.

As shown in Fig. 7, the concentration of alkane 2C continuously increases to values greater than the maximum concentrations attained by either the alcohol or the alkene. The overall time-dependence of alkane formation corresponds roughly to that for DBK decomposition, implying that DBK reduction to form the alcohol is the rate-determining step for formation of the alkane. This is consistent with the observation that the alkene, and in particular the alcohol, do not build up substantial concentrations.

The fastest reaction in the pathway when starting with DBK appears to be dehydration of the alcohol 2F, since the alcohol reacts most rapidly to the lowest maximum concentration. This is consistent with the observation of rapid reaction when starting with alcohol 2F, and consistent with published work on alcohol dehydration under hydrothermal conditions (Xu et. al, 1997; Antal et. al, 1998; Akiya and Savage, 2001; Anikeev and Ermakova, 2003; Hunter and Savage, 2004). This previous work has led to a suggested mechanism for alcohol dehydration that involves acid catalysis, with the first step being protonation of the -OH to form  $-\text{OH}_2^+$ , which is a leaving group. The acid is formed in the self-dissociation of  $\text{H}_2\text{O}$  under the reaction conditions.  $\text{H}_2\text{O}$  elimination then follows either an E1 mechanism, where the  $-\text{OH}_2^+$  leaves as  $\text{H}_2\text{O}$  to give a carbon-centered cation that then loses a proton, or an E2 mechanism where the  $\text{H}_2\text{O}$  ( $-\text{OH}_2^+$ ) leaves and the proton is lost to  $\text{H}_2\text{O}$  simultaneously. Whether the E1 or the E2 mechanism is followed for a particular alcohol seems to depend upon the structure of the alcohol and the reaction conditions, in particular temperature (Akiya and Savage, 2001). By microscopic reversibility, alcohol hydration presumably follows the same

mechanism(s) in reverse. Both reduction reactions (i.e., DBK to alcohol, and alkene to alkane) are slower than the alcohol dehydration. If DBK reduction is rate-determining for formation of the alkane, as suggested by the kinetic data, then reduction of the alkene is faster than reduction of the DBK. Compared to alcohol dehydration (and the corresponding alkene hydration), the detailed mechanisms of reduction of double bonds under hydrothermal conditions have not been extensively studied and potential mechanisms are thus discussed in more detail here.

It is important to remember that the experimental systems are sealed, which means the hydrogen atoms required for the reduction reactions must come from either the reactants themselves or from H<sub>2</sub>O. As indicated above, although there are uncertainties in our estimate of the detailed hydrogen balance for these reactions, evidently the majority of the hydrogen atoms required for the reduction reactions come from the other organic structures, and ultimately from DBK itself. An accurate description of the kinetics of the reduction reactions is difficult, since the concentrations of the reducing species presumably vary with time. However, the rate of reaction of the reducing species with the double bonds must at least contribute to the overall reaction rate to account for the observed difference in the reactivities of C=O and C=C bonds, C=O being reduced more slowly than C=C. If the reduction of the C=O and C=C bonds occurs via the same mechanism, then the different observed reactivities can be used to give insight into the reduction mechanism.

The standard mechanisms of hydrogenation reactions in solution involve either sequential addition of hydride (H<sup>-</sup> or equivalent) followed by addition of a proton (H<sup>+</sup>), or sequential addition of two hydrogen atoms (or equivalent; Smith and March, 2007).

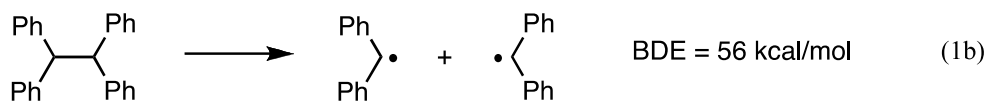
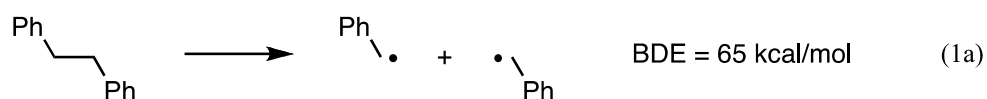
The hydride/proton mechanism for reduction of either DBK or alkene 2E seems unlikely under the experimental conditions for two reasons. First, there is no reasonable source of hydride (or equivalent) in aqueous solution, since under the reaction conditions hydride should react very rapidly with H<sub>2</sub>O. Second, hydride and its equivalents are nucleophilic, and if the rate of reduction were determined by the rate of addition of hydride to the C=C and C=O bonds, the more electrophilic C=O bond would be expected to react faster than the C=C bond, but the opposite is observed. From these observations we conclude that the mechanism of reduction of C=C and C=O under the experimental conditions is unlikely to involve the rate-determining addition of hydride or equivalent.

Although there is no obvious source of hydride ions, there is an obvious source of hydrogen atoms, i.e., from homolytic C-H bond cleavage. Indeed, many of the coupling products are best understood as being derived from radicals formed via bond homolysis reactions. If the reduction mechanism involves rate-determining addition of a hydrogen atom (or equivalent) to the C=C and C=O bonds, then the stronger C=O bond would be expected to react more slowly than the weaker C=C bond, as observed.

If reduction occurs via sequential addition of hydrogen atoms, it is worth asking whether such a reduction reaction is reasonable from a kinetic perspective. A minimal mechanism for the reduction reaction of DBK to form the alcohol 2F, which contains the essential features of the DBK reactivity under our reaction conditions, is shown in Fig. 8. The reactive hydrogen atoms can be generated as a result of C-H bond homolysis in the benzylic position of DBK as shown in step (1) of Fig. 8. The literature value for this bond dissociation enthalpy (BDE) has been reported to be 83 kcal mol<sup>-1</sup> (Bordwell and Harrelson, 1990). Two such dissociations are required to reduce one molecule of DBK to

alcohol 2F. Although the bond dissociation enthalpies discussed here are for 298 K, their values are very weakly temperature dependent. Specifically, Blanksby and Ellison (2003) point out that for many organic structures, bond dissociation enthalpies at 298 K are almost numerically equivalent to the corresponding bond dissociation enthalpies at 0 K. Therefore, we assume that the enthalpies estimated here are valid at 300°C within the range of uncertainty.

Reduction of DBK also involves dissociation of the  $\pi$ -bond component of the C=O double bond.  $\pi$ -Bond enthalpies are difficult to measure, however, a recent *ab initio* calculation (Chen et al., 2011) provides a value of 76 kcal mol<sup>-1</sup> for C=O bonds, which we assume to be valid for DBK. The literature BDEs for the two bonds to hydrogen that are made: the O-H bond of step (2) and the C-H bond adjacent to oxygen of step (3), are 104 and 94 kcal mol<sup>-1</sup>, respectively (Luo, 2007). The homolytic C-H bond dissociation step (1) generates two benzylic radicals, and enthalpy is gained when they recombine in step (4). The BDE for the C-C bond that is formed in this case is not known, but can safely be assumed to lie between those for 1,2-diphenylethane (Reaction 1a) and 1,1,2,2-tetraphenylethane (Reaction 1b),

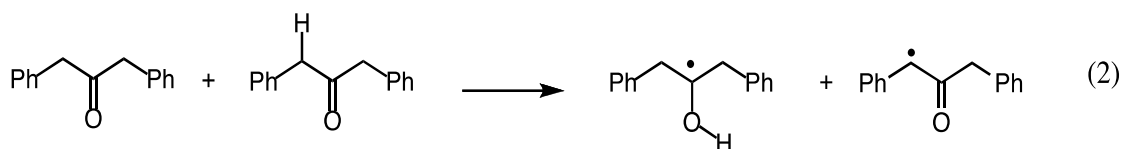


*i.e.* greater than 56 kcal mol<sup>-1</sup> and less than 65 kcal mol<sup>-1</sup> (Pedley et al., 1986; Luo, 2007).

The overall reaction thus converts 3 molecules of DBK into alcohol 2F and the structure

formed in step (4), which is reminiscent of many of the products of the coupling and the dimeric pathway for DBK. Based on the literature BDEs we determine that the reaction mechanism outlined in Fig. 8 is enthalpically favorable by between 14 and 21 kcal mol<sup>-1</sup>. This mechanism is oversimplified; for example there are several different possible structures that can liberate hydrogen from a benzylic position, and indeed there are several reduction reactions involving DBK, its derivatives, and many different coupling products. The contribution of entropy and any medium effects on the BDEs are also ignored. However, the reaction is sufficiently exothermic, and presumably exergonic, that the reaction mechanism is at least plausible.

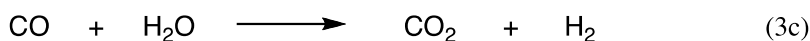
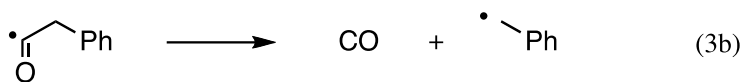
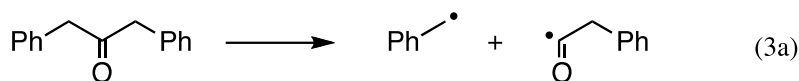
The rate-determining step in the mechanism of Fig. 8 is C-H bond dissociation, which has an enthalpic barrier of 83 kcal mol<sup>-1</sup>. An alternate mechanism for reduction via hydrogen atom transfer involves direct transfer to the oxygen atom of the C=O group of DBK from the benzylic position of another DBK, or another structure with benzylic hydrogens, without the intermediacy of a free hydrogen atom, as illustrated in Reaction 2:



The advantage of the hypothetical hydrogen atom transfer process of Reaction 2 is that the kinetic enthalpic requirements are significantly reduced compared to the mechanism of Fig. 8, since the enthalpy costs of breaking the C-H and the C=O  $\pi$ -bonds (83 and 76 kcal mol<sup>-1</sup>, respectively) are offset by the simultaneous gain in enthalpy associated with formation the O-H bond (104 kcal mol<sup>-1</sup>), for a total enthalpy barrier of 55 kcal mol<sup>-1</sup>. Although the hydrogen atom transfer mechanism is more favorable kinetically, and

hydrogen atom transfer in various kinds of chemical systems has previously been reported in the literature, the specific process shown in Reaction 2 has not been described, and there may still be a substantial kinetic barrier to the reaction above the 55 kcal mol<sup>-1</sup> required by the bond dissociation enthalpies (Mayer, 2010). We cannot support or rule out either mechanism based on the product distributions alone.

Another possible source of hydrogen atoms is associated with the water/gas shift reaction, as illustrated in Reactions 3a-3c:



As discussed further below, dibenzylketone can undergo homolytic C-C bond dissociation to form a benzyl radical and a phenacetyl radical (Reaction 3a). The phenacetyl radical may then undergo rapid decarbonylation (Reaction 3b) to form carbon monoxide and a second benzyl radical (Gould et al., 1987). Under the experimental conditions, carbon monoxide should react with H<sub>2</sub>O to form carbon dioxide and hydrogen (Reaction 3c; Seewald et al., 2006). If the molecular hydrogen formed this way is the source of hydrogen atoms for the reduction reactions through a mechanism that is similar to that of Fig. 8, the rate-determining step will then be homolytic bond cleavage of molecular hydrogen to form two hydrogen atoms. The H-H BDE is 104 kcal mol<sup>-1</sup> (Blanksby and Ellison, 2003), *i.e.* significantly larger than the benzylic C-H bond dissociation enthalpy (83 kcal mol<sup>-1</sup>). For this reason, molecular hydrogen may be a less



important source of reducing hydrogen atoms than the organic structures with benzylic hydrogen atoms. The hydrogen balance calculations described above that gave values around 100% excluded the hydrogen atoms formed in the water gas shift reaction, therefore this process is not necessarily a contributor to the reduction process.

A final mechanistic possibility that needs to be considered is that the bond cleavage reactions are catalyzed by the surface of the gold reaction capsule. As an example, adsorption of the organic structures to the gold surface might weaken covalent bonds and facilitate hydrogen atom transfer in a manner similar to conventional metal-catalyzed hydrogenation reactions (Rylander, 1967). Gold is generally considered to be minimally catalytic in hydrothermal reactions; nevertheless, in their work on decarboxylation of acetic acid, Bell et al. (1994) were unable to completely rule out gold catalysis. Such catalysis cannot be completely ruled out in the present experiments either, although we have independent evidence for freely diffusing carbon-centered radicals that formed as a result of bond homolysis (see below).

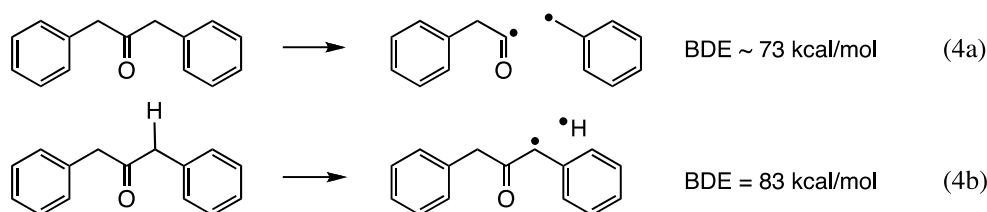
To summarize, the experiments demonstrate reversible interconversion reactions of functional groups all the way from ketone to alkane that are able to compete with other reactions of the various functional groups. The time sequence experiments provide direct evidence for the reaction sequence. The most plausible mechanism involves sequential addition of hydrogen atoms, although the mechanism for reduction cannot be confirmed solely on the basis of the product studies described here.

### 2.4.3. Mechanisms of C-C and C-H bond cleavage pathways

One of the goals of the project was to determine the extent to which C-C bond cleavage could compete with the reduction and functional-group-interconversion pathways. Dibenzylketone was anticipated to be useful in this regard because cleavage of the C-C bond adjacent to the C=O group is facilitated by formation of a resonance-stabilized benzylic intermediate (Fig. 2). As mentioned above, the preponderance of coupling products points to the formation of radicals via homolytic bond fragmentation, *i.e.* the critical intermediate in Fig. 2 appears to be a resonance-stabilized benzyl radical. One of the major products at all reaction times is toluene, indicating that C-C bond cleavage is indeed a major reaction pathway. The toluene concentration grows steadily throughout the duration of the experiment and corresponds closely to the decrease in concentration of the DBK as shown in Fig. 9.

The C-C bond cleavage products can be understood according to the processes indicated in Reactions 3a and 3b. Exactly the same mechanistic steps occur in the photochemically induced decompositions of DBK (Robbins and Eastman, 1970; Gould et al., 1987): initial fragmentation of the benzylic C-C bond to form a benzyl radical and a phenacetyl radical, Reaction 3a, followed by decarbonylation to form a second benzyl radical and carbon monoxide, Reaction 3b. That the thermal and photochemical reactions proceed via the same mechanism is understandable since the active excited state in DBK photochemistry is the triplet state, and both the triplet and ground states correlate with a radical pair upon bond stretching (whereas the excited singlet state correlates with an ion pair; Turro, 1991).

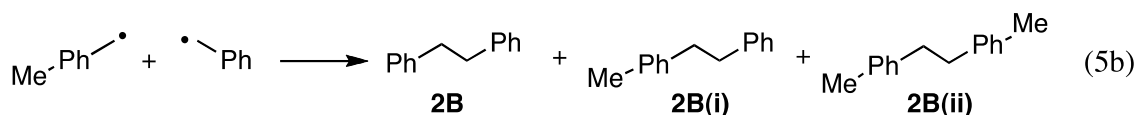
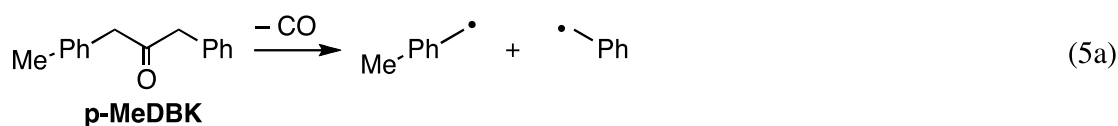
The homolytic bond dissociation enthalpy for the benzylic C-C bond in DBK is reported to be 65 kcal mol<sup>-1</sup> in a review by McMillen and Golden (1982), although several other measurements of benzylic carbon-carbonyl carbon BDEs put this number closer to 73 kcal mol<sup>-1</sup> (Luo, 2007). The C-C BDE is thus smaller than the C-H BDE, as shown in Reaction 4,



nevertheless, products associated with both of these bond fragmentations are observed. Indeed, essentially all of the bond fragmentation products require *both* C-C and C-H bond cleavage, the only exception is bibenzyl 2B. The BDE for cleavage of the C-C bond to the benzene ring in DBK has not been reported, however, this is almost certainly much larger than those in Reactions 4a and 4b. The larger BDE in this case presumably accounts for the fact that the products requiring this bond cleavage, benzene (1A) and diphenylmethane (2A), form in significantly lower yields than those that require cleavage at the benzylic carbon, such as toluene (see Table 1).

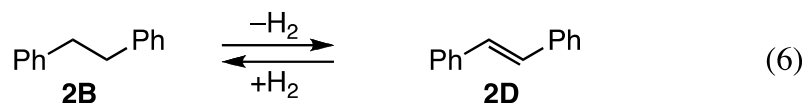
Strong evidence in favor of the formation of freely diffusing carbon-centered radicals that are formed *via* homolytic C-C bond cleavage at the benzylic carbon is provided by an experiment that starts with an asymmetrical analog of DBK, *p*-methyldibenzylketone (*p*-MeDBK). In this case, two different kinds of benzyl radicals are generated, a simple unsubstituted benzyl radical and one with a *p*-methyl substituent.

It is known that photolysis of *p*-MeDBK results in formation of freely diffusing benzyl radicals that form three different bibenzyl products (Turro and Weed, 1983). To check for freely diffusing benzyl radicals under the conditions of our experiments, we reacted *p*-MeDBK under the same hydrothermal conditions as DBK. Although an even larger number of products are formed compared to DBK itself, as a consequence of the additional methyl group in many of the products, we focused our attention on the three possible bibenzyl products 2B, 2B(i) and 2B(ii), formed according to:



All three bibenzyls were observed after 70 h, and the product distribution was 0.42:1.14:0.50 mmolal for 2B:2B(i):2B(ii). The formation of significant concentrations of the cross-coupling products 2B and 2B(ii) in this experiment provides strong support for the formation of benzyl radicals that diffuse freely in solution, and couple to form bibenzyls. Indeed, the product distribution is close to the expected 1:2:1 ratio expected for completely random radical coupling. The deviation from the pure statistical ratio is presumably a consequence of the fact that the benzyl radicals are involved in other reactions in addition to the formation of bibenzyls.

As mentioned above, bibenzyl (2B) is the only product of DBK decomposition that requires C-C bond homolysis solely. Loss of two hydrogen atoms from bibenzyl forms stilbene (2D) as shown in Reaction 6,



which is observed as a product, predominantly as the *trans*-stereoisomer under the conditions of the experiments. The hydrogens are lost from bibenzyl presumably in the course of reduction of DBK or alkene 2E or stilbene 2D, according to the mechanisms discussed above. As shown in Fig. 10, the concentration of *trans*-stilbene 2D is larger than that of bibenzyl at earlier reaction times, although this situation reverses at later times. One explanation for this behavior is that at earlier times, bibenzyl provides the hydrogen atoms required for the various reduction reactions, and at later times, larger structures such as 3C and 4B start to accumulate that have liberated hydrogen atoms that can push the reversible reaction (Reaction 6) back towards bibenzyl. The significance of this is that the reversible reactivity observed in the DBK system, specifically the bibenzyl/*trans*-stilbene interconversion (Reaction 6), appears to adjust rapidly to changing local conditions, which is one of the reasons for the time-dependent product distributions.

A plausible first step for formation of the three- and four-benzene-ring coupling products is shown in step 4 of Fig. 8. Further C-C and C-H bond breaking, combined with reduction pathway reactions of the kind that DBK itself undergoes, can explain the formation of the three- and four-ring structures illustrated in Fig. 4. The time

dependencies of the concentrations of representative three- and four-ring structures are given in Figs. 11 and 12, and the dehydrogenated coupling products exhibit steady increases in concentration. These are presumably favored thermodynamically since by losing hydrogen atoms they become increasingly conjugated. The bulk of these hydrogens are consumed in the formation of toluene, which is another major product of the reaction at later times as shown in Fig. 9. As shown in Fig. 11, the major coupling product that accumulates at later times is the three-ring structure 3C<sup>III</sup>, which is relatively stable since it is highly conjugated.

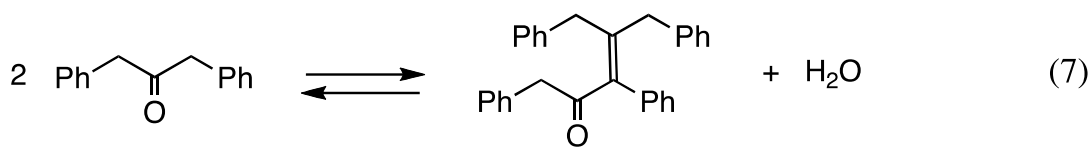
#### *2.4.4. Ionic reaction pathways*

The cross-coupling experiment provides strong support for carbon-carbon bond cleavage via homolysis to form radicals, and the product distribution is also consistent with this proposal. It is important to note that although homolytic C-C bond cleavage is favored for DBK because of resonance stabilization of the intermediate benzyl radicals, heterolytic cleavage to form a benzyl anion or cation would also be favored for the same reason, i.e. resonance stabilization. Thus, although DBK was chosen specifically to enhance the C-C bond cleavage pathway, it is not pre-determined to undergo homolytic cleavage, although this does appear to be at least the dominant mechanism for bond fragmentation under the present conditions. However, reactions that proceed via ionic mechanisms almost certainly also occur in the DBK system. Specifically, the hydrothermal dehydration of alcohols to form alkenes was previously shown to proceed via an ionic mechanism (Xu et. al, 1997; Antal et. al, 1998; Akiya and Savage, 2001;

Anikeev and Ermakova, 2003; Hunter and Savage, 2004), and we have no reason to believe that the same mechanism does not apply under our experimental conditions. Of course, the principle of microscopic reversibility dictates that the reverse formation of alcohol from alkene is also ionic.

An ionic mechanism for another process is also suggested by experiments on DBK performed in deuterated water, where we observe very rapid exchange of hydrogen and deuterium. Hydrothermal reaction of DBK at 300°C and 70 MPa for 24 h resulted in a shift of the molecular ion peak for DBK from m/z 210 to m/z 214, which reflects hydrogen-deuterium exchange at all four benzylic positions. The mechanism of this H/D exchange almost certainly involves reversible formation of an enol via an acid catalyzed ionic mechanism (Smith and March, 2007).

This observation suggests that reactions of enols should at least be considered. A possible reaction is formation of the aldol condensation product via nucleophilic addition of the enol of DBK to a second DBK molecule, followed by dehydration (Smith and March, 2007), as illustrated by



However, no evidence for an aldol product was obtained. Aldol formation is known to be reversible, suggesting that the equilibrium lies on the side of DBK under the conditions of the experiment. Although an aldol product was not observed, the rapid dehydration of 1,3-diphenyl-2-propanol and hydrogen-deuterium exchange of DBK suggest ionic reaction pathways co-existed with radical reaction pathways in these experiments.

#### 2.4.5. Carboxylic acids

As mentioned above, ketones are the functional group in which C-C bond cleavage must occur in order to form carboxylic acids in the reaction scheme illustrated in Fig. 1. Results from this study show that C-C bond cleavage is a dominant pathway for the hydrothermal reactions of DBK. However, *carboxylic acids were not found* in our DBK experiments, at least at our GC detection limits of ~0.05 millimolal. Other less oxidized products, such as benzaldehyde and benzyl alcohols, were also not observed. Evidently, bond cleavage fails to form the oxygenated carboxylic acids in appreciable amounts under the conditions of our experiments. A possible explanation is that because the system is sealed, the primary products of C-C bond homolysis tend to accept the hydrogen atoms that are generated in parallel reactions. Alternatively, the results might suggest that to form oxygenated products such as aldehydes or carboxylic acids, a heterolytic bond cleavage pathway may be required to form a primary cation intermediate that could then react with H<sub>2</sub>O. Additional experiments in which the oxidation state is externally buffered may help to elucidate these mechanistic details.

### 2.5. Conclusions

There are several major conclusions of this study of hydrothermal reactions of the model ketone DBK:

(1) Time sequence experiments provide direct evidence for the functional group interconversion reaction sequence of Fig 1 within a single system, supporting the use of



this scheme for interpreting the products of organic hydrothermal reactions. For the reaction sequence ketone to alcohol to alkene to alkane, alcohol dehydration seems to be the fastest reaction, followed by alkene reduction, with ketone reduction being slowest of all.

(2) Reversible interconversion over the entire range of functional groups from alkane to ketone is observed, with the dominant reaction directions responding quite rapidly to changes in the product distribution and thus reaction environment.

(3) Functional group interconversion occurs together with homolytic bond cleavage reactions that result in freely diffusing radicals in the case of C-C bond fragmentation. Bond cleavage predominates at longer reaction times, with the products tending toward formation of dehydrogenated coupling products and the hydrogen atoms being consumed in formation of toluene.

(4) Ionic reactions are much less important than radical reactions at the conditions of these hydrothermal experiments (300°C, 70 MPa).

(5) Although C-C bond cleavage is the dominant reaction, no carboxylic acids are formed under these experimental conditions. Carboxylic acid formation evidently requires the introduction of additional oxidizing agents, or hydrogen loss, either of which may prevail in natural systems.

Additional implications for natural systems require extrapolation from the experimental results to conditions that prevail in sedimentary basins and hydrothermal systems, many of which operate at lower temperatures and pressures than used in this experimental study, and include mineral reactions that have the potential to alter reaction pathways. Nevertheless, based on our experimental results for DBK, we can make

general observations of relevance to geochemical processes. Reversibility of reactions among ketones, alcohols, alkenes and alkanes provides strong support for the concept that metastable equilibria are regularly and commonly attained among aqueous organic compounds. As a consequence, these results support the validity of assumptions underlying thermodynamic representations of diverse organic geochemical processes (Amend and Shock, 1998; Shock and Schulte, 1998; Amend and Shock, 1998; Shock, 2000; Schulte and Shock, 2004; Shock and Canovas, 2010). However, the inability of the current experimental efforts to produce carboxylic acids raises questions about the irreversible reactions involved in natural organic transformation processes. The conversion of ketones to carboxylic acids may be a rate-limiting step in the overall conversion of alkanes, which would be a variation on the scheme proposed by Seewald (2001; 2003).

**Table 1.** Concentrations (mmolal) of various products for DBK in H<sub>2</sub>O at 300 °C and 70 MPa, their mass-to-charge values, the mass and hydrogen balances, and percent conversion of DBK, at the various reaction times.<sup>a,b</sup>

RT <sup>c</sup>	Product	m/z	0 h	12 h	24 h	46 h	70 h	168 h	290 h	528 h
1.98	1A	78	1.16	1.10	1.52	1.88	2.74	2.88	2.88	2.90
2.26	1B	92	0.46	2.38	4.52	8.66	16.65	36.32	62.45	146.2
2.75	1C	106	na	na	na	na	0.16	0.54	1.44	3.62
9.17	2A	168	na	na	na	na	0.14	0.36	0.40	1.22
10.25	2B	182	na	0.12	0.30	0.68	1.24	2.68	3.18	5.16
11.79	2C	196	na	0.40	1.02	1.40	2.20	6.58	8.40	10.65
12.42	2D	180	0.28	1.16	1.44	1.82	2.06	0.92	0.42	0.42
12.65	2E	194	0.48	2.42	2.24	1.66	1.66	1.28	0.72	0.62
13.25	DBK	210	988.9	984.3	981.9	968.5	958.9	931.5	899.1	850.8
13.58	2F	212	1.70	0.24	0.08	0.06	na	na	na	na
13.74	-	-	2.26	0.74	0.90	0.64	0.32	0.20	0.18	0.48
13.97	-	-	na	na	na	na	na	na	0.26	0.48
14.16	-	-	na	na	na	na	na	0.40	0.78	1.86
17.44	3A	284	na	0.06	0.09	0.17	0.18	0.26	0.38	0.57
17.56	3A'	284	na	0.09	0.12	0.17	0.17	0.23	0.54	0.87
17.92	-	-	na	na	na	na	na	na	na	0.30
18.02	3B	282	na	0.05	0.08	0.17	0.24	0.32	0.47	0.68
18.15	3C	310	na	0.03	0.05	0.12	0.18	0.54	1.43	3.67
18.27	3D	298	0.08	0.11	0.26	0.45	0.63	1.04	1.47	3.07
18.75	3E	300	na	na	0.11	0.15	0.20	0.36	0.41	0.62
18.81	3C'	310	na	na	na	na	na	0.57	2.15	3.85
19.02	3C''	310	na	na	na	na	na	0.36	1.61	4.44
19.33	3F	312	na	na	na	na	0.08	0.32	1.07	2.26
19.77	3C'''	310	na	0.23	0.53	1.47	2.84	6.45	14.64	23.24
19.90	-	-	na	na	0.12	0.20	0.26	0.36	0.47	0.71
21.68	4A	400	0.35	0.71	1.14	1.97	2.47	3.61	3.99	5.55

22.64	4A'	400	na	na	na	na	na	na	0.32	0.60
23.41	4B	384	na	na	na	na	na	0.18	0.33	0.50
23.92	4A''	400	0.08	0.26	0.44	0.69	0.84	0.92	1.02	1.14
24.50	4A'''	400	na	0.20	0.30	0.51	0.66	0.71	0.84	0.95
Mass Balance (%) <sup>d</sup>								88	96	116
Hydrogen Balance (%) <sup>d</sup>								89	93	119
Conversion (%) <sup>e</sup>			0.7	1.1	1.4	2.7	3.7	6.4	9.7	14.5

<sup>a</sup> The products that are included in this table were those detected above minimum concentrations in DCM, as defined in the Experimental section. Products that are given a number (see Fig 4) and m/z value are those that were either identified using purchased standards, or whose mass was measured and a likely structure determined. A product that is a structural or stereoisomer of another product with an earlier retention time is identified using the ' symbol; additional structural and stereoisomers are identified using '' and '''.

<sup>b</sup> na means that the amount formed is too small to be accurately determined at that particular reaction time.

<sup>c</sup> The retention time (in minutes) on GC chromatograms.

<sup>d</sup> Mass and hydrogen balances are estimated as described in the text, and only for DBK conversion greater than 5%. The estimated errors are  $\pm 12\%$  and  $\pm 15\%$  for the mass and hydrogen balances, respectively.

<sup>e</sup> Percent conversion of DBK.

**Table 2.** Concentrations (mmolal) of products from hydrothermal reactions starting with DBK, alcohol (2F) or alkane (2C) in H<sub>2</sub>O at 300 °C and 70 MPa, starting concentrations, conversions, and percent reduction pathway products for two reaction times.<sup>a,b</sup>

<b>Product</b>	<b>DBK (24 h)</b>	<b>Alcohol (2F) (24 h)</b>	<b>DBK (70 h)</b>	<b>Alkane (2C) (70 h)</b>
1B	4.52	104.3	16.65	351.5
1C	Na	23.61	0.16	56.23
2B	0.30	18.21	1.24	2.82
2C	1.02	188.3	2.20	724.2
2D	1.44	3.40	2.06	1.84
2E	2.24	1.66	1.66	9.28
DBK	981.9	21.41	958.9	7.00
2F	0.08	na	na	0.34
Starting Conc. <sup>c</sup>	996.5	980.5	996.3	1024.5
% Conversion <sup>d</sup>	1.4	>99	3.7	29
% Reduction <sup>e</sup>	~22	~21	~10	~6

<sup>a</sup> All concentrations are in mmolal. Only the concentrations of the major products containing one and two benzene rings are given, see text. See Fig 4 for the assignment of the structure numbers.

<sup>b</sup> na means that the amount formed is too small to be accurately determined at that particular reaction time.

<sup>c</sup> Concentrations of the starting compound, DBK, alcohol 2F, and alkane 2C.

<sup>d</sup> Percent conversion of the starting compound, DBK, alcohol 2F, and alkane 2C.

<sup>e</sup> Estimated as the percentage of the sum of the concentrations of the structures that contribute to the reduction pathway relative to the concentration of the reacted starting material. When starting with DBK, these structures are the alcohol 2F, the alkene 2E and the alkane 2C. When starting with alcohol 2F, the structures are the alkene 2E, the

alkane 2C and DBK. When starting with the alkane 2C, the structures are the alkene 2E,  
the alcohol 2F and DBK.

**Fig. 1.** Schematic illustration of the proposed oxidation and reduction (horizontal), and hydration/dehydration (vertical) pathways that interconvert hydrocarbon and carboxylic acid functionalities at hydrothermal conditions (Seewald, 2003). Note the central position of ketones. Most reactions are thought to be reversible, and that irreversible C-C bond breaking in ketones leads to carboxylic acids.

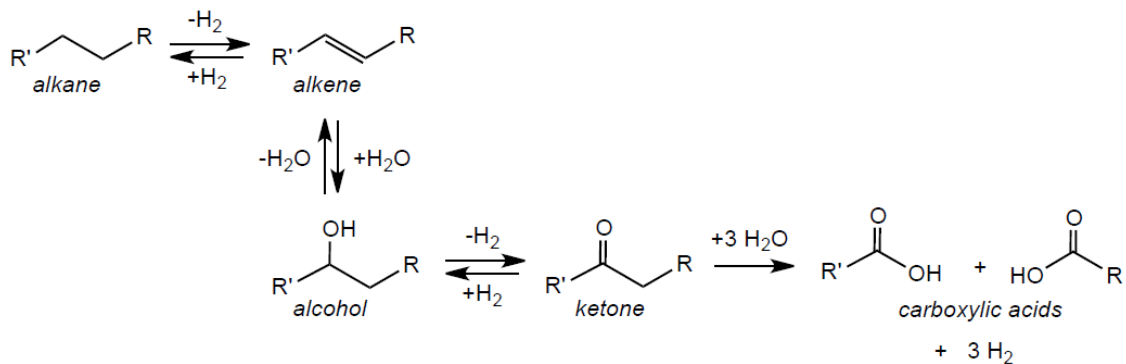


**Fig. 2.** Dibenzylketone (DBK) and a schematic C-C bond fragmentation reaction to form two transient species, where the \* represents an ion or radical site. The transient in the box is benzylic and will be resonance stabilized, which should facilitate bond fragmentation via homolysis or heterolysis.

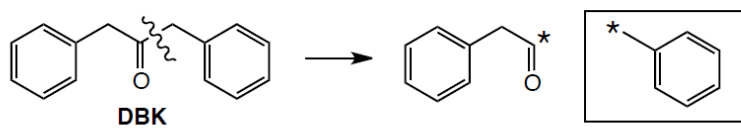




**Fig. 3.** Gas chromatograms showing the products of hydrothermal transformation of DBK in water at 300 °C and 70 MPa, after 290 h reaction time (the ordinate corresponds to relative intensity). The upper chromatogram shows the one- and two-benzene-ring structures at earlier retention times, the lower chromatogram shows the three- and four-benzene-ring structures at later retention times. DCM refers to the dichloromethane solvent and the peaks labeled S1 and S2 correspond to decane and dodecane, respectively, which are used as relative internal standards for quantification of peak areas. The structures of the labeled peaks are given in Fig 4.

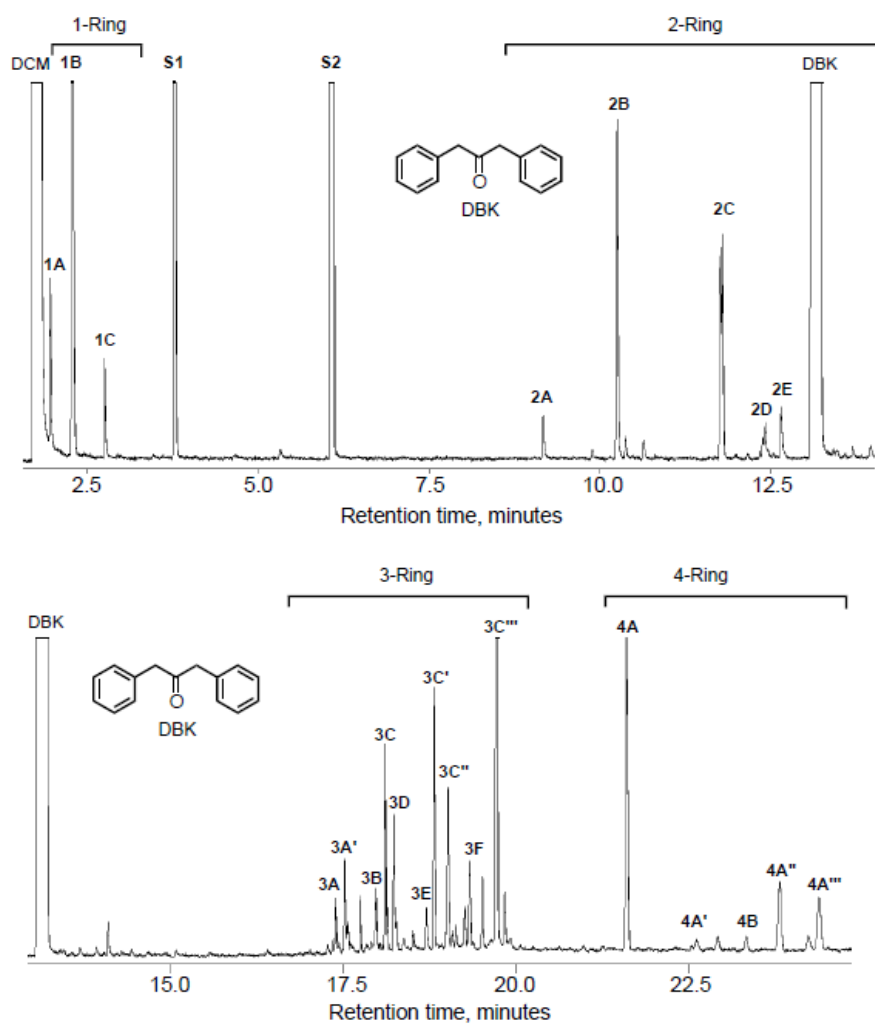


**Fig. 4.** Structures of major product types observed for hydrothermal transformation of DBK in H<sub>2</sub>O at 300 °C and 70 MPa. Structures are categorized by the number of benzene rings they contain. Several of the structures have structural and/or stereoisomers with the same molecular mass; where multiple isomers are observed, they are also identified in Fig. 3 and in Table 1 using the ' symbol.

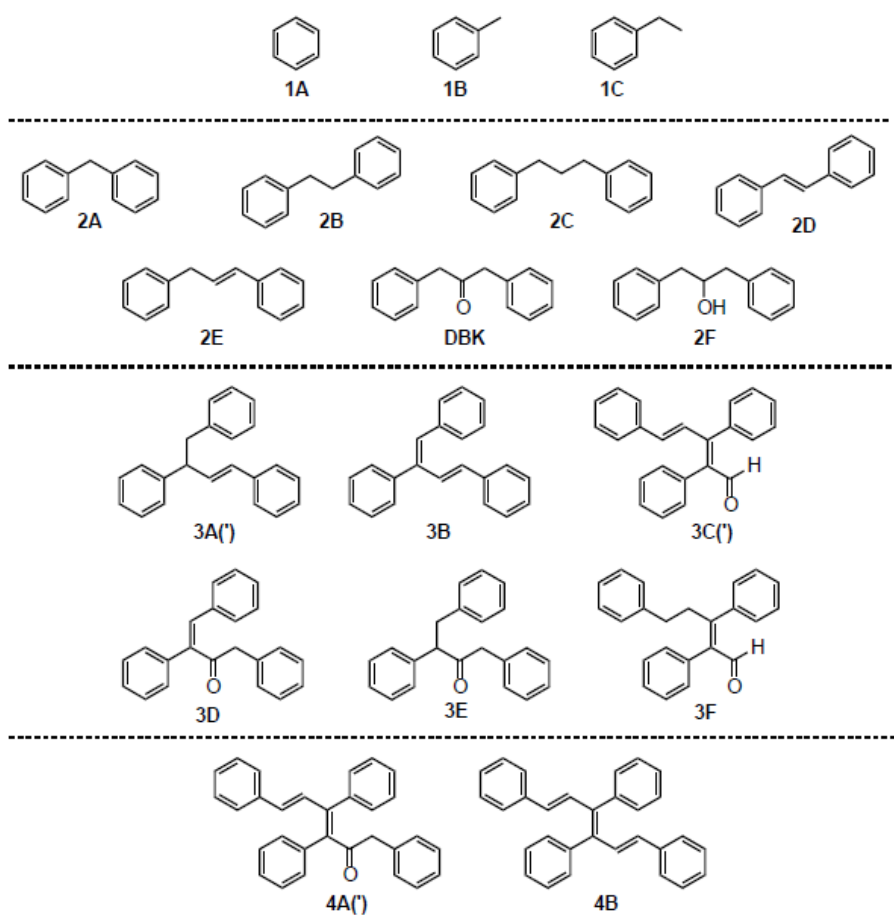


**Fig. 5.** Mass spectrum and assigned fragments for the four-benzene-ring structure 4A. Other products have the same molecular ion peak at 400 m/z, and presumably represent stereoisomers associated with the carbon-carbon double bonds. The stereochemistry of the structure assigned as 4A, or the other structures that have the same molecular ion peak, are not actually known.

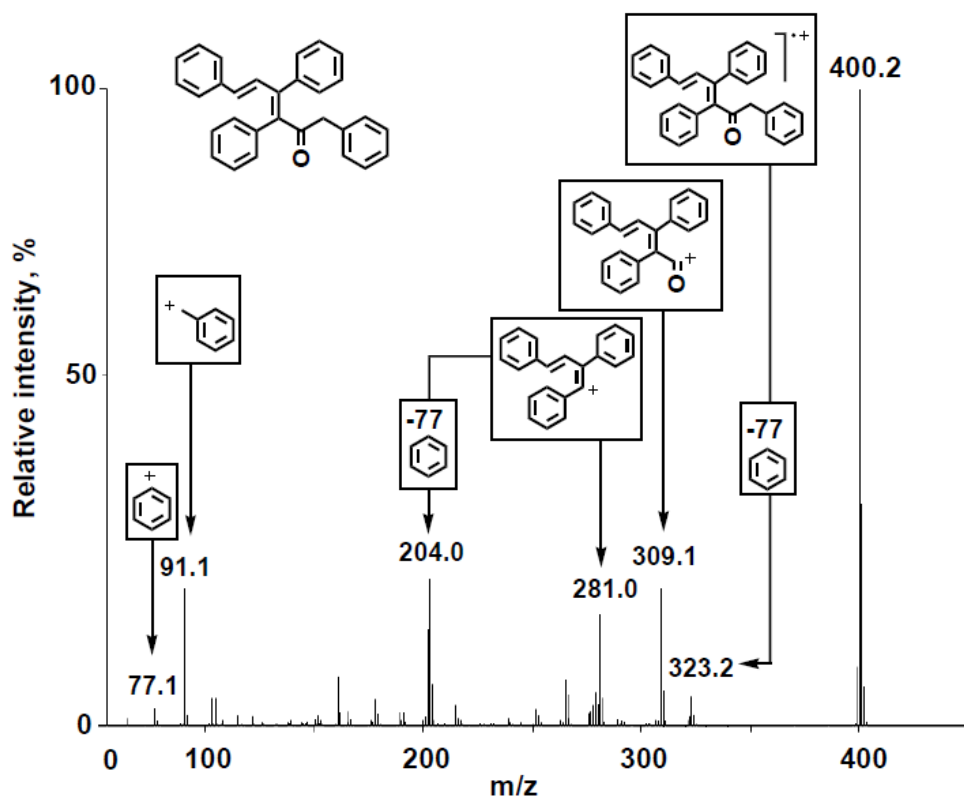


**Fig. 6.** Schematic representation of the main reaction pathways for hydrothermal transformations of DBK. The reduction pathway (lower left) results ultimately in formation of the alkane 2C. The two bond homolysis pathways are necessarily interrelated; only bibenzyl, 2B, requires no C-H bond homolysis, all other products require some combination of C-C and C-H bond fragmentation.

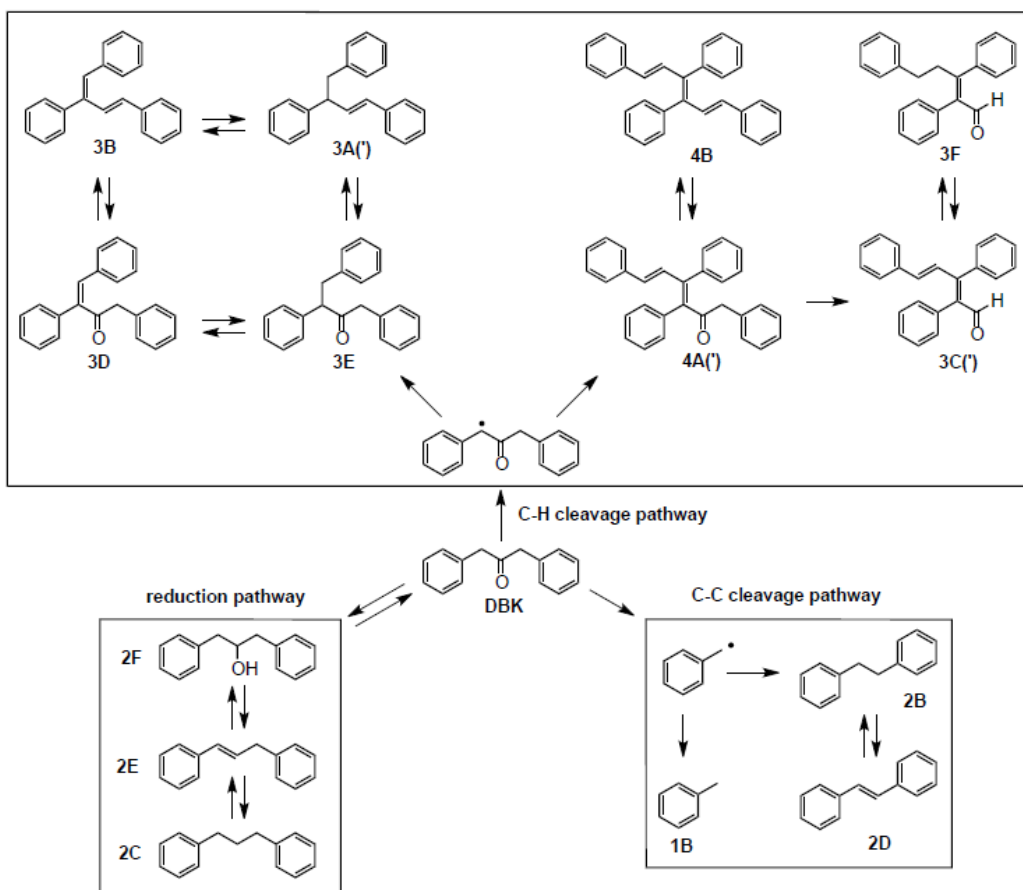


**Fig. 7.** Time dependencies of the concentrations of DBK (filled circles) and the products of the reduction pathway, alcohol 2F (triangles), alkene 2E (diamonds) and alkane 2C (open circles), that are formed in the hydrothermal reactions of DBK in H<sub>2</sub>O at 300 °C and 70 MPa. The lower panel expands the early time behavior outlined in the box at the lower left of the upper panel.

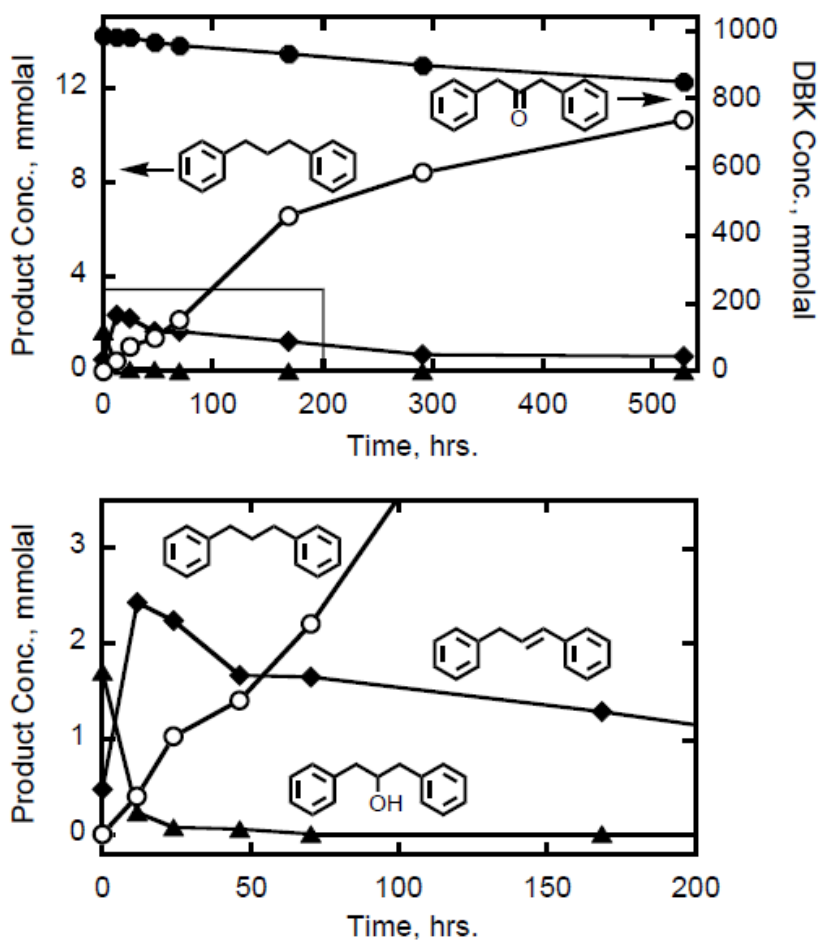


**Fig. 8.** Proposed minimal mechanism for reduction of DBK to alcohol 2F via hydrogen atom addition to the C=O double bond. The literature bond dissociation enthalpies in bold are for bonds that are broken, and those in italics are for bonds that are formed. The bond dissociation enthalpy for the C-C bond formed in Reaction (4) can only be estimated (see text). This reaction scheme is exothermic by between 14 and 21 kcal mol<sup>-1</sup>.

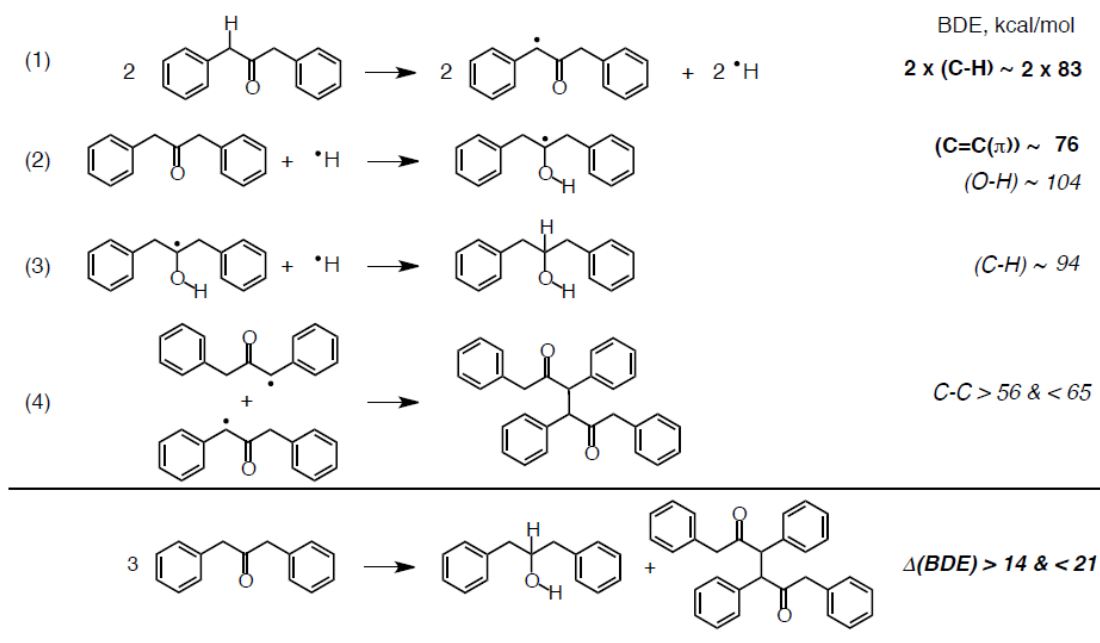


**Fig. 9.** Time dependencies of the concentrations of DBK (filled circles) and toluene 1B (open circles), a major product of the reaction of DBK in H<sub>2</sub>O at 300 °C and 70 MPa.

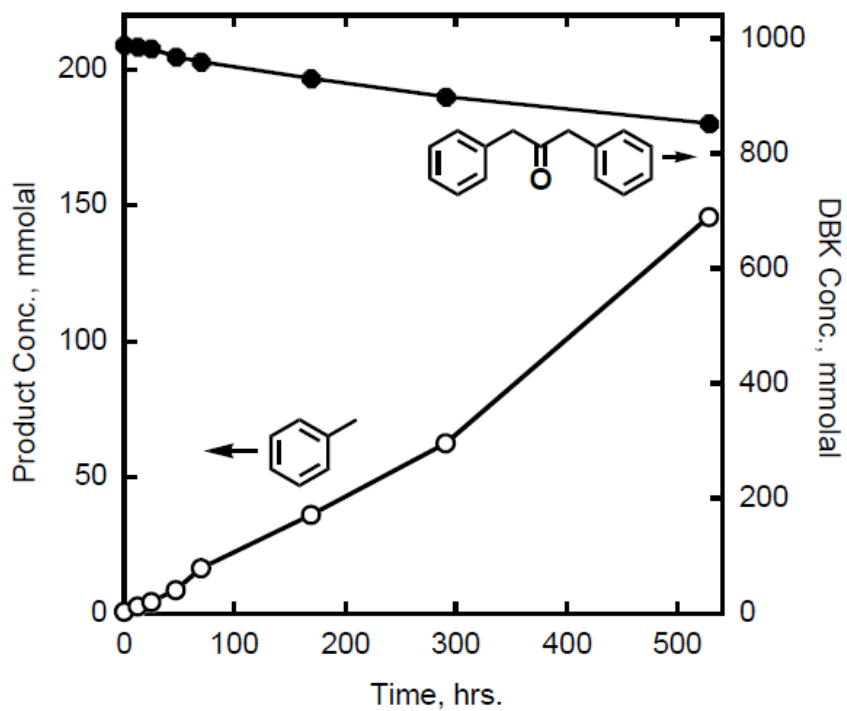


**Fig. 10.** Time dependencies of the concentrations of DBK (filled circles), *trans*-stilbene 2D (diamonds), bibenzyl 2B (open circles) in H<sub>2</sub>O at 300 °C and 70 MPa.

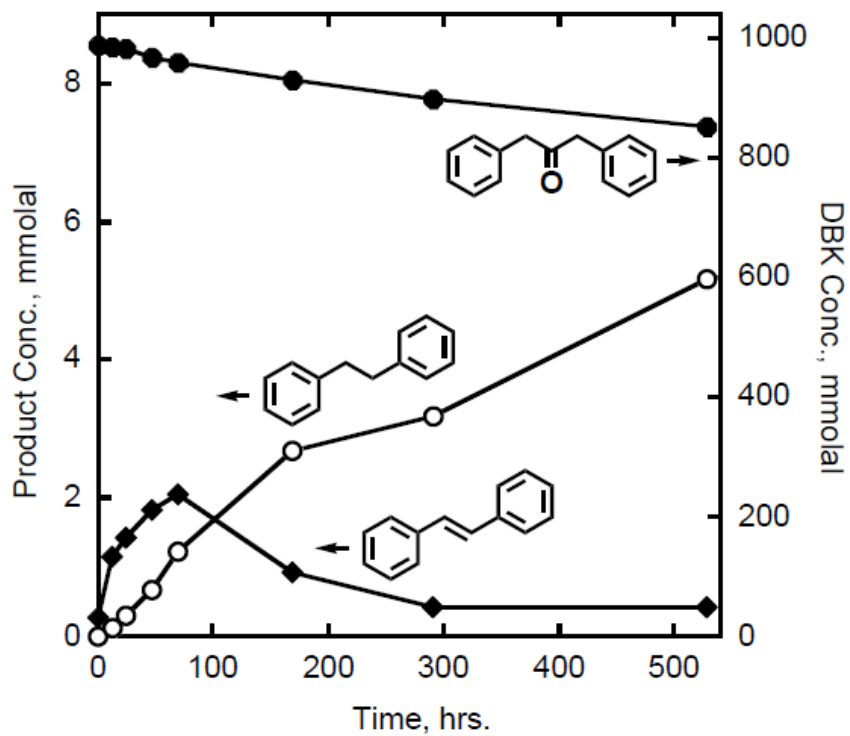




**Fig. 11.** Time dependencies of the concentrations of DBK (filled circles), and the two three-ring products 3C<sup>'''</sup> (open circles), and 3D (diamonds) in H<sub>2</sub>O at 300 °C and 70 MPa.

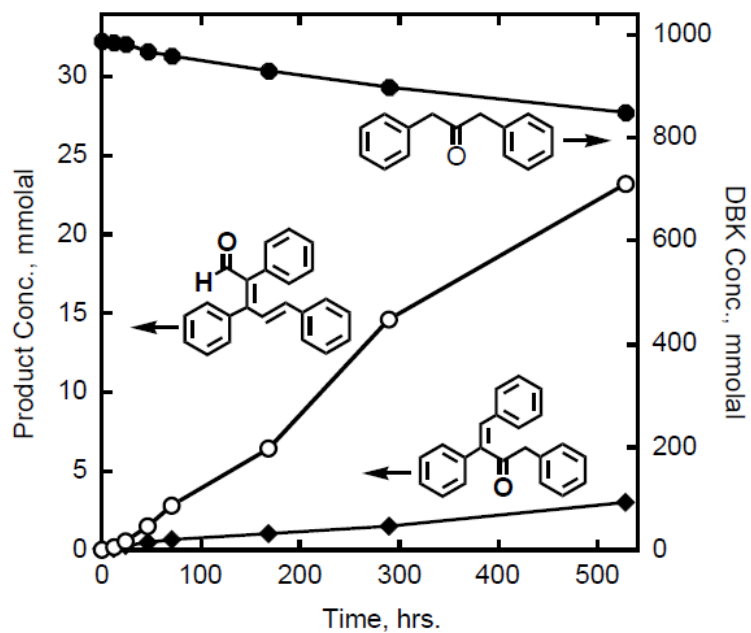
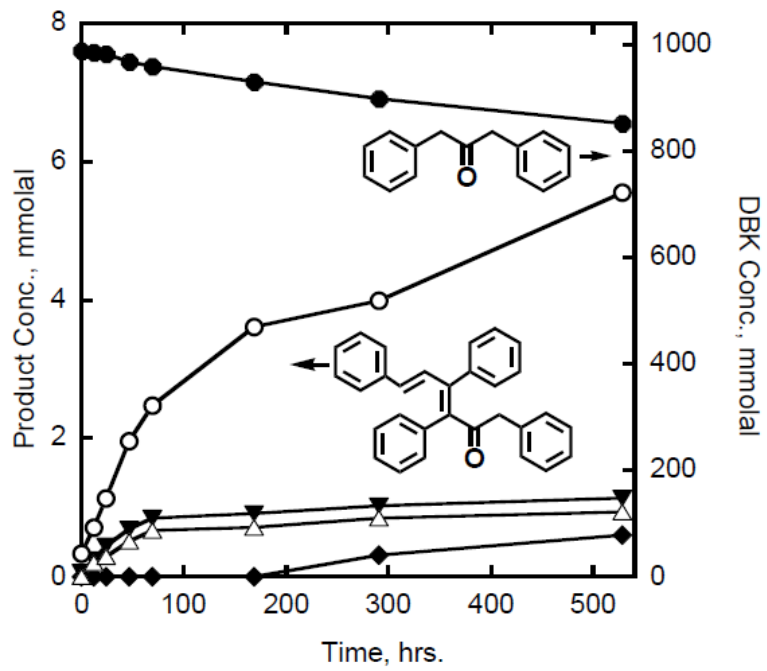


**Fig. 12.** Time dependencies of the concentrations of DBK (filled circles), and four isomeric structures with the same molecular ion that correspond to structure 4A of Fig. 4 in H<sub>2</sub>O at 300 °C and 70 MPa.



## 2.6. References

- Adlhart C. and Uggerud E. (2007) Mechanisms for the dehydrogenation of alkanes on platinum: insights gained from the reactivity of gaseous cluster cations,  $Pt_n^+$   $n = 1-21$ . *Chem. Eur. J.* **13**, 6883-6890.
- Akiya N. and Savage P. E. (2001) Kinetics and mechanism of cyclohexanol dehydration in high-temperature water. *Ind. Eng. Chem. Res.* **40**, 1822–1831.
- Amend J. P. and Helgeson H. C. (1997) Calculation of the standard molal thermodynamic properties of aqueous biomolecules at elevated temperatures and pressures. Part I. L- $\alpha$ -amino acids. *J. Chem. Soc., Faraday Trans.* **93**, 1927–1941.
- Amend J. P. and Helgeson H. C. (2000) Calculation of the standard molal thermodynamic properties of aqueous biomolecules at elevated temperatures and pressures. Part II. Unfolded proteins. *Biophys. Chem.* **84**, 105–136.
- Amend, J. P. and Shock, E. L. (1998) Energetics of amino acid synthesis in hydrothermal ecosystems. *Science* **281**, 1659-1662.
- Andersson E. and Holm N. G. (2000) The stability of some selected amino acids under attempted redox constrained hydrothermal conditions. *Origins Life Evol. Bios.* **30**, 9-23.
- Anikeev V. I. and Ermakova A. (2003) The influence of the density of supercritical water on the rate constant for the dehydration of isopropanol. *Russ. J. Phys. Chem.* **77**, 211-214.
- Antal M. J., Carlsson M., Xu X. and Anderson D. G. M. (1998) Mechanism and kinetics of the acid-catalyzed dehydration of 1- and 2-propanol in hot compressed liquid water. *Ind. Eng. Chem. Res.* **37**, 3820-3829.
- Bell J. L. S., Palmer D. A., Barnes H. L., and Drummond S. E. (1994) Thermal decomposition of acetate. 3. Catalysis by mineral surfaces. *Geochim. Cosmochim. Acta* **58**, 4155-4177.
- Bell J. L. S. and Palmer D. A. (1994) Experimental studies of organic acid decomposition. *Organic Acids in Geological Processes* (eds. E. D. Pittman and M. D. Lewan). Springer- Verlag, New York. pp. 226-269.
- Blanksby S. J. and Ellison G. B. (2003) Bond dissociation energies of organic molecules. *Acc. Chem. Res.* **36** (4), 255-263.

- Bordwell F. G. and Harrelson J. A. (1990) Acidities and homolytic bond dissociation energies of the  $\alpha$ C-H bonds in ketones in DMSO. *Can. J. Chem.* **68**, 1714-1718.
- Chen J.-X., Kim C. K., Lee H. W., Xue Y. and Kim C. K. (2011) Reexamination of the  $\pi$ -bond strengths within  $H_2C_5XH_n$  systems: A theoretical study. *J. Comput. Chem.* **32**, 1361–1367.
- Coan S. B. and Becker E. I. (1954) Synthesis of unsymmetrical 1,3-diphenyl-2-propanes. *J. Am. Chem. Soc.* **76**, 501-503.
- Coan S. B. and Becker E. I. (1963) *Organic Synthesis*, Wiley, New York, Volume **4**, 174-177.
- Dick J. M., LaRowe D. E., and Helgeson H. C. (2006) Group additivity calculation of the standard molal thermodynamic properties of aqueous amino acids, polypeptides, and unfolded proteins as a function of temperature, pressure and ionization state. *Biogeosciences* **3**, 311-336.
- Gould I. R., Baretz B. H. and Turro N. J. (1987) Primary processes in the Type 1 photocleavage of dibenzyl ketones. A pulsed laser and photochemically induced dynamic nuclear polarization study. *J. Phys. Chem.* **91**, 925-929.
- Head I. M., Jones D. M. and Larter S. R. (2003) Biological activity in the deep subsurface and the origin of heavy oil. *Nature* **426**, 344-352.
- Helgeson H. C., Knox A. M., Owens C. E. and Shock E. L. (1993) Petroleum, oil field waters and authigenic mineral assemblages: Are they in metastable equilibrium in hydrocarbon reservoirs? *Geochim. Cosmochim. Acta* **57**, 3295-3339.
- Helgeson H. C., Owens C. E., Knox A. M. and Richard L. (1998) Calculation of the standard molal thermodynamic properties of crystalline, liquid, and gas organic molecules at high temperatures and pressures. *Geochim. Cosmochim. Acta* **62**, 985-1081.
- Helgeson H. C., Richard L., McKenzie W. F., Norton D. L. and Schmitt A. (2009) A chemical and thermodynamic model of oil generation in hydrocarbon source rocks. *Geochim. Cosmochim. Acta* **73**, 594-695.
- Hinrichs K.-U., Hayes J. M., Bach W., Spivak A. J., Hmelo L. R., Holm N. G., Johnson C. G. and Sylva S. P. (2006) Biological formation of ethane and propane in the deep marine subsurface. *Proc. Natl. Acad. Sci. USA* **103**, 14684-14689.
- Hunter S. E. and Savage P. E. (2004) Recent advances in acid- and base-catalyzed organic synthesis in high-temperature liquid water. *Chem. Eng. Sci.* **59**, 4903–4909.

- Katritzky A. R., Nichols D. A., Siskin M., Murugan R. and Balasubramanian M. (2001) Reactions in high-temperature aqueous media. *Chem. Rev.* **101**, 837-892.
- Lang S. Q., Butterfield D. A., Schulte M., Kelley D. S., and Lilley M. D. (2010) Elevated concentrations of formate, acetate and dissolved organic carbon found at the Lost City hydrothermal field. *Geochim. Cosmochim. Acta* **74**, 941-952.
- Larter S. R., Wilhelms A., Head I., Koopmans M., Aplin A., Di P. R., Zwach C., Erdmann M. and Telnaes N. (2003) The controls on the composition of biodegraded oils in the deep subsurface: Part I - Biodegradation rates in petroleum reservoirs. *Org. Geochem.* **34**, 601-613.
- LaRowe D. E. and Dick J. M. (2012) Calculation of the standard molal properties of crystalline peptides. *Geochim. Cosmochim. Acta* **80**, 70-91.
- LaRowe D. E. and Helgeson H. C. (2006a) Biomolecules in hydrothermal systems: Calculation of the standard molal thermodynamic properties of nucleic-acid bases, nucleosides, and nucleotides at elevated temperatures and pressures. *Geochim. Cosmochim. Acta* **70**, 4680-4724.
- LaRowe D. E. and Helgeson H. C. (2006b) The energetics of metabolism in hydrothermal systems: Calculation of the standard molal thermodynamic properties of magnesium complexed adenosine nucleotides and NAD and NADP at elevated temperatures and pressures. *Thermochim. Acta* **448**, 82-106.
- Leif R. N. and Simoneit B. R. T. (1995) Ketones in hydrothermal petroleum and sediment extract from Guaymas Basins, Gulf of California. *Org. Geochem.* **23**, 889-904.
- Luo Y-R. (2007) *Comprehensive Handbook of Chemical Bond Energies*. CRC Press: Boca Raton, FL.
- Mayer J. M. (2010) Understanding hydrogen atom transfer: From bond strengths to Marcus theory. *Acc. Chem. Res.* **44**, 36-46.
- McCollom T. M., Ritter G. and Simoneit B. R. T (1999) Lipidsynthesis under hydrothermal conditions by Fischer-Tropsch-type reactions. *Orig. Life Evol. Bios.* **29**, 153-166.
- McCollom T. M. and Seewald J. S. (2003a) Experimental constraints on the hydrothermal reactivity of organic acids and acid anions: I. Formic acid and formate. *Geochim. Cosmochim. Acta* **67**, 3625-3644.

- McCollom T. M. and Seewald J. S. (2003b) Experimental study of the hydrothermal reactivity of organic acids and acid anions: II. Acetic acid, acetate, and valeric acid. *Geochim. Cosmochim. Acta* **67**, 3645-3664.
- McCollom T. M. and Seewald J. S. (2007) Abiotic synthesis of organic compounds in deep-sea hydrothermal environments. *Chem. Rev.* **107**, 382-401.
- McMillen D. F., Golden D. M. (1982) Hydrocarbon bond dissociation energies. *Ann. Rev. Phys. Chem.* **33**, 493-532.
- Morooka S., Matubayasi N. and Nakahara M. (2007) Kinetic study on disproportionations of C1 aldehydes in supercritical water: Methanol from formaldehyde and formic acid. *J. Phys. Chem. A* **111**, 2697-2705.
- Palmer D. A. and Drummond S. E. (1986) Thermal decarboxylation of acetate. 1. The kinetics and mechanism of reaction in aqueous solution. *Geochim. Cosmochim. Acta* **50**, 813-823.
- Pedley J. B., Naylor R. D. and Kirby S. P. (1986) *Thermochemical Data of Organic Compounds*. 2nd Ed., Chapman and Hill: New York.
- Pittman E. D. and Lewan M. D. (1994) *Organic Acids in Geological Processes*. Springer-Verlag, Berlin, Germany.
- Plyasunova N. V., Plyasunov A. V. and Shock E. L. (2004) Database of thermodynamic properties for aqueous organic compounds. *Int. J. Thermophys.* **25**, 351-360.
- Plyasunov A. V. and Shock E. L. (2000) Standard state Gibbs energies of hydration of hydrocarbons at elevated temperatures as evaluated from experimental phase equilibria studies. *Geochim. Cosmochim. Acta* **64**, 2811-2833.
- Plyasunov A. V. and Shock E. L. (2003) Prediction of the vapor-liquid distribution constants for volatile nonelectrolytes in H<sub>2</sub>O up to the critical temperature of water. *Geochim. Cosmochim. Acta* **67**, 4981-5009.
- Richard L. (2001) Calculation of the standard molal thermodynamic properties as a function of temperature and pressure of some geochemically important organic sulfur compounds. *Geochim. Cosmochim. Acta* **65**, 3827-3877.
- Richard L. and Helgeson H. C. (1998) Calculation of the thermodynamic properties at elevated temperatures and pressures of saturated and aromatic high molecular weight solid and liquid hydrocarbons in kerogen, bitumen, petroleum, and other organic matter of biogeochemical interest. *Geochim. Cosmochim. Acta* **62**, 3591-3636.

- Robbins W. K. and Eastman R. H. (1970) Photodecarbonylation in solution. 2. Trapping of intermediates in the photolysis of dibenzyl ketone. *J. Am. Chem. Soc.* **92**, 6077-6079.
- Rylander P. N. (1967) *Catalytic Hydrogenation over Platinum Metals*. Academic Press, New York.
- Schulte M. and Shock E. L. (2004) Coupled organic synthesis and mineral alteration on meteorite parent bodies. *Meteorit. Planet. Sci.* **39**, 1577-1590.
- Seewald J. S. (1994) Evidence for metastable equilibrium between hydrocarbons under hydrothermal conditions. *Nature* **370**, 285-287.
- Seewald J. S. (2001) Aqueous geochemistry of low molecular weight hydrocarbons at elevated temperatures and pressures: Constraints from mineral buffered laboratory experiments. *Geochim. Cosmochim. Acta* **65**, 1641-1664.
- Seewald J. S. (2003) Organic-inorganic interactions in petroleum producing sedimentary basins. *Nature* **426**, 327-333.
- Seewald J. S.; Zolotov M. Y. and McCollom T. M. (2006) Experimental investigation of single carbon compounds under hydrothermal conditions. *Geochim. Cosmochim. Acta* **70**, 446-460.
- Shock E. L. (1988) Organic acid metastability in sedimentary basins. *Geology* **16**, 886-890.
- Shock E. L. (1989) Calculation of the thermodynamic and transport properties of aqueous species at high pressures and temperatures: Standard partial molal properties of inorganic neutral species. *Geochim. Cosmochim. Acta* **53**, 2157-2183.
- Shock E. L. (1994) Catalysing methane production. *Nature* **368**, 499-500.
- Shock E. L. (1995) Organic acids in hydrothermal solutions: Standard molal thermodynamic properties of carboxylic acids, and estimates of dissociation constants at high temperatures and pressures. *Am. J. Sci.* **295**, 496-580.
- Shock E. L. (2000) Thermodynamic response of organic compounds in geochemical processes of sedimentary basins. *Reviews in Economic Geology*, Vol. **9** (eds: T. H. Giordano, R. M. Kettler, S. A. Wood). Society of Economic Geologists, Inc., Littleton, CO., pp. 105-117.
- Shock E. L. and Canovas P. C. (2010) The potential for abiotic organic synthesis and biosynthesis at seafloor hydrothermal systems. *Geofluids* **10**, 161-192.

- Shock E. L. and Helgeson H. C. (1990) Calculation of the thermodynamic and transport properties of aqueous species at high pressures and temperatures: Standard partial molal properties of organic species. *Geochim. Cosmochim. Acta* **54**, 915-945.
- Shock E. L. and Schulte M. D. (1998) Organic synthesis during fluid mixing in hydrothermal systems. *J. Geophys. Res.* **103**, 28513-28527.
- Siskin M. and Katritzky A. R. (1991) Reactivity of organic compounds in hot water-geochemical and technological implications. *Science* **254**, 231-237.
- Smith M. B. and March J. (2007) *March's Advanced Organic Chemistry*. 6th Edition, Wiley, New York.
- Turro N. J. (1991) *Modern Molecular Photochemistry*. University Science Books, Sausalito, CA.
- Turro N. J. and Weed G. C. (1983) Micellar systems as "supercages" for reactions of geminate radical pairs - Magnetic effects. *J. Am. Chem. Soc.* **105**, 1861-1868.
- Williams L. B., Hervig R. L., Holloway J. R. and Hutcheon I. (2001) Boron isotope geochemistry during diagenesis. Part 1. Experimental determination of fractionation during illitization of smectite. *Geochim. Cosmochim. Acta* **65**, 1769-1782.
- Windman T., Zolotova N., Schwandner F. and Shock, E. L. (2007) Formate as an energy source for microbial metabolism in chemosynthetic zones of hydrothermal ecosystems. *Astrobiology* **7**, 873-890.
- Xu X., Antal M. J. and Anderson D. G. M. (1997) Mechanism and temperature-dependent kinetics of the dehydration of tert-butyl alcohol in hot compressed liquid water. *Ind. Eng. Chem. Res.* **36**, 23-41.



## CHAPTER 3:

### HYDROTHERMAL PHOTOCHEMISTRY AS A MECHANISTIC TOOL IN ORGANIC GEOCHEMISTRY – THE CHEMISTRY OF DIBENZYL KETONE

Revised with permission from Yang Z., Lorance E. D., Bockisch C., Williams L. B., Hartnett H. E., Shock E. L. and Gould I. R. (2014) Hydrothermal photochemistry as a mechanistic tool in organic geochemistry. The chemistry of dibenzylketone. *J. Org. Chem.* (Accepted manuscript).

#### 3.1. Abstract

Hydrothermal organic transformations under geochemically relevant conditions can result complex product mixtures that form via multiple reaction pathways. The hydrothermal decomposition reactions of the model ketone dibenzylketone (**DBK**) form a mixture of reduction, dehydration, fragmentation, and coupling products that suggest simultaneous and competitive radical and ionic reaction pathways under the reaction conditions. This work shows how the photochemistry of **DBK** can be used to independently generate radical intermediates under hydrothermal conditions, and how at high temperatures benzyl radicals undergo coupling and radical abstraction reactions that do not occur at ambient conditions. The photochemical method allows the primary radical coupling products of the thermal reaction to be identified and the kinetics of the follow-up ionic reactions of these primary products to be studied. In this way the radical and ionic thermal reaction pathways can be studied separately.

### 3.2. Introduction

Over 99.99% of the Earth's organic carbon does not actively participate in the biospheric carbon cycle, but is located within the crust, mainly in continental and marine sedimentary basins in the form of kerogen (Falkowski et al., 2000; McSween et al., 2003). It is estimated that more than 15,000,000 Gt of organic matter is located beneath the surface of the Earth (McSween et al., 2003). The reactions of this huge quantity of organic matter contribute to a wide range of geochemically important processes. Specifically, reactions of organic material in the Earth's crust represent an important component of the deep, or geochemical, carbon cycle, which is an important factor in controlling atmospheric carbon dioxide levels (Dasgupta, 2013). Subsurface organic reactions are critical to petroleum generation and maturation processes (Helgeson et al., 2009), can provide energy sources for deep microbial communities (e.g., Horsfield et al., 2006), and have been implicated in the formation of ore deposits (Shock et al., 2013).

From an organic chemistry perspective, it is interesting that the solvent for most of these reactions is water, usually at elevated temperatures and pressures (e.g., McCollom et al., 2007; Tassi et al., 2007). Geochemically relevant hydrothermal organic reactions can have a wide temperature range, but the majority of the important processes take place between ca. 150 - 300°C, i.e., well below the critical point of water at 374°C and 221 bar (e.g., Seewald, 2003; McCollom and Seewald, 2007; Tassi et al., 2007). A wide range of reactions have now been identified in hot subcritical water (and associated confining pressures), which include fragmentations into smaller structures, additions to make larger structures, and functional group interconversions, and it is also interesting

that these reactions occur without the addition of any external reagents or catalysts (e.g., Siskin and Katritzky, 1981; Katritzky et al., 2001; Siskin and Katritzky, 2001; Akiya and Savage, 2002; Hunter and Savage, 2004; Watanabe et al., 2004). For these reasons, organic chemical reactions under conditions that mimic geochemical conditions are being studied as potential “green chemistry” systems (Avola et al., 2013; Shanab et al., 2013).

Many hydrothermal reactions are somewhat surprising when compared to the corresponding processes close to ambient conditions. Examples include the endothermic elimination of hydrogen from alcohols and alkanes to form carbonyls and alkenes and the dehydration of alcohols to form alkenes (e.g., Antal et al., 1987; Kuhlmann et al., 1994; Seewald, 1994; Xu et al., 1997; Akiya and Savage, 2001; Katritzky et al., 2001; Ott et al., 2006). Alcohol dehydration is particularly surprising since water is the solvent. The equilibrium between alcohol and alkene plus water is strongly temperature dependent, and for butanol, as an example, the equilibrium is on the side of butene plus water at temperatures above 200°C at the vapor-liquid saturation pressure of water (see Shock et al., 2013). At higher temperatures the entropic contribution to the free energy increases, so that eventually water elimination, which increases entropy, becomes favorable despite being endothermic. In general, hydrothermal organic reactions tend to be controlled by thermodynamics and entropy, as opposed to kinetics and enthalpy which are the primary controlling factors closer to ambient. Hydrothermal reactions are also unlike those at ambient conditions in that both ionic and radical reaction mechanisms can occur under the same conditions, although it is generally thought that ionic reactions are more prevalent at lower temperatures whereas radical reactions dominate at higher temperatures (Burdige, 2006; LaRowe and Van Cappellen, 2011).

Although a large number of hydrothermal organic reactions have been studied, the emphasis has been mainly on product distributions; reports of mechanistic studies have been less frequent, and direct evidence for proposed intermediates is often lacking. This is partly because many hydrothermal reactions give complex product mixtures, and many reactions are reversible (e.g., McCollom and Seewald, 2003a, b; Seewald, 2003; Seewald et al., 2006; Yang et al., 2012; Shipp et al., 2013). The need for high-pressure experimental apparatus can also complicate the use of many routine analytical procedures. Other than kinetic measurements (Belsky et al., 1999; Li and Brill, 2001; McCollom and Seewald, 2003a, b), and in some cases isotope effects (Hoering, 1984; Yamamoto et al., 2004; McCollom et al., 2010; Reeves et al., 2012), the mechanistic toolbox for hydrothermal organic reactions has been somewhat limited to date. One of the goals of this work is to develop a new experimental probe for hydrothermal organic reaction mechanisms.

The most abundant organic functional groups found in geochemically relevant environments are alkanes and carboxylic acids (Seewald, 2003). Seewald (2001, 2003) has proposed a reaction scheme that shows how acids and alkanes might be linked by a series of reversible and irreversible functional group interconversions (Scheme I). The critical structure in this scheme is the ketone, since it occupies the position where irreversible carbon-carbon bond cleavage must occur. The hydrothermal reactions of a model ketone, dibenzylketone (**DBK**), were studied in order to investigate how bond cleavage might compete with the functional group interconversions (Yang et al., 2012). Under the hydrothermal conditions of 300°C and 700 bar, all of the reactions of Scheme I were observed, except that carbon-carbon bond cleavage occurred to give mainly

coupling products rather than carboxylic acids (Yang et al., 2012). The coupling products were explained as arising from homolytic bond cleavage of **DBK** to give benzyl and related radicals, although the hydrothermal coupling products and their distributions were very different from those expected based on the known **DBK**-derived radical chemistry at ambient temperature (Robbins and Eastman, 1970a, b; Turro, 1982; Gould et al., 1987; GarciaGaribay et al., 1991; Turro, 2000). Independent evidence for the intermediacy of radicals in the bond cleavage reactions of **DBK** under hydrothermal conditions was thus sought.

The ambient photochemistry of **DBK** and its analogues has been extensively studied in a variety of reaction media (e.g., Robbins and Eastman, 1970a, b) and the primary photophysical and chemical processes are well established. This work found that using photochemistry at high temperature and pressure in water to independently generate radicals helps to rationalize the product distributions observed in the hydrothermal reactions of **DBK**. Specifically, an analysis of the product distributions and the quantum yields for the corresponding hydrothermal photolysis reaction provides convincing evidence for the previously proposed radical mechanisms for the thermal reactions of **DBK**, and reveals how the radical reactions are different under hydrothermal compared to ambient conditions. The shorter timescale of the photochemical hydrothermal reaction also allows the primary thermal reaction products to be identified and their follow-up reactions to be monitored directly, which is not possible in the closed hydrothermal thermal reaction vessel. In short, hydrothermal photochemistry is found to be a very useful mechanistic tool.

### 3.3. Results and discussion

#### 3.3.1. Hydrothermal reactions of DBK

Water at high temperatures and pressures acts as an excellent solvent for many organic reactions (Siskin and Katritzky, 2001). The hydrothermal decomposition reactions of **DBK** give a complex mixture of products that has been described in detail previously (Yang et al., 2012). Scheme II summarizes the main reaction products that are relevant to the present work. One reaction pathway involves reduction, dehydration and further reduction to give the corresponding alcohol (**2c**), alkene (**2d**) and alkane (**2e**) (although the alcohol **2c** does not accumulate significantly due to rapid dehydration to form the alkene **2d**), which corresponds to the functional group interconversion reactions shown in Scheme I. The majority of the reaction products, however, are derived from carbon-carbon and carbon-hydrogen bond cleavage reactions and subsequent coupling processes, presumably via radical intermediates. Cleavage of **DBK** to give benzyl radicals would be expected to give bibenzyl (**2a**), which is certainly observed, although in relatively low yield compared to other three- and four-ring coupling products. The bond cleavage products are most easily categorized in terms of the number of benzene rings they contain: specifically, toluene (**1**); bibenzyl (**2a**) and stilbene (**2b**); and products that contain three benzene rings (**3a - 3d**); and products that contain four benzene rings (**4a - 4b**).

The previously reported thermal reactions were performed by heating and pressurizing the samples in small, sealed, gold tubes with an argon headspace. Most

organic reactions that are designed to mimic geochemically relevant conditions are often run over extended time periods, from days to months, and avoiding inadvertent catalysis by the reaction container is a significant issue (e.g., Palmer and Drummond, 1986). Gold is generally considered to be one of the more inert materials for hydrothermal reactions (Palmer and Drummond, 1986) and, because it is malleable, the pressure inside a gold tube can be controlled by applying an external pressure using water in a stainless steel reaction vessel. Gold cannot be used for photochemical hydrothermal reactions, and so the hydrothermal decomposition of **DBK** in fused-silica glass tubes was first studied.

**DBK** is essentially insoluble in water at ambient temperature, but the solubility increases with increasing temperature so that a 1 molal solution can be obtained at 300°C (Yang et al., 2012). In a sealed fused-silica tube the internal pressure is determined by the water vapor pressure at the experiment temperature, which is 86 bar at 300°C (Johnson et al., 1992). A higher pressure was used in the gold tube experiments (700 bar) to ensure a single phase under those conditions. The lower pressure in the fused-silica experiments results in a headspace above the solution. The hydrothermal photochemical reactions do not occur in the headspace, as evidenced by the observation that irradiation in this region leads to no decomposition of **DBK**. The hydrothermal reaction of **DBK** was performed for 3 days at 300°C in a fused-silica tube, in a gold tube at 700 bar, and in a gold tube that was sealed inside a fused-silica tube. This last experiment allows a reaction in a gold container but at the same pressure as the experiments run in fused-silica tubing. The reaction time period was selected to minimize secondary follow-up reactions (see below). The observed products are essentially identical for the hydrothermal reaction of **DBK** in fused-silica glass, in gold at high pressure and in gold at the fused-

silica tube pressure, but the product distributions are slightly different. As an example, the yields of the alkane **2e** (Scheme II) formed by reduction of DBK are higher in the gold experiments than in the fused-silica tube by a factor of ca. three. The **DBK** conversions are also somewhat different, being 3.6%, 2.9%, and 2.1% in high-pressure gold, low-pressure gold, and fused-silica, respectively. This suggests increased reactivity in the gold reaction containers. The hydrogen balance is close to 100% for the hydrothermal reactions of **DBK**, and the hydrogen atoms that enable **DBK** reduction to alkanes (and other reduced products) should come from dehydrogenation reactions that form more oxidized organic products. A gas chromatogram showing the product distribution for a 7-day thermolysis experiment in the fused-silica tube is shown in Figure 1A. This longer reaction time period allows direct comparison to the photochemical experiments, but the product distribution is similar to that observed after 3 days.

### 3.3.2. *Ambient photochemistry of DBK*

The products of the 7-day thermal reaction were compared to those from 33-minute photolysis at room temperature in methanol and 33-minute hydrothermal photolysis at 300°C. The **DBK** conversions were all 5–8%, allowing direct comparison of the product distributions. Again, conversions were deliberately kept low to minimize secondary reactions. In agreement with the earlier literature (Robbins and Eastman, 1970a, b), photochemical excitation of **DBK** in homogeneous methanol solution at ambient temperature yields bibenzyl as the only detectable product, Figure 1C. The photochemical reaction of **DBK** in micelles and other constrained media has been



observed to additionally form small quantities of isomers of the starting material as a result of coupling of the primary benzyl and phenacyl radicals in the *ortho*- and *para*-positions (Lehr and Turro, 1981). However, benzyl radical/benzyl radical coupling tends to form only bibenzyl and no other isomers. Although bibenzyl is the only product of **DBK** photolysis at ambient conditions, the hydrothermal photochemistry yields quite different products that depend upon the initial **DBK** concentration.

### 3.3.3. *Hydrothermal photochemistry of DBK*

Photolysis of 1 molal **DBK** for 33 minutes at 300°C in water gives the product distribution shown in Figure 1B. Although the bibenzyl (**2a**) that is formed in the room temperature photolysis is observed, the major products are now toluene (**1**) and some of the three- and four-benzene ring coupling products of Scheme II. The product distribution resembles a simpler version of that obtained from the 7-day thermal reaction, shown in Figure 1A. The photochemical conversion of **DBK** is linear with time, as is formation of the toluene, bibenzyl and the coupling products. Figure 2 shows the product yields as a function of irradiation time for the hydrothermal photochemical reaction compared to the photochemical reaction in methanol at room temperature, corrected for the different **DBK** conversions under the two conditions. This plot clearly shows the large change in product distribution for the photochemical reaction at the higher temperature.

A mechanism that accounts for the fragmentation and coupling products under hydrothermal conditions is shown in Scheme III. Based on the known photochemistry of

**DBK**, excitation to the first excited singlet state is followed by intersystem crossing to the excited triplet state, which undergoes efficient homolytic bond cleavage to form a geminate benzyl and a phenacyl radical. From the previously measured activation parameters (Turro et al., 1983), decarbonylation of the phenacyl radical to yield another benzyl radical should occur in less than 2 ns at 300°C. The geminate benzyl radical pair is formed in an overall triplet state, and efficient diffusive separation of this primary radical pair is expected to occur in fluid solution, since recombination is spin forbidden (Gould et al., 1984). The non-photochemical thermal reaction forms the same geminate benzyl/phenacyl radical pair, in this case with in an overall singlet spin state. Separated benzyl radicals then form by decarbonylation and diffusive separation.

The hydrothermal reaction of the benzyl radicals that does not take place under ambient conditions is hydrogen atom abstraction from **DBK** to yield toluene (**1**) and a **DBK** derived radical, **DBK**<sup>•</sup>. Coupling of **DBK**<sup>•</sup> with a benzyl radical generates the primary three-ring structures **3a**, which form as a mixture of three structural isomers indicated as **3a**<sup>1</sup>, **3a**<sup>2</sup> and **3a**<sup>3</sup> in Figure 1B. Coupling of two **DBK**<sup>•</sup> generates the primary four-ring structures **4a** (two stereoisomers are formed), which undergo thermal dehydration to form structures **4b** (again, several isomers are formed). The primary products of the hydrothermal photochemical radical reactions are thus **1** (toluene), **2a** (bibenzyl), **3a** and **4a**, Scheme III.

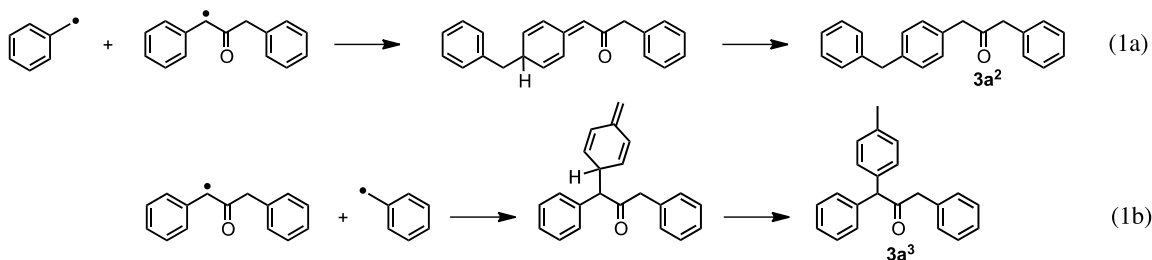
The hydrogen atom abstraction process occurs *in competition* with the conventional benzyl radical coupling to form bibenzyl. Therefore, changing the reaction conditions to change the relative rates of the competing processes should influence the product distribution. Formation of bibenzyl is kinetically second-order with respect to

benzyl radical concentration, whereas the competing hydrogen atom abstraction with **DBK** is pseudo-first-order. The relative rates of these reactions should thus depend upon the radical concentration, which can be varied by changing the light intensity. At higher light intensities (no attempt was made to quantify the various light intensities) the radical concentration is higher and the yield of bibenzyl compared to the coupling products is indeed observed to be higher.

Support for the mechanism of Scheme III is also obtained from experiments performed in the presence of Cu (II) ion, which is known to trap benzyl radicals *via* oxidation (Turro and Weed, 1983). Hydrothermal photolysis of **DBK** was performed in the presence of 0.5 molal Cu (II) chloride for 15 minutes. The extent of **DBK** conversion was similar to that without Cu (II), but the yields of all of the radical products **1**, **2a**, **3a** and **4a** were dramatically reduced by a factor of 80 - 90%. New oxidized products were detected in the presence of Cu (II) by gas chromatography, which included benzaldehyde, benzoic acid, and phenylacetic acid. This provides strong evidence for benzyl and benzylic radicals being the precursors to the various coupling products of the hydrothermal photochemistry of **DBK**.

Three structural isomers assigned to the coupling products **3a** are observed in the gas chromatogram/mass spectra of the product mixture from hydrothermal photolysis. One, with the shortest retention time in Figure 1B, is formed in significantly higher yield compared to the other two. These products are not isolable (the conversions are low and the reaction mixtures are complex), therefore only tentative assignments can be made. Coupling of a benzyl and a **DBK**<sup>•</sup> radical could in principle occur at various positions since the spins are delocalized. For the benzyl radical the measured spin densities are

3.19, 1.0 and 1.22 for the benzylic, *ortho*- and *para*-positions, respectively (Dust and Arnold, 1983). These spin densities do not explain the coupling of two benzyl radicals at ambient in fluid solution since coupling only occurs at the benzylic position under these conditions. Exclusive formation of bibenzyl is readily understood, however, since coupling at other positions initially forms a structure that has lost aromaticity. On this basis it is anticipated that the major coupling product for the **DBK**<sup>•</sup> radical would arise from coupling at the benzylic position to yield structure **3a<sup>1</sup>**, Scheme IV. Non-benzylic coupling has occasionally been observed, however, in photochemical reactions of **DBK** at ambient (e.g., Lehr and Turro, 1981). Two equivalent processes for the coupling of a benzyl radical and a **DBK**<sup>•</sup> radical are shown in Eqns. 1a and 1b, which yield **3a<sup>2</sup>** and **3a<sup>3</sup>** respectively, Scheme IV.



**3a<sup>2</sup>** and **3a<sup>3</sup>** are shown as *para*-coupling isomers, although a mixture of *ortho*- and *para*- isomers could be formed, and not be detected if they did not separate well under the chromatography conditions. **3a<sup>2</sup>** and **3a<sup>3</sup>** are formed in lower yields than **3a<sup>1</sup>** since they must be formed via intermediates that have lost aromaticity. Formation of non-benzylic coupling products under hydrothermal conditions points to higher reactivity and lower selectivity in the reactions of benzylic radicals at the higher temperatures. The

assignments of **3a<sup>1</sup>**, **3a<sup>2</sup>**, and **3a<sup>3</sup>** to the first, second and third peaks in the gas chromatogram of Figure 1 is supported by their mass spectra, and also the observed follow-up thermal chemistry discussed below. The mass spectra for the peaks assigned to **3a<sup>1</sup>** and **3a<sup>2</sup>** are very similar and contain m/z fragments 181 and 209 that are consistent with cleavage on both sides of the carbonyl group to give benzyl ions (Scheme IV). In the mass spectrum for the structure assigned to **3a<sup>3</sup>**, however, the 209 m/z fragment is very small and the 181 m/z is the base peak, since in the case of **3a<sup>3</sup>** the 181 m/z corresponds to a more stable diarylmethyl ion (see supporting information).

Five products assigned to structures that contain four benzene rings are formed at the early reaction times in sufficient quantity for mass spectral analysis, Figure 1B. Unlike the three-ring products, the time-dependencies of the concentrations of these structures are non-linear, see Figure 3. Two of these structures are formed in equal abundance and have identical mass spectra suggesting that they are the meso/(*d,l*) diastereomer pair formed by coupling of two **DBK<sup>•</sup>**, indicated as **4a** in Figure 1B and Scheme III. The other four-ring products indicated as **4b<sup>1</sup>** and **4b<sup>2</sup>** in Figure 1B are isomers with a molecular ion mass of 400, consistent with formal loss of water compared to the **4a** isomers. The rate of formation of the **4b** isomers also increases as a function of irradiation time, Figure 3, consistent with formation of the **4b** by secondary thermal dehydration reactions of **4a**.

That the **4b<sup>1</sup>** and **4b<sup>2</sup>** isomers are derived from the **4a** isomers is readily demonstrated by an experiment in which hydrothermal photolysis was *followed* by thermolysis without light at 300°C for a further 30 minutes. In this experiment it was found that the two peaks that were formed in the initial photolysis and assigned to **4a** had

completely disappeared in a follow-up thermal reaction, and the peaks assigned to the **4b** isomers were correspondingly larger. This explains the non-linear behavior of the **4a** and **4b**<sup>1</sup> with time shown in Figure 3. The dehydration reactions that convert **4a** into the **4b** isomers are discussed in detail below.

Further support for the mechanism of Scheme III comes from analysis of the product and quantum yields. According to Scheme III, one molecule of toluene is formed for each one of the three-ring coupling structures that are formed, and two molecules of toluene are formed for each one of the four-ring coupling structures. Therefore, the concentration of toluene in the product mixture [**1**] should be equal to the sum of the concentrations of all of the three-ring products ( $\Sigma$  [three-ring]) plus twice the sum of the concentrations of all of the four-ring structures ( $\Sigma$  [four-ring]), Eqn. 2. The concentrations of toluene and the concentrations of the three and four ring products summed according

$$[\mathbf{1}] = \Sigma [\text{three-ring}] + 2 \Sigma [\text{four-ring}] \quad (2)$$

to Eqn. 2 are shown as a function of time in Figure 4. The slopes of these plots are similar, supporting Eqn. 2 and also the mechanism of Scheme III. The small differences in the slopes are probably consequences of the necessary assumptions for the gas chromatography response factors for the various coupling products, which are assumed as 1.5 and 2.0 times larger than **DBK** for the three and four ring structures, respectively (see supporting information for details).

The formation of toluene and the coupling products requires consumption of more **DBK** molecules per photon compared to the ambient **DBK** photochemistry. The quantum yield for bibenzyl formation for ambient photochemical excitation of **DBK** is ca. 0.7 and is essentially solvent independent (e.g., Robbins and Eastman, 1970a, b). The quantum yield for product formation is the same as the quantum yield for formation of separated benzyl radicals since all separated benzyl radicals form coupling products. According to Scheme III, formation of a three-ring coupling product and the accompanying toluene consumes two **DBK** molecules. The quantum yield for formation of the three-ring structures should thus be twice as large as that for formation of bibenzyl. Formation of a four-ring coupling product (and the accompanying two toluenes) will correspondingly have a quantum yield that is three times larger than that for bibenzyl formation, since three **DBK** molecules are consumed in this case. Based on the observed product distribution for hydrothermal photolysis, the quantum yield for **DBK** consumption can thus be calculated relative to that under corresponding conditions where bibenzyl is the only product.

Bibenzyl formation does not depend upon the **DBK** concentration whereas the hydrogen atom abstraction reaction is pseudo-first-order with respect to **DBK**. It was found that the product distributions could be varied controllably by changing the **DBK** concentration. Hydrothermal photolysis of **DBK** at a concentration of 0.05 molal gave bibenzyl as the major product, whereas at 1 molal concentration toluene and the coupling products dominated the distribution, Figure 1. The quantum yields for formation of the coupling products can thus be obtained by comparing experiments at different concentrations of **DBK**.

Hydrothermal photolysis of **DBK** at 0.05 molal and 1.0 molal was compared to photolysis of **DBK** at ambient, where bibenzyl was the only product, and at concentrations that had the same light absorption as the two hydrothermal samples (details are given in the supporting information). It was found that the **DBK** consumption for hydrothermal photolysis is higher per absorbed photon at the higher **DBK** concentration compared to the low concentration by a factor of ca. 1.3. The calculated hydrothermal quantum yield at 1 molal concentration, based on the observed product distribution and assuming that each of the three- and four-ring structures consume 2 and 3 **DBK** molecules, respectively, is 1.37, which agrees quite well with the experimentally determined difference. The product distributions and quantum yields thus both support the mechanism of Scheme III.

The critical step in the mechanism is hydrogen atom abstraction from **DBK** by the benzyl radicals. This process is responsible for the new products and, at the same time, consumes more than one **DBK** molecule per initial photochemically-induced fragmentation reaction. The H-atom abstraction reaction has been examined computationally using B3LYP/aug-cc-pVDZ as implemented in *Gaussian 09* (Frisch et al., 2010). Methyl benzyl ketone (**MBK**) was used instead of **DBK** for computational economy. **MBK** was optimized both in the gas phase and in solvent (modeled using the polarizable continuum model, PCM) at 300°C and 700 bar. Starting with the optimal conformer of **MBK**, the benzyl radical was fixed at 2.5Å from the  $\alpha$ -hydrogen of the **MBK**, Figure 5, and the distance-constrained complex was fully optimized. From this geometry, the distance to the benzylic carbon of the radical,  $C_{\text{benzyl}}-H_{\alpha}$ , was shortened by 0.1Å steps to 1.5Å and then by 0.05Å steps until a distance of 1.35Å (optimizing the



distance-constrained complex at each distance), at which point the  $C_{\alpha}-H_{\alpha}$  bond separation distance in the **MBK** became quite large ( $>3\text{\AA}$ ), consistent with the breaking of this bond. A search for the transition state located an extremely steep apex to the reaction coordinate (Figure 5). This structure at this apex was characterized by an associated vibration frequency of  $-1528\text{ cm}^{-1}$ , which corresponds to the desired hydrogen transfer motion. The decrease in energy after the transition state is reached is artificially steep as a consequence of constraining only the  $C_{\text{benzyl}}-H_{\alpha}$  coordinate and none of the other relevant bond distances. The reaction is found to be exothermic, as expected for a reaction that generates a more resonance-stabilized radical, by a value of 29 kJ/mol. This is in excellent agreement with the differences in the experimentally measured  $C_{\text{benzyl}}-H_{\alpha}$  and  $C_{\alpha}-H_{\alpha}$  bond dissociation energies of 30 kJ/mol, i.e., 377 kJ/mol for the benzylic C–H bond in toluene (Blanksby and Ellison, 2003) and 347 kJ/mol for the benzylic ( $\alpha$ -) C–H bond in **MBK** (Bordwell and Harrelson, 1990) (bond dissociation enthalpies are essentially independent of temperature). The activation free energy is computed to be 132.4 kJ/mol at 300°C, which translates into a bimolecular rate constant of  $10.3\text{ M}^{-1}\text{ s}^{-1}$  using transition state theory (Fernandez-Ramos et al., 2006). The corresponding activation energy and rate constant at ambient are calculated to be 119.0 kJ/mol and  $8.9 \times 10^{-9}\text{ M}^{-1}\text{ s}^{-1}$ .

Hydrogen atom abstraction is competitive with benzyl radical recombination at 300°C, since both bibenzyl and abstraction products are observed. However, the hydrogen atom abstraction rate constant is predicted to be ca.  $10^9$  times slower at ambient compared to 300°C. Therefore, it is not surprising that hydrogen atom abstraction cannot

compete with radical recombination at ambient and that bibenzyl is the only observable product at this temperature.

#### 3.3.4. *Hydrothermal dehydration*

In addition to providing insight into the thermal radical reactions, the photochemical technique allows the follow-up ionic thermal reactions to be more easily isolated. The photochemical reaction clearly reveals the primary three-ring and four-ring radical coupling products **3a** and **4a** that are difficult to identify in the thermal reaction due to simultaneous formation of secondary products. In the pure thermal reactions the major primary three-ring isomers **3a**<sup>1</sup> are not among the most abundant products, and the primary four-ring isomers **4a** are not even observed, Figure 1A. The secondary products can be mostly understood as arising from follow-up dehydration reactions of the **3a** and **4a** structures. Note again that dehydration occurs efficiently despite the fact that the solvent is water and there are no added reagents or catalysts.

Dehydration of alcohols is perhaps the best-characterized hydrothermal reaction from a mechanistic perspective (e.g., Xu et al., 1997; Akiya and Savage, 2001; Ott et al., 2006). These reactions proceed by conventional acid-catalyzed elimination of water. The acid catalyst is supplied by the water. Under hydrothermal conditions it is well known that the  $K_w$  for water increases (Harvey and Friend, 2004), the dielectric constant of water decreases (Harvey and Friend, 2004), and, with the increased thermal energy, the reactivity of the hydronium and hydroxide ions is increased. The mechanisms of the dehydration reactions of the ketones **3a** and **4a** are not as obvious, however, since these

are not alcohols, but the photochemical approach was again found to provide useful mechanistic insight.

Further photolysis-followed-by-thermolysis experiments were performed in order to obtain a more quantitative description of the dehydration reactions of **3a** and **4a**. Photolysis was performed at 300°C for 2 minutes with high light intensity, followed by thermolysis at the same temperature for variable time periods. A high light intensity was used to quickly generate a sufficient concentration of the **3a** and the **4a** before significant thermal dehydration started to occur. The rates of follow-up thermal dehydration were found to be very different for the **3a** isomers and the **4a** isomers. Reaction of both diastereomers of **4a** was complete within ca. 15 minutes after the light was shut off (both reacted at the same rate), whereas the reactions of the **3a** isomers were much slower. The different isomers of **3a** decreased in concentration at different rates, but none decreased by more than a factor of ca. 2 over a period of one day. The reactions of the **3a** isomers were so slow that accurate measurement of their reaction kinetics was not possible, since they were also being formed by thermal (non-photochemical) decomposition of **DBK** during the post-photolysis thermal reaction period. However, the kinetics of the conversions of the diastereomers of **4a** to the **4b** isomers were readily measured by quenching photolysis samples after different follow-up thermolysis periods, Figure 6. Dehydration of the **4a** isomers to the **4b** isomers was remarkably fast, and the pseudo-first-order rate constant is ca. 0.25 min<sup>-1</sup>. Although a corresponding rate constant for the **3a** reactions could not be obtained, it is clear that the reactivities of the **3a** and the **4a** are very different, and that any proposed dehydration mechanism needs to account for the different reactivity.

Possible acid-catalyzed dehydration reactions were investigated both computationally and by using some model reactions. For these large structures the semiempirical PM6 method was selected (Stewart, 2007; Frisch et al., 2010). Calculations were performed at 300°C and 700 bar (the conditions of the original gold tube experiments) in simulated hot pressurized water using the PCM (details provided in supporting information). A plausible mechanism for the dehydrations of **4a** and **3a** involves protonation of a carbonyl, followed by formation of the corresponding enols (**4e** and **3e**), rearrangement to form alcohol **4f** and **3f** followed by conventional acid-catalyzed elimination of water to generate dienones or dienes, **4b<sup>2</sup>** and **3b**, respectively, as shown in Scheme V. Most of these structures could be formed in multiple stereo- or structural isomeric forms, as indicated by the (') symbols in Scheme V, and as observed in the final dehydration products **3b** and **4b<sup>2</sup>** in the gas chromatograms of Figure 1.

Heats of formation for the relevant intermediate structures are summarized in Scheme V. Formation of the enol was found to be slightly endothermic for both **3a** and **4a**, as expected, and the isomerization **3e/4e** to **3f/4f** was almost thermoneutral. Deprotonation of the initially protonated carbonyl may skip the enol and form the alcohols **3f/4f** directly, but the energy changes along the two reaction pathways to the dienes **3b** and the dienones **4b<sup>2</sup>**, including the final dehydration step, are very similar, and cannot account for the large observed difference in reaction rates for **3a** and **4a**. One of the products of dehydration of **4a** is formed in significantly higher yield than the others, Figure 1B. The isomeric dienones **4b<sup>2</sup>** shown in Scheme V are sterically congested and extensive conjugation is not observed in any of the calculated structures, see Figure 7, for example. This lack of conjugation due to steric crowding is also observed in the enol and

alkene isomers **3e/4e** and **3f/4f**. The heats of formation of the four stereoisomers of the dienones **4b<sup>2</sup>** were found to be similar, although the (*3Z,5E*)-isomer was the most stable computationally and was visually the least crowded, Figure 7. The uncertainty in the heats of formation of isomeric organic structures such as those in Scheme V has been estimated to be ca. 16 kJ/mol (Isegawa et al., 2013). The energy of the (*3Z,5E*) isomer is lower than the others by ca. 30 kJ/mol (i.e. by more than the reported estimated uncertainty in the heats of formation), but this energy difference is not enough to account for this isomer being formed with significantly higher abundance than the others. However, another dehydration pathway is available to the **4a** that can form a product that is even more stable than the dienones.

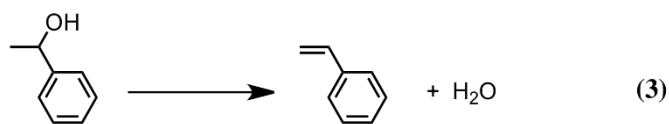
The protonated **4a** can undergo the known Paal-Knorr cyclization to form a furan (Amarnath and Amarnath, 1995), whereas the corresponding protonated **3a** cannot, Scheme V. This additional reaction pathway readily accounts for the significantly increased rate of dehydration of **4a** compared to **3a**. The reaction forms a furan **4b<sup>1</sup>** that is a structural isomer of the dienones **4b<sup>2</sup>** of Scheme V, Figure 7. Computationally, this furan is found to be significantly more stable than the dienones by ca. 60 kJ/mol (at 300°C and 700 bar), which in turn suggests that it is the major dehydration isomer observed with the shortest retention time in the gas chromatograms of Figure 1. Although still sterically congested, the furan **4b<sup>1</sup>** is more conjugated than the least hindered dienone, Figure 7, which presumably contributes to its increased stability.

Isomers are possible for the dienones, but not for the furan **4b<sup>1</sup>**. Three dehydration isomers are clearly observed in the gas chromatograms shown in Figure 1, and smaller peaks due to other isomers can also be detected at longer reaction times.

Dehydration may form all of the isomers, or interconversion among the dienone isomers could also occur via protonation and deprotonation reactions. The development of true thermodynamic equilibrium among the various isomers is unlikely, however, due to further follow-up reactions of the **4b<sup>2</sup>** dienones discussed below.

Studies of model reactions support the mechanisms of Scheme V. Enolization of ketones **3a** and **4a** (illustrated as acid-catalyzed in Scheme V, although base catalysis is also possible) can be tested using **DBK** itself as a model. As mentioned above, the inherent Brønsted acid and base catalytic activity in water is expected to be high at 300°C. The hydrothermal reaction of **DBK** in deuterated water at 300°C for 10 minutes resulted in complete incorporation of four deuteriums in the unreacted **DBK**, as determined by mass spectrometry, presumably as a consequence of exchange of the four enolizable hydrogens in **DBK** (e.g., Siskin et al., 1995). Thus, enolization readily occurs on the timescale of the dehydration reaction. The second isomerization step can also be readily understood as proceeding via acid catalysis, protonation followed by deprotonation, similar to enolization, Scheme V. That this process could also be fast on the timescale of the **4a** dehydration is supported by the calculated heats of formation that indicate that the process **4e** to **4f** is even less endothermic than the enolization step, as well as observation of rapid interconversions among isomeric alkenes under similar conditions (e.g., Shipp et al., 2013).

The final step in the mechanism of Scheme V is dehydration of the alcohol, which was modeled by studying the same reaction in 1-phenylethanol, Eqn. 3. Thermolysis of 1-phenylethanol for 1 hour at 300°C resulted in conversion of ca. 50% of the alcohol to



styrene. The mechanism of hydrothermal alcohol dehydration has previously been shown to proceed via protonation of the oxygen followed by conventional E1 or E2 elimination (e.g., Akiya and Savage, 2001). The rate of this dehydration is intermediate between those observed for the overall more complex dehydrations of **3a** and **4a**, and suggests that the reactions of Scheme V are plausible on the observed timescales.

### 3.3.5. Follow-up ionic reactions

The photochemical reaction effectively separates the radical reactions from the mainly ionic secondary dehydration reactions that occur simultaneously with the radical reactions in the pure thermal reaction, Scheme III. This separation allowed us to construct the reaction scheme for the formation of the fragmentation and coupling products, Scheme III, which was not possible from the previous thermal-only studies (e.g., Yang et al., 2012).

Hydrothermal photolysis followed by thermolysis eventually results in a product distribution that resembles that of the pure thermolysis reaction, Figure 1A. As mentioned above, thermolysis after photolysis results in the complete removal of the **4a** isomers via dehydration. Thermolysis after photolysis does not completely remove the **3a** isomers, but their product distribution changes compared to that after short-time

photolysis alone. In particular, the major product of hydrothermal photolysis, **3a<sup>1</sup>**, becomes the least abundant of the **3a** isomers upon thermolysis, and additional three-ring structures are observed, although in greater yields than could be accounted for by reactions of the **3a** alone.

This observation is explained by recognizing that the structure assigned to **3a<sup>1</sup>** can undergo the same dehydration reaction as **4a** to give **3b** isomers, Scheme III. The structures assigned to **3a<sup>2</sup>** and **3a<sup>3</sup>**, however, cannot undergo the corresponding dehydration, but could in principle undergo reactions similar to **DBK** itself. Under the experimental conditions and timescales, conversion to secondary products would be expected to be minimal since the reactions of **DBK** itself are relatively slow (Yang et al., 2012). Toluene would be expected to be a major product of these reactions, but structural isomers of bibenzyl (**2a**) and other coupling products would also be expected to eventually form. In support of this, small peaks in the gas chromatograms, close to authentic bibenzyl, are observed upon extended thermolysis and appear to be bibenzyl isomers based on mass spectral analysis, Figure 1.

After extended thermolysis the major three-ring structure is the aldehyde **3d** (formed as multiple stereoisomers), Scheme III. This reaction has not yet been investigated in detail, however, the aldehyde yield after extended reaction time is sufficiently large that it cannot be formed from reactions of the primary three-ring products **3a**. A potential alternate source of **3d** is via bond homolysis in the dienones **4b<sup>2</sup>**, Scheme III. The other product of this reaction would be toluene **1**, although formation of **3d** and **1** from **4b<sup>2</sup>** requires two hydrogen atoms. With extended reaction times, stilbene (**2b**, mainly the *trans*-isomer) becomes a major product in the two-benzene ring region at the expense of



bibenzyl, Figure 1A. The conversion to stilbene from bibenzyl formally generates hydrogen atoms that could be used in the formation of **3d** from **4b**<sup>2</sup>.

### 3.4. Conclusions

Hydrothermal photolysis of dibenzylketone allows identification of the primary radical coupling products in the corresponding thermal reactions and reveals unexpected reactions of benzylic radicals in high temperature water. Hydrothermal photolysis also allows separation of the radical and ionic reactions that occur simultaneously in the purely thermal experiment without photolysis. Reactions of the benzyl radicals at high temperature that do not occur at ambient include *ortho*- and *para*-coupling and hydrogen atom abstraction from **DBK** itself. The increased thermal energy and increased  $K_w$  facilitate rapid Brønsted acid- and base-catalyzed reactions that are not observed at ambient, specifically dehydration of the ketones **3a** and **4a**. Although alcohol dehydration has been observed many times in other hydrothermal organic reactions, this work points to dehydration as a generally favorable process for different kinds of structures in addition to alcohols (Shock et al., 2013). The follow-up reactions of Scheme V are mainly Brønsted acid-catalyzed, and it is well known that natural geologic systems are characterized by widely varying pH and distributions of organic materials and functional groups (McSween et al., 2003). Isolation of the ionic pH-dependent reactions is thus a valuable tool to aid in the understanding of the complex schemes that often characterize geologically relevant organic processes.

### 3.5. Supporting information

#### 3.5.1. *Experimental*

##### 3.5.1.1. *Materials*

Most of the chemicals were available from previous work (Yang et al., 2012). Copper chloride ( $\text{CuCl}_2$ , 98%) was purchased from Sigma-Aldrich and used without purification.

##### 3.5.1.2. *Experimental procedures*

The hydrothermal photolysis experiments were carried out in narrow fused silica glass tubes (GM Associates, Inc.) that had a 6 mm outside diameter and a 2 mm inside diameter. Dibenzyl ketone (**DBK**) was weighed into the tubes and 0.2 mL of argon-purged deionized water was added, to obtain solutions that, when heated, ranged in concentration from 0.035 to 1 molal. It was previously confirmed that **DBK** is soluble at all experimental concentrations at 300°C (Yang et al., 2012). The samples were frozen in liquid nitrogen, evacuated using three pump-freeze-thaw cycles and then sealed under vacuum with hydrogen flame to a length of ~12 cm. The sample occupied ~8 cm of the tube length at room temperature (RT) and the remainder was evacuated headspace. The volume of the headspace was diminished by water expansion at 300°C since the density

of water decreases ca. 30% from RT to 300°C. At 300°C the pressure in the tube is determined to be ca. 86 bar using SUPCRT 92 (Johnson et al., 1992). The sealed fused silica tubes were placed vertically in a large brass block that was heated using cartridge heaters. A thermocouple inside the brass block next to the sample tube was used to monitor the reaction temperature. The samples were pre-heated in the brass block at 300°C for 5 minutes before irradiation for time periods of 2 to 33 minutes. The 5-minute preheating time was determined to be suitable in an experiment where the temperature was measured directly using a thermocouple placed inside the same silica glass tube containing silicone oil. The light source was a 200 watt W mercury arc lamp (Osram HBO200W) equipped with Oriel Arc Lamp Power Supply system (model 8500, Stamford, Conn, USA). A filter solution of potassium chromate and sodium carbonate was used to isolate the 313 nm emission line and control the light intensity (Murov et al., 1993). At the end of the irradiation period the sample tubes were quenched immediately in a cold-water bath.

For longer timescale (thermolysis only) experiments, the samples were heated in a gas chromatograph oven at 300°C for 3, 7, or 12 days. Thermolysis experiments in gold tubes at 300°C and 700 bar were performed using the apparatus and methods described previously (Yang et al., 2012). A low pressure gold capsule hydrothermal experiment at 300°C and 86 bar was performed by sealing a gold capsule inside a larger fused silica tube with a 12 mm outside diameter and a 6 mm inside diameter, which was placed in a Swagelok pipe that contained water to equalize the pressure inside and outside the fused silica tube to prevent fracture. Room temperature photolysis of **DBK** were carried out in

the same fused silica tubes and apparatus as the high temperature photolysis experiments. Radical trapping experiments were performed using 0.5 molal  $\text{CuCl}_2$  at 300°C and 86 bar.

The extraction and analytical procedures were as described previously (Yang et al., 2012). Gas chromatography with flame ionization detection (FID) was used for quantitative analysis of the reaction mixtures in the quantum yield and kinetics experiments. Because of the low conversions and the number of products, it was not possible to isolate the coupling products that contained three and four benzene rings. As described previously (Yang et al., 2012), the gas chromatography FID response factors for coupling structures for which there was no independent standards were estimated based on the number of benzene rings that they contained; specifically, 1.5 and 2.0 times larger than that for **DBK** for the three-benzene-ring and the four-benzene-ring structures, respectively.

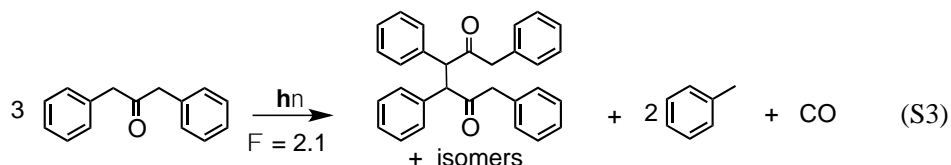
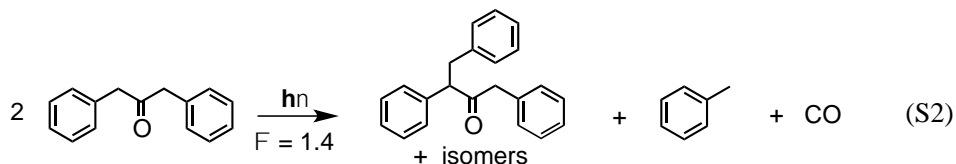
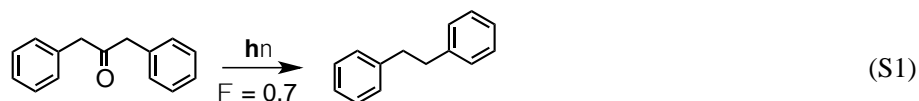
### *3.5.1.3 Electronic structure calculations*

All calculations were accomplished with Gaussian 09 Rev. A.02 (Frisch et al., 2009), using either the B3LYP hybrid DFT method (Becke, 1993) as implemented in Gaussian (Stephens et al., 1994; Hertwig and Koch, 1997; Scuseria and Staroverov, 2005) with Dunning's correlation-consistent double-zeta basis set augmented with diffuse functions (aug-cc-pVDZ) (e.g., Dunning, 1989; Kendall et al., 1992; Davidson, 1996), or the PM6 method (Stewart, 2007). All calculations used tight constraints and ultrafine integrals in the DFT evaluation and were run at 573.15 K and 700 bar, the conditions of the original gold tube thermolysis experiments. High-temperature, high-pressure water

(“hi-PT water”) was simulated in both the DFT and the PM6 calculations using a polarizable continuum model via the integral-equation formalism (IEF-PCM) (Scalmani and Frisch, 2010). The relevant solvent parameters and their values were: dielectric constant 25.296, density 0.02760533 molecules/Å<sup>3</sup> (Becke, 1993), and molar volume 21.8146299 cm<sup>3</sup>/mole. The data were taken from NIST *Thermophysical Properties of Physical Systems* (<http://webbook.nist.gov/chemistry/fluid/>), except the dielectric constant, which was calculated from interpolation formulas found in Uematsu and Franck (1980). The PCM solvation model was used with Bondi cavity-building radii, evaluated at an average point density of 10/Å<sup>2</sup>, and was corrected for dispersion, repulsion, and cavitation terms.

### 3.5.2. Quantum yield calculations

The quantum yield for bibenzyl formation for ambient photochemical excitation of **DBK** is ca. 0.7, Eqn. S1, which is also the quantum yield for consumption of **DBK** since bibenzyl is the only product at ambient (e.g., Robbins and Eastman, 1970a, b). As



described in the main text, the quantum yield for consumption of **DBK** is expected to be higher than 0.7 under the hydrothermal experimental conditions since, according to the proposed reaction Scheme III in the main text, formation of the three- and four-ring coupling products requires consumption of more than one **DBK** molecule per absorbed photon. Formation of a three-ring coupling product and the accompanying toluene consumes two **DBK** molecules, giving an expected quantum yield for formation (if it is the only product) of 1.4, based on a quantum yield of 0.7 for **DBK** consumption, Eqn. S2. Correspondingly, formation of a four-ring coupling product (and the two accompanying toluenes) has a quantum yield (if it is the only product) of 2.1, Eqn. S3, since three **DBK** molecules are consumed in this case. Based on the observed product distribution, a prediction of the quantum yield for **DBK** consumption upon hydrothermal photolysis,  $\Phi_p$ , can thus be made by measuring the chemical yields of the biphenyl, the three-ring structures and the four-ring structures as a fraction of the sum of the chemical yields of these products,  $f$  (bibenzyl),  $f$  (three-ring) and  $f$  (four-ring), respectively, Eqn. S4.

$$\Phi_p = 0.7 f(\text{bibenzyl}) + 1.4 f(\text{3-ring}) + 2.1 f(\text{4-ring}) \quad (\text{S4})$$

Chemical yield data were obtained as a function of time for photolysis of 1 molal **DBK** at 300°C and 86 bar, and the fractional yields were found to be essentially independent of the photolysis time, Table S1. From this data, together with Eqn. S4, an average predicted quantum yield of 1.37 was determined.

To determine the experimental quantum yield for **DBK** consumption, hydrothermal photolysis was compared to room temperature photolysis. Taking into

account the expansion of water with temperature, a 1 molal solution of **DBK** in water at 300°C and 86 bar has the approximately the same light absorptivity as a 0.7 molal solution of **DBK** in methanol at room temperature. The conversion with time was thus compared for photolysis of these two solutions, Figure S1A. The **DBK** conversion is higher in high temperature water than in room temperature methanol, consistent with destruction of more **DBK** molecules per photon at the higher temperature. The ratio of the slopes of Figure S1A is 1.23, and taking the quantum yield for decomposition of **DBK** in methanol to be 0.7, the quantum yield in the high temperature water is thus be estimated to be 0.86. However, this does not take into account differences in refractive index and other optical effects associated with irradiation of samples in round tubes in the brass block apparatus. To correct for these effects, a 0.05 molal **DBK** solution in high temperature water was compared to a 0.035 molal **DBK** solution in methanol at room temperature. A solution of 0.035 molal **DBK** in methanol is assumed to have approximately the same light absorbance as a 0.05 molal **DBK** aqueous solution at high temperature, because hydrothermal photolysis of a 0.05 molal **DBK** solution at 300°C generates mainly bibenzyl, and much smaller quantities of the three- and four-ring coupling products. Comparing the two lower **DBK** concentration solutions, the conversion as a function of time is found to be larger in the room temperature methanol samples than in the high temperature water, Figure S1B. It is assumed that the quantum yield for **DBK** consumption is 0.7 in both of these lower concentration solutions, since bibenzyl is the major product in each case, and that the different rates of **DBK** consumption shown in Figure S1B reflect optical differences in the two experiments. The ratio of the slopes of the plots in Figure S1B is 1.5, and correcting the 0.86 quantum

yield determined from the high concentration experiments by this ratio results in a final estimated quantum yield of 1.3 for hydrothermal photolysis of the high concentration **DBK**. This is close to the predicted quantum yield of 1.37 based on Scheme III of the main text discussed above.

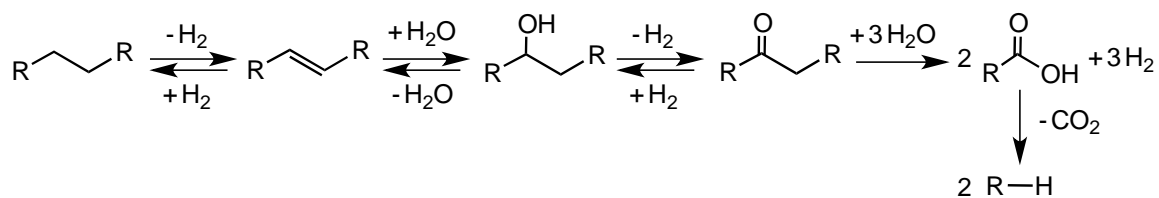
This analysis assumes that the quantum yield for **DBK** fragmentation in high temperature water is the same as in room temperature methanol. This is a reasonable assumption for the following reasons. Bond cleavage occurs in the first excited triplet state, the lifetime of which is much shorter than that of the excited singlet state (Arbour and Atkinson, 1989). Radiative and radiationless decay to ground state and intersystem crossing in excited singlets are not activated, and are thus expected to be temperature independent (Turro et al., 2010). The excited triplet state has a very short lifetime (Arbour and Atkinson, 1989), which is consistent with an essentially pure repulsive energy surface for dissociation. The bond dissociation process is therefore also likely to be temperature independent. Diffusive separation of the radicals and decarbonylation of the primary phenacyl radical will be temperature dependent, however, these processes do not influence the quantum yield for **DBK** destruction, since the geminate radical pair is formed in the triplet state and the radicals undergo essentially complete separation in fluid solution (Turro et al., 2010). Thus, any increase in the rate of separation or decarbonylation will not increase the final yield of separated benzyl radicals.



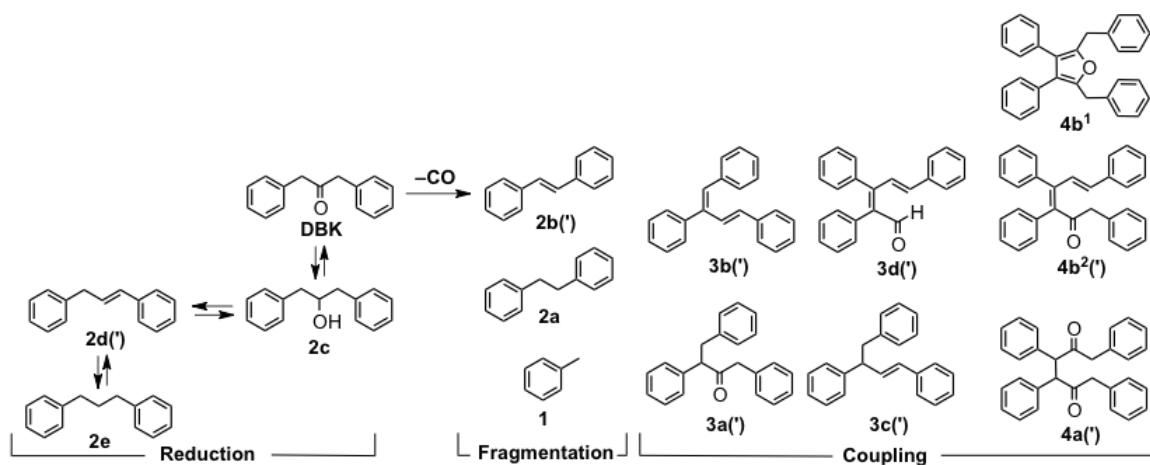
### 3.5.3. *Product characterization via gas chromatography/mass spectrometry*

The products observed at early reaction times for hydrothermal photolysis of **DBK** are toluene, **1**, bibenzyl, **2a**, and the three- and four-ring coupling products **3a**, **4a** and **4b**. The products that contain one and two benzene rings are readily identified in the gas chromatogram of the product mixture using authentic standards (Yang et al., 2012). The primary three- and four-ring coupling product structures are assigned based on analysis of the product distribution, the quantum yields and the follow-up thermal chemistry, as described in the main text, and on the mass spectra given in Figures S2 - S4.

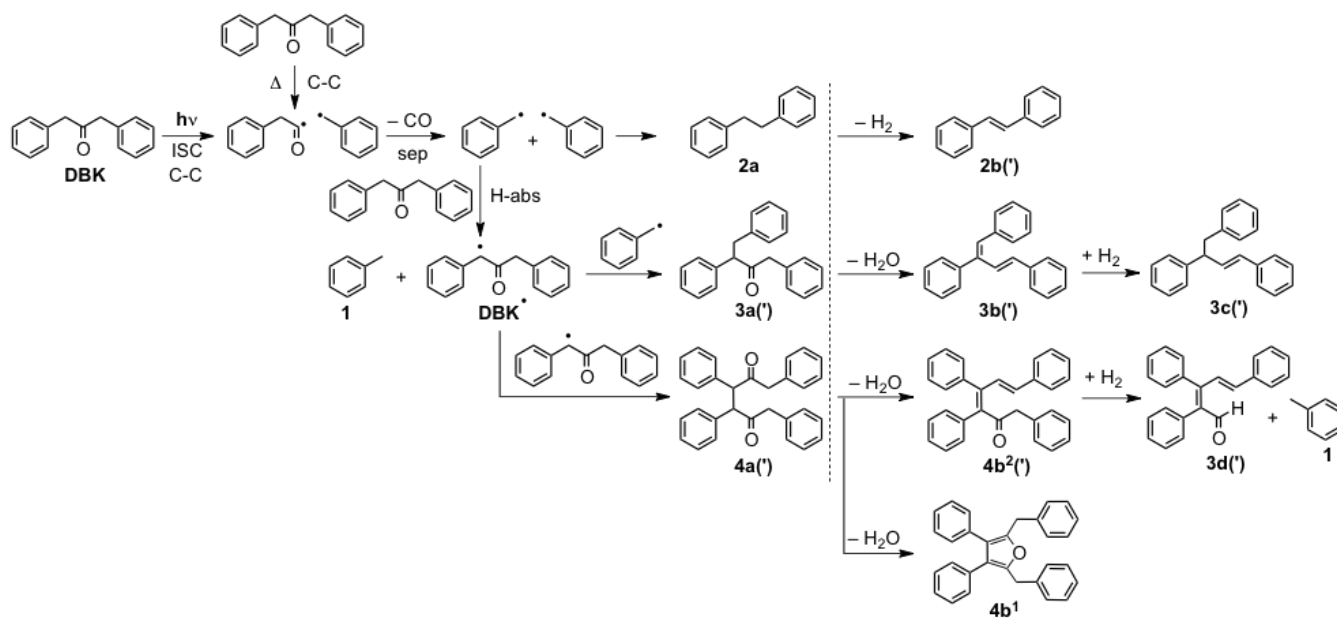
**Scheme I.** Schematic representation of functional group interconversions that connect simple hydrocarbons and carboxylic acids, proposed by Seewald (2001, 2003) for hydrothermal organic reactions.



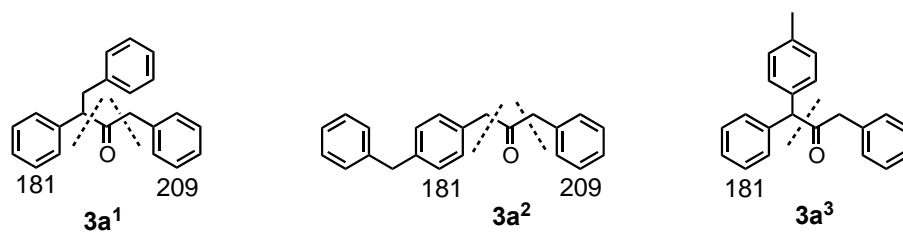
**Scheme II.** Summary of the main products of the hydrothermal reaction of **DBK** at 300°C and 700 bar (Yang et al., 2012). Fragmentation and coupling reactions that give the products **1**, **2a**, **2b**, **3a-d** and **4a,b** compete with reduction and dehydration reactions that form alcohol **2c**, alkene **2d** and alkane **2e**. The (') symbol means that the product is formed in more than one stereo- and/or structural isomeric form (**4b<sup>1</sup>** and **4b<sup>2</sup>** (') are structural isomers).



**Scheme III.** Proposed mechanism for the formation of the fragmentation and coupling products of the hydrothermal reaction of **DBK** at 300°C. The steps to the left of the dotted line are the radical processes that are observed in the hydrothermal photochemical reaction, while those to the right of the dotted line are the follow-up thermal reactions that are mainly ionic. The first step in the photochemical reaction combines excitation of **DBK** to the first singlet state ( $h\nu$ ), followed by intersystem crossing to the triplet state (ISC), and finally homolytic cleavage (C-C) to form a benzyl and a phenacyl radical. This radical pair is also formed in the thermal (non-photochemical) reaction, although much more slowly and in an overall singlet state. The second step (-CO/sep) includes decarbonylation and separation of the radicals in the geminate pair (sep). A separated benzyl radical reacts with **DBK** via hydrogen atom abstraction (H-abs) to yield toluene and a **DBK**-derived radical **DBK<sup>•</sup>**. The (') symbol associated with a structure indicates that more than one stereo- or structural isomer is formed. The products **4b<sup>1</sup>** and **4b<sup>2</sup>** (') are structural isomers.



**Scheme IV.** Structural isomers assigned as products of benzyl/**DBK** radical (**DBK**<sup>•</sup>) coupling observed in the gas chromatogram of Figure 1B. The major product is assigned to **3a<sup>1</sup>**. **3a<sup>2</sup>** and **3a<sup>3</sup>** are shown as *para*-coupling isomers, although *ortho*-coupling structures could also form. The dashed lines indicate the bonds that cleave to yield the *m/z* fragments indicated. For **3a<sup>3</sup>** the 181 peak in the mass spectrum is much larger than the 209 *m/z* peak.



**Scheme V.** The proposed mechanisms for Brønsted acid-catalyzed dehydration of **3a** and **4a** into **3b**(') and **4b**<sup>1</sup> and **4b**<sup>2</sup>(') (the ' symbol indicates stereo and/or structural isomers), via enol (**3e**(') and **4e**(')) and conjugated alkene intermediates (**3f**(') and **4f**(')). Acid can catalyze each step; only the first protonated intermediate is shown. Cyclization of the primary protonated intermediate is possible for **4a** (but not for **3a**) to give the furan **4b**<sup>1</sup>, a structural isomer of the dienones **4b**<sup>2</sup>('). The numbers in red are the heats of formation in kJ/mol at 300°C and 700 bar, calculated using the PM6 method with the solvent modeled using PMC as detailed in the supporting information. The values for the **3b**('), the **4b**<sup>2</sup>(') and **4b**<sup>1</sup> include the heat of formation of the water that is liberated in the last reaction, which is calculated to be -271 kJ/mol using the PM6/PCM method. The furan **4b**<sup>1</sup> is calculated to be more stable than the corresponding dienones **4b**<sup>2</sup>(') by ca. 60 kJ/mol under these conditions and using this method.

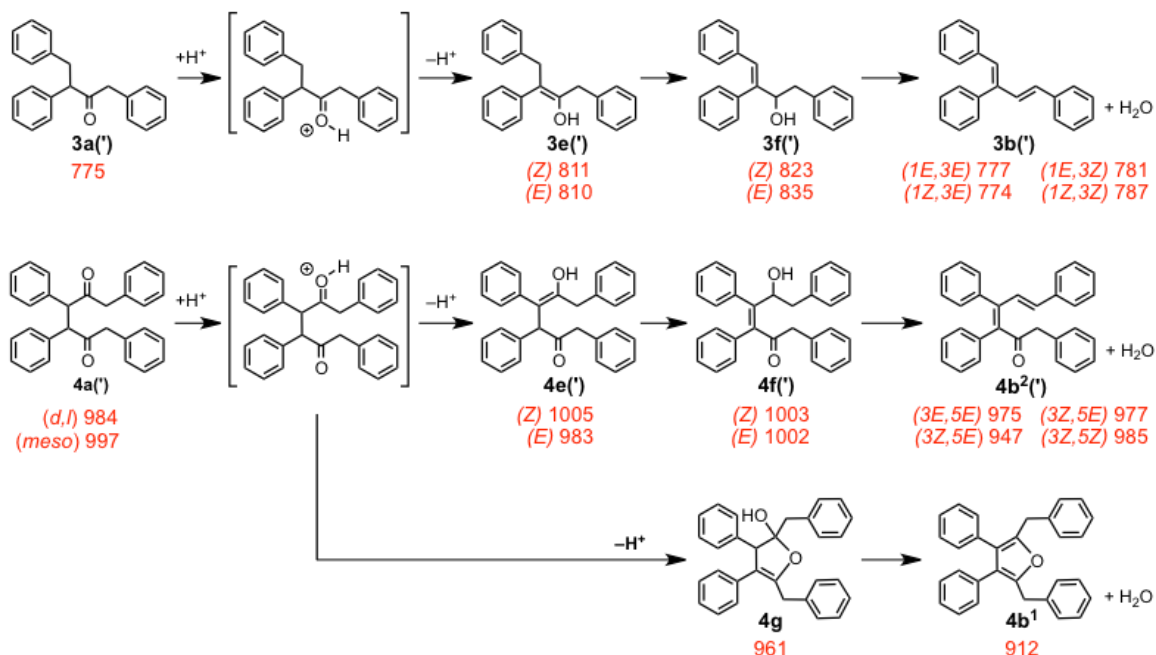


**Figure 1.** Gas chromatograms showing the product distributions for: (A, black) thermal reaction of **DBK** in water at 300°C and 86 bar (no light) for a time period of 7 days; (B, red) hydrothermal photolysis in water at 300°C and 86 bar for a time period of 33 mins; (C, blue) photolysis of **DBK** in methanol at room temperature (RT) for a time period of 33 mins. As indicated, the various products separate chromatographically into those that contain one, two, three and four benzene rings.

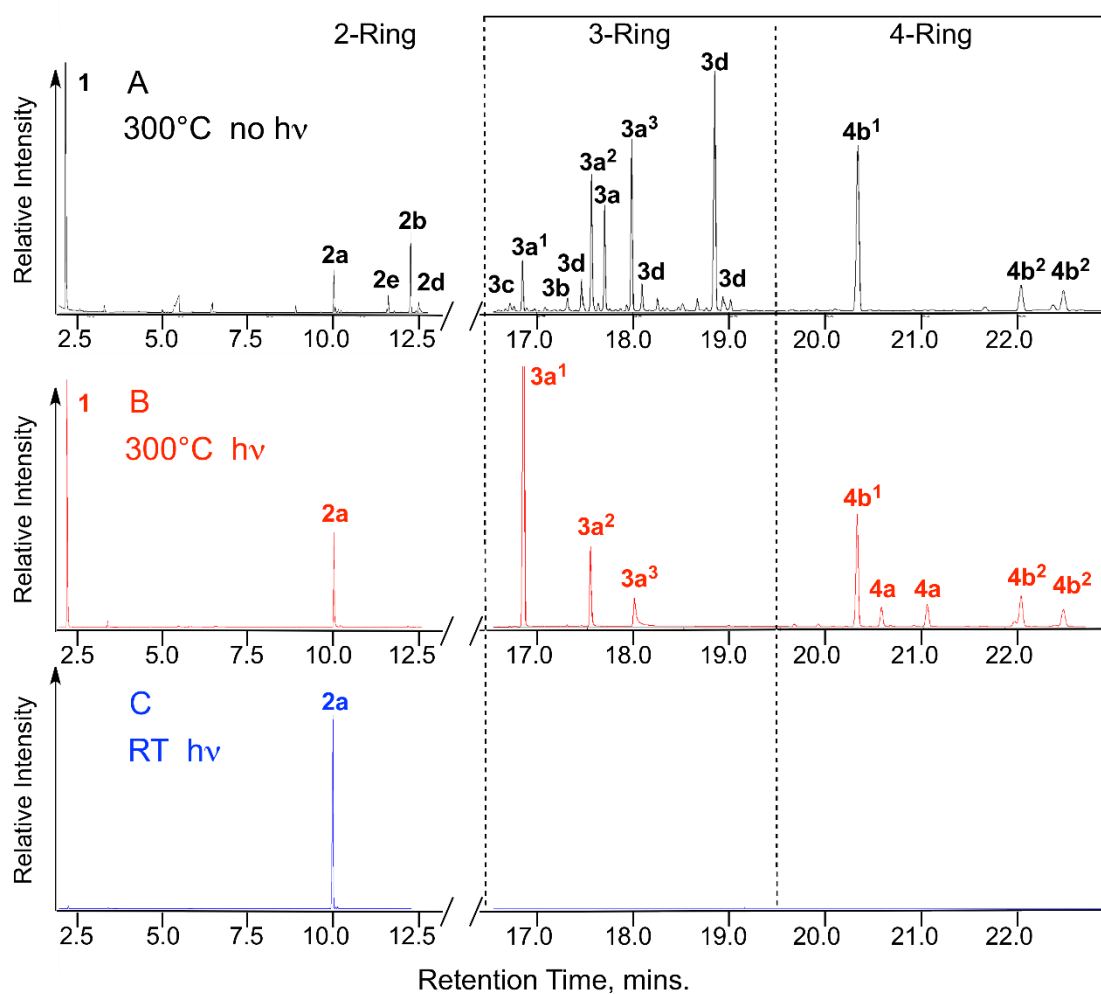


**Figure 2.** Comparison of product concentration versus irradiation time for the photolysis of **DBK** showing the formation of bibenzyl **2a** (blue, closed circles) as the only product in methanol at room temperature (RT), and the formation of bibenzyl **2a** (red, closed circles), toluene **1** (red, open circles), and the three-ring coupling product **3a<sup>1</sup>** (red, open triangles) in water at 300°C and 86 bar. The concentrations of the products at 300°C are corrected for the different conversions of **DBK** at the two reaction temperatures to allow direct comparison of their relative chemical yields to that of bibenzyl at room temperature.

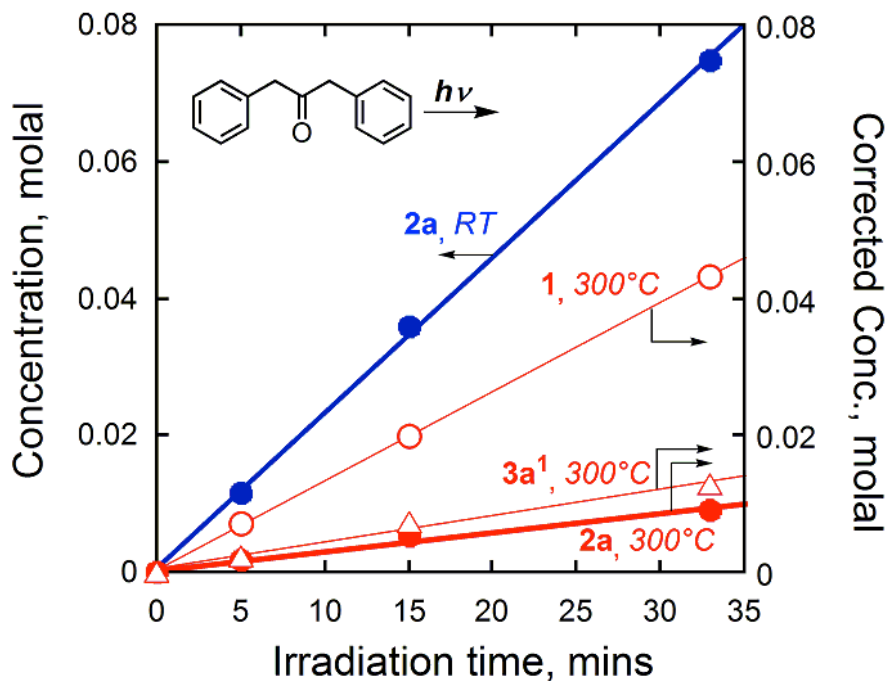




**Figure 3.** Concentration versus time plot for photolysis of **DBK** in water at 300°C at 86 bar for (open circles) the primary coupling product **4a** with the smaller retention time of the two diastereomers in Figure 1B, and (closed circles) the dehydrated four-ring product **4b<sup>1</sup>**.

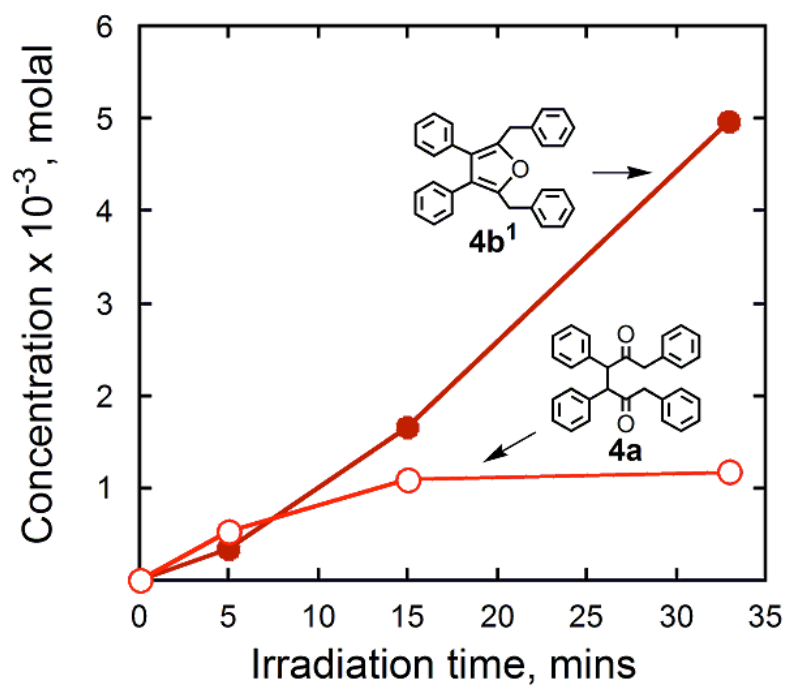


**Figure 4.** The time dependence of the concentration of toluene **1** compared to the sum of the concentrations of 3-ring products plus twice the sum of the concentration of the 4-ring products. These should be equal according to Eqn. 2, the small difference may be a consequence of assumed gas chromatography response factors for the coupling products (see supporting information) or other experimental uncertainties.

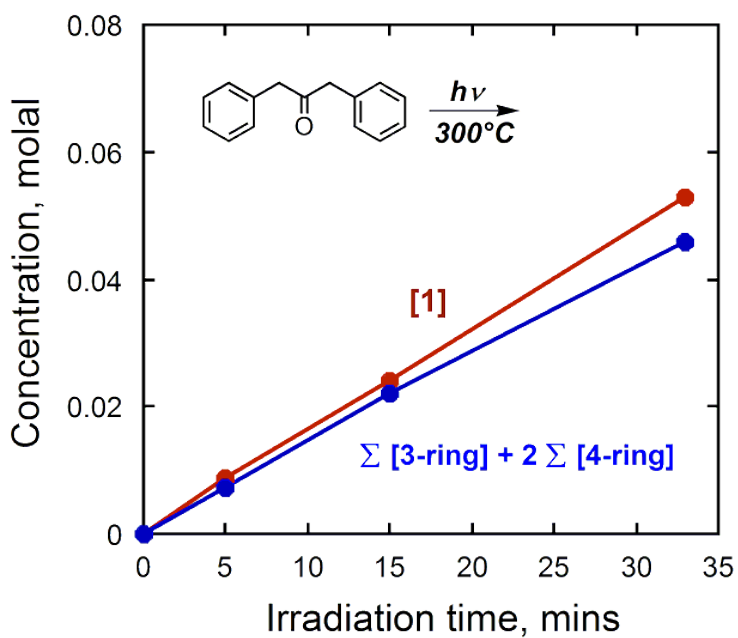


**Figure 5.** Electronic energy versus  $\alpha$ -hydrogen-benzylic carbon separation distance,  $r_{\text{C-H}\alpha}$ , for hydrogen atom abstraction from methylbenzylketone (**MBK**) by a benzyl radical, and the computed transition state structure located at an  $r_{\text{C-H}\alpha}$  of 1.41 Å, computed using B3LYP/aug-cc-pVDZ and PCM to model the solvent. The energies are referenced to **MBK** plus benzyl radical at infinite separation distance. The reaction is computed to be exothermic by 29 kJ/mol at 300°C and 700 bar. The computed free energy barrier for the reaction is 132 kJ/mol at 300°C and 700 bar.

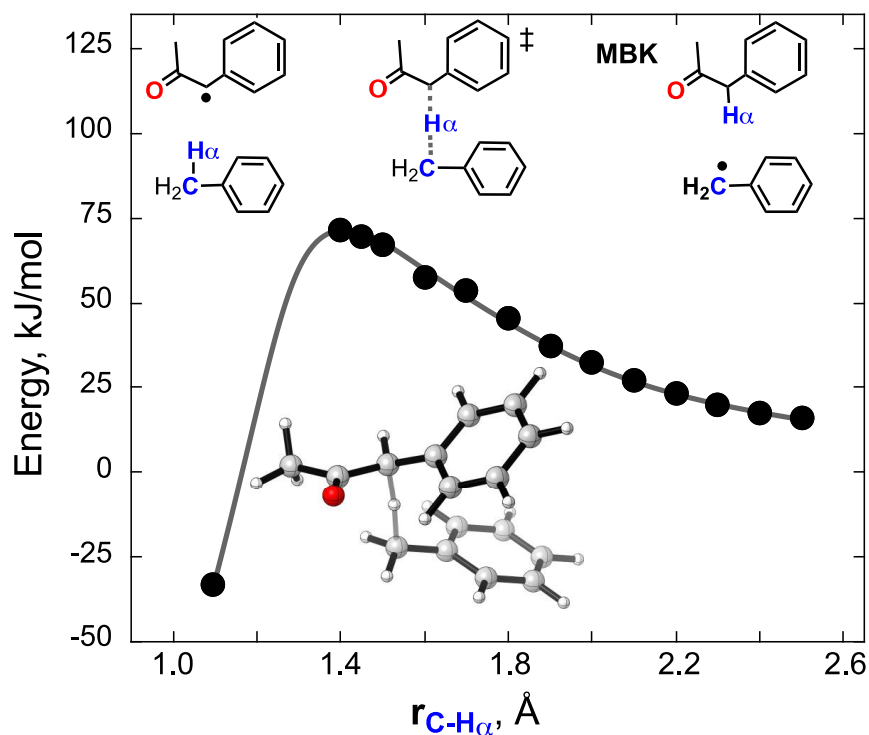


**Figure 6.** The time dependence of the concentration of **4a** as a fraction of the sum of the **4a** and **4b<sup>1</sup>** concentrations, for the dehydration reaction of **4a** to form the furan **4b<sup>1</sup>**, in water at 300°C and 86 bar. The **4a** stereoisomer is the one with the shorter gas chromatographic retention time in Figure 1B. **4a** is formed by hydrothermal photolysis of **DBK** for 2 minutes, followed by thermal dehydration for the various times indicated in the graph. The curve through the data corresponds to a pseudo-first order rate constant of 0.25 min<sup>-1</sup>.

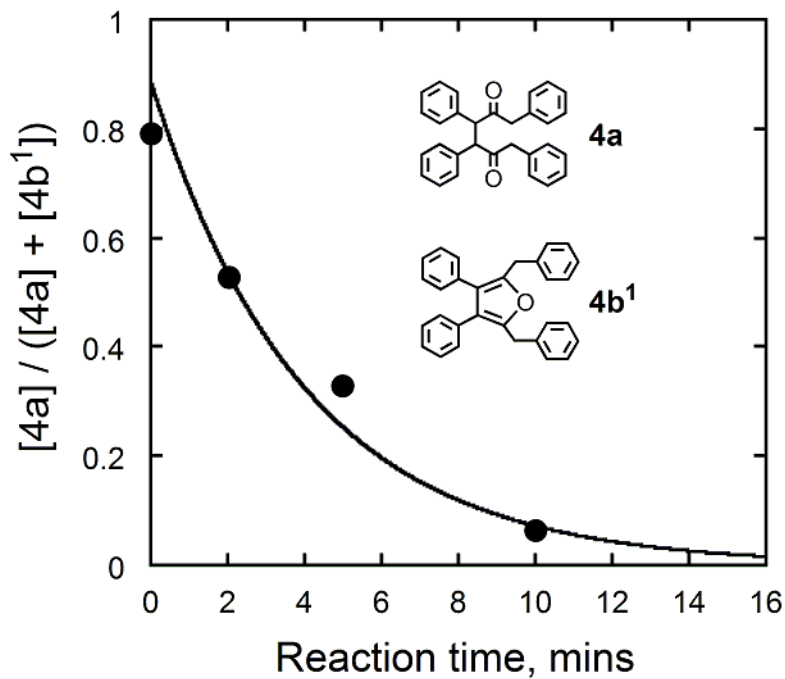


**Figure 7.** Computed structures of (left) the *(3Z,5E)*-isomer of the dienone **4b<sup>2</sup>**, and (right) the furan **4b<sup>1</sup>**, using the semi-empirical PM6 method, and using PCM to model water as the solvent, showing the lack of planarity and lack of conjugation between the carbon-carbon and carbon-oxygen double bonds in the dienone and increased planarity in the furan.

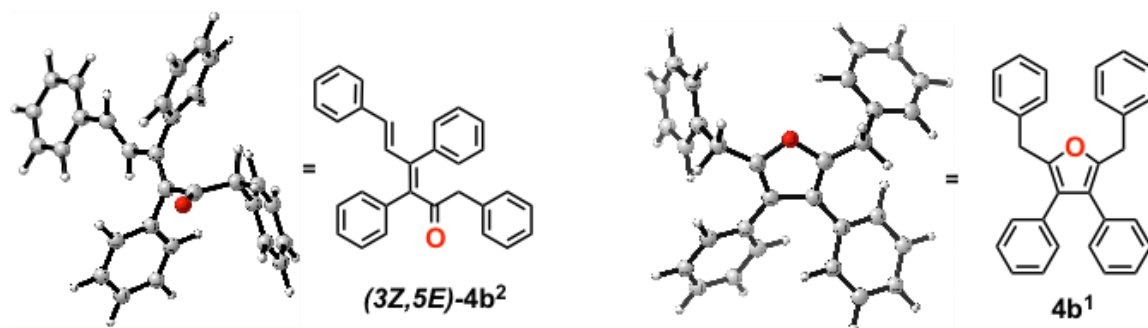


**Table S1.** Fractional chemical yields of products for hydrothermal photolysis of DBK at 300°C and 86 bar, at three different irradiation times, and the corresponding predicted quantum yields,  $\Phi_p$ , calculated using Eqn. S4.<sup>a</sup>

<b>Irradiation Time</b>	<b>Fractional yield of Bibenzyl</b>	<b>Fractional yield of 3-Ring products</b>	<b>Fractional yield of 4-Ring products</b>	<b><math>\Phi_p</math></b>
5 min	0.28	0.47	0.25	1.38
15 min	0.28	0.50	0.22	1.36
33 min	0.26	0.50	0.24	1.38

<sup>a</sup>The fractional yields are defined in the text.

**Figure S1.** (A) Percentage conversion of **DBK** as a function of irradiation time for (red) hydrothermal photolysis of 1 molal **DBK** in water at 300°C and 86 bar, and (blue) 0.7 molal **DBK** in methanol at room temperature. The ratio of the slopes is 1.23. (B) Percentage conversion of **DBK** as a function of irradiation time for (red) hydrothermal photolysis of 0.05 molal **DBK** in water at 300°C and 86 bar, and (blue) 0.035 molal **DBK** in methanol at room temperature. The ratio of the slopes is 1.5.

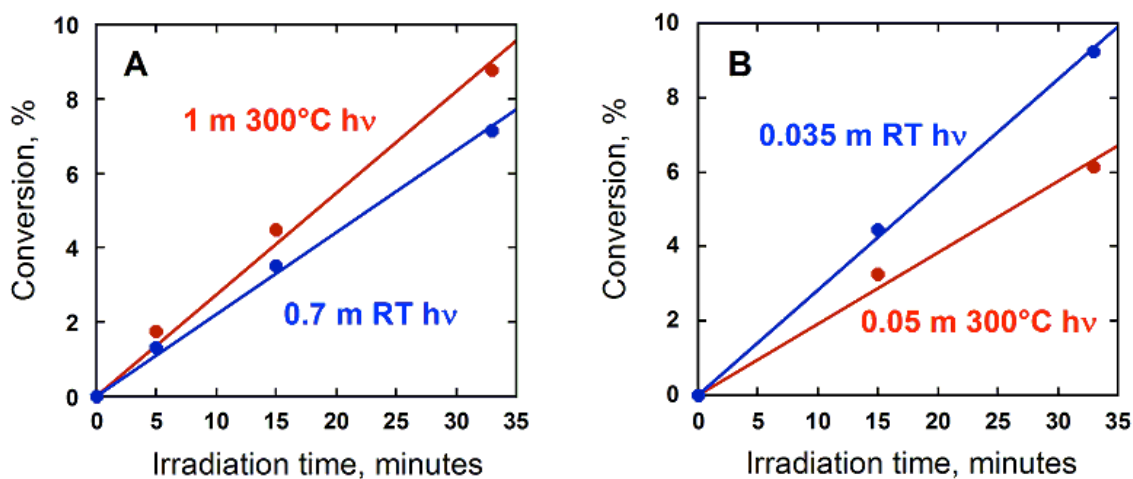


**Figure S2.** Mass spectra of products **3a<sup>1</sup>**, **3a<sup>2</sup>**, and **3a<sup>3</sup>**, with molecular ion of 300 m/z. The gas chromatography (GC) retention times refer to Figure 1B of the main text.

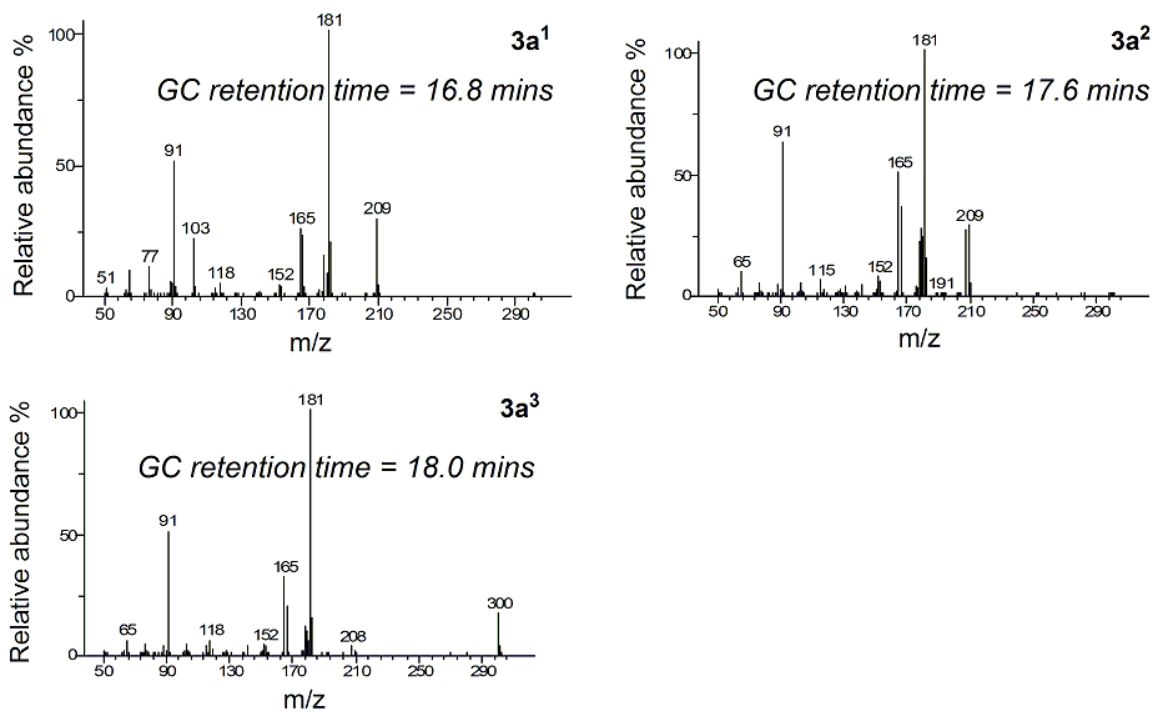




**Figure S3.** Mass spectra of the isomeric products **4a**. The molecular ion peak at 418 m/z is very small, but the major fragments with m/z of 327 and 91 sum to 418. The gas chromatography (GC) retention times refer to Figure 1B of the main text.

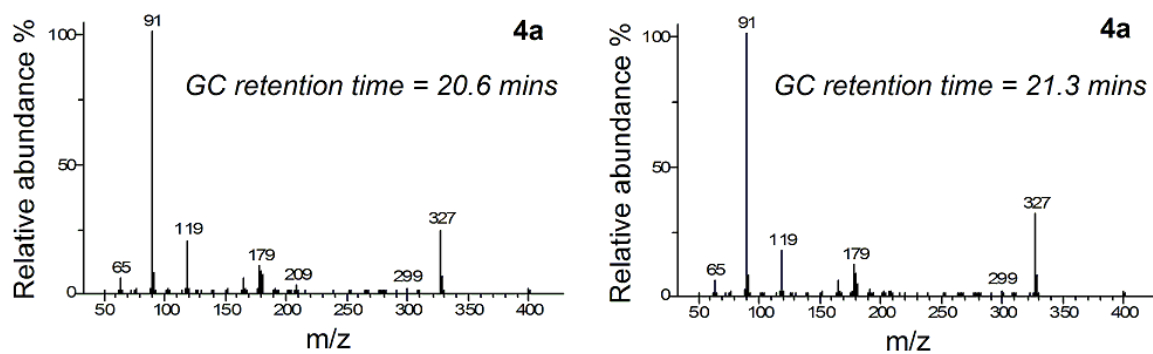
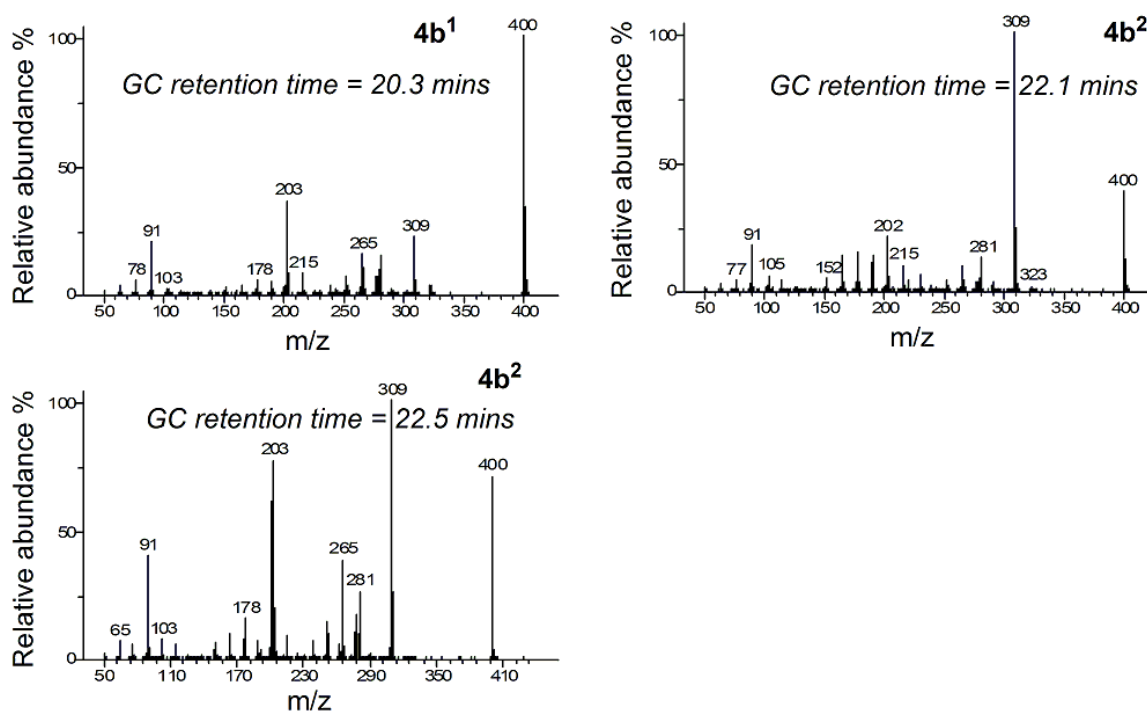


**Figure S4.** Mass spectra of the isomeric dehydration products **4b** with a molecular ion of 400 m/z. The structure assigned to the furan is **4b<sup>1</sup>**, which has a larger molecular ion peak than those of the two dienones indicated here as **4b<sup>2</sup>**, and a smaller fragmentation peak of m/z 309. The gas chromatography (GC) retention times refer to Figure 1B of the main text.



### 3.6. References

- Akiya N. and Savage P. E. (2001) Kinetics and mechanism of cyclohexanol dehydration in high-temperature water. *Ind. Eng. Chem. Res.* **40**, 1822-1831.
- Akiya N. and Savage P. E. (2002) Roles of water for chemical reactions in high-temperature water. *Chem. Rev.* **102**, 2725-2750.
- Amarnath V. and Amarnath K. (1995) Intermediates in the Paal-Knorr synthesis of furans. *J. Org. Chem.* **60**, 301-307.
- Antal M. J., Brittain A., DeAlmeida C., Ramayya S., Roy J. C. (1987) Heterolysis and hemolysis in supercritical water. *ACS Sym. Ser.* **329**, 77-86.
- Arbour C. and Atkinson G. H. (1989) Picosecond photodissociation of dibenzyl ketone. *Chem. Phys. Letts.* **159**, 520-525.
- Avola S., Guillot M., da Silva-Perez D., Pellet-Rostaing S. and Kunz W.; Goettmann F. (2013) Organic chemistry under hydrothermal conditions. *Pure Appl. Chem.* **85**, 89-103.
- Becke A. D. (1993) Density functional thermochemistry. III. The role of exact exchange. *J. Chem. Phys.* **98**, 5648-5652.
- Belsky A. J., Maiella P. G. and Brill T. B. (1999) Spectroscopy of hydrothermal reactions – 13. Kinetics and mechanisms of decarboxylation of acetic acid derivatives at 100-260°C under 275 bar. *J. Phys. Chem. A* **103**, 4253-4260.
- Blanksby S. J. and Ellison G. B. (2003) Bond dissociation energies of organic molecules. *Acc. Chem. Res.* **36** (4), 255-263.
- Bordwell F. G. and Harrelson J. A. (1990) Acidities and homolytic bond dissociation energies of the  $\alpha$ C-H bonds in ketones in DMSO. *Can. J. Chem.* **68**, 1714-1718.
- Burdige D. J. (2006) *Geochemistry of Marine Sediments*. Princeton University Press: Princeton, NJ.
- Dasgupta, R. (2013) Ingassing, storage, and outgassing of terrestrial carbon through geologic time. *Rev. Mineral. Geochem.* **75**, 183-229.

- Davidson E. R. (1996) Comment on “Comment on Dunning’s correlation-consistent basis sets”. *Chem. Phys. Lett.* **260**, 514-518.
- Dunning T. H. (1989) Gaussian basis sets for use in correlated molecular calculations. I. The atoms boron through neon and hydrogen. *J. Chem. Phys.* **90**, 1007-1023.
- Dust J. M. and Arnold D. R. (1983) Substituent effects on benzyl radical ESR hyperfine coupling constants. The .sigma..alpha..cntdot. scale based upon spin delocalization. *J. Am. Chem. Soc.* **105**, 1221-1227.
- Falkowski P., Scholes R. J., Boyle E., Canadell J., Canfield D., Elser J., Gruber N., Hibbard K., Hogberg P., Linder S., Mackenzie F. T., Moore B., Pedersen T., Rosenthal Y., Seitzinger S., Smetacek V. and Steffen W. (2000) The global carbon cycle: A test of our knowledge of earth as a system. *Science* **290**, 291-296.
- Fernandez-Ramos A., Miller J. A., Klippenstein S. J. and Truhlar D. G. (2006) Modeling the kinetics of bimolecular reactions. *Chem. Rev.* **106**, 4518–4584.
- Frisch M. J. et al. (2009) Gaussian 09, revision A.02. Gaussian, Inc., Wallingford, CT.
- Frisch M. J. et al. (2010) Gaussian 09, revision C.01. Gaussian, Inc., Wallingford, CT.
- GarciaGaribay M. A., Zhang Z. and Turro N. J. (1991) Diffusion and percolation of radical pairs in zeolite media – A product analysis study. *J. Am. Chem. Soc.* **113**, 6212-6218.
- Gould I. R., Baretz B. H. and Turro N. J. (1987) Primary processes in the Type I photocleavage of dibenzyl ketones - A pulsed laser and photochemically induced dynamic nuclear-polarization study. *J. Phys. Chem.* **91**, 925-929.
- Gould I. R., Turro N. J. and Zimmt M. B. (1984) In *Advances in Physical Organic Chemistry* (eds: Gold V. and Bethell D.). Academic Press, New York. Vol. 20, 1-51.
- Harvey A. H. and Friend D. G. (2004) In *Aqueous Systems at Elevated Temperatures and Pressures* (eds: Palmer D. A., Fernandez-Prini R. and Harvey A. H.). Elsevier, San Diego, CA.
- Helgeson H. C., Richard L., McKenzie W. F., Norton D. L. and Schmitt A. (2009) A

chemical and thermodynamic model of oil generation in hydrocarbon source rocks. *Geochim. Cosmochim. Acta* **73**, 594-695.

Hertwig R. H. and Koch W. (1997) On the parameterization of the local correlation functional. What is Becke-3-LYP? *Chem. Phys. Lett.* **268**, 345-351.

Hoering T. C. (1984) Thermal reactions of kerogen with added water, heavy water and pure organic substances. *Org. Geochem.* **5**, 267-278.

Horsfield B., Schenk H. J., Zink K., Ondrak R., Dieckmann V., Kallmeyer J., Mangelsdorf K., di Primo R., Wilkes H., Parkes R. J., Fry J. and Cragg B. (2006) Living microbial ecosystems within the active zone of catagenesis: Implications for feeding the deep biosphere. *Earth Planet. Sci. Lett.* **246**, 55-69.

Hunter S. E. and Savage P. E. (2004) Recent advances in acid-and base-catalyzed organic synthesis in high-temperature liquid water. *Chem. Eng. Sci.* **59**, 4903-4909.

Isegawa M., Fiedler L., Leverentz H. R., Wang Y., Nachimuthu S., Gao J. and Truhlar D. G. (2013) Polarized molecular orbital model chemistry. 3. The PMO method extended to organic chemistry. *J. Chem. Theory Comput.* **9**, 33-45.

Johnson J. W., Oelkers E. H. and Helgeson H. C. (1992) SUPCRT92: A software package for calculating the standard molal thermodynamic properties of minerals, gases, aqueous species, and reactions from 1 to 5000 bar and 0 to 1000°C. *Comput. Geosci.* **18**, 899-947.

Katritzky A. R., Nichols D. A., Siskin M., Murugan R. and Balasubramanian M. (2001) Reactions in high-temperature aqueous media. *Chem. Rev.* **101**, 837-892.

Kendall R. A., Dunning T. H. and Harrison R. J. (1992) Electron affinities of the first-row atoms revisited. Systematic basis sets and wave functions. *J. Chem. Phys.* **96**, 6796-6806.

Kuhlmann B., Arnett E. M. and Siskin M. (1994) Classical organic reactions in pure superheated water. *J. Org. Chem.* **59**, 3098-3101.

LaRowe D. E. and Van Cappellen P. (2011) Degradation of natural organic matter: A thermodynamic analysis. *Geochim. Cosmochim. Acta* **77**, 2030-2042.

Lehr G. F. and Turro N. J. (1981) Measurement of rate processes of free radicals in homogeneous and micellar solutions by cidnp. *Tetrahedron* **37**, 3411-3420.

- Li J. and Brill T. B. (2001) Spectroscopy of hydrothermal solutions 18: pH-dependent kinetics of itaconic acid reactions in real time. *J. Phys. Chem. A* **105**, 10839-10845.
- McCollom T. M. and Seewald J. S. (2003a) Experimental constraints on the hydrothermal reactivity of organic acids and acid anions: I. Formic acid and formate. *Geochim. Cosmochim. Acta* **67**, 3625-3644.
- McCollom T. M. and Seewald J. S. (2003b) Experimental study of the hydrothermal reactivity of organic acids and acid anions: II. Acetic acid, acetate, and valeric acid. *Geochim. Cosmochim. Acta* **67**, 3645-3664.
- McCollom T. M. and Seewald J. S. (2007) Abiotic synthesis of organic compounds in deep-sea hydrothermal environments. *Chem. Rev.* **107**, 382-401.
- McCollom T. M., Lollar B. S., Lacrampe-Couloume G. and Seewald J. S. (2010) The influence of carbon source on abiotic organic synthesis and carbon isotope fractionation under hydrothermal conditions. *Geochim. Cosmochim. Acta* **74**, 2717-2740.
- McSween H., Richardson S. and Uhle M. (2003) *Geochemistry: Pathways and Processes* (Second Edition). Columbia University Press, New York.
- Murov S. L., Carmichael I. and Hug G. L. (1993) *The Handbook of Photochemistry, 2nd Edition*. CRC Press, Boca Raton.
- Ott L., Bicker M. and Vogel H. (2006) Catalytic dehydration of glycerol in sub- and supercritical water: A new chemical process for acrolein production. *Green Chem.* **8**, 214-220.
- Palmer D. A. and Drummond S. E. (1986) Thermal decarboxylation of acetate. Part I. The kinetics and mechanism of reaction in aqueous solution. *Geochim. Cosmochim. Acta* **50**, 813-823.
- Reeves E. P., Seewald J. S. and Sylva S. (2012) Hydrogen isotope exchange between n-alkanes and water under hydrothermal conditions. *Geochim. Cosmochim. Acta* **77**, 582-599.
- Robbins W. K. and Eastman R. H. (1970a) Photodecarbonylation in solution. I. Quantum yields and quenching results with dibenzyl ketones. *J. Am. Chem. Soc.* **92**, 6076-6077.

- Robbins W. K. and Eastman R. H. (1970b) Photodecarbonylation in solution. II. Trapping of intermediates in the photolysis of dibenzyl ketone. *J. Am. Chem. Soc.* **92**, 6077-6079.
- Scalmani G. and Frisch M. J. (2010) Continuous surface charge polarizable continuum models of solvation. I. General formalism. *J. Chem. Phys.* **132**, 114110.
- Scuseria G. E. and Staroverov V. N. (2005) In *Theory and Applications of Computational Chemistry: The First 40 Years (A Volume of Technical and Historical Perspectives)* (eds: Dykstra C. E., Frenking G. and Kim K. S.). Elsevier, Amsterdam.
- Seewald J. S. (1994) Evidence for metastable equilibrium between hydrocarbons under hydrothermal conditions. *Nature* **370**, 285-287.
- Seewald J. S. (2001) Aqueous geochemistry of low molecular weight hydrocarbons at elevated temperatures and pressures: constraints from mineral buffered laboratory experiments. *Geochim. Cosmochim. Acta* **65**, 1641-1664.
- Seewald J. S. (2003) Organic-inorganic interactions in petroleum producing sedimentary basins. *Nature* **426**, 327-333.
- Seewald J. S., Zolotov M. Y. and McCollom T. (2006) Experimental investigation of single carbon compounds under hydrothermal conditions. *Geochim. Cosmochim. Acta* **70**, 446-460.
- Shanab K., Neudorfer C., Schirmer E. and Spreitzer H. (2013) Green solvents in organic synthesis: An overview. *Curr. Org. Chem.* **17**, 1179-1187.
- Shipp J., Gould I., Herckes P., Shock E., Williams L., and Hartnett H. (2013) Organic functional group transformations in water at elevated temperature and pressure: Reversibility, reactivity, and mechanisms. *Geochim. Cosmochim. Acta* **104**, 194-209.
- Shock E. L., Canovas P., Yang Z., Boyer G., Johnson K., Robinson K., Fecteau K., Windman T., and Cox A. (2013) Thermodynamics of organic transformations in hydrothermal fluids. *Rev. Mineral. Geochem.* **76**, 311-350.
- Siskin M. and Katritzky A. R. (1991) Reactivity of organic compounds in hot water – Geochemical and technological implications. *Science* **254**, 231-237.

- Siskin M. and Katritzky A. R. (2001) Reactivity of organic compounds in superheated water: general background. *Chem. Rev.* **101**, 826-835.
- Siskin M., Katritzky A. R. and Balasubramanian M. (1995) Aqueous organic chemistry. 9. Reactivity of 1,5-, 1,6-, 1,7- and 2,6-dihydroxynaphthalenes, dibenzofuran, 2-hydroxydibenzofuran, carbazole, 2-hydroxycarbazole, acridine and 4-hydroxyacridine. *Fuel* **74**, 1509-1511.
- Stephens P. J., Devlin F. J., Chabalowski C. F. and Frisch M. J. (1994) Ab initio calculation of vibrational absorption and circular dichroism spectra using density functional force fields. *J. Phys. Chem.* **98**, 11623-11810.
- Stewart J. J. P. (2007) Optimization of parameters for semiempirical methods V: Modification of NDDO approximations and application to 70 elements. *J. Mol. Model.* **13**, 1173-1213.
- Tassi F., Vaselli O., Capaccioni B., Montegrossi G., Barahona F. and Caprai A. (2007) Scrubbing process and chemical equilibria controlling the composition of light hydrocarbons in natural gas discharges: An example from the geothermal fields of El Salvador. *Geochm. Geophys. Geosys.* **8**, doi:10.1029/2006GC001487.
- Turro N. J. (1982) Laser flash spectrometric investigations of biradicals and caged radical pairs. *Tetrahedron* **38**, 809-917.
- Turro N. J. (2000) From boiling stones to smart crystals: Supramolecular and magnetic isotope control of radical-radical reactions in zeolites. *Acc. Chem. Res.* **33**, 637-646.
- Turro N. J. and Weed G. C. (1983) Micellar systems as "supercages" for reactions of geminate radical pairs - Magnetic effects. *J. Am. Chem. Soc.* **105**, 1861-1868.
- Turro N. J., Gould I. R. and Baretz B. H. (1983) Absolute rate constants for decarbonylation of phenylacetyl and related radicals. *J. Phys. Chem.* **87**, 531-532.
- Turro N. J., Ramamurthy V. and Scaiano J. C. (2010) *Modern Molecular Photochemistry of Organic Molecules*. University Science Books, Sausalito, CA.
- Uematsu M. and Franck E. U. (1980) Static dielectric constant of water and steam. *J. Phys. Chem. Ref. Data* **9**, 1291-1306.



- Watanabe M., Sato T., Inomata H., Smith Jr. R. L., Arai K., Kruse A. and Dinjus E. (2004) Chemical reactions of C<sub>1</sub> compounds in near-critical and supercritical water. *Chem Rev.* **104**, 5803-5821.
- Xu X., Antal M. J. and Anderson D. G. M. (1997) Mechanism and temperature-dependent kinetics of the dehydration of tert-butyl alcohol in hot compressed liquid water. *Ind. Eng. Chem. Res.* **36**, 23-41.
- Yamamoto M., Yokota Y., Oshima K. and Matsubara S. (2004) H-D exchange reaction on benzene ring of polystyrene in hydrothermal deuterium oxide with platinum (IV) oxide catalyst. *Chem. Comm.* **15**, 1714-1715.
- Yang Z., Gould I. R., Williams L., Hartnett H., and Shock E. L. (2012) The central role of ketones in reversible and irreversible hydrothermal organic functional group transformations. *Geochim. Cosmochim. Acta* **98**, 48-65.

## CHAPTER 4:

### INFLUENCE OF MINERALS ON HYDROTHERMAL REACTIONS OF KETONES

#### 4.1. Abstract

Hydrothermal organic transformations occurring in geochemical processes can be influenced by surrounding environments including minerals. This work focused on the influence of several common iron-containing minerals on the hydrothermal reactions of a model ketone, dibenzylketone (DBK). The ketone group was chosen for study because they play a central role in many hydrothermal organic functional group transformations, including those between hydrocarbons and oxygen-bearing compounds. Specific effects of the individual mineral were observed from the hydrothermal reactions of DBK. Quartz ( $\text{SiO}_2$ ) and corundum ( $\text{Al}_2\text{O}_3$ ) had no detectable effect, whereas hematite ( $\text{Fe}_2\text{O}_3$ ), magnetite ( $\text{Fe}_3\text{O}_4$ ), and troilite ( $\text{FeS}$ ) all increased DBK reactivity to various extents. Under the experimental conditions (300°C, 70 MPa, and up to 168 h), magnetite elevated DBK reactivity by almost an order of magnitude, when compared to DBK in  $\text{H}_2\text{O}$  alone. Primary products distributions were examined at early reaction times, and it indicated that the fragmentation products were more dominating in the presence of hematite or magnetite than  $\text{H}_2\text{O}$  alone, while much more reduced products from DBK were observed in the presence of troilite. Potential roles of the iron-containing minerals were additionally explored by attempting the hydrogen balance calculation, the dissolved  $\text{H}_2$  measurement, and the experiments as a function of added mineral surface areas. The facilitated DBK decomposition rates with the iron oxides minerals appear to be mainly

attributed to mineral surface-promoted reactions, while troilite was likely to expedite the reduction products formation by contributing dissolved inorganic compounds in solution and delivering hydrogen atoms from H<sub>2</sub>O to organic compounds.

## **4.2. Introduction**

The hydrothermal chemistry of organic compounds influences a wide range of critical geochemical processes, including the degradation and transport of organic matter in sedimentary systems (Seewald, 2003), the formation of oil and gas reservoirs (Head et al., 2003; Larter et al., 2003; Jones et al., 2008), and as part of the metabolic cycles of microbes in subsurface environments (Head et al., 2003; D'Hondt et al., 2004; Simoneit et al., 2004; Hinrichs et al., 2006; Horsfield et al., 2006; McCollom and Seewald, 2007; Mason et al., 2010; Shock and Canovas, 2010). The chemistry of a large number of organic structures under hydrothermal conditions has been reported (Bell and Palmer, 1994; Cody et al., 2001; Katrizky et al., 2001; McCollom and Seewald, 2003; Watanabe et al., 2004; McCollom, 2013), and thermodynamic properties and models of many organic compounds in the gas and aqueous phase are available (Shock and Helgeson, 1990; Shock, 1995; Helgeson et al., 1998; Plyasunov and Shock, 2000, 2003; Shock, 2000; LaRowe and Helgeson, 2006; Helgeson et al., 2009; LaRowe and Dick, 2012). Attempts to systematically study the chemistry of various organic functional groups have also been made at various elevated temperatures and pressures in aqueous media (Savage, 1999; Andersson and Holm, 2000; Akiya and Savage, 2001; Katrizky et al., 2001; Siskin

and Katrizky, 2001; McCollom and Seewald, 2007; Yang et al., 2012; Shipp et al., 2013; McCollom, 2013).

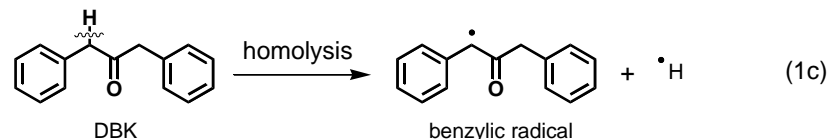
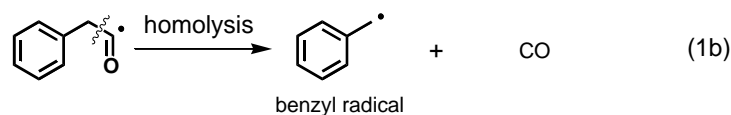
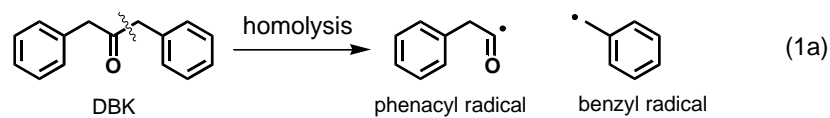
Geochemical processes involving organic compounds take place not just in an aqueous medium, but with gases and electrolytes, variable pH, and perhaps most importantly, inorganic materials such as minerals and clay substrates. Suggestions that minerals can, and perhaps should, influence organic hydrothermal reactivity have been made for decades (Jurg and Eisma, 1964; Shimoyam and Johns, 1971; Espitalié et al., 1980; Simoneit, 1992; Seewald, 2001; McCollom and Seewald, 2003). There have been impressive reports of the ways in which naturally occurring inorganic substrates can influence the stability of organic structures under hydrothermal conditions (Leif and Simoneit, 2000; Cody et al., 2001; Seewald, 2001; Foustoukos and Seyfried, 2004; Fu et al., 2008; Williams et al., 2010). In addition, many hydrothermal studies took the aid of mineral assemblages, because variables including the oxidation state, the pH, and the dissolved sulfur species of hydrothermal environment can be controlled experimentally (Seewald, 1994, 2001; Andersson and Holm, 2000; McCollom and Seewald, 2003; Reeves et al., 2012; McCollom 2013). For instance, pyrite-pyrrhotite-magnetite, hematite-magnetite, and hematite-magnetite-pyrite assemblages have been used to regulate the activities of dissolved  $H_2$  and  $H_2S$  in hydrothermal solution (e.g., Seewald 2001). Different roles of these iron-containing minerals in organic hydrothermal reactions have been found, including the promotion of bond cleavage processes on the mineral surface, and the alteration of solution properties such as ionic strength, pH, and dissolved metals and sulfur inorganic species. As an example, Reeves et al. (2012) used a pyrite-pyrrhotite-magnetite mineral assemblage to provide a redox-buffered

hydrothermal environment for C<sub>1</sub>-C<sub>5</sub> n-alkanes at 323°C and 350 bar, where they observed reversible and extensive water-derived hydrogen incorporation into C<sub>2</sub>-C<sub>5</sub> n-alkanes, but comparatively little exchange for CH<sub>4</sub>. They suggest that the occurrence of isotopic exchange should be within reversible equilibration between the alkane and the corresponding alkene. McCollom (2013) studied the influence of iron oxide and sulfide minerals on hydrothermal decomposition of amino acids norvaline and alanine, using hematite-magnetite-pyrite and pyrite-pyrrhotite-magnetite assemblages. The observed fact that both amino acids decomposed more rapidly and with altered product distributions in the presence of minerals compared water alone, allows him to successfully propose that the mineral effects were due to both surface catalysis and solution chemistry change.

Although mineral assemblages own the advantage of regulating hydrothermal fluid chemistry, the understanding of potential contribution of each individual mineral, such as among those common iron oxides and sulfides, may remain complicated. Which specific minerals enhance, suppress, or do not influence organic hydrothermal reactivity? Which minerals initiate new reaction pathways? When they influence reactions, which minerals are responsible for surface-promoted reactions and which behave as reactants by changing water chemistry? Additionally, the mineral effects on hydrothermal reactions of ketones have not been addressed yet. In an attempt to provide an entry to answering these questions, here a study of individual mineral influence on the hydrothermal chemistry of ketones, has been initiated. In the previous work, the reaction pathways and mechanisms of a model ketone, dibenzylketone (DBK), has been systematically studied in the absence of minerals under specific hydrothermal conditions (Yang et al., 2012).

As a derived project, this work summarizes the first results from hydrothermal experiments with DBK in the presence of common iron-containing minerals, hematite ( $\text{Fe}_2\text{O}_3$ ), magnetite ( $\text{Fe}_3\text{O}_4$ ), and troilite ( $\text{FeS}$ ). For comparison, corundum ( $\text{Al}_2\text{O}_3$ ) and quartz ( $\text{SiO}_2$ ), which are expected to be insensitive to redox reactions, are also included.

The ketone functional group has been selected for study since ketones occupy a central role in the reaction pathway proposed by Seewald (2003) that links alkanes with carboxylic acids (Fig. 1). Ketones represent the critical point at which carbon-carbon (C-C) bond cleavage must occur in order to form carboxylic acids. It was found that DBK is a useful model ketone because the benzylic position adjacent to the carbonyl carbon allows relatively facile C-C bond fragmentation, which enables the reactions to occur on a reasonable laboratory timescale. An in-depth analysis of the hydrothermal reaction products for DBK reveals extensive C-C bond cleavage, although it is noteworthy that carboxylic acids were not formed in detectable quantities in  $\text{H}_2\text{O}$  alone under the experimental conditions (Yang et al., 2012). Many of the observed products were consistent with radical coupling reactions, which support the interpretation that homolytic C-C bond cleavage forms a pair of radicals as primary intermediates (Eqns. 1a, 1b and 1c).



Toluene was observed as the major C-C bond cleavage product. Fragmentation of the carbon-hydrogen (C-H) bond at the benzylic position was also observed, and this process provides a source of hydrogen atoms (Eqn. 1c), which can be used in the formation of reduced products. Reduced products form in the reaction sequence from ketone to alcohol to alkene to alkane (Fig. 1), which was previously named as the reduction pathway (Yang et al., 2012). Many oxidized (dehydrogenated) radical coupling products are also produced, and approximate hydrogen balance is observed under the experimental conditions of a sealed gold capsule. Two benzyl radicals can be formed via homolytic cleavage of a C-C bond in DBK, since the phenacyl radical formed in Eqn. 1a decarbonylates rapidly in Eqn. 1b. Benzyl radicals were precursors to many primary coupling products (see Chapter 2). Many of the primary coupling products can undergo further bond cleavage, or functional group transformations, to form secondary alkenes and alkanes that are analogous to the DBK reduction pathway. Almost all of the observed products from DBK can be understood arising from Eqns. 1a, 1b and 1c and the reversible pathways in Fig. 1.

Building upon the previous observations in the absence of minerals, the goals of this work are: (1) to perform hydrothermal reactions with DBK in the presence of different kinds of minerals, and to look for changes in DBK decomposition rates, products distribution, and the reaction pathways (i.e., the reduction pathway and the bond fragmentation pathways); (2) to investigate the potential contribution of individual mineral on the reactivity of ketones, whether it initiates surface-promoted reactions or serves as a reagent, and (3) to explore new reaction pathways of ketones with the aid of minerals, in particular formation of carboxylic acids. In order to minimize complications associated with secondary reactions, the same strategy was applied as in the previous work that was to run the reactions to low conversions. It is thus helpful for interpreting the kinetics and product distributions of the reactions at early times, rather than establishing and measuring thermodynamic equilibrium at longer reaction durations.

### **4.3. Experimental**

#### *4.3.1. Reagents*

Most of the organic chemicals were available from previous work (see Chapter 2). Minerals used in this work include finely powered synthetic hematite ( $\text{Fe}_2\text{O}_3$ , 99.5%, metals basis, -325 mesh), magnetite ( $\text{Fe}_3\text{O}_4$ , 97%, metals basis, -325 mesh), corundum ( $\text{Al}_2\text{O}_3$ , 99.9%, metal basis, -325 mesh), and quartz ( $\text{SiO}_2$ , 99.5%, metal basis, -325 mesh), all purchased from Alfa Aesar. Troilite ( $\text{FeS}$ , 99.9%, metal basis, Alfa Aesar) was powdered further using a McCone Mill (to reach -325 mesh). The compositions and



purities of all used minerals were verified by X-ray diffraction (XRD) analysis using a Siemens D-5000 spectrometer, and the XRD patterns revealed their crystal structures were >95% consistence with database. The surface area of each mineral was measured by the Brunauer, Emmett and Teller (BET) gas adsorption technique using N<sub>2</sub> as the adsorptive species in Tristar II 3020. The hematite, magnetite, and powdered troilite were found to have BET surface areas of 12.90 m<sup>2</sup>/g, 7.82 m<sup>2</sup>/g and 9.29 m<sup>2</sup>/g, respectively. Quartz and corundum were found to be 5.32 m<sup>2</sup>/g and 5.28 m<sup>2</sup>/g, respectively. To remove any tiny or nano-sized particulates, a clean-up protocol was attempted with a magnetite sample by repeated sonication and centrifugation. The size distribution of the magnetite particles that were treated this way showed a slight decrease in the relative number of smaller particles upon scanning electron microscopy (SEM). The BET surface area for the treated magnetite was measured to be 7.68 m<sup>2</sup>/g, which is slightly lower than the untreated magnetite, 7.82 m<sup>2</sup>/g.

#### 4.3.2. Procedures

Experiments were performed using gold capsules (5 mm outer diameter, 4 mm inner diameter, and length of ~37.5 mm) with an internal volume of roughly 1.75 mL. The capsules were cleaned by treating with concentrated HCl, followed by boiling in deionized water, and then annealing at 580°C for 12 h before use. The capsules were first arc-welded at one end using a precision welder before loading solids and water. Oxygen was removed by gently purging the empty capsule with ultra-high purity argon for one minute. 42 mg of purified DBK and different amounts of minerals were added in

separate experiments. 200  $\mu\text{L}$  of argon-purged deionized water was then added to the capsules to make the DBK concentration as one molal, followed by a second purging of the headspace using argon before pinching the end closed. Capsules were quickly frozen using liquid nitrogen, and submerged in a methanol:ice (1:1) cold bath to minimize evaporative losses during the arc welding.

The gold capsules were placed into a 51 cm stainless steel cold seal pressure vessel (Williams et al., 2001) that was filled with DI water to pressurize the gold capsules to 70 MPa (10,150 psi) at 300°C. Temperature was monitored by a thermocouple inside the pressure vessel directly adjacent to the reacting capsules. Hematite, magnetite and troilite experiments were performed in time series up to 168 h, using a constant surface area of  $\sim 1.29 \text{ m}^2$  (Table 1). Because of the large heat capacity, the pressure vessel required ca. 3 h for the furnace to heat the sample up to 300°C, so the time zero point for each experiment was taken to be the time when the temperature reached 298°C. Experiments using various mineral surface areas were also conducted at a fixed reaction time of 70 h at 300°C, 70 MPa (Table 2). Other than  $1.29 \text{ m}^2$ , surface areas of  $\sim 0.53 \text{ m}^2$  and  $\sim 0.91 \text{ m}^2$  were also used for all the five minerals, and  $0.31 \text{ m}^2$  was additionally selected for magnetite. After the desired experimental duration, the pressure vessels were quenched rapidly in an ice bath and the gold capsules were removed. The experiments

were determined to be successful only if the gold capsule weights before and after each experiment were consistent using a 0.01 mg-scale balance.

#### *4.3.3. Product analysis*

The extraction procedures of products were similar to those described in the previous Chapters. Briefly, the capsules were frozen in liquid nitrogen before cutting open with a scalpel. The organic products in the opened capsules were extracted using 3.0 mL of DCM containing decane and dodecane as internal standards in a 4 mL silanized glass vial (Supelco Inc.) with shaking using a Vortex Genie 2 for two minutes. The suspended mineral powders were allowed to settle before transferring the DCM solution into 1.5 mL silanized glass vials for gas chromatography (GC) analysis. A Varian CP-3800 gas chromatograph equipped with a poly capillary column (5% diphenyl/95% dimethylsiloxane, Supelco Inc.) and a flame ionization detector was used to analyze the organic products. The detection limit for carboxylic acids was found to be near 0.05 mmolal. The reaction products were identified by co-injecting purchased standard samples (if available) in the GC, together with comparing mass spectra data obtained from high resolution gas chromatography-mass spectrometry (HR-GC-MS). For those ambiguous products with relatively high molecular weights, possible structures were deduced both from molecular ion fragmentation patterns on the mass spectra and comparing to multi-benzene-ring structures determined in the DBK in water alone results.

The mass balance for the reactions was estimated using the same method described in Chapter 2, i.e., comparing the total number of benzene rings in the products

to the total number of benzene rings in the consumed DBK molecules. The concentrations of the products containing multi-benzene-rings were quantified based on the measured or estimated GC response factors (see Chapter 2). Because of the increasing complexity and large number of products observed in longer hydrothermal experiments in the presence of iron-bearing minerals, some small unidentified products were not included in the mass balance calculations. Errors in the mass balance calculations vary from  $\pm 10$ -20% depending on the duration of the experiment, as well as the extent of conversion of DBK. The average uncertainty was estimated to be  $\pm 15\%$ .

Hydrogen balance was estimated based on the numbers of hydrogen atoms in the organic products and the reacted DBK. To maximize the differences, the five hydrogen atoms on the benzene rings of consumed DBK and the aromatic products were not counted. Since the accuracy of the hydrogen balance calculation essentially depends on the accuracy of the mass balance, and the average uncertainty of hydrogen balance was estimated to be  $\pm 18\%$ . In the presence of the minerals, the hydrogen balance calculations were only attempted at early reaction times, when the DBK conversion was relatively low and the product distributions were relatively simple.

To test the validity of hydrogen balance calculations, measurements of dissolved  $H_2$  have been attempted using gas chromatography with reducing compound photometer detection (GC-RCP, Peak Laboratories, LLC). Once the desired duration was reached, the hydrothermal experiment was quickly quenched, and the gold capsule was transferred into a sealed and argon-purged gas vial (Labco Exetainer®) with a known empty volume ( $\sim 12$  mL). The background concentration of  $H_2$  in the argon-purged vial was pre-determined by triplicate injections of 25  $\mu$ L gas samples, and the percent error was found

less than 5%. Calibration cuves that were built using H<sub>2</sub> gas standards were used to quantify the concentration of H<sub>2</sub> in the vial. A solid needle inserted through the septum on the vial cap was used to puncture the gold capsule and to release the gases at room temperature. After one-minute shaking and equilibrating, three 25  $\mu$ L of gas mixture were taken from the sample vial using a gas-tight syringe and injected into the GC. The actual concentration of H<sub>2</sub> was calculated by subtracting the background concentration from the measured value. With ideal gas assumption, moles and molality of H<sub>2</sub> in the gold capsule can thus be estimated (Table 2). The standard detection limit of molecular hydrogen in GC-RCP can reach as low as 800 ppt (part per trillion). Several repeated H<sub>2</sub> measurement experiments were also conducted using separate gold capsules, and the average analytical uncertainty was estimated to be  $\pm 25\%$ .

#### **4.4. Results and discussion**

##### *4.4.1. Decomposition of DBK*

Hydrothermal reactions of DBK were performed in the presence of five different minerals: hematite, magnetite, troilite, corundum and quartz, with varying masses of mineral in the gold capsule, but with a constant surface area of  $\sim 1.29 \text{ m}^2$ . This surface area is dictated by the quantity of mineral that could be loaded into the capsule. Of these, hematite, magnetite, and troilite substantially influenced the rates of DBK decomposition and the reaction product distributions, whereas corundum and quartz had no detectable influence under the conditions of the experiment. The effects are easily seen in the DBK

percent conversion as a function of reaction time, as shown in Fig. 2. It appears that the decomposition of DBK is much faster in the presence of the three iron-containing minerals compared to water alone, with magnetite in particular being most effective. As an example, after a 70-h reaction progress, the DBK conversion with magnetite was ca. 24%, whereas only a ca. 3.7% of DBK decomposed in hydrothermal water alone. More experimental data for the time-dependent experiments for magnetite, hematite and troilite are summarized in Table 1.

The DBK conversion in the presence of magnetite is sufficiently large to attempt a kinetic analysis. Shown as an inset in Fig. 2 is the yield of DBK plotted versus time. The yield is determined as the percentage of the DBK that is remaining (e.g., 100% yield at time zero by definition). By assuming a pseudo-first-order reaction with respect to DBK and a complete conversion, the reaction rate constant was estimated to be  $3.7 \pm 0.3 \times 10^{-3} \text{ hr}^{-1}$  in the magnetite experiments, where the observed maximum DBK conversion was ca. 46.8% over 168 hours (Table 1). Similarly, the reaction rate constant in the absence of minerals was found to be  $3.0 \pm 0.6 \times 10^{-4} \text{ hr}^{-1}$ , where the maximum DBK conversion was only 14.5% over 528 h (Table 1). Under the assumptions, the increase in pseudo-first-order rate constant is at least an order of magnitude in the presence of magnetite compared to water alone. If assigning this rate constant increase to the influence of magnetite, the absolute rate constant of the DBK-magnetite reaction will be ca.  $3.4 \times 10^{-3} \text{ hr}^{-1}$  for a mineral surface area of  $1.29 \text{ m}^2$ , or an area ratio (DBK molecules surface area/mineral surface area) of ca. 33 (see further below).

In common with many hydrothermal reactions of organic structures, DBK can form rather a large number of products, although many of them were possibly from

secondary or follow-up reactions. Interpretation of product distributions is thus most readily accomplished at the early reaction times before the accumulation of appreciable quantities of secondary products. Shown in Fig. 3 are the main hydrothermal reaction pathways for DBK, with an abbreviated summary of the main product structure types. Three major reaction pathways are included: the fragmentation pathway, the reduction pathway, and the acid pathway. The products in the fragmentation pathway are associated with the C-C and C-H hemolytic cleavage and radical coupling reactions. The main difference between Fig. 3 and Fig. 1 is that the fragmentation pathway is expanded to show the various structure types that are formed via bond cleavage. The reduction pathway gives the alcohol R1, the alkene R2 through alcohol dehydration, and alkane R3 through further reduction of the alkene. The acid pathway yields benzoic acid A1 and phenylacetic acid A2, when magnetite is present. A major product under all conditions is toluene, C1, which requires C-C bond fragmentation, followed by addition of a hydrogen atom. The only product that requires only C-C bond fragmentation is bibenzyl, C2, which is formed by coupling of two benzyl radicals, as shown in Eqns. 1a and 1b above. Dehydrogenation of bibenzyl forms stilbene, C3. The other main products (H1 – H7, with isomers) are included in the C-H cleavage pathway, although many of them may also require C-C bond fragmentation and coupling to form structures that contain three or four benzene rings. At short reaction durations, the primary product distributions in the presence of minerals can be seen in the gas chromatograms (see below).

#### 4.4.2. Reaction products with hematite and magnetite

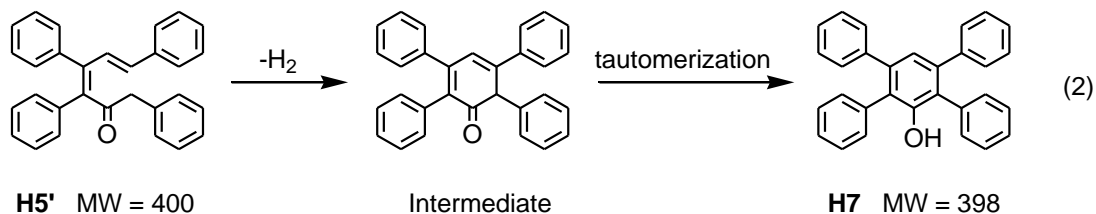
Shown in Figs. 4 and 5 are gas chromatograms showing the products of hydrothermal reaction of DBK with hematite and magnetite after a 5-h reaction time, compared to H<sub>2</sub>O alone after a 46-h reaction time. The reaction durations with hematite and magnetite are shorter, because they were chosen to match as closely as possible the DBK conversion in H<sub>2</sub>O alone. It is evident that the product distribution is simpler in the presence of hematite or magnetite. Specifically, the abundances of the products in the reduction pathway (R1 - R3) were much lower than in water alone. Toluene (C1) was still a major product, but bibenzyl (C2) was formed in very small quantity compared to its dehydrogenated equivalent stilbene (C3) at this early reaction time. In the three- and four-benzene-ring regions of the gas chromatograms (i.e., GC retention time between 15 and 25 mins), two of the major structure types that are formed in water alone were observed, specifically H5' (three isomers formed) and H6' (two or three isomers formed). A new five-ring product, H7, was discovered in both hematite and magnetite experiments, but it was not detected in the water alone experiments.

Formation of the products H5' and H6' can be understood starting with C-H bond fragmentation, followed by radical coupling to form intermediate structure D1, as shown in steps 1 and 2 in Fig. 6. A series of functional group transformations, specifically reduction to the alcohol, dehydration to the alkene, and further dehydrogenation, steps 3, 5 and 6, convert D1 into H5'. Steps 3 and 5 in Fig. 6 are analogous to those in the reduction pathway, although step 6 in this case is dehydrogenation (oxidation) instead of the hydrogenation (reduction). The C-C bond cleavage in D1, step 4, is similar to that in



DBK itself, and it results in product H6' via the same functional group transformations. Nevertheless, the order of the functional group transformation and C-C bond cleavage reactions that form H5' and H6' cannot be determined only from the observations of product distributions. As an example, H6' could be either generated from H5' via C-C bond cleavage or derived from any other intermediates in the D1 to H5' path. Both H5' and H6' structures are highly conjugated and are relatively stable towards further reaction.

The five-benzene-ring product, H7, was observed in the gas chromatograms with hematite and magnetite (Figs. 4 and 5). GC-MS analysis gave a molecular ion peak at 398 for H7, with virtually no fragmentation observed in the mass spectrum. The molecular ion is smaller by two mass units than that for H5', suggesting that H7 was probably formed from structure H5' by losing two hydrogen atoms (Eqn. 2). Loss of two hydrogen atoms in H5' can occur with formation of a six-membered cyclohexadiene ring, which may rapidly tautomerize (rearrange) into tetraphenylphenol (Eqn. 2) under the experimental conditions. Although the assignment of H7 to tetraphenylphenol has not been confirmed by an authentic standard, aryl-substituted phenols typically undergo almost no fragmentation in mass spectrometry, which seems consistent with the observed mass spectrum of H7 (Kuck, 2004). The four-benzene-ring product H5' is one of the most dehydrogenated products observed in hydrothermal reactions of DBK in H<sub>2</sub>O alone, the further C-H bond breaking of H5' to give H7 thus implies that the bond fragmentation pathway was greatly promoted by the presence of hematite and magnetite.



Another piece of evidence that supports C-H bond fragmentation promotion is that at early reaction times, the C-C bond cleavage product bibenzyl, C2, was formed in much lower and even undetectable yield compared to its dehydrogenated form stilbene, C3, when hematite or magnetite was present (Fig. 4 and 5). In water alone, however, the bibenzyl/stilbene ratio looks much higher. It again suggests that more C-H bond cleavage occurred with the aid of the oxide minerals under the studied hydrothermal conditions.

Hematite and magnetite not only facilitated C-H bond cleavage, but also expedited formation of C-C bond fragmentation products, such as toluene, C1, and bibenzyl, C2. Fig. 7 illustrates the production of C1 as a function of reaction progress in the presence of the minerals, compared to in H<sub>2</sub>O alone. It clearly shows that magnetite and hematite substantially enhanced the toluene production over the same reaction times as studied in water alone, and particularly for magnetite, the toluene concentration was almost an order of magnitude higher than that in water alone through the 168-h duration. Similar observation can be seen in Fig. 8, where the accumulation of bibenzyl was plotted time-dependently. Again, both hematite and magnetite dramatically increased the bibenzyl concentration in comparison with H<sub>2</sub>O alone, and the follow-up C-H bond fragmentation also occurred to convert bibenzyl to stilbene as another bond cleavage product.

Despite it seems likely that many observed products were formed through C-H bond fragmentation with loss of hydrogen atoms in the presence of hematite and magnetite, the whole organic system was not necessarily hydrogen deficient because the formation of major/dominant products such as toluene would need consume many hydrogen atoms, presumably via H-abstraction reactions by benzyl radicals. Indeed, as implied by the hydrogen balance calculations (Table 1), the DBK-hematite/magnetite system could reach approximate hydrogen balance just as the DBK in water alone system. Additional evidence to support hydrogen balance was obtained from the H<sub>2</sub> measurement experiments, where the amount of dissolved molecular hydrogen in gold capsules were quantified using GC-RCP. As shown in Table 2, when no minerals were added, the detected amounts of dissolved H<sub>2</sub> in water alone hydrothermal experiments were ca. 46.1 and 47.7 nanomoles after 46 h and 168 h, respectively. In contrast to the micromoles of DBK reacted in each experiment (Table 2), the amount of molecular hydrogen present in hydrothermal solution was substantially small. In hematite and magnetite hydrothermal experiments, the dissolved H<sub>2</sub> were measured at shorter reaction times. As examples, 5- and 24-h reaction durations were chosen to match up with the DBK conversions in 46- and 168-h water alone experiments, respectively. Control experiments were also conducted by loading only minerals and water in gold capsules without DBK, where the detected molecular hydrogen was approximate 1 nanomole during the studied reaction durations.

When DBK was added, 7.2 and 10.9 nanomoles of molecular hydrogen were detected in the 5-h hematite and magnetite experiments respectively. These values were both smaller than the 46.1 nanomoles observed in the 46-h H<sub>2</sub>O alone experiment. In the

24-h hydrothermal experiments, the detected H<sub>2</sub> were 23.6 and 14.8 nanomoles for hematite and magnetite respectively, which again were smaller than the 47.6 nanomoles in the 168-h water alone experiment (Table 2). It implies that hematite and magnetite might interact with some dissolved hydrogen in solution under the studied experimental conditions. However, even at a longer reaction time, when the DBK conversion was ca. 20% after 70 h, both hematite and magnetite experiments still yielded nanomoles of molecular hydrogen, comparing to micromoles of DBK that was consumed. It seems likely that the DBK-hematite/magnetite hydrothermal system maintained a relatively low level of dissolved hydrogen, although the formation of C-C and C-H bond cleavage products were greatly facilitated by the minerals. The fact that these iron oxide minerals did not promote molecular hydrogen generation suggests a balance of organic hydrogen atoms in the hydrothermal system, which also seems consistent with the hydrogen balance calculations as described before.

The DBK hydrothermal product distributions were time dependent and became more complex at longer durations. Two carboxylic acids, benzoic acid A1 and phenylacetic acid A2, were first observed in the presence of magnetite when reaction progress was greater than 70 h (Table 1). Although the yields of the acids were as low as ca. 1% among all the organic products, it is a new finding since no appreciable amounts of carboxylic acids were detected in water alone for reaction timescales of up to 528 h (Yang et al., 2012). Interestingly, the acids were not detected at earlier reaction times (less than 70 h) for magnetite or hematite, implying that they were probably not the primary products from DBK, but were formed through secondary reactions. The observed yield of benzoic acid was always higher than that of phenylacetic acid at all

studied reaction times, and after 168 h, the concentration of phenylacetic acid was even undetectable while the benzoic acid still continued to accumulate. This probably suggests that phenylacetic acid decarboxylated faster than benzoic acid under the hydrothermal conditions, presumably as a consequence of the facile C-C bond cleavage at its benzylic position (e.g., Glein et al., 2012).

To look for changes in different reaction pathways of DBK, it was informative to compare the reduction pathway versus the fragmentation pathway in the studied hydrothermal systems. This can be done by comparing the total yields of the reduction pathway products (R1, R2, and R3) to the total yields of all the other products, assuming a mass balance of 100%. In purpose of this comparison, the carboxylic acids were considered as fragmentation products, since they also require the C-C bond breaking. The reduction pathway percentage was calculated via dividing the sum of benzene rings in products R1 - R3 by the sum of benzene rings in all the products (DBK excluded). The acid pathway percentage was calculated the same way, counting the total number of benzene rings in the formed acids, A1 and A2. The fragmentation pathway percentage was simply 100% minus the reduction pathway percentage. The calculated data were included in Tables 1 and 3, and the pathway percentage versus reaction time was plotted in Fig. 9. In the presence of hematite and magnetite, the fragmentation pathway was dominating more than 95% of total reaction pathways all the time from 5 h to 168 h, whereas in H<sub>2</sub>O alone it took more than 46 h to reach 90%. It thus suggests that the C-C and C-H bond fragmentation was more favorable when hematite and magnetite were added, compared to water alone. Although the reduction pathway percentage for hematite/magnetite was extremely low (Fig. 9), the absolute yields of the reduction

products (R1 - R3) were found similar to those in water alone (Fig. 10). The decreased percentage of reduction pathway does not mean the reduction was prohibited, but means that fragmentation and coupling products were formed more abundantly than those in the water alone condition. As an example illustrated in Figs. 7 and 8, both toluene and bibenzyl concentrations increased dramatically compared to water alone. It is thus consistent with the fact that the accumulation of both smaller (e.g., C1 and C2) and larger (e.g., H5' and H6') cleavage products from DBK is facilitated by the presence of hematite and magnetite.

#### *4.4.3. Reaction products with troilite*

The product distributions in DBK-troilite (FeS) hydrothermal experiments are diverge from those in water alone, with hematite and magnetite, particularly at early reaction times (Figs. 4 and 5). After a 24 h reaction, shown in Fig. 11, the DBK reduction products R1 (alcohol), R2 (alkene), and R3 (alkane) were formed almost exclusively, whereas the bond cleavage products were hardly observed. The reduction of DBK seems preferable to occur compared to the bond fragmentation at the early durations, which is opposite to what observed in the iron oxides experiments. Fig. 12 shows the time dependence of the reduction pathway products in the presence of troilite, comparing to H<sub>2</sub>O alone under the same concentration scale. The yield of the reduced alkane R3 grows substantially with troilite, and more surprisingly, the alcohol R1 concentration remains high (>16 mmolal) even after 168 h, whereas in pure water, R1 reacts very rapidly and no appreciable concentration was detected in 24 h (Yang et al.,

2012). As reduction products of DBK, R1 and R3 were formed much more efficiently with troilite than in H<sub>2</sub>O alone and than in the presence of hematite or magnetite. Fig. 9 compares the percentage of reduction and fragmentation for troilite, and it clearly shows that the reduction pathway was preferred over fragmentation at early reaction times. However, at extended reaction progress, the fragmentation products eventually accumulate and become dominant. As an example, after 70 h, the concentration of major fragmentation product toluene, C1, became higher than that in water alone (Fig. 7). An explanation to this is that the reactions along the reduction pathway are reversible, whereas the cleavage products are formed irreversibly (see Chapter 2). The products from the irreversible fragmentation pathway would ultimately accumulate at the expense of the reversible reduction pathway products.

In troilite early time experiments, the fact that the reduction products are much more abundant suggests that DBK actually needs additional source of hydrogen atoms to compensate for the reduction products formation. The calculated hydrogen balance in Table 1 were estimated as 172%, 144%, and 136% for the 5-, 24-, and 70-h troilite experiments, respectively, which are all greater than the  $\pm 18\%$  experimental uncertainty. This means that there were more hydrogen atoms in the organic products than those in the reacted DBK molecules, and in other words, the incorporated hydrogen atoms should come from sources other than the organic compounds. The most likely and the only hydrogen source in the hydrothermal system should be water, and troilite presumably played a role in delivering hydrogen atoms from water through geochemical reactions. In hot water, it is known that iron sulfide minerals such as pyrrhotite (Fe<sub>1-x</sub>S) can potentially elevate concentrations of dissolved inorganic sulfur species (primarily H<sub>2</sub>S and HS<sup>-</sup>) as

the reducing power, and in some cases when H<sub>2</sub>S is added, some H<sub>2</sub> could also form in the processes such as pyrite formation (Drobner et al., 1990; Cody, 2004; McCollom, 2013). As an example, Drobner et al. (1990) demonstrated that starting with 200 mg pyrrhotite and 2 mmol H<sub>2</sub>S in aqueous solution at 100°C for 14 days under a CO<sub>2</sub> atmosphere resulted in production of ca. 20 μmol of H<sub>2</sub> and pyrite formation, whereas in the control experiment without H<sub>2</sub>S, only a ca. 0.2 μmol of H<sub>2</sub> was produced in the pyrrhotite alone experiment. As an analogous mineral to pyrrhotite, troilite at elevated temperature could also be expected to make H<sub>2</sub>S and H<sub>2</sub>, so attempts have been made to measure dissolved molecular hydrogen in the DBK hydrothermal experiments with troilite. When DBK was not added, the detected amounts of H<sub>2</sub> in the presence of troilite were 66.6 and 17.4 nanomoles after 5 and 70 h respectively, which are much greater than the ca. 1 nanomole in hematite/magnetite water alone experiments. The fact that the measured H<sub>2</sub> concentrations were not constant at different reaction times is probably because the systems had not reached equilibria within such short durations. Although it seems likely that troilite produced small quantities of hydrogen under these hydrothermal conditions, the amount of hydrogen looks too small to be the main reducing reagent or hydrogen donor for the DBK reduction products, since as much as ca. 1.7 and 10.8 μmoles of molecular hydrogen would be required to compensate for a 100% hydrogen balance in the 5 and 70 h experiments, respectively. Also to be noted, the experiments of troilite with DBK after 5 and 70 h yielded 78.8 and 22.6 nanomoles of H<sub>2</sub>, which are similar to those found in troilite without DBK. It might imply that the produced dissolved H<sub>2</sub> from troilite was not much affected or used by the DBK organic system



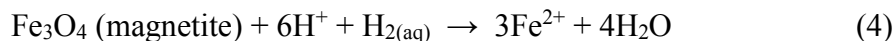
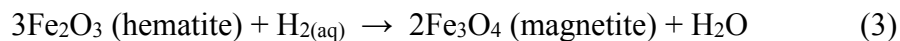
inside the gold capsules, but it is more likely that dissolved sulfur species should act as the main hydrogen contributors for the DBK reduction in the hydrothermal solutions.

To briefly summarize, for DBK with troilite during short reaction times (< 24 h), the reduction pathway mainly occurs, whereas at longer times, the fragmentation pathway begins to lead. Additional source of hydrogen atoms is required to generate the reduction pathway products, where the reaction between troilite and water is most likely to be responsible. For DBK with hematite and magnetite, on the contrary, the fragmentation pathway always dominates. Although hematite and magnetite greatly promote the bond cleavages, an approximate 100% hydrogen balance presumably suggests that these iron oxides potentially serve as a mineral catalyst rather than a reagent.

#### *4.4.4. Roles of the minerals*

Potential roles of minerals in hydrothermal organic reactions can include changing the inorganic components in the aqueous solution, and providing mineral surface to promote organic bond breaking and forming (e.g., McCollom, 2013). The results from the time-dependent experiments indicate that the studied iron-bearing minerals exert an evident influence on the DBK decomposition rates, reaction pathways, and product distributions. The product distributions described above indicate that much more C-C and C-H bond fragmentation products were formed apparently in the presence of hematite and magnetite than in water alone. The expedited decomposition rates and increased production of fragmentation products suggest the iron oxides greatly facilitate homolytic bond cleavage, however, the analysis of the hydrogen atom distributions did

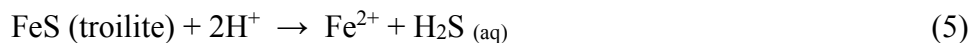
not illustrate a hydrogen deficit in the yielded organic products relative to the starting DBK (Table 1). It implies that hematite and magnetite serve principally as catalytic surfaces for the organic transformation processes. Nevertheless, possibility that the minerals can act partially as a reagent could not be totally ruled out, because the H<sub>2</sub> measurement results also showed that the detected molecular hydrogen were lower with hematite and magnetite than in water alone, when DBK conversions were comparable (Table 2). It seems likely that these minerals could influence or maybe buffer the reaction conditions by taking away the hydrogens liberated from the organics. Possible ways that hematite and magnetite potentially regulate or consume dissolved H<sub>2</sub> can be through reactions such as:



Because of the very low level of H<sub>2</sub> concentration, small volume of aqueous solution (0.2 mL), and the high mineral-to-water ratio, it was difficult to observe or identify any small changes in the mineral phase or in the solution, the mineral transformations still remained unclear under the experimental conditions. The fact that the detected hydrogen were higher in hematite experiments than in magnetite (24 and 70 h, Table 2) probably suggest that magnetite was more efficient to slightly decrease the hydrogen levels for the DBK hydrothermal system, although it is generally thought that hematite exists in a more oxidized form compared to magnetite in nature. It also seems to be evident from the product distributions in the reduction pathway (Fig. 10), where the most reduced product

alkane (R3) accumulated faster in the presence of hematite than magnetite. Possible explanations are (1) magnetite could be more susceptible to molecular hydrogen reduction than hematite in this specific hydrothermal system, so there would be less dissolved hydrogen present in the magnetite environment that can react in the DBK reduction pathway; (2) although magnetite was more powerful to facilitate C-C bond cleavage than hematite, it is possible that hematite could be more helpful in breaking C-H bonds on its surface and making more dissolved hydrogen in the system; and (3) it is also likely that the DBK reduction pathway was not controlled by the redox states of the minerals, but by the network organic reactions such as bond fragmentation and addition, where the minerals only played a catalytic role rather than a reactant.

Troilite plays a quite different role from hematite and magnetite. Instead of promoting bond fragmentation, it accelerates the reduction of DBK, especially at early reaction times. The abundant reduction pathway products not only suggest troilite is a reducing reagent, the greatly increased hydrogen balance numbers also indicate H<sub>2</sub>O should be heavily involved as a hydrogen contributor. Although the exact reducing power for DBK has not been identified, formation of dissolved H<sub>2</sub>S or other sulfur species from troilite can be speculated via reactions such as:



In fact, in troilite hydrothermal experiments, there was always a “rotten egg” smell when opening the gold capsules, and it possibly suggests the presence of H<sub>2</sub>S. H<sub>2</sub>S is a well-

known reducing reagent used in organic synthesis (Smith and March, 2007), and experiments using  $\text{H}_2\text{S}$  and  $\text{FeS}$  in hot aqueous solutions have also been conducted to explore whether the mineral-involved reactions could promote model organic reactions under geologically relevant conditions (Cody et al., 2004). A variety of organic structures have been investigated, as an example, Blochl et al. (1992) reported that the reduction of nitrate to form ammonia, reduction of ethyne and acetaldehyde to both form ethylene and ethane, and reduction of thiol compounds to form ethene, all occurred in aqueous media at  $100^\circ\text{C}$  in the presence of  $\text{FeS}/\text{H}_2\text{S}$ , and an intermediary and reductive role for  $\text{H}_2\text{S}$  was proposed. Although these organic reduction by  $\text{FeS}/\text{H}_2\text{S}$  could be subject to specific conditions, it seems very likely that dissolved sulfide species were formed in the troilite hydrothermal experiments, serving as the source of the reducing power for DBK.

Other than acting as a reducing reagent, surface-promoted reaction mechanism by troilite cannot be eliminated as an alternative possibility, since some bond fragmentation products also accumulated more quickly than water alone, toluene C1 for instance (Fig. 7). Troilite may serve both as a reactant and a catalytic surface in the DBK hydrothermal system.

Summarized in Table 3 and illustrated in Fig. 13 are the results of hydrothermal experiments in which the surface areas of the minerals were varied, for a fixed reaction time of 70 h. The purpose of conducting the mineral surface area-dependent experiments is to investigate the surface effects on DBK hydrothermal transformation, considering a potential surface-promoted reaction mechanism. Fig. 13 shows that the iron-bearing minerals all promoted the extent of DBK conversion at various mineral surface areas,

whereas the non-iron minerals, quartz and corundum, had no detectable effects on DBK at any of the surface areas studied (0.53 and 0.91 m<sup>2</sup>). It suggests that the iron may be required in the mineral structures for accelerating DBK decomposition. Of the minerals that influence the reactions, magnetite, hematite, and troilite show a roughly linear dependence on the surface areas (Fig. 13), or more exactly, the quantities of the mineral that were loaded into the gold capsule. Note that the lines through the data points are to guide the eyes only, not meant to imply a strictly linear relationship. The fact that the conversion efficiency depends almost linearly upon the added mineral surface area is evident in favor of a surface-promoted reaction mechanism, which again suggests the potential catalytic roles of these iron-containing minerals.

The area ratio between DBK and the minerals in the gold capsules experiments is large. The area of a single DBK molecule, when it is completely flat (Fig. 14), is ca. 75 Å<sup>2</sup>. If DBK is allowed to fold into a minimum energy conformation, the largest area accessible to a surface is ca. 35 Å<sup>2</sup>. The number of DBK molecules started in the mineral experiments is ca. 10<sup>20</sup>, which means that the area DBK can cover is between ca. 42 m<sup>2</sup> (folded) to 90 m<sup>2</sup> (flat) (Fig. 14). These numbers are much larger than the surface areas of any of the minerals used (see section 4.3.1.). If assuming an optimum situation, where all the DBK molecules are folded and the measured mineral surface area accessible to N<sub>2</sub> (BET method) is equally accessible to DBK, the theoretical minimum area ratio (DBK molecules/1.29 m<sup>2</sup> mineral surface) is ca. 33, which means the mineral surface will need at least 33 turnovers to be able to cover all the DBK molecules loaded in the gold capsule. As shown in Fig. 13, the roughly linear dependence on the mineral surface area suggests a model of mineral action that requires DBK binding to the surface. If the

surface chemistry or structure of the minerals is altered after the first interplay with DBK, the roughly linear conversion curve would not be expected under the conditions of an excess of DBK. In other words, it is more likely that the minerals promote the reactivity of DBK on the same surface over and over again, but without changing the mineral surface properties. It could be especially practical for hematite and magnetite, which elevated a much higher DBK conversion than troilite.

In addition, to eliminate any possible effects of nano-sized mineral particulates in the purchased synthetic minerals powders, a 70 h DBK experiment with a sample of magnetite that was further cleaned by repeated sonication and centrifugation (see experimental section) was conducted under the same hydrothermal conditions. The specific surface area of the treated magnetite was measured to be  $7.68 \text{ m}^2/\text{g}$ , and the estimated total area was  $\sim 1.18 \text{ m}^2$ . As shown in Table 3 and Fig. 13, the DBK conversion with cleaned magnetite was  $\sim 26.7\%$ , which falls closely to the DBK conversion curve with untreated magnetite. The product distribution of the treated magnetite is almost identical to that obtained using the untreated magnetite under the same experimental conditions. It seems that if there were any nano-sized particles present in the magnetite sample, they are not mainly responsible for the observed effects on DBK transformations.

In summary, both surface-promoted and reagent roles of the studied iron-containing minerals have been observed in the DBK hydrothermal reactions. Magnetite and hematite strongly promoted the DBK decomposition, most likely through catalytic effect by the mineral surface. The primary effects of magnetite and hematite are to facilitate bond fragmentation processes by generating the dominating C-C and C-H bond

cleavage products. The reduction of DBK was substantially facilitated by the presence of troilite, which presumably provided inorganic species, such as dissolved sulfur compounds, to the aqueous solutions, and took a role in supplying reducing hydrogen source from the water. Surface-promoted organic reactions may have also occurred on the troilite surface, but obviously not as strong as on hematite or magnetite.

#### **4.5. Conclusions**

This study initiates an exploration on the potential impact of common iron-bearing minerals on the behavior of ketones in hydrothermal geochemical systems. Specific influences of minerals on the hydrothermal reactions of ketones have been found under the experimental conditions. Quartz and corundum had virtually no influence on DBK transformations compared to that in the absence of minerals, while hematite, magnetite, and troilite, in contrast, exhibited strong effects on both the DBK conversion and the reaction pathways. The overall ketone conversion increases most dramatically with magnetite, followed by hematite and troilite. At early reaction times, the product distributions were examined in the presence of the different iron-bearing minerals, where selective formation of specific products was observed. In the case of hematite and magnetite, the products are mostly included in the fragmentation pathway, whereas for troilite, the products are more reduced and the reduction pathway is preferred. Carboxylic acids were formed in the presence of magnetite only at longer reaction times, probably not through primary reactions of DBK. Potential roles of the minerals can be a combination of mineral surface promoting and solution chemistry changing, and this

study suggests the ketone decomposition mostly depends on the mineral surface for hematite and magnetite, but mainly relies on the dissolved reducing species generated by troilite in the solution. The organic model system provides a useful method for studying mineral-ketone-water interactions under hydrothermal conditions. In natural hydrothermal environments, factors such as pH, ionic strengths, may also be involved in controlling ketones and other organic matter transformations, and these factors should be considered in the future study.



**Table 1.** Conversions, reaction pathways percentages, and estimated mass and hydrogen balances from the hydrothermal reaction of the ketone DBK at 300°C and 70 MPa, in the absence and presence of the minerals. Experiments are taken at various reaction times, with a constant mineral surface area of ~1.29 m<sup>2</sup>.

Time (hr)	Conversion (%)	Reduction pathway <sup>a</sup> (%)	Fragmentation pathway <sup>b</sup> (%)	Acid pathway <sup>c</sup> (%)	Mass balance <sup>d</sup> (%)	Hydrogen balance <sup>e</sup> (%)
no mineral						
0	0.7	26.0	74.0	n.a.	89	n.a.
12	1.1	22.9	77.1	n.a.	86	n.a.
24	1.4	16.7	83.3	n.a.	108	n.a.
46	2.7	10.4	89.6	n.a.	85	88
70	3.7	8.1	91.9	n.a.	88	90
168	6.4	8.8	91.2	n.a.	88	89
290	9.7	6.3	93.7	n.a.	96	98
528	14.5	3.9	96.1	n.a.	112	104
hematite						
0	0.8	8.5	91.5	n.a.	94	n.a.
5	2.3	2.5	97.5	n.a.	109	87
24	7.1	1.8	98.2	n.a.	90	93
70	17.3	1.9	98.1	n.a.	84	108
96	21.0	2.3	97.7	n.a.	82	n.a.
168	26.4	2.2	97.8	n.a.	80	n.a.
magnetite						
5	2.1	3.3	96.7	n.a.	84	83
24	8.4	1.1	98.9	n.a.	83	94
70	24.1	0.7	99.3	0.9	89	102
96	28.7	1.5	98.5	1.7	80	n.a.
168	46.8	0.7	99.3	1.1	76	n.a.
troilite						
5	0.6	76.5	23.5	n.a.	86	172
24	2.4	69.4	30.6	n.a.	91	144
70	7.6	47.3	52.7	n.a.	83	136
168	14.5	31.0	69.0	n.a.	80	125

<sup>a</sup> Percentage of the products that are assigned to the reduction reaction pathway, as defined in the text and illustrated in Fig. 8.

<sup>b</sup> Percentage of the products that are assigned to the fragmentation reaction pathway, as defined in the text and illustrated in Fig. 8. Note that the acid percentage is included in the fragmentation pathway percentage since the acids also require C-C bond cleavage.

<sup>c</sup> Percentage of the products that are assigned to the acid reaction pathway, as defined in the text. n.a. means the yield of the acids is too small to be detected under the experimental conditions.

<sup>d</sup> Mass balance calculated according to the method described in the experimental section. n.a. means the data is unavailable due to low accuracy.

<sup>e</sup> Hydrogen balance calculated according to the method described in the experimental section. n.a. means the data is unavailable due to low accuracy.

**Table 2.** Conversions, micromoles of DBK reacted, nanomoles of hydrogen detected, dissolved concentration of H<sub>2</sub>, and estimated hydrogen balances from the hydrothermal reaction of the ketone DBK at 300°C and 70 MPa, in the absence and presence of the minerals. Experiments are taken at various reaction times, with a constant mineral surface area of ~1.29 m<sup>2</sup>. Controls for H<sub>2</sub> measurements were conducted for the three iron-bearing minerals without DBK added.

Time (hr)	Conversion (%)	Reacted DBK (μmoles)	H <sub>2</sub> (nmoles)	Log activity of H <sub>2</sub>	Hydrogen balance (%)
no mineral					
46	2.7	5.4	46.1	-3.64	88
168	6.4	12.5	47.6	-3.62	89
hematite without DBK					
5	-	-	0.7	-5.47	-
hematite with DBK					
5	2.3	4.5	7.2	-4.45	87
24	7.1	13.9	23.6	-3.93	93
70	17.3	34.1	33.2	-3.78	108
magnetite without DBK					
5	-	-	1.0	-5.30	-
70	-	-	1.0	-5.31	-
magnetite with DBK					
5	2.1	4.2	10.9	-4.27	83
24	8.4	16.1	14.8	-4.13	94
70	24.1	47.4	15.8	-4.10	102
troilite without DBK					
5	-	-	66.6	-3.48	-
70	-	-	17.4	-4.06	-
troilite with DBK					
5	0.6	1.2	78.8	-3.40	172
70	7.6	15.0	22.6	-3.95	136

**Table 3.** Conversions, reaction pathways percentages, and estimated mass balances from the hydrothermal reaction of the ketone DBK at 300°C and 70 MPa, in the absence and presence of minerals. Experiments are taken at a fixed reaction time of 70 hours, but with different mineral surface areas.

Mineral surface area (m <sup>2</sup> )	Conversion (%)	Reduction pathway <sup>a</sup> (%)	Fragmentation pathway <sup>b</sup> (%)	Acid pathway <sup>c</sup> (%)	Mass balance <sup>d</sup> (%)
no mineral					
0	3.7	8.1	91.9	n.a.	88
quartz					
0.53	3.1	8.3	91.7	n.a.	101
0.90	3.5	5.9	94.1	n.a.	90
corundum					
0.53	3.3	11.0	89.0	n.a.	83
0.91	2.7	8.1	91.9	n.a.	84
hematite					
0.54	9.7	2.1	97.9	n.a.	115
0.91	14.4	1.8	98.2	n.a.	92
1.29	17.3	1.9	98.1	n.a.	81
magnetite					
0.30	12.2	0.4	99.6	n.a.	108
0.57	17.6	0.4	99.7	0.3	103
0.91	23.1	0.6	99.7	0.4	94
1.18 <sup>e</sup>	26.7	1.2	98.8	1.3	101
1.27	27.9	0.9	99.1	1.0	83
troilite					
0.53	5.5	43.9	56.1	n.a.	94
0.91	6.2	46.2	53.8	n.a.	84
1.29	7.6	47.3	52.7	n.a.	83

<sup>a</sup> Percentage of the products that are assigned to the reduction reaction pathway, as defined in the text.

<sup>b</sup> Percentage of the products that are assigned to the fragmentation reaction pathway, as defined in the text. Note that the acid percentage is included in the fragmentation pathway percentage since the acids also require C-C bond cleavage.

<sup>c</sup> Percentage of the products that are assigned to the acid reaction pathway, as defined in the text. n.a. means that the yield of the acids is too small to be detected under the experimental conditions.

<sup>d</sup> Mass balance calculated according to the method described in the experimental section.

<sup>e</sup> Experimental data of DBK with the cleaned magnetite, shown as the used mineral surface area, the calculated DBK conversion, percentage of pathways, and the mass balance. The conversion is also plotted in Fig. 12 to compare with the data points for the untreated magnetite with different surface areas.

**Figure 1.** Schematic sequence of functional group interconversions that link alkanes to carboxylic acids, shown as oxidation/reduction reactions (horizontal arrows) and non-redox reactions (vertical arrows). Ketones, in the grey box, occupy an important position in this reaction sequence since they represent the point at which C-C bond fragmentation reactions occur, accompanied either by oxidation to give carboxylic acids, or with radical fragmentation and coupling reactions, such as in the case of the model ketone studied here.

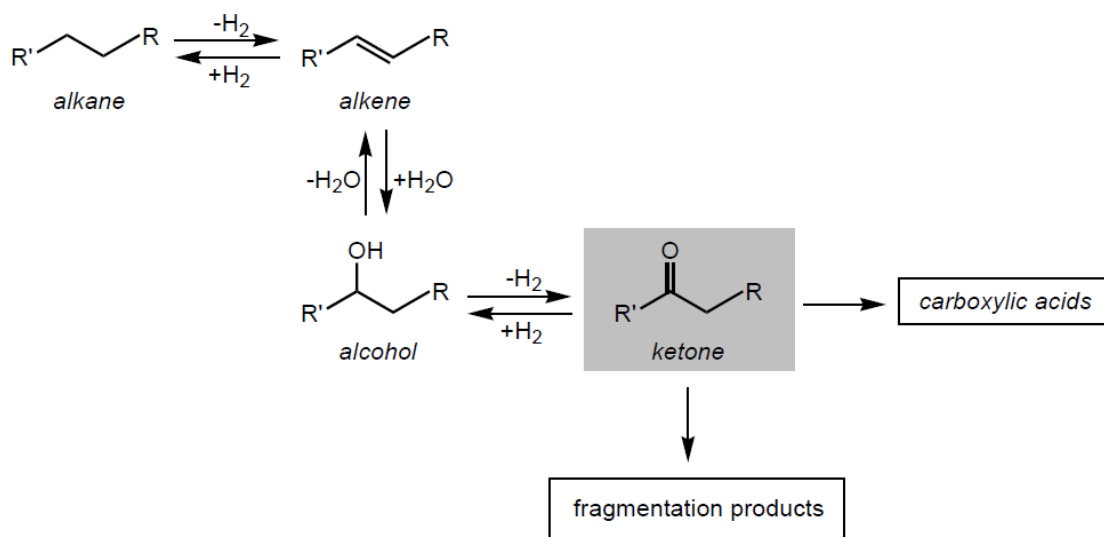


**Figure 2.** Percent conversion as a function of time for hydrothermal reaction of the ketone DBK at 300°C and 70 MPa, in H<sub>2</sub>O alone (open circles), and in the presence of ferrous sulfide (closed diamonds), hematite (open diamonds), and magnetite (closed circles). The added iron-bearing minerals have different masses but the same surface area, ~1.29 m<sup>2</sup>. Single time points of 70 hours are shown in the presence of quartz (closed inverted triangle) and corundum (open triangles), which are indistinguishable from the corresponding conversion in H<sub>2</sub>O alone. The mineral surface areas for quartz and corundum are both ~0.91 m<sup>2</sup>. The data points with error bars represent repeated experiments. The inset is a first-order kinetic fit to the magnetite data, which yields a pseudo first-order rate constant of  $\sim 3.7 \times 10^{-3} \text{ hr}^{-1}$  (see text for details).

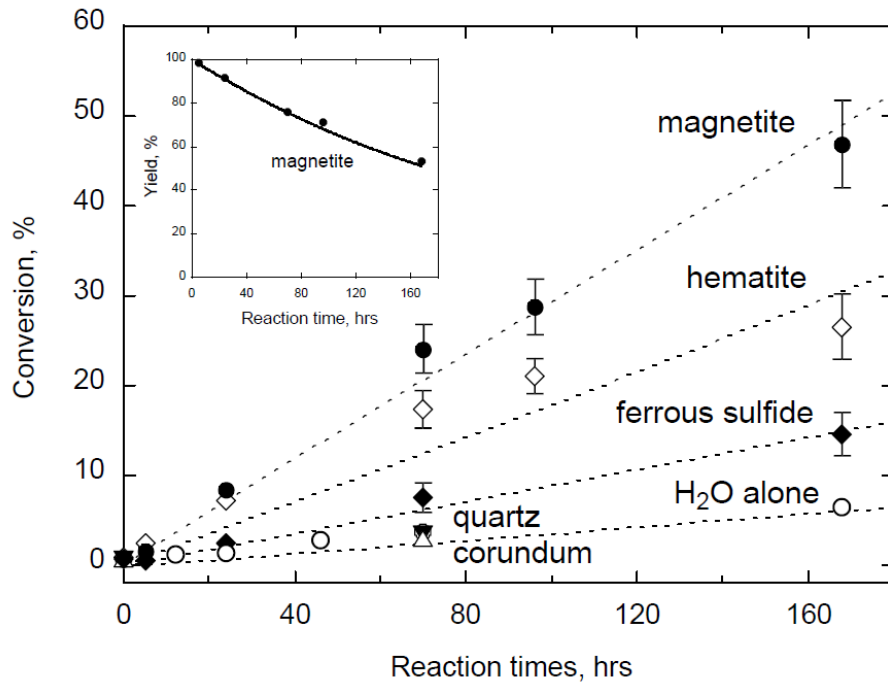


**Figure 3.** Summary of the products from the hydrothermal reactions of the ketone DBK at 300°C and 70 MPa. The prime symbol (') in the product designation indicates the presence of more than one structural or stereoisomer isomer of that particular structure. Four main reaction pathways can be identified, i.e., the reduction pathway, the C-C cleavage and C-H cleavage pathways, and the acid pathway. The reduction pathway is the same as in Fig. 1 and connects the ketone with the alkane. The C-C and C-H pathways are the fragmentation pathways in Fig. 1, and are highly interconnected. Reduction pathway type products are also observed in the cleavage pathways. The acid pathway yields carboxylic acids as shown in Fig 1. In the presence of the minerals, the major products are indicated by the outlined boxes.

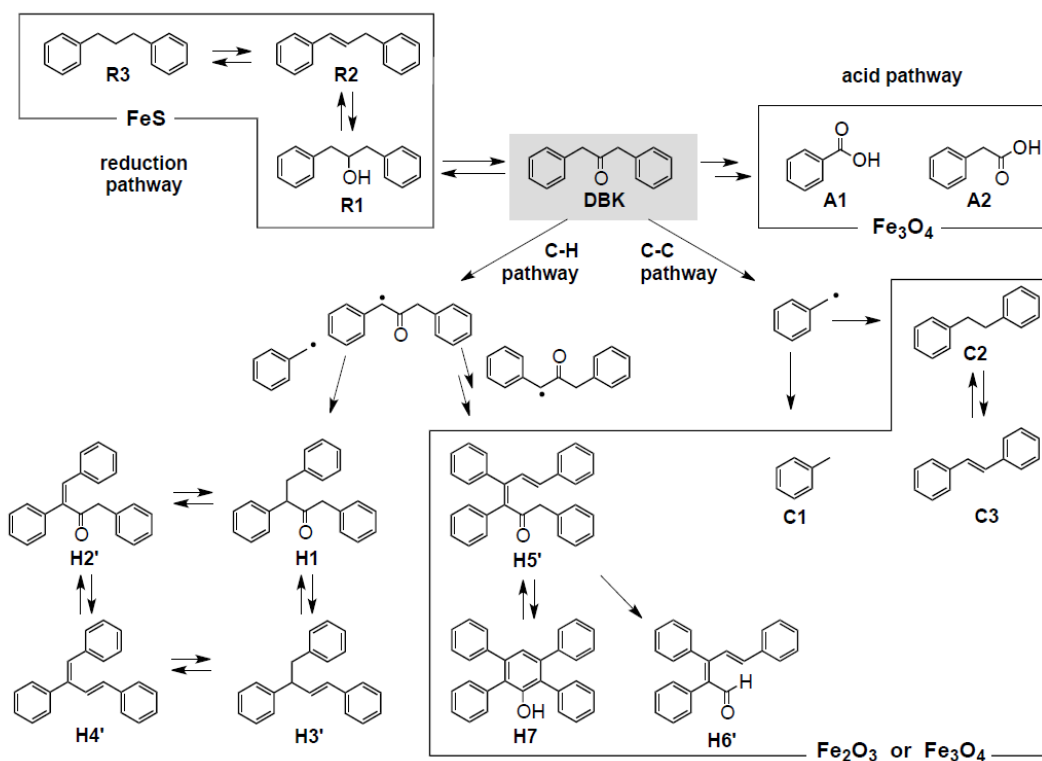




**Figure 4.** Gas chromatograms comparing the products of hydrothermal reactions of the ketone DBK at 300°C and 70 MPa, in the presence of hematite with a surface area of  $\sim 1.29 \text{ m}^2$  after a 5-hour reaction time, and in  $\text{H}_2\text{O}$  alone after a reaction period of 46 hours. The DBK conversions are similar, which are  $\sim 2.3\%$  in the presence of hematite and  $\sim 2.7\%$  in  $\text{H}_2\text{O}$  alone. The upper chromatograms show the one- and two-benzene-ring products at earlier retention times, the lower chromatograms show the three-, four- and five-benzene-ring products at later retention times.

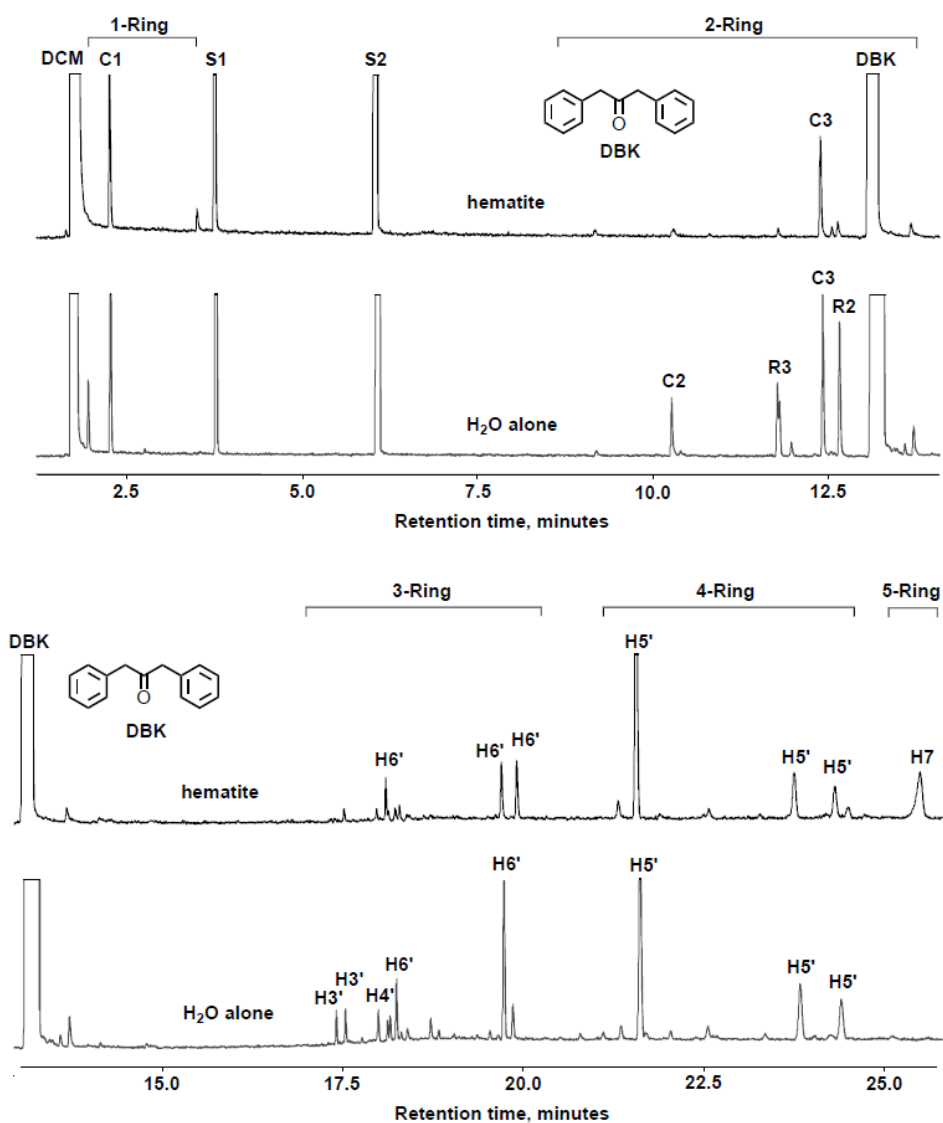


**Figure 5.** Gas chromatograms comparing the products of hydrothermal reactions of the ketone DBK at 300°C and 70 MPa, in the presence of magnetite with a surface area of  $\sim 1.29 \text{ m}^2$  after a 5-hour reaction time, and in  $\text{H}_2\text{O}$  alone after a reaction period of 46 hours. The DBK conversions are similar, which are  $\sim 1.5\%$  in the presence of magnetite and  $\sim 2.7\%$  in  $\text{H}_2\text{O}$  alone. The upper chromatograms show the one- and two-benzene-ring products at earlier retention times, the lower chromatograms show the three-, four- and five-benzene-ring products at later retention times.

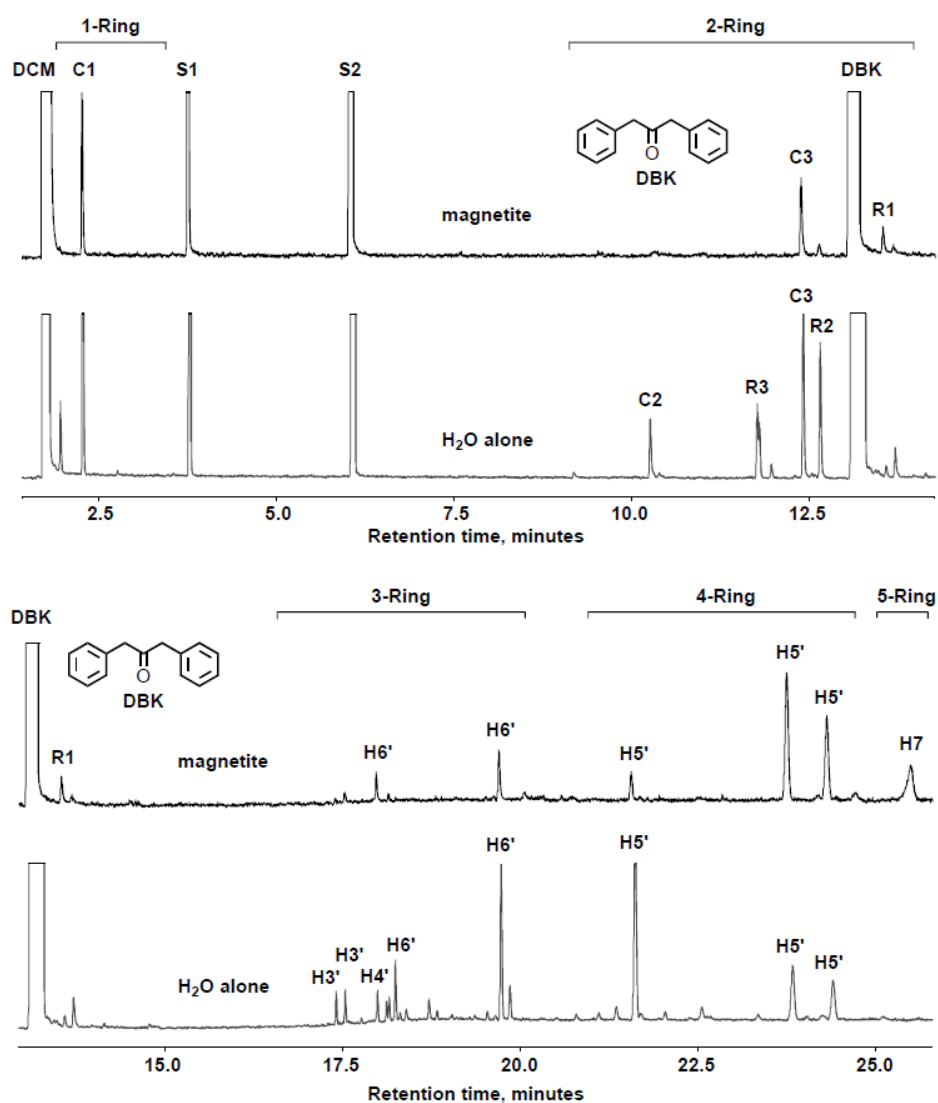


**Figure 6.** Proposed reaction scheme for formation of the coupling products H5' and H6' from DBK (the ' symbol indicates structural and/or stereoisomers). The C-H bond cleavage (step 1) forms two benzylic radicals that can couple into a ketone dimer, D1 (step 2), which probably undergoes either functional groups transformations that start with hydrogenation (step 3) to reach the conjugated H5', or C-C bond cleavage (step 4) to eventually form H6' via the same functional group transformations. The order of step 3 and step 4 to produce H6' can be reversed, and step 4 could also occur at other intermediates along the path from D1 to H5'.

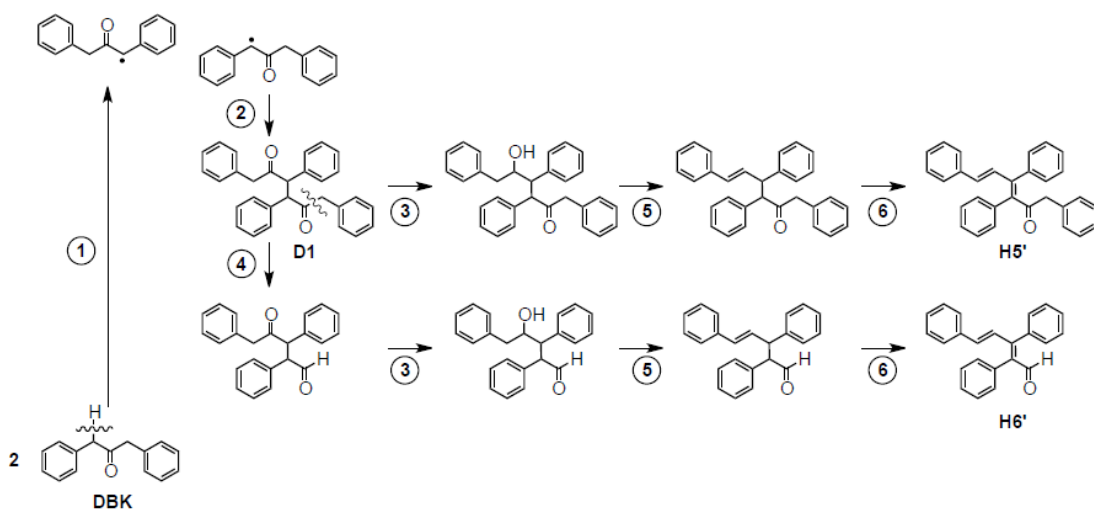


**Figure 7.** Time dependence of concentrations of the C-C bond cleavage and the major product toluene, C1, from hydrothermal decomposition of DBK at 300°C and 70 MPa, in H<sub>2</sub>O alone (dashed line and open circles), in the presence of hematite (solid line and open diamonds), magnetite (solid line and closed circles), and ferrous sulfide (solid line and closed diamonds), using a constant mineral surface area of ~1.29 m<sup>2</sup>.

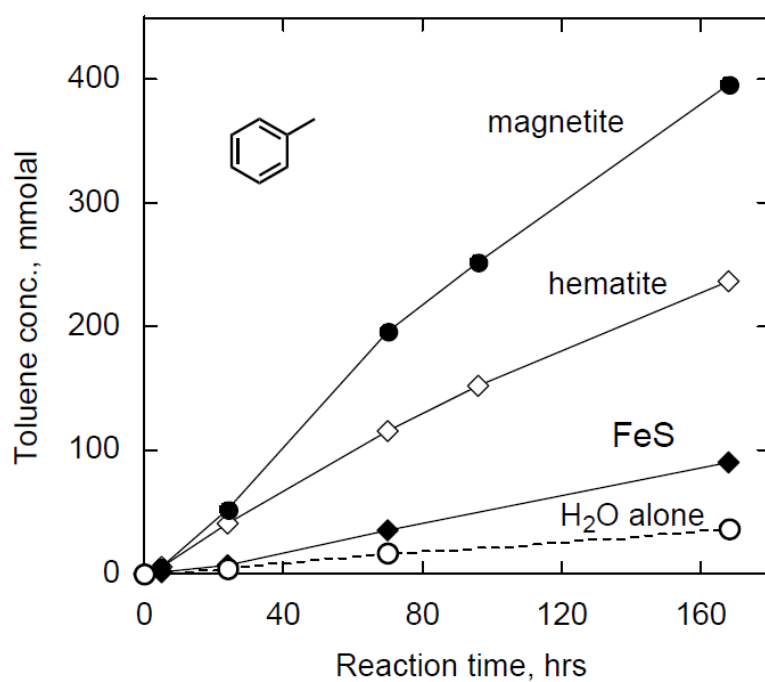


**Figure 8.** Time dependence of concentrations of the C-C bond cleavage and the major product bibenzyl, C2, from hydrothermal decomposition of DBK at 300°C and 70 MPa, in H<sub>2</sub>O alone (dashed line and open circles), in the presence of hematite (solid line and open diamonds), magnetite (solid line and closed circles), and troilite (solid line and closed diamonds), using a constant mineral surface area of ~1.29 m<sup>2</sup>.

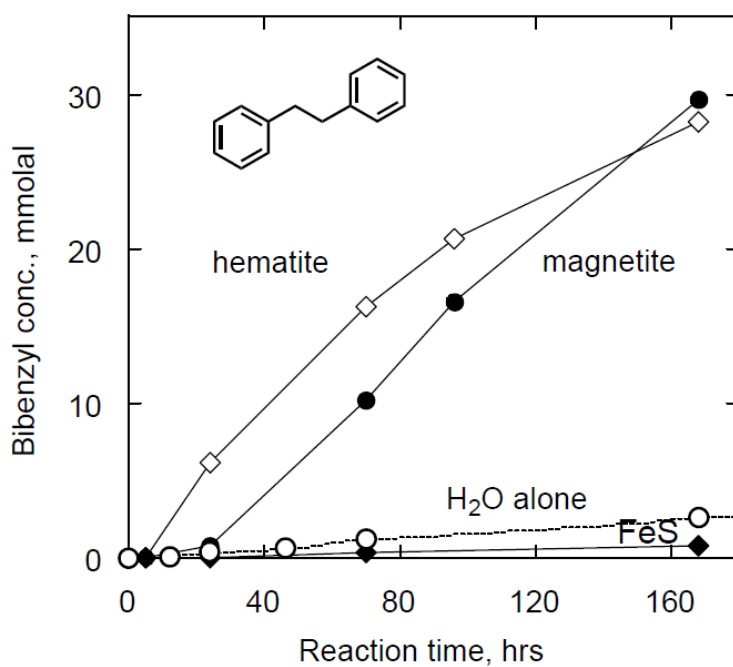


**Figure 9.** Percentage reduction and fragmentation pathways for hydrothermal reactions of DBK at 300°C and 70 MPa, in H<sub>2</sub>O alone on the left hand side, and in the presence of hematite (triangles), magnetite (inverted triangles), and ferrous sulfide (diamonds) on the right hand side. In both figures, the closed symbols indicate the fragmentation pathway percentage, and the open symbols indicate the reduction pathway percentage. For the oxides minerals, the fragmentation dominates at all reaction times. For the ferrous sulfide, the reduction dominates at early reaction times, but at later times, the fragmentation overtakes. Note that the decrease of the reduction percentage does not mean a decrease in the amount of the reduction pathway products; it should represent a slower accumulation of the reduction pathway products comparing to the fragmentation pathway.

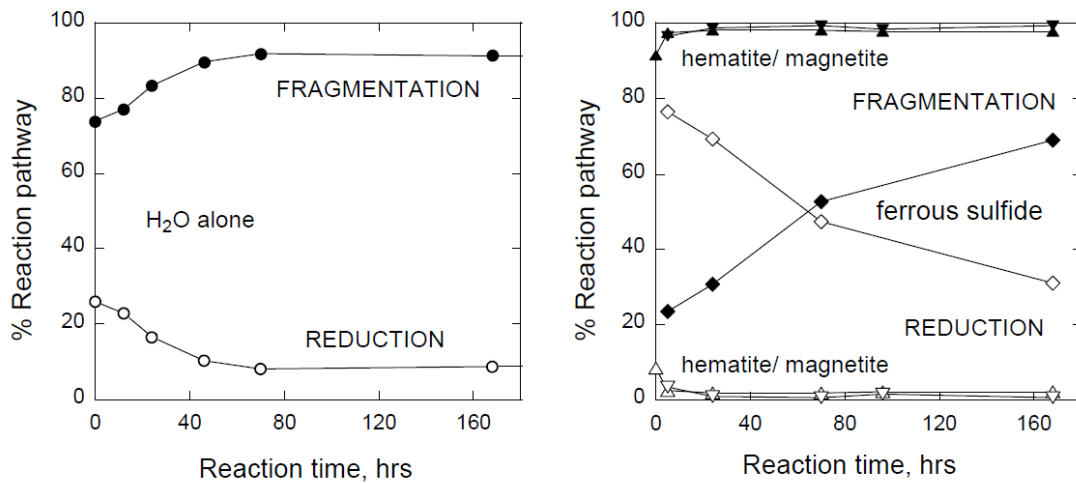


**Figure 10.** Time dependence of concentrations of the reduction pathway products, alcohol (R1), alkene (R2), and alkane (R3), from hydrothermal transformation of DBK in H<sub>2</sub>O alone (left), in the presence of hematite (center), and magnetite (right) with a constant mineral surface area of ~1.29 m<sup>2</sup>. The yields of the reduction pathway products with hematite and magnetite are roughly comparable to H<sub>2</sub>O alone over the reaction time period, although their time dependencies are different (see text).

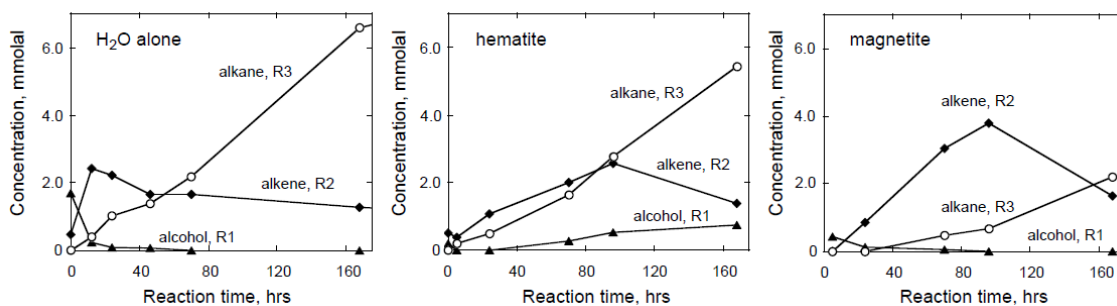


**Figure 11.** Gas chromatograms comparing the products of hydrothermal reactions of the ketone DBK at 300°C and 70 MPa, in the presence of ferrous sulfide (troilite) with a surface area of  $\sim 1.29 \text{ m}^2$  after a 24-hour reaction time, and in  $\text{H}_2\text{O}$  alone after a reaction period of 46 hours. The DBK conversions are similar, which are  $\sim 2.4\%$  in the presence of ferrous sulfide and  $\sim 2.7\%$  in  $\text{H}_2\text{O}$  alone. The upper chromatograms show the one- and two-benzene-ring products at earlier retention times, the lower chromatograms show the three-, four- and five-benzene-ring products at later retention times.

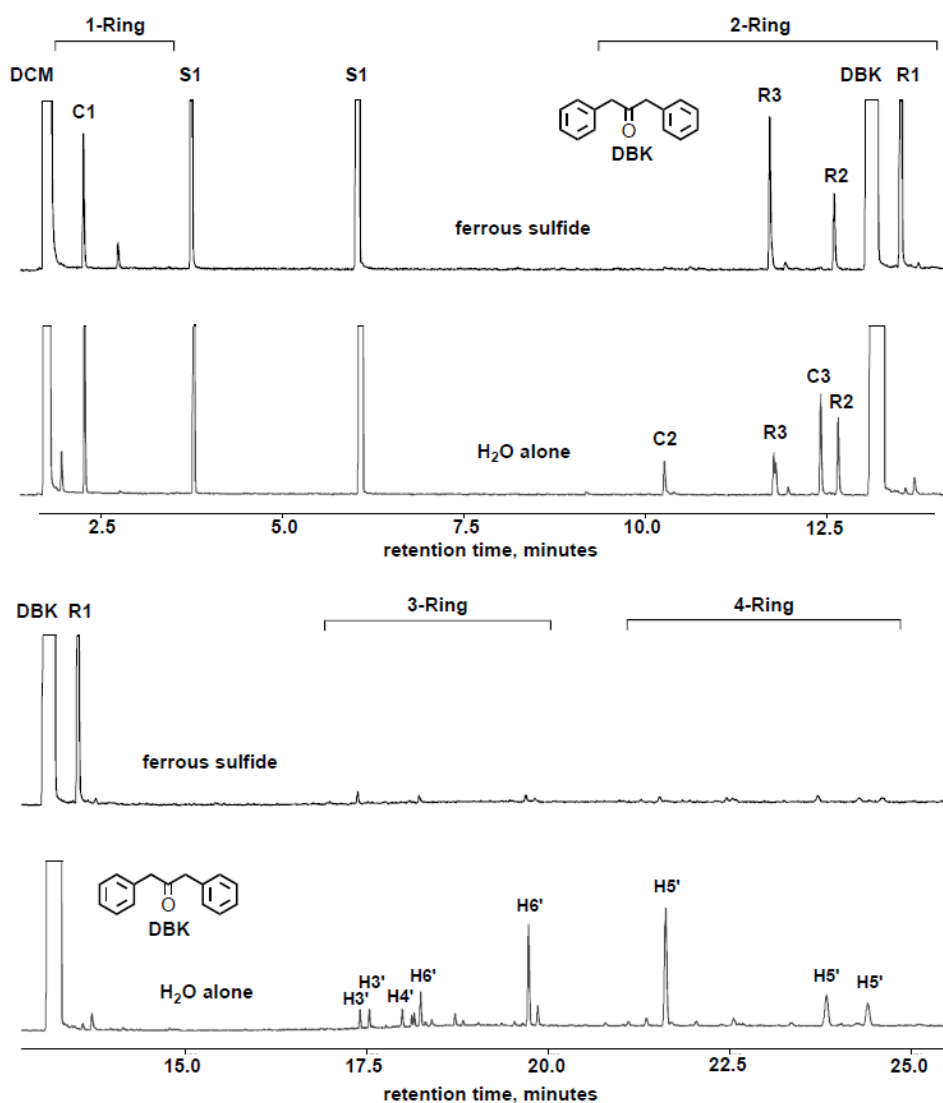




**Figure 12.** Time dependence of concentrations of the reduction pathway products, alcohol (R1), alkene (R2), and alkane (R3), from hydrothermal transformation of DBK in H<sub>2</sub>O alone (left), and in the presence of ferrous sulfide (right) with a constant mineral surface area of ~1.29 m<sup>2</sup>. The same vertical scale emphasizes the fact that the yields of the reduction pathway products with ferrous sulfide are much larger than the yields in H<sub>2</sub>O alone. The H<sub>2</sub>O alone data are plotted on an expanded scale in Fig. 9.

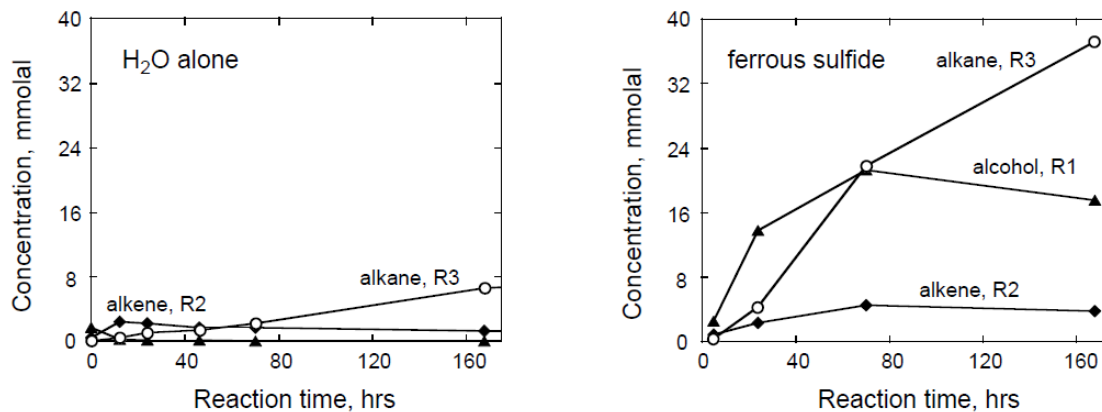


**Figure 13.** DBK conversion at a fixed reaction period of 70 hours as a function of the surface area for the added mineral, corundum (open triangles), quartz (closed inverted triangles), ferrous sulfide (closed diamonds), hematite (open diamonds), and magnetite (closed circles). The cleaned-magnetite experiment is indicated as the open circle. The horizontal dashed line at bottom represents the conversion in H<sub>2</sub>O alone. The other straight dashed lines through the data points are for guidance, they do not essentially imply a linear relationship (see text). The data points with error bars represent repeated experiments.

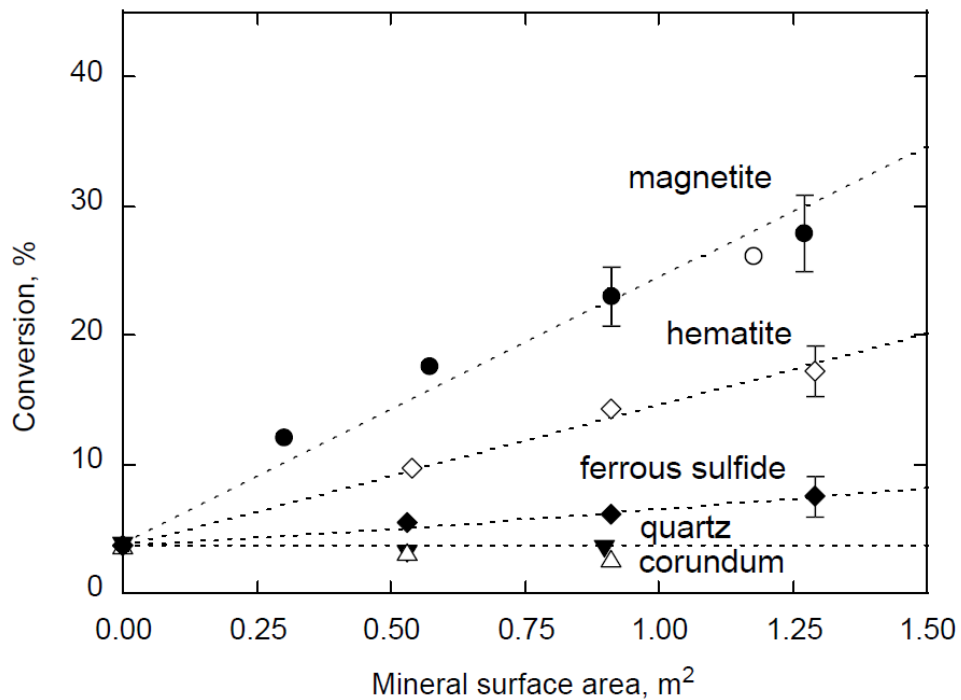
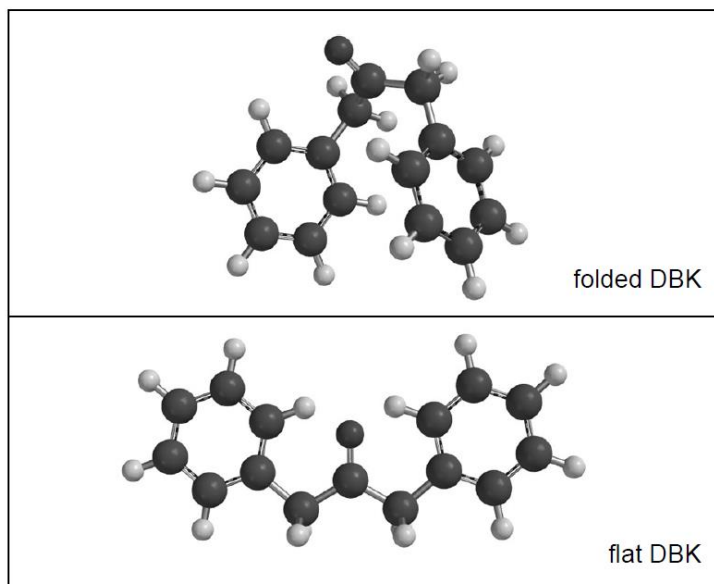


**Figure 14.** Representations of a completely flat DBK molecule (bottom), which covers an area of ca.  $75 \text{ \AA}^2$ , and a folded DBK molecule (top) that covers an area of ca.  $35 \text{ \AA}^2$ . Each experiment used ca.  $1.2 \times 10^{20}$  DBK molecules, which give a total area of DBK coverage between ca.  $62$  (folded) and  $29$  (flat)  $\text{m}^2$ .



#### 4.6. References

- Akiya N. and Savage P. E. (2001) Kinetics and mechanism of cyclohexanol dehydration in high-temperature water. *Ind. Eng. Chem. Res.* **40**, 1822–1831.
- Andersson E. and Holm N. G. (2000) The stability of some selected amino acids under attempted redox constrained hydrothermal conditions. *Origins Life Evol. Bios.* **30**, 9-23.
- Bell J. L. S. and Palmer D. A. (1994) Experimental studies of organic acid decomposition. *Organic Acids in Geological Processes* (eds. E. D. Pittman and M. D. Lewan). Springer- Verlag, New York. pp. 226-269.
- Cody G. D., Boctor N. Z., Hazen R. M., Brandes J. A., Morowitz H. J., Yoder H. S. (2001) Geochemical roots of autotrophic carbon fixation: Hydrothermal experiments in the system citric acid, H<sub>2</sub>O-(±FeS)-(±NiS). *Geochim. Cosmochim. Acta* **65**, 3557-3576.
- Cody G. D. (2004) Transition metal sulfides and the origins of metabolism. *Annu. Rev. Earth Planet. Sci.* **32**, 569-599.
- D'Hondt S., Jørgensen B. B., Miller D. J., Batzke A., Blake R., Cragg B. A., Cypionka H., Dickens G. R., Ferdelman T., Hinrichs K.-U., Holm N. G., Mitterer R., Spivak A., Wang G., Bekins B., Engelen B., Ford K., Gettemy G., Rutherford W. D., Sass H., Skilbeck C. G., Aiello I. W., Guèrin G., House C. H., Inagaki F., Meister P., Naehr T., Niitsuma S., Parkes R. J., Schippers A., Smith D. C., Teske A., Wiegel J., Padilla C. N. and Acosta J. L. S. (2004) Distributions of microbial activities in deep seafloor sediments. *Science* **306**, 2216-2221.
- Drobner E., Huber H., Wächtershäuser G., Rose D. and Stetter K. O. (1990) Pyrite formation linked with hydrogen evolution under anaerobic conditions. *Nature* **346**, 742-744.
- Espitalie J., Madec M. and Tissot B. (1980) Role of mineral matrix in kerogen pyrolysis – influence on petroleum generation and migration. *AAPG Bulletin-American Association of Petroleum Geologists.* **64**, 59-66.
- Foustoukos D. I. and Seyfried Jr. W. E. (2004) Hydrocarbons in hydrothermal vent fluids: the role of chromium-bearing catalysts. *Science* **304**, 1002-1005.
- Fu Q., Foustoukos D. I., Seyfried Jr. W. E. (2008) Mineral catalyzed organic synthesis in hydrothermal systems: An experimental study using time-of-flight secondary ion mass spectrometry. *Geophys. Res. Lett.* **35**, L07612.

- Glein C. R. (2012) *Theoretical and experimental studies of cryogenic and hydrothermal organic geochemistry*. Doctoral dissertation, Arizona State University. Ann Arbor: ProQuest/UMI. (Publication No. 3521607).
- Head I. M., Jones D. M. and Larter S. R. (2003) Biological activity in the deep subsurface and the origin of heavy oil. *Nature* **426**, 344-352.
- Helgeson H. C., Owens C. E., Knox A. M. and Richard L. (1998) Calculation of the standard molal thermodynamic properties of crystalline, liquid, and gas organic molecules at high temperatures and pressures. *Geochim. Cosmochim. Acta* **62**, 985-1081.
- Helgeson H. C., Richard L., McKenzie W. F., Norton D. L. and Schmitt A. (2009) A chemical and thermodynamic model of oil generation in hydrocarbon source rocks. *Geochim. Cosmochim. Acta* **73**, 594-695.
- Hinrichs K.-U., Hayes J. M., Bach W., Spivak A. I., Hmelo L. R., Holm N. G., Johnson C. G. and Sylva S. P. (2006) Biological formation of ethane and propane in the deep marine subsurface. *Proc. Natl. Acad. Sci. USA*. **103**, 14,684-14,689.
- Horsfield B., Schenk H. J., Zink K., Ondrak R., Dieckmann V., Kallmeyer J., Mangelsdorf K., Primio R. D., Wilkes H., Parkes R. J., Fry J. and Cragg B. (2006) Living microbial ecosystems within the active zone of catagenesis: Implications for feeding the deep biosphere. *Earth Planet Sc. Lett.* **246.1-2**, 55-69.
- Johnson J. W., Oelkers E. H., Helgeson H. C. (1992) SUPCRT92: A software package for calculating the standard molal thermodynamic properties of minerals, gases, aqueous species, and reactions from 1 to 5000 bar and 0 to 1000°C. *Computers Geosci.* **18**, 899-947.
- Jones D. M, Head I. M., Gray N. D., Adams J. J., Rwan A. K., Aitken C. M., Bennett B., Huang H., Brown A., Bowler B. F. J., Oldenburg T., Erdmann M. and Larter S. R. (2008) Crude-oil biodegradation via methanogenesis in subsurface petroleum reservoirs. *Nature* **451**, 176-180.
- Jurg J. W. and Eisma E. (1964) Petroleum hydrocarbons – generation from fatty acid. *Science* **144**, 1451-1452.
- Katritzky A. R., Nichols D. A., Siskin M., Murugan R. and Balasubramanian M. (2001) Reactions in high-temperature aqueous media. *Chem. Rev.* **101**, 837-892.

- Kuck, D. (2004) Mass spectrometry and gas-phase ion chemistry of phenols. The Chemistry of Phenols (ed. Z. Rappoport). Wiley, New York. p. 259.
- Larter S. R., Wilhelms A., Head I., Koopmans M., Aplin A., Di P. R., Zwach C., Erdmann M. and Telnaes N. (2003) The controls on the composition of biodegraded oils in the deep subsurface: Part I - Biodegradation rates in petroleum reservoirs. *Org. Geochem.* **34**, 601-613.
- LaRowe D. E. and Dick J. M. (2012) Calculation of the standard molal properties of crystalline peptides. *Geochim. Cosmochim. Acta* **80**, 70-91.
- LaRowe D. E. and Helgeson H. C. (2006a) Biomolecules in hydrothermal systems: Calculation of the standard molal thermodynamic properties of nucleic-acid bases, nucleosides, and nucleotides at elevated temperatures and pressures. *Geochim. Cosmochim. Acta* **70**, 4680-4724.
- Leif R. N. and Simoneit B. R. T. (2000) The role of alkenes produced during hydrous pyrolysis of a shale. *Org. Geochem.* **31**, 1189-1208.
- Mason O. U., Nakagawa T., Rosner M., Van Nostrand J. D., Zhou J., Maruyama A., Fisk M. R. and Giovannoni S. J. (2010) First investigation of the microbiology of the deepest layer of ocean crust. *PLoS ONE*. **5**, 1-11.
- McCullom T. M. and Seewald J. S. (2003a) Experimental constraints on the hydrothermal reactivity of organic acids and acid anions: I. Formic acid and formate. *Geochim. Cosmochim. Acta* **67**, 3625-3644.
- McCullom T. M. and Seewald J. S. (2003b) Experimental study of the hydrothermal reactivity of organic acids and acid anions: II. Acetic acid, acetate, and valeric acid. *Geochim. Cosmochim. Acta* **67**, 3645-3664.
- McCullom T. M. and Seewald J. S. (2007) Abiotic synthesis of organic compounds in deep-sea hydrothermal environments. *Chem. Rev.* **107**, 382-401.
- McCullom T. M. (2013) The influence of minerals on decomposition of the n-alkyl-alpha-amino acid norvaline under hydrothermal conditions. *Geochim. Cosmochim. Acta* **104**, 330-357.
- Plyasunov A. V. and Shock E. L. (2000) Standard state Gibbs energies of hydration of hydrocarbons at elevated temperatures as evaluated from experimental phase equilibria studies. *Geochim. Cosmochim. Acta* **64**, 2811-2833.
- Plyasunov A. V. and Shock E. L. (2003) Prediction of the vapor-liquid distribution constants for volatile nonelectrolytes in H<sub>2</sub>O up to the critical temperature of water. *Geochim. Cosmochim. Acta* **67**, 4981-5009.

- Reeves E. P., Seewald J. S. and Sylva S. (2012) Hydrogen isotope exchange between n-alkanes and water under hydrothermal conditions. *Geochim. Cosmochim. Acta* **77**, 582-599.
- Savage P. E. (1999) Organic chemical reactions in supercritical water. *Chem. Rev.* **99**, 603-621.
- Seewald J. S. (1994) Evidence for metastable equilibrium between hydrocarbons under hydrothermal conditions. *Nature* **370**, 285-287.
- Seewald J. S. (2001) Aqueous geochemistry of low molecular weight hydrocarbons at elevated temperatures and pressures: Constraints from mineral buffered laboratory experiments. *Geochim. Cosmochim. Acta* **65**, 1641-1664.
- Seewald J. S. (2003) Organic-inorganic interactions in petroleum producing sedimentary basins. *Nature* **426**, 327-333.
- Shimoyam A. and Johns W. D. (1971) Catalytic conversion of fatty acids to petroleum-like paraffins and their maturation. *Nature Physical Science* **232**, 140-144.
- Shipp J., Gould I. R., Herckes P., Shock E. L., Williams L. B. and Hartnett H. E. (2013) Reversibility, reactivity and reaction mechanisms for organic reactions under hydrothermal conditions. *Geochim. Cosmochim. Acta.* **104**, 194-209.
- Shock E. L. (1995) Organic acids in hydrothermal solutions: Standard molal thermodynamic properties of carboxylic acids, and estimates of dissociation constants at high temperatures and pressures. *Am. J. Sci.* **295**, 496-580.
- Shock E. L. (2000) Thermodynamic response of organic compounds in geochemical processes of sedimentary basins. *Reviews in Economic Geology*, Volume **9** (eds: T. H. Giordano, R. M. Kettler, S. A. Wood). pp. 105-117.
- Shock E. L. and Helgeson H. C. (1990) Calculation of the thermodynamic and transport properties of aqueous species at high pressures and temperatures: Standard partial molal properties of organic species. *Geochim. Cosmochim. Acta* **54**, 915-945.
- Shock E. L. and Canovas P. C. (2010) The potential for abiotic organic synthesis and biosynthesis at seafloor hydrothermal systems. *Geofluids* **10**, 161-192.
- Simoneit, B. R. T. (1992) Aqueous organic geochemistry at high temperature/high pressure. In *Marine Hydrothermal Systems and the Origin of Life*, Holm N.G. Ed., Kluwer, Dordrecht, Netherlands, Chapter 4.

Simoneit, B. R. T., Lein, A. Y. Peresykin, V. I., Osipov, G. A. (2004) Composition and origin of hydrothermal petroleum and associated lipids in the sulfide deposits of the Rainbow field (Mid-Atlantic Ridge at 36°N). *Geochim. Cosmochim. Acta* **68**, 2275-2294.

Smith M. B. and March J. (2007) *March's Advanced Organic Chemistry: Reactions, Mechanisms, and Structure*. Wiley-Interscience, Hoboken, New Jersey.

Watanabe M., Sato T., Inomata H., Smith, Jr., R. L., Arai K., Kruse A. and Dinjus E. (2004) Chemical reactions of C<sub>1</sub> compounds in near-critical and supercritical water. *Chem Rev.* **104**, 5803-5821.

Williams L. B., Holloway J. R., Canfield B., Glein C., Dick J., Hartnett H. and Shock E. L. (2010) Birth of biomolecules from the warm wet sheets of clays near spreading centers. In *Earliest Life on Earth* (eds. Golding S. and Glikson M.). Springer Publishing. Chapter 4.

Yang Z., Gould I. R., Williams L. B., Hartnett H. E., and Shock E. L. (2012) The central role of ketones in reversible and irreversible hydrothermal organic functional group transformations. *Geochim. Cosmochim. Acta* **98**, 48-65.



## CHAPTER 5:

### OXIDATION BY COPPER (II) IN HYDROTHERMAL ORGANIC REACTIONS

#### 5.1. Introduction

Copper is an abundant metal in the Earth's crust and has been extensively used in industrial society and daily life with great economic value (Marshall and Fairbridge, 1999). The geochemistry of copper plays important roles in the transport and deposit of copper in the crustal environment, and influences ore formation in related hydrothermal systems (Marshall and Fairbridge, 1999). It is thought that copper ore is predominantly derived from porphyry copper deposits, which are mostly associated with hydrothermal processes (e.g., Candela and Holland, 1986; Marshall and Fairbridge, 1999; Kesler and Wilkinson, 2008). Also, principal copper sulfide minerals such as chalcocite ( $\text{Cu}_2\text{S}$ ) and chalcopyrite ( $\text{CuFeS}_2$ ) are commonly observed in natural hydrothermal fluids (e.g., Tivey, 1995).

The understanding of the geochemistry of copper under hydrothermal conditions comes from a variety of subjects, among which solubility and speciation have been a significant research focus for copper. Copper readily goes into solution, and two common valence states exist in aqueous solution, the +2 (cupric) state and the +1 (cuprous) state. At ambient temperature, the solubility of cuprous salts is normally much lower than cupric salts. As an example, cupric chloride is highly soluble in aqueous solution, whereas cuprous chloride is normally considered to be insoluble in pure water, with a solubility product constant ( $K_{\text{sp}}$ ) of ca.  $1.72 \times 10^{-7}$  at 25°C (Patnaik, 2003). At

elevated temperatures, however, cuprous species become more soluble and stable in water, and various soluble cuprous complexes have been characterized under hydrothermal conditions (e.g., Crerar and Barnes, 1976; Var'yash, 1992; Liu et al., 2001). Solubility experiments of elemental copper and copper minerals including chalcopyrite, bornite, and chalcocite have been performed in hydrothermal sodium chloride and sulfide solutions as early as 1976 by Crerar and Barnes, who concluded that the main dissolved form of Cu is aqueous  $\text{CuCl}$  in the temperature range of 200 - 350°C. Many follow-up studies also indicated that copper mainly exists in the form of cuprous ( $\text{Cu}^{\text{I}}$ ) in hydrothermal solutions (e.g., Hemley et al., 1992; Seyfried and Ding, 1993; Xiao et al., 1998). Chloride is usually considered to be the critical counter ion in ore-forming hydrothermal fluids (Barnes, 1979; Heinrich et al., 1989). Copper-chloride complexes at high temperatures have thus been a particular focus in geochemical studies (Haynes and Bloom, 1987; Sverjensky, 1987; Liu et al., 2001), although uncertainties remain as to the exact structure of the predominant copper chloride complexes in hydrothermal solutions (Xiao et al., 1998; Archibald et al., 2002; Migdisov et al., 2014). In addition to chloride, aqueous complexation of copper with organic anions (e.g., acetate) has been investigated under hydrothermal conditions. Shock and Koretsky (1993) predicted that the dissociation of copper-acetate aqueous complexes become less thermodynamically favorable at higher temperature, and Liu et al. (2001) experimentally confirmed this by measuring the thermodynamic properties of cuprous acetate complexes in hydrothermal water up to 250°C.

Another important property of aqueous copper that is not well understood under geochemically relevant conditions is potential redox chemistry. The stability of cuprous

species in water at elevated temperatures and pressures suggests a relatively high potential for oxidation of copper (I) to copper (II). There is strong evidence in the inorganic chemistry literature that complexes of copper (II) can be involved in redox chemistry with organic structures under hydrothermal conditions (e.g., Zhang, 2005; Chen and Tong, 2007). There is also a suggestion in the literature that aqueous copper (II) can be reduced to copper (I) in the presence of aromatic ligands (Yaghi and Li, 1995), although the mechanism of the reduction has not been investigated, specifically whether it involves single electron transfer or not. Under conditions close to ambient, copper has been widely used in various oxidations of organic structures, including alkanes, alkenes, alcohols, aldehydes/ketones, and nitrogen containing compounds (Nigh, 1973; Gamez et al., 2001). In essentially all of these reactions, however, oxygen or hydrogen peroxide is the oxidizing reagent and the role of copper (II) is usually a catalyst (Allen et al., 2013). Taken as an example, cupric ions ( $\text{CuCl}_2$  or  $\text{CuBr}_2$ )-facilitated oxidation of benzyl alcohol to benzaldehyde can be achieved with good yields in hours only in the presence of molecular oxygen and other inorganic or ligand additives, such as  $\text{CsCO}_3$  and TEMPO (2,2,6,6-tetramethylpiperidine-1-oxyl) (e.g., Gamez et al., 2003; Liang et al., 2010). Oxidation reactions using copper (II) have been reported, but these reactions also require the presence of strong bases, also, the reactions only proceed if enolizable hydrogens are present (Nigh, 1973). To the best of my knowledge, there are no reports of the pure use of aqueous copper (II) ions to oxidize organic compounds under *anaerobic* hydrothermal solution. Copper (II) is a considerably milder oxidizing agent than those conventionally used in organic chemistry, which are based on Cr (VI) and Mn (VI) reagents (Smith and March, 2007), and the ability to perform oxidations in water using copper (II) would be

of great interest to both the geochemistry and the green chemistry communities. In this Chapter, novel reactions are reported in which aqueous copper (II) ions are found to oxidize model aromatic compounds, including phenylacetic acids, benzyl alcohols, and benzaldehydes, with good chemical yields in deoxygenated H<sub>2</sub>O at 250°C and 40 bar, during reaction times as short as hours or even minutes.

## 5.2. Experimental

The following materials were obtained from the commercial sources indicated: phenylacetic acid (Aldrich, 99%), p-fluorophenylacetic acid (Alfa Aesar, 98%), p-methylphenylacetic acid (Alfa Aesar, 99%), p-tert-butylphenylacetic acid (Matrix Scientific, 98%), p-trifluoromethyl-phenylacetic acid (Aldrich, 97%), p-methoxyphenylacetic acid (Aldrich, 99%), benzaldehyde (Sigma-Aldrich, 99%), p-trifluoromethyl-benzaldehyde (Acros Organics, 98%), p-methylbenzaldehyde (Aldrich, 97%), benzylalcohol (Sigma-Aldrich, 99.8%), p-trifluoromethyl-benzylalcohol (Sigma-Aldrich, 98%), p-methylbenzylalcohol (Aldrich, 98%), p-methoxybenzylalcohol (Aldrich, 98%), hydrochloric acid (Alfa Aesar), sodium hydroxide (Alfa Aesar, 98%), cupric chloride (Aldrich, 97%), dichloromethane (Fisher Scientific, 99.9%), n-decane (Sigma-Aldrich, 99%). Fresh solutions of cupric chloride with concentrations from 0.05 to 0.2 molal were prepared using high-purity water obtained from Diamond Ultrapure water system (18.2 MΩ·cm resistivity). Sodium phenylacetate was prepared by neutralizing phenylacetic acid with sodium hydroxide. The purity of all used organic materials were verified by gas chromatography.

Hydrothermal experiments were performed in fused silica glass tubes (GM Associates, Inc.) with a 6mm inside diameter and a 12mm outside diameter. The relatively large diameter tubes allow easy loading of the solid starting materials and also guarantee an adequate quantity of the organic structures for analysis after the experiments. The starting organic structure (0.10 mmol) together with 2.0 mL argon-purged cupric chloride solution were loaded into each tube to obtain a molality of 0.05 for the organic species. The samples were frozen in liquid nitrogen, degassed using pump-freeze-thaw cycles, and then sealed with a hydrogen flame under vacuum. Each fused silica glass tube (~15 cm long) was placed into a small steel pipe (~21 cm long) before heating in a gas chromatography (GC) oven at 250°C. At 250°C the pressure in the silica glass tube is calculated to be ca. 40 bar using SUPCRT 92 (Johnson et al., 1992). A thermocouple inside the GC oven next to the sample tubes was used to verify the reaction temperature. The estimated uncertainty in the temperature of the sample was within  $\pm 2^\circ\text{C}$  over the experimental duration. It was found that 10 mins of pre-heating time was necessary for the samples to reach the experimental temperature of 250°C.

The experimental reaction times ranged from 10 mins to 8 hrs at 250°C and 40 bar, depending on the particular reaction. When the desired reaction time was reached, the experiment was quenched by placing the steel pipe into a room temperature water bath. The extraction procedure was similar to that described in the previous chapters. After the fused silica tube was opened using a tube cutter, the sample was transferred into a 20 mL glass vial, and the reaction tube was then rinsed twice with 10.0 mL dichloromethane solution containing the GC internal standard n-decane (0.067% by volume). The water and dichloromethane phases were combined in the 20 mL vial. For

the phenylacetic acids and the sodium phenylacetate samples, two drops of one molar aqueous HCl was added to the reaction tubes after opening to ensure protonation of any organic acid species and extraction into the organic layer. The 20 mL vials were capped and shaken repeatedly to facilitate extraction of the organics into the dichloromethane phase. The aqueous layer was separated into a small centrifuge tube, and any suspended solid particles (e.g., CuCl) were separated by centrifugation before the analysis of cupric ion in clear aqueous solutions.

Quantitative analysis was performed for both the organic species in the dichloromethane and the aqueous species that remained in the water. The organic species were analyzed using a Varian CP-3800 gas chromatography with a flame ionization detector. Reproducibility was ensured by triplicate injections with a Varian CP-8400 autosampler. The identities of the organic products were verified by using authentic standards, and their quantities were determined based on the calibration curves that were referenced to the internal standard. Mass balance was calculated in the same way as described in previous Chapters by comparing the number of benzene rings in the products and the reactants. The aqueous samples were analyzed quickly after centrifugation, in order to minimize any air oxidation of cuprous ions to cupric. UV-Vis photospectrometer was used to measure the light absorption due to the copper (II) ions in solution at 700 nm at room temperature. The concentrations of copper (II) were determined using a calibration curve that was built with known copper (II) standards, from 0.01 to 0.20 molal. The 700 nm wavelength was selected to ensure a measurable absorbance ( $< 1.0$ ) for the concentrations of copper (II) that were studied. Measurement of the copper (I) concentration in the aqueous sample was not attempted since the solubility of copper (I)

chloride is low at room temperature (Patnaik, 2003). Triplicate measurements were taken to ensure reproducibility of the copper (II) measurements using the photospectrometer.

### **5.3. Results and discussion**

#### *5.3.1. Decomposition of the carboxylic acids, alcohols, and aldehydes*

The effect of copper (II) on the hydrothermal chemistry of phenylacetic acid, benzyl alcohol and benzaldehyde (and their derivatives) was investigated. The reactivities of these species were first measured in water alone under the experimental conditions of 250°C in the fused silica tube. It was reported previously that the conversions of one molal phenylacetic acid and sodium phenylacetate in water at 300°C and 1034 bar in gold capsules were ca. 20% and 60% after 6 hours, respectively (Glein, 2012). In both cases, toluene was observed as the dominant organic product. In contrast, the conversions of both phenylacetic acid and the sodium salt were found to be less than 8% in water alone at 250°C and 40 bar in a fused silica tube after a 6-h duration. Similarly, the reactivities of benzaldehyde and benzylalcohol were also quite low at 250°C. The conversions were less than 3% after 6 hours.

In the presence of cupric chloride (0.05 – 0.20 molal in H<sub>2</sub>O), however, the hydrothermal reactivities of all of these compounds are dramatically increased. Data from hydrothermal experiments with phenylacetic acids at 250°C are summarized in Table 1. Data for reactions of benzyl alcohols and benzaldehydes are given in Tables 2 and 3, respectively. The conversion of 0.05 molal phenylacetic acid in the presence of

0.20 molal copper (II) was ca. 68% after only 0.17 hours, whereas in water alone, the conversion was less than ca. 2%. The conversion of the carboxylate salt of phenylacetic acid, sodium phenylacetate, for the same reaction time was even greater at 85%. For 0.05 molal benzylalcohol in the presence of 0.10 molal copper (II) the conversion was 65% after 1 hour, and that of benzaldehyde was ca. 14% after 2 hours. The presence of cupric ion enhances the rate of decomposition of these organic compounds by orders of magnitude compared water alone at the experimental conditions.

More impressively, these reactions in the presence of copper (II) did not generate complex mixture of products. For the phenylacetic acids and sodium phenylacetates, benzaldehydes were observed as the dominant organic product (ca. >90%). Small quantities of benzyl alcohol were observed as a minor product, depending upon the reaction conditions, but always less than 5% of the total moles of products. The corresponding reaction of the benzyl alcohols in the presence of copper (II) was also selective. Conversions of the benzyl alcohols greater than 17% were obtained for reaction times of 0.5 and 1 h (depending upon the particular alcohol and initial cupric ion concentration, Table 2) that gave the corresponding benzaldehydes in yields of more than 80%. Small quantities (ca. <20%) of the corresponding benzoic acids were also observed when higher cupric ion concentrations (e.g., 0.20 molal) were used. The experiments starting with the benzaldehydes were exceptionally clean in that the corresponding benzoic acids were mostly observed as the only detectable products for an 8-h reaction time at 250°C and 40 bar. Satisfactory mass balance was observed for all the experiments (>90%), as shown in Tables 1 - 3. Replicate experiments were also performed to check the reproducibility of the experiments. For benzaldehyde as an



example, the conversion was found to be reproducible within less than 4% for multiple experiments (Table 3).

The reactions of phenylacetic acid and benzyl alcohol with copper (II) both yield benzaldehyde as the common major product, suggesting a linked reaction pathway among these functional groups. A plausible reaction pathway starting with phenylacetic acid is shown in Scheme I. Starting with phenylacetic acid, copper (II) can act as a one-electron oxidant for the deprotonated carboxylate, which forms a carboxyl radical that is known to undergo very rapid decarboxylation in less than microseconds at room temperature (Hilborn and Pincock, 1991). Decarboxylation forms a benzyl radical, which is known to be oxidized by copper (II) to form a benzyl cation (Turro et al., 1981), which will react with water to form a benzyl alcohol. Benzyl alcohol is proposed as a reaction intermediate in the conversion of phenylacetic acid to benzaldehyde because a small amount of benzyl alcohol was observed in short-time phenylacetic acid experiments, and it was found to be highly reactive in the presence of copper (II) under the studied conditions. Observations that are consistent with benzyl radicals being the precursors to benzyl alcohol, benzaldehyde, and benzoic acid comes from the DBK hydrothermal photolysis described earlier in this thesis, where these products were detected in abundance when benzyl radicals were generated independently in the presence of cupric chloride (Chapter 3). Further evidence in support of Scheme I was obtained from studies of the reaction stoichiometries and the ring substituent effects.

### 5.3.2. *Reaction stoichiometries*

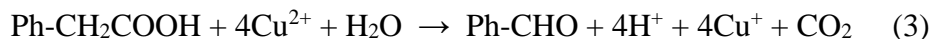
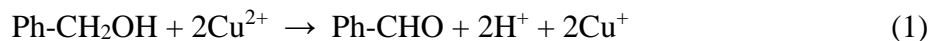
In order to determine the stoichiometry of the reactions, experiments were performed with varying concentration ratios between the starting organic compound and the copper (II) ions (Tables 1, 2, and 3). With the constant starting concentration for the organic structures of 0.05 molal, initial concentrations of copper (II) were selected to be 0.05, 0.10, and 0.20 molal, i.e., 1, 2, and 4 equivalents compared to the quantity of the organic compounds. Although measurement of reaction kinetics was not the focus of this study, the rates of disappearance of the carboxylic acids, alcohols, and aldehydes all increased with increasing copper (II) concentration. As examples, after 0.5 hours at 250°C and 40 bar, the conversions of benzyl alcohol were ca. 18, 29, and 43% in the presence of 1, 2, and 4 equivalent moles of copper (II), respectively (Table 2). Starting with benzaldehyde, conversions were ca. 14 and 23% in the presence of 2 and 4 equivalents copper (II), respectively, after 2 hours at 250°C (Table 3). These observations suggest that the copper (II) ion is involved in the rate-determining step for these reactions in Scheme I.

The conversions of phenylacetic acid to benzaldehyde, benzyl alcohol to benzaldehyde, and benzaldehyde to benzoic acid are all oxidation reactions. Each of these reactions was observed to occur with corresponding reduction of cupric ions. The disappearance of cupric ions in solution could be readily observed as a change in solution color from sky blue to colorless. In addition, white solid precipitates were usually found in the unopened fused silica tubes after the reactions at room temperature. The white-colored precipitate seems consistent with formation of solid copper (I) chloride in an

oxygen-free environment (Greenwood and Earnshaw, 1997), but inconsistent with formation of copper oxides (yellow or red for  $\text{Cu}_2\text{O}$ , black or brown for  $\text{CuO}$ ), copper hydroxide (pale blue or green), or elemental copper (orange or red). Oxidation of the organics appears to be associated with conversion of soluble cupric chloride into insoluble cuprous chloride in the aqueous solutions.

Summarized in Table 4 are the ratios of the number of moles of consumed copper (II) ions to the number of moles consumed of the starting organic. The moles of consumed copper (II) were calculated by measuring the concentration of copper (II) ions that remained in the aqueous solution photospectrometrically. The number of moles of consumed organics was quantified by gas chromatography, as discussed in the experimental section. The computed mole ratios (cupric ion/organic) fall in the range 3.5 - 3.9 for conversion of phenylacetic acid to benzaldehyde, 1.8 - 2.4 for conversion of benzyl alcohol to benzaldehyde, and 2.0 - 2.4 for conversion of benzaldehyde to benzoic acid (Table 4). Possible reasons why the mole ratios exhibited some variation include: (1) formation of minor products that may consume copper (II) but were not quantified; (2) impurities in the starting organic structures may react with copper (II); (3) small amounts of dissolved copper (I) ions may have undergone disproportionation into elemental copper and cupric ions in air (Greenwood and Earnshaw, 1997), although the spectrophotometric measurements were performed as quickly as possible to minimize this potential problem; and (4) any reduction of Cu (I) to Cu (0) under the reaction conditions would lower the apparent Cu (II) consumption (however, no obvious black solid Cu (0) was visually observed after the hydrothermal experiments). Although these minor factors would lead to small uncertainties, the rounded stoichiometric ratios for the acid, alcohol,

and aldehyde reactions were 4, 2, and 2, respectively (Table 4), which seem consistent with the balanced equations for the reactions shown in Eqns. 1 - 3.



### 5.3.3. Ring substituent effects

Ring substituent effects were investigated using both electron donating substituents (e.g., CH<sub>3</sub>, CH<sub>3</sub>O and tert-butyl) and electron withdrawing substituents (e.g., F and CF<sub>3</sub>) in the *para*-positions for the benzyl alcohol, benzaldehyde, and phenylacetic acid reactions. An increase in reaction rate with an electron donating substituent (and/or decrease with an electron withdrawing substituent) would suggest formation of a positively charged intermediate in the rate-determining step where the charge is delocalized into the benzene ring, since electron donating groups stabilize cations and radical cations. A lack of substituent effect would suggest that the rate-determining step does not delocalize charge into the benzene ring. The substituent effects observed for the three kinds of functional group, alcohol, aldehyde, and carboxylic acid, were quite different.

Experiments with ring-substituted benzyl alcohols revealed a strong influence of the *para*-substituents, Table 2. Reaction at 250°C and 40 bar with 2 equivalents of copper (II) for 0.5 hours resulted in a conversion of ca. 17% for the -CF<sub>3</sub> substituent,

compared to 29% conversion of the unsubstituted alcohol (i.e., slower reaction with the electron withdrawing substituent). With the  $-CH_3$  and  $-OCH_3$  substituents, however, the corresponding conversions were ca. 92% and 99% (i.e., much faster reaction with increasing donating ability of the substituent). These results clearly suggest formation of a cation or a radical cation intermediate in the rate-determining step for the benzyl alcohol reaction.

Experiments with the carboxylic acids revealed a very different effect of the substituents. Reaction at 250°C and 40 bar with 4 equivalents of copper (II) for 0.17 hours resulted in a conversion of ca. 66-69% for the  $-F$ ,  $-t$ -butyl,  $-CH_3$  and  $-CF_3$  substituents, compared to a 68% conversion of the unsubstituted acid. It indicates that neither electron-donating nor -withdrawing substituents substantially influenced the rate of the reaction, which in turn suggests that development of charge on the benzene ring does not occur in the rate-determining step. The reactivity of the deprotonated form of phenylacetic acid, however, was measurably higher than that of the acid itself. An 85% conversion was found for sodium phenylacetate compared to 68% for the acid. This probably suggests that it was the deprotonated form of the carboxylic acid that is reactive in the copper (II) reaction (Scheme I).

Ring-substituted benzaldehydes experiments revealed an intermediate influence of the *para*-substituents, Table 3. Reaction at 250°C and 40 bar with 4 equivalents of copper (II) for 6 hours resulted in a conversion of ca. 31% for the  $-CF_3$  substituent, compared to 39% conversion of the unsubstituted aldehyde. Reaction under the same conditions with  $-CH_3$  substituted benzaldehyde resulted in a conversion of ca. 45%. Reaction for 8 hours with 2 equivalents copper (II) gave ca. 41% for the unsubstituted

aldehyde compared to ca. 29% for the p-CF<sub>3</sub>-benzaldehyde. These results somewhat suggest a slower reaction with the electron withdrawing -CF<sub>3</sub> substituent and a faster reaction with the electron donating -CH<sub>3</sub> substituent, although the substituent effects seem to be somewhat smaller than those observed in benzyl alcohols experiments.

#### 5.3.4. Oxidation mechanisms

**Carboxylic Acids.** Decarboxylation is perhaps one of the best studied reaction of carboxylic acids (March, 1985). One of the simplest form of decarboxylations that occur under oxidative conditions is the Kolbe electrolysis (Vijh and Conway, 1967): the carboxylic acid is in equilibrium with the carboxylate, and the carboxylate undergoes one-electron oxidation at an electrode to form a carboxyl radical, which undergoes very rapid decarboxylation to form an alkyl radical. Two of these alkyl radicals then dimerize to form an alkane. Side products will form in the Kolbe electrolysis reaction when the intermediate carbon radicals can experience one-electron oxidation at the electrode. Radical oxidation generates carbocations, which in water would rapidly undergo nucleophilic addition with ultimate formation of an alcohol. One-electron oxidation is also frequently encountered in metal ion oxidations of a variety of organic structures (Sheldon and Kochi, 1981), and it has been shown that copper (II) was more effective than other metals in oxidation of radicals to corresponding carbocations (Kochi, 1967; 1974). Based on the mechanisms of the known Kolbe electrolysis and other metal ion oxidations, one-electron transfer mechanism can be proposed as the basis for the copper

(II) oxidation of the phenylacetic acids. A detailed proposed reaction sequence is given in Scheme II for hydrothermal conversion of the carboxylic acid to benzyl alcohol.

Analogous to Kolbe electrolysis reaction, it can be expected that carboxylate anion would undergo one-electron oxidation to form a carboxyl radical. This is consistent with the observation that the hydrothermal reaction proceeds more rapidly when starting with the carboxylate compared to the acid. The kinetics of one-electron transfer reactions are determined from the energy change associated with electron transfer, which in turn can be determined from the difference in the potentials for the appropriate redox couples. Accurate measurements of the potentials cannot be made for many of the redox couples relevant to the copper (II) oxidations discussed here, since redox equilibrium cannot be attained due to rapid follow-up or competing reactions of one or both partners in the couples, especially for the organic species. Nevertheless, some estimates can be found in the literature, and they are summarized in Table 5.

From Table 5 it can be seen that one-electron transfer from the carboxylate anion to the copper (II) ion ( $et_1$ ) is endothermic by ca. 1.9 eV. Electron transfer from the benzyl radical to copper (II) is also endothermic ( $et_2$ ), but significantly less, ca. 0.7 eV. One-electron oxidation of benzyl radicals should thus be much faster than oxidation of the carboxylate anion. Copper (II) is known to trap carbon-centered radicals efficiently (Sheldon and Kochi, 1981), and benzyl radicals in particular have been shown to be trapped efficiently even at room temperature in water (Turro et al., 1981). Furthermore, evidence of trapping of benzyl radicals under hydrothermal conditions has also been collected in hydrothermal photolysis of DBK (see Chapter 3), where benzyl radicals were trapped with Cu (II) and generated the oxidized products such as benzyl alcohol,

benzaldehyde and benzoic acid. The experimental observations are thus consistent with the rapid electron transfer from benzyl radicals to copper (II) under the experimental conditions.

As mentioned previously, decarboxylation of the carboxyl radical ( $-CO_2$ ) is expected to be very fast. Addition of water to the benzyl cation ( $+H_2O$ ) should also be fast (Anslyn and Dougherty, 2005), as should the final deprotonation step ( $-H^+$ ) in hot water. It thus suggests that the rate-determining step in Scheme II should be the first electron transfer reaction ( $et_1$ ) from the carboxylate to copper (II).

Estimation of the rate constant,  $k_{et}$ , for this electron transfer process, can be attempted using Marcus electron transfer theory (Marcus and Sutin, 1985). In Eqn. 4a,  $k$  is Boltzmann's constant,  $h$  is Planck's constant, and  $\Delta G^\ddagger$  is the activation free energy for the electron transfer reaction. The activation free energy is given by Eqn. 4b, where  $\Delta G$  is the free energy for the reaction, given by the difference in the redox potentials (Table 5), and  $\lambda$  is the reaction reorganization energy. The reorganization energy is not precisely known, but for ionic reactions in water,  $\lambda$  is presumably large, perhaps around 40 kcal/mol (Ebersson, 1988). If using this value for the reorganization energy in Eqns. 4, ca.  $0.01 \text{ hr}^{-1}$  can be estimated for  $k_{et}$  at the experimental temperature of  $250^\circ\text{C}$ . Based on the observation of ca. 68% conversion of the phenylacetic acid in 0.17 hours, the actual rate constant was estimated as ca.  $2 \text{ hr}^{-1}$ . However, it is found that the calculated rate constant is very sensitive to the values of the redox potentials, and those in Table 5



$$k_{\text{et}} = \frac{kT}{h} e^{-\frac{\Delta G^\ddagger}{RT}} \quad (4a)$$

$$\Delta G^\ddagger = \frac{(\lambda + \Delta G)^2}{4\lambda} \quad (4b)$$

almost certainly do not apply to the experimental conditions, particularly that for the Cu(I)/Cu(II) couple. The Cu(I)/Cu(II) value in Table 5 is for fully solvated ions in water at room temperature, and at 250°C the copper (II) ions should be more associated with anions (e.g., Shock and Koretsky, 1993), which will probably raise the electron transfer rate constant. Furthermore, if the Cu (II) is associated with the carboxylate anion, weak ionic bonds will be formed between them, and an additional increase in the rate constant would be expected, because the electron transfer across weak bonds should be faster than via bimolecular collision (Marcus and Sutin, 1985). Hence, the rate-determining single electron transfer seems plausible on the reaction timescale.

Also consistent with rate-determining carboxylate one-electron oxidation is the observed substituent effects. The carboxylate anion is not directly conjugated with the benzene ring, so benzene-ring substituents should not much influence the oxidation for the carboxylate anion. One-electron oxidation of the phenylacetate anion should occur at the carboxylate rather than the benzene ring, since the carboxylate has a lower redox potential than toluene (Table 5), which can be a reasonable model for the benzene ring of phenylacetic acid. Finally, the stoichiometry experiments suggest that two Cu (II) ions should be consumed to generate each benzyl alcohol, which is also consistent with Scheme II.

***Benzyl Alcohols.*** One-electron transfer is a common mechanism for metal cation oxidations of organics (Sheldon and Kochi, 1981), and a mechanism for copper (II) oxidation of benzyl alcohol can be written based on one-electron transfer that is consistent with the experimental observations, Scheme III. The oxidation potential for benzyl alcohol is not known, but the potential for a model mono-benzene substituted toluene has been reported to be ca. 2.6 V vs. Standard Hydrogen Electrode (SHE), Table 5. Electron transfer from benzyl alcohol to copper (II) is thus more endothermic than from the carboxylate anion. Oxidation of benzyl alcohol can generate an aromatic radical cation. Aromatic radical cations with benzylic hydrogens are known to be strong Brønsted acids (Nicholas and Arnold, 1982), so deprotonation should be rapid, to generate a benzylic radical (Scheme III). As discussed previously, one-electron oxidation of benzyl radicals by copper (II) was rapid and efficient. The product of one-electron oxidation of this benzyl radical is the protonated benzaldehyde, which will also deprotonate rapidly as a strong Brønsted acid. The rate-determining step for Scheme III is thus the initial one-electron oxidation of the alcohol ( $et_1$ ).

Although an accurate oxidation potential for benzyl alcohol has not been documented, it is presumably larger than that for phenyl acetate because of the inductive effect of the oxygen in the -OH group. Benzyl alcohol oxidation using copper (II) can thus be predicted to be slower than the corresponding reaction with phenyl acetate, and this is indeed observed in the hydrothermal experiments. Furthermore, since oxidation of benzyl alcohol will generate a positive charge directly on the benzene ring, substituent effects are expected to be substantial, and this is also observed. Electron-donating substituents greatly accelerated the reaction and the electron-withdrawing substituents

slowed the reaction down, again are consistent with Scheme III. In addition, the measured reaction stoichiometry also supports the proposed oxidation scheme for benzyl alcohol.

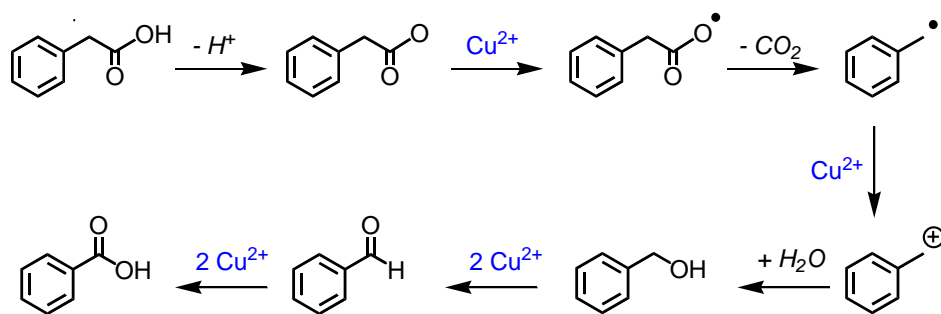
***Benzaldehydes.*** A possible reaction sequence for hydrothermal conversion of benzaldehyde to benzoic acid with copper (II) is proposed in Scheme IV. Oxidation of aldehydes to carboxylic acids in aqueous media almost always involves the intermediacy of a hydrate (Smith and March, 2007). Hydrate formation occurs by addition of H<sub>2</sub>O to the C=O bond of the aldehyde (Scheme IV). This addition is usually Brønsted acid or base catalyzed (Smith and March, 2007), and such catalysts are readily available in high temperature water where establishment of aldehyde/hydrate equilibrium should be rapid. Once formed, conversion of the hydrate to the benzoic acid could follow the same mechanism as oxidation of benzyl alcohol to the aldehyde (Scheme III), so the rate-determining step in Scheme IV will again be expected to be the first one-electron oxidation reaction (*et*<sub>1</sub>). However, there is a pre-equilibrium situation in this case, because the overall rate of the reaction will be modified by the equilibrium concentration of the hydrate. Although little is known about the equilibrium concentration of hydrates under hydrothermal conditions, the equilibrium should lie on the side of the aldehyde in the case of benzaldehyde in water close to ambient conditions (Smith and March, 2007), and since dehydration seems to be favored at higher temperatures (Shock et al., 2013), a low equilibrium concentration of hydrate would be expected under the experimental conditions. For this reason, oxidation of benzaldehyde will probably be slower than oxidation of benzyl alcohol, and this is indeed observed.

Although the relative reactivities of the aldehyde and the alcohol seem consistent with the proposed Schemes, the experimental data did not provide direct evidence for the intermediacy of a hydrate. Substituent effects were observed for the benzaldehyde oxidations. Electron-donating substituents are expected to increase the rate of the first electron transfer reaction, as observed with the benzyl alcohols, however, the formation of hydrate should be less favorable for benzaldehydes that have electron-donating groups. In fact, in some oxidation reactions of benzaldehydes that involve hydrate formation, electron-donating substituents can decrease the reaction rate due to a lower equilibrium concentration of the hydrate (Stewart, 1964). Wiberg and Richardson (1961) reported that donating substituents accelerated the oxidations of benzaldehydes using manganese (III or IV) ions as the oxidant, but the opposite effect was observed using chromic acid as the oxidant, which involves formation of a chromate ester but not via a one-electron oxidation process. Therefore, according to Scheme IV, there will probably be opposing effects of substituents in the benzene ring of benzaldehydes. The observed substituent effects for the benzaldehydes were in the same direction as for the benzyl alcohols, but the effects were diminished compared to the alcohols. This observation seems consistent with the opposing substituent effects predicted by Scheme IV, but concretizing the reaction mechanisms should require more information such as equilibrium concentrations of hydrates under the hydrothermal conditions.

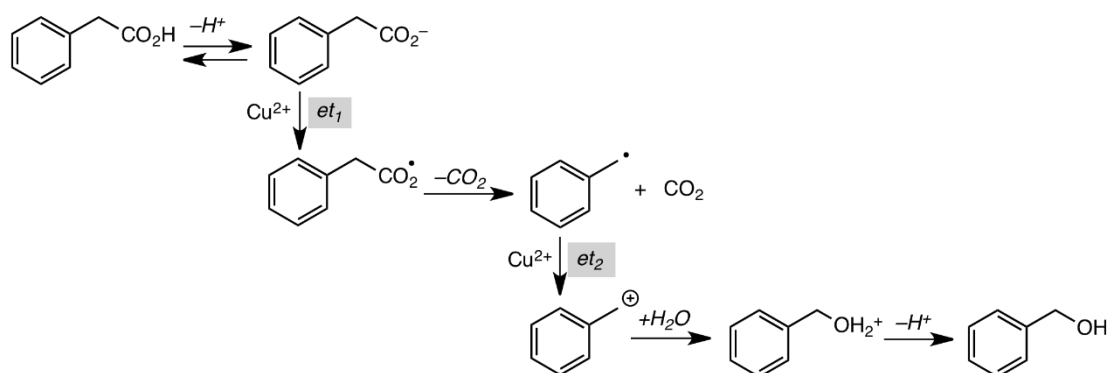
## 5.4. Conclusions

This work describes new oxidation reactions using the mild oxidant copper (II) under hydrothermal conditions. The excellent conversions and high selectivity of these reactions have implications in both organic chemistry and geochemistry. From a perspective of conventional organic chemistry, the reactions use an inexpensive and mild oxidant in water solvent, with no need for oxygen or any other additives. From a geochemist perspective, the results suggest that the hydrothermal chemistry of copper and other metal ions may be involved in many other geological processes in addition to ore formation, such as controlling natural organic hydrothermal transformations. Some remaining questions from this study may include understanding the scope of the copper (II) oxidation in more organic hydrothermal reactions, and to what extent other di- and tri-valent metal cations might do similar reactions. More detailed investigation of reaction kinetics and studies of the possible role of hydrates in the aldehyde oxidations would be desirable. Finally, a study of the speciation of copper (II) ions under the reaction conditions will also be necessary in order to develop a full understanding of the mechanisms of these interesting reactions.

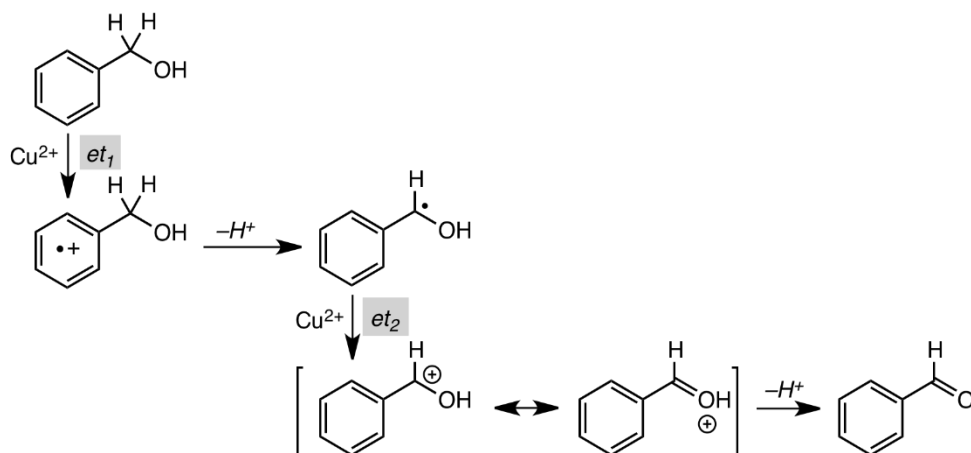
**Scheme I.** Proposed cupric ion hydrothermal oxidation pathway from phenylacetic acid through benzyl alcohol, benzaldehyde to benzoic acid in H<sub>2</sub>O at 250°C and 40 bar.



**Scheme II.** Proposed reaction sequence for hydrothermal conversion of phenylacetic acid to benzyl alcohol with copper (II) ions. Each single electron transfer reaction (*et*) results in conversion of one copper (II) ion into one copper (I) ion.



**Scheme III.** Proposed reaction sequence for hydrothermal conversion of benzyl alcohol to benzaldehyde with copper (II) ions. Each single electron transfer reaction (*et*) results in conversion of one copper (II) ion into one copper (I) ion.





**Scheme IV.** Proposed reaction sequence for hydrothermal conversion of benzaldehyde to benzoic acid with copper (II) ions. Each single electron transfer reaction (*et*) results in conversion of one copper (II) ion into one copper (I) ion.

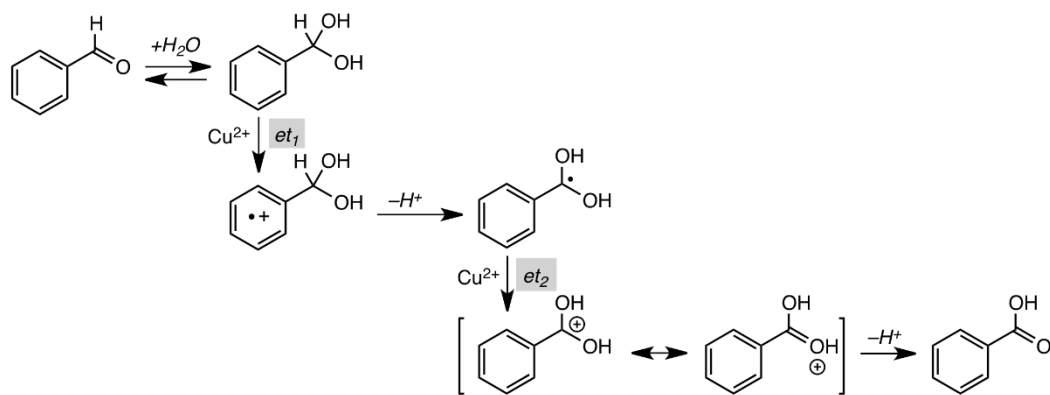


**Table 1.** Abundances of organic compounds and cupric ion from experiments with phenylacetic acids and sodium phenylacetate in H<sub>2</sub>O (2.0 mL) at 250°C and 40 bar in fused silica tubes. Initial acid/acetate stands for the appropriate phenylacetic acid (non-substituted or substituted) and sodium phenylacetate, final acid represents for the dichloromethane extracted phenylacetic acids after acidifying with one molar aqueous HCl, and final aldehyde means the corresponding benzaldehyde which was produced as the dominant product in these experiments. ND means not detected (<1 μmol), and NA means not available. To be noted that other products with small quantity such as benzyl alcohol and benzoic acid were observed but not included in this table.

Starting Material	Temp. (°C)	Time (hrs)	Conv. (%)	Initial Acid/acetate (μmol)	Initial Cu <sup>2+</sup> (μmol)	Final Acid (μmol)	Final Cu <sup>2+</sup> (μmol)	Final Aldehyde (μmol)	Mass Balance (%)
Phenylacetic acid	250	8	<5	100	0	97	0	ND	98
Phenylacetic acid	250	8	25	101	100	75.2	10	20.4	97
Phenylacetic acid	250	8	98	100	400	1.4	44	89	95
Phenylacetic acid	250	2	96	99	400	2.4	<10	97	99
p-F-phenylacetic acid	250	2	97	99	400	2.9	<10	84	94
p-tert-Butyl-phenylacetic acid	250	2	98	99	400	1.8	<10	92	95
Sodium phenylacetate	250	2	99	100	400	ND	<10	96	102
Phenylacetic acid	250	0.5	98	100	400	1.2	<10	95	101
p-F-phenylacetic acid	250	0.5	98	101	400	1.5	<10	94	97
p-tert-Butyl-phenylacetic acid	250	0.5	97	100	400	2.1	<10	87	94
p-CH <sub>3</sub> -phenylacetic acid	250	0.5	96	100	400	3.2	<10	92	97

Sodium phenylacetate	250	0.5	99	100	400	1.1	<10	96	101
Phenylacetic acid	250	0.17	68	100	400	32.6	140	64.2	101
p-F-phenylacetic acid	250	0.17	66	101	400	35.1	152	63.4	100
p-tert-Butyl-phenylacetic acid	250	0.17	68	102	400	32.1	142	65.5	98
p-CH <sub>3</sub> -phenylacetic acid	250	0.17	67	100	400	32.8	159	63.6	97
p-CF <sub>3</sub> -phenylacetic acid	250	0.17	69	100	400	30.1	NA	62.5	96
Sodium phenylacetate	250	0.17	85	101	400	15.6	88	82.3	98

**Table 2.** Abundances of organic compounds and cupric ion from experiments with benzyl alcohols in H<sub>2</sub>O (2.0 mL) at 250°C and 40 bar in fused silica tubes. Initial and final alcohol stand for the appropriate benzyl alcohol (non-substituted or substituted), final aldehyde means the corresponding benzaldehyde which was produced as the dominant product in these experiments. ND means not detected (<1 μmol), and NA means not available. To be noted that other products with small quantity such as benzoic acid were observed but not included in this table.

Starting Material	Temp. (°C)	Time (hrs)	Conv. (%)	Initial Alcohol (μmol)	Initial Cu <sup>2+</sup> (μmol)	Final Alcohol (μmol)	Final Cu <sup>2+</sup> (μmol)	Final Aldehyde (μmol)	Mass Balance (%)
Benzyl alcohol	250	1	41	100	100	58.1	22	36.7	92
Benzyl alcohol	250	1	65	100	200	34.4	42	62.2	97
p-CF <sub>3</sub> -benzyl alcohol	250	1	27	100	200	68.7	NA	25.8	95
p-CH <sub>3</sub> -benzyl alcohol	250	1	92	100	200	8.2	NA	87.5	97
p-CH <sub>3</sub> O-benzyl alcohol	250	1	99	100	200	ND	NA	78.3	93
Benzyl alcohol	250	0.5	18	100	100	81.8	68	16.8	98
Benzyl alcohol	250	0.5	29	100	200	70.6	NA	27.2	97
Benzyl alcohol	250	0.5	43	100	400	56.6	298	36.2	96
p-CF <sub>3</sub> -benzyl alcohol	250	0.5	17	100	200	82.6	NA	14.7	99
p-CH <sub>3</sub> -benzyl alcohol	250	0.5	78	100	200	31.7	NA	66.8	98
p-CH <sub>3</sub> O-benzyl alcohol	250	0.5	99	100	200	ND	NA	77.1	92

**Table 3.** Abundances of organic compounds and cupric ion from experiments with benzaldehydes in H<sub>2</sub>O (2.0 mL) at 250°C and 40 bar in fused silica tubes. Initial and final aldehyde stand for the appropriate benzaldehyde (non-substituted or substituted), final acid means the corresponding benzoic acid which was produced as the dominant product in these experiments. NA means not available.

Starting Material	Temp. (°C)	Time (hrs)	Conv. (%)	Initial Aldehyde (μmol)	Initial Cu <sup>2+</sup> (μmol)	Final Aldehyde (μmol)	Final Cu <sup>2+</sup> (μmol)	Final Acid (μmol)	Mass Balance (%)
Benzaldehyde	250	8	41	100	200	55.3	108	40.4	96
p-CF <sub>3</sub> -benzaldehyde	250	8	29	100	200	71.6	136	25.5	98
Benzaldehyde	250	6	38	100	400	61.3	316	37.1	98
Benzaldehyde <sup>a</sup>	250	6	39	100	400	60.6	NA	38.2	99
p-CF <sub>3</sub> -benzaldehyde	250	6	32	100	400	65.7	322	40.2	96
p-CF <sub>3</sub> -benzaldehyde <sup>a</sup>	250	6	30	100	400	67.3	NA	29.8	97
p-CH <sub>3</sub> -benzaldehyde	250	6	44	100	400	54.4	302	41.8	98
p-CH <sub>3</sub> -benzaldehyde <sup>a</sup>	250	6	45	100	400	53.5	NA	42.4	97
Benzaldehyde	250	2	12	100	200	87.2	174	10.4	97
Benzaldehyde <sup>a</sup>	250	2	16	100	200	83.8	162	15.6	99
Benzaldehyde	250	2	23	100	400	76.5	344	21.2	98

<sup>a</sup>, Experiments were performed in the same run to ensure reproducibility.

**Table 4.** Mole ratios and stoichiometric ratios between the consumed cupric ions and the consumed starting organic compounds in H<sub>2</sub>O (2.0 mL) at 250°C and 40 bar in fused silica tubes. The starting moles of the organic compounds were all ca. 100, whereas the starting moles of cupric ions were varied between 100 and 400 in these hydrothermal experiments. The stoichiometric ratios were estimated as 4, 2, and 2 for the reactions between phenylacetic acid and Cu<sup>2+</sup>, benzyl alcohol and Cu<sup>2+</sup>, and benzaldehyde and Cu<sup>2+</sup>, respectively.

Starting Material	Temp. (°C)	Time (hrs)	Conv. (%)	Consumed Cu <sup>2+</sup> (μmol)	Consumed Organics (μmol)	Consumed mole ratio	Estimated Stoichiometric ratio
Acid/acetate							
Phenylacetic acid <sup>a</sup>	250	8	25	90	25.8	3.5	4
Phenylacetic acid <sup>b</sup>	250	8	98	356	98.6	3.6	4
Phenylacetic acid <sup>b</sup>	250	0.17	68	260	67.4	3.9	4
p-F-phenylacetic acid <sup>b</sup>	250	0.17	66	248	65.9	3.8	4
p-tert-Butyl-phenylacetic acid <sup>b</sup>	250	0.17	68	258	69.9	3.7	4
p-CH <sub>3</sub> -phenylacetic acid <sup>b</sup>	250	0.17	67	241	67.2	3.6	4
Sodium phenylacetate <sup>b</sup>	250	0.17	85	312	85.4	3.7	4
Alcohol							
Benzyl alcohol <sup>a</sup>	250	1	41	78	41.9	1.9	2
Benzyl alcohol <sup>c</sup>	250	1	65	158	65.6	2.4	2
Benzyl alcohol <sup>a</sup>	250	0.5	18	32	18.2	1.8	2
Benzyl alcohol <sup>b</sup>	250	0.5	43	102	43.4	2.3	2
Aldehyde							
Benzaldehyde <sup>c</sup>	250	8	41	92	44.7	2.1	2

p-CF <sub>3</sub> - benzaldehyde <sup>c</sup>	250	8	29	64	28.4	2.3	2
Benzaldehyde <sup>b</sup>	250	6	38	84	38.7	2.2	2
p-CF <sub>3</sub> - benzaldehyde <sup>b</sup>	250	6	32	78	34.3	2.3	2
p-CH <sub>3</sub> - benzaldehyde <sup>b</sup>	250	6	42	98	45.6	2.1	2
Benzaldehyde <sup>c</sup>	250	2	12	26	12.8	2.0	2
Benzaldehyde <sup>c,d</sup>	250	2	16	38	16.2	2.3	2
Benzaldehyde <sup>b</sup>	250	2	23	56	23.5	2.4	2

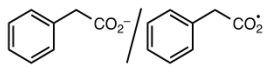
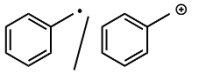
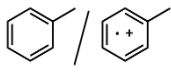
<sup>a</sup>, Experiments were started with 1 equivalent of copper (II) chloride;

<sup>b</sup>, Experiments were started with 4 equivalents of copper (II) chloride;

<sup>c</sup>, Experiments were started with 2 equivalents of copper (II) chloride;

<sup>d</sup>, Experiments were performed in the same run to ensure reproducibility.

**Table 5.** Estimated redox potentials for oxidation of the carboxylate anion, the benzyl radical, toluene, and copper (I) ion that are relevant to single electron transfer processes. The redox potentials are relative to the standard hydrogen electrode (SHE) as a reference.

Structure				Cu(I) / Cu(II)
$E_{\text{redox}}$ (V vs. SHE)	~2.1 <sup>a</sup>	~0.9 <sup>b</sup>	~2.6 <sup>c</sup>	~0.2 <sup>d</sup>

<sup>a</sup> See reference (Eberson, 1988);

<sup>b</sup> See reference (Wayner and Griller, 1985);

<sup>c</sup> See reference (Howell et al., 1984);

<sup>d</sup> See reference (James and Williams, 1961).



## 5.5. References

- Allen S. E., Walvoord R. R., Padilla-Salinas R. and Kozlowski M. C. (2013) Aerobic copper-catalyzed organic reactions. *Chem. Rev.* **113**, 6234-6458.
- Anslyn E. and Dougherty D. (2005) *Modern Physical Organic Chemistry*. University Science Books, Sausalito, CA.
- Archibald S. M., Migdisov A. A. and Williams-Jones A. E. (2002) An experimental study of the stability of copper chloride complexes in water vapor at elevated temperatures and pressures. *Geochim. Cosmochim. Acta* **66**, 1611-1619.
- Barnes H. L. (1979) Solubility of ore minerals. *Geochemistry of Hydrothermal Ore Deposits* (ed. H. L. Barnes). John Wiley & Sons, New York.
- Candela P. and Holland H. D. (1986) A mass transfer model for copper and molybdenum in magmatic hydrothermal systems; the origin of porphyry-type ore deposits. *Econ. Geol.* **81**, 1-19.
- Chen X. and Tong M. (2007) Solvothermal in situ metal/ligand reactions: A new bridge between coordination chemistry and organic synthetic chemistry. *Acc. Chem. Res.* **40**, 162-170.
- Crerar D. A. and Barnes H. L. (1976) Ore solution chemistry. V. Solubilities of chalcopyrite and chalcocite assemblages in hydrothermal solution at 200 to 350°C. *Econ. Geol.* **71**, 772-794.
- Eberson L. (1988) *Electron Transfer Reactions in Organic Chemistry*. Springer-Verlag, New York.
- Gamez P., Arends I., Reedijk J. and Sheldon R. A. (2003) Copper (II)-catalysed aerobic oxidation of primary alcohols to aldehydes. *Chem. Comm.* **19**, 2014-2015.
- Gamez P., Aubel P. G., Driessen W. L. and Reedijk R. (2001) Homogeneous bio-inspired copper-catalyzed oxidation reactions. *Chem. Soc. Rev.* **30**, 376-385.
- Greenwood N. N. and Earnshaw A. (1997) *Chemistry of the Elements*, 2nd ed., Butterworth-Heinemann, Oxford, UK.
- Haynes D. W. and Bloom M. (1987) Stratiform copper deposits hosted by low-energy sediments: III. Aspects of metal transport. *Econ. Geol.* **82**, 635-648.

- Heinrich C. A., Henley R. W. and Seward T. M. (1989) *Hydrothermal Systems*. Australian Mineral Foundation, Adelaide.
- Hemley J. J., Cygan G. L., Fein J. B., Robinson G. R., and D'Angelo W. M. (1992) Hydrothermal ore-forming process in the light of studies in rock-buffered systems, I. Iron-copper-zinc-lead sulfide solubility relations. *Econ. Geol.* **87**, 1-22.
- Hilborn J. W. and Pincock J. A. (1991) Rates of decarboxylation of acyloxy radicals formed in the photocleavage of substituted 1-naphthylmethyl alkanoates. *J. Am. Chem. Soc.* **113**, 2683-2686.
- Howell J. O., Goncalves J. M., Amatore C., Klasinc L., Wightman R. and Kochi J. K. (1984) Electron transfer from aromatic hydrocarbons and their  $\pi$ -complexes with metals. Comparison of the standard oxidation potentials and vertical ionization potentials. *J. Am. Chem. Soc.* **106**, 3968-3976.
- James B. R. and Williams R. J. P. (1961) The oxidation-reduction potentials of some copper complexes. *J. Chem. Soc.* 2007-2019.
- Kesler S. E. and Wilkinson B. H. (2008) Earth's copper resources estimated from tectonic diffusion of porphyry copper deposits. *Geology*. **36**, 255-258.
- Kochi J. K. (1967) Mechanisms of organic oxidation and reduction by metal complexes. *Science* **155**, 415-424.
- Kochi J. K. (1974) Electron-transfer mechanisms for organometallic intermediates in catalytic reactions. *Accts. Chem. Res.* **7**, 351-360.
- Liang, L.; Rao, G.; Sun, H.-L.; Zhang, J.-L. (2010) Aerobic oxidation of primary alcohols catalyzed by copper salts and catalytically active  $\mu$ -hydroxyl-bridged trinuclear copper intermediate. *Adv. Synth. Catal.* **352**, 2371-2377.
- Liu W., McPhail D. C. and Brugger J. (2001) An experimental study of copper (I)-chloride and copper (I)-acetate complexing in hydrothermal solutions between 50°C and 250°C and vapor-saturated pressure. *Geochim. Cosmochim. Acta* **17**, 2937-2948.
- Lu J. Y. (2003) Crystal engineering of Cu-containing metal-organic coordination polymers under hydrothermal conditions. *Coord. Chem. Rev.* **246**, 327-347.
- March J. (1985) *Advanced Organic Chemistry: Reactions, Mechanisms, and Structure* (third edition). Wiley, New York.
- Marcus R. A. and Sutin N. (1985) Electron transfers in chemistry and biology. *Biochim. Biophys. Acta* **811**, 265-322.

- Marshall C. P. and Fairbridge R. W. (1999) *Encyclopedia of Geochemistry*. Kluwer Academic Publishers, The Netherlands.
- Migdisov A. A., Bychkov A. Y., Williams-Jones A. E. and Hinsberg V (2014) A predictive model for the transport of copper by HCl-bearing water vapour in ore-forming magmatic-hydrothermal systems: Implications for copper porphyry ore formation. *Geochim. Cosmochim. Acta* **129**, 33-53.
- Nicholas A. and Arnold D. (1982) Thermochemical parameters for organic radicals and radical ions. I. The estimation of the  $pK_a$  of radical cations based on thermochemical calculations. *Can. J. Chem.* **60**, 2165-2179.
- Nigh W. G. (1973) Oxidation by cupric ion. In *Oxidation in Organic Chemistry* (ed. Trahanovsky W. S.). Vol. 5-B. Academic Press, New York.
- Patnaik P. (2003) *Handbook of Inorganic Chemicals*. McGraw-Hill, New York.
- Seyfried Jr. W. E. and Ding K. (1993) The effect of redox on the relative solubility of copper and iron in Cl-bearing aqueous fluid at elevated temperature and pressures: An experimental study with application to subseafloor hydrothermal systems. *Geochim. Cosmochim. Acta* **57**, 1905-1918.
- Sheldon R. A. and Kochi J. K. (1981) *Metal-catalysed Oxidations of Organic Compounds*. Academic Press, New York.
- Shock E. L., Canovas P., Yang Z., Boyer G., Johnson K., Robinson K., Fecteau K., Windman T., and Cox A. (2013) Thermodynamics of organic transformations in hydrothermal fluids. *Rev. Mineral. Geochem.* **76**, 311-350.
- Shock E. L. and Koretsky C. M. (1993) Metal-organic complexes in geochemical processes: Calculations of standard partial molal thermodynamic properties of aqueous acetate complexes at high pressures and temperatures. *Geochim. Cosmochim. Acta* **57**, 4899-4922.
- Smith M. B. and March J. (2007) *March's Advanced Organic Chemistry: Reactions, Mechanisms, and Structure*. Wiley-Interscience, Hoboken, New Jersey.
- Stewart R. (1964) *Oxidation Mechanisms*. Benjamin Press, New York. p. 49.
- Sverjensky D. A. (1987) The role of migrating oil field brines in the formation of sediment-hosted Cu-rich deposits. *Econ. Geol.* **82**, 1130-1141.

- Tivey M. K. (1995) The influence of hydrothermal fluid composition and advection rates on black smoker chimney mineralogy: Insights from modeling transport and reaction. *Geochim. Cosmochim. Acta* **59**, 1933–1949.
- Turro N. J., Chow M-F., Chung C-J., Tanimoto Y. and Weed G. (1981) Time-resolved laser flash spectroscopic study of benayl radical pairs in micelle cages. *J. Am. Chem. Soc.* **103**, 4574-4576.
- Var'yash L. N. (1992) Cu (I) complexing in NaCl solutions at 300 and 350°C. *Geochem. Intl.* **29**, 84-92.
- Vijh A. K. and Conway B. E. (1967) Electrode kinetic aspects of the Kolbe reaction. *Chem. Rev.* **67**, 623-664.
- Wayner D. and Griller D. (1985) Oxidation and reduction potentials of transient free-radicals. *J. Am. Chem. Soc.* **107**, 7764-7765.
- Wiberg K. B. and Richardson W. H. (1961) The chromic acid oxidation of aromatic aldehydes. Some observations concerning the oxidation by the chromium species of intermediate valence. *J. Am. Chem. Soc.* **84**, 2800-2807.
- Xiao Z., Gammons C. H. and Williams-Jones A. E. (1998) Experimental study of copper (I) chloride complexing in hydrothermal solutions at 40 to 300°C and saturated water vapor pressure. *Geochim. Cosmochim. Acta* **62**, 2949-2964.
- Yaghi O. M. and Li H. (1995) Hydrothermal synthesis of a metal-organic framework containing large rectangular channels. *J. Am. Chem. Soc.* **117**, 10401-10402.
- Zhang X. (2005) Hydro(solvo)thermal in situ ligand syntheses. *Coord. Chem. Rev.* **249**, 1201-1219.

## CHAPTER 6:

### SUMMARY OF CHAPTERS AND OUTLOOK FOR FUTURE WORK

#### 6.1. Summary of current work

One of the main themes of the work described in this dissertation is the use of conventional mechanistic and physical organic techniques to provide insight into geochemically relevant hydrothermal organic transformations. As detailed in the previous Chapters, model organic structures have been used as tools to probe hydrothermal reaction mechanisms, dibenzylketone (DBK) in particular. The benzylic positions of DBK stabilize reaction intermediates which facilitate fragmentation and formation of coupling products. Ketones are not as abundant as alkanes/alkenes and carboxylic acids in natural systems, but they link these functional groups via functional group interconversions (e.g., Seewald, 2003). A detailed experimental study of DBK in hydrothermal water alone identified both reversible and irreversible reactions for this specific ketone. Many of the products are consistent with previously proposed reaction schemes, but some are different. For DBK, reversibility was observed across the ketone, alcohol, alkene and alkane functional groups within a single chemical structure family for the first time, in support of the Seewald reaction scheme (Figure 1). Irreversible bond fragmentation occurred to generate a range of smaller fragmentation and larger coupling products. Nevertheless, no carboxylic acids were observed in water alone for hydrothermal reaction of a ketone that is specifically designed to facilitate bond fragmentation, at least under the conditions of the experiments described in this thesis.

The complexity of hydrothermal organic products has always been a challenge for organic geochemists, and DBK is not an exception in this regard. Chapter 3 of this thesis describes the use of hydrothermal photochemistry as a novel tool for organic geochemistry, which was particularly useful in unraveling the complex reaction pathways for DBK. For ketones, photochemistry represents a good method for generating radical species. Conducting photolysis of DBK under hydrothermal allowed the primary radical products of conventional hydrothermolysis to be isolated. Photolysis followed by thermolysis further allowed the follow-up ionic reactions to be studied, which is not possible in pure hydrothermal reactions.

Having mapped out the detailed reaction pathways, the hydrothermal chemistry of DBK in water alone represented a firm foundation for studying the interactions between ketones and inorganic species, specifically minerals and metal ions, under hydrothermal conditions. Some dramatic and selective mineral effects were observed for the model ketone DBK. The iron-bearing oxide minerals magnetite and hematite had a very different effect than the iron sulfide mineral troilite. Magnetite and hematite were found to facilitate carbon-carbon bond breaking at the benzylic position of DBK, so that bond fragmentation and radical coupling products were predominant with these minerals. Additionally, small quantities of carboxylic acids were found with the oxide minerals, possibly suggesting that mineral interactions are required for formation of these functional groups. Troilite also increased ketone hydrothermal reactivity, but in this case reduced products formed via functional group interconversions were the predominant products. Compared to water alone, the reduced alcohol, alkene, and alkane products were formed abundantly. In addition to solid minerals, the aqueous metal ion  $\text{Cu}^{2+}$  was

found to be a strong hydrothermal oxidant for various organic functional groups. Clean and rapid reactions that converted alcohols to aldehyde and aldehydes to carboxylic acids were observed. Very rapid decarboxylation accompanied by oxidation of phenylacetic acids was also observed in cupric hydrothermal solutions. These results are surprising since the cupric ion is generally considered to be unreactive towards organic structures at ambient. This work points towards possible extensions of hydrothermal geochemistry into conventional organic chemistry.

## **6.2. What we learned from the hydrothermal organic reactions**

Two different kinds of natural hydrothermal organic environments can be envisioned. One includes long-term transformations that allow organic matter to reach metastable equilibria in a geological time scale, examples include sedimentary basins where the reactions are under thermodynamic control. The other includes shorter-time transformations such as might occur upon the initial mixing of organic matter with hydrothermal fluids, where the reactions may be under kinetic control. The work described in this thesis focused on shorter timescale experiments in order to identify primary reaction products and to allow mechanistic analysis, and thus may be more relevant to the second scenario.

In the Seewald scheme (Figure 1), the interconversions between alkanes, alkenes, alcohols, ketones, and carboxylic acids were proposed. Much of what was known about the various functional group interconversions came from the work of Siskin and Katrizky, McCollom and Seewald and others, as described in the preceding Chapters.

Many individual reactions have previously been described, but little was known about the relative rates for the various reactions. Alcohols were known to dehydrate quickly under hydrothermal conditions (e.g., Akiya and Savage, 2002), but exactly how fast compared to the other reactions of the Seewald scheme was not clear. The kinetic study of hydrothermal decomposition of model ketone DBK confirmed the order of the functional group interconversions should be that alcohol dehydration was faster than alkene reduction, which was faster than ketone reduction, which was comparable to carbon-carbon bond cleavage, in water alone at 300°C and 700 bar (Chapter 2). These results suggest that under conditions of kinetic control, alcohol and alkene concentrations will be low due to high reactivity, and that alkane should accumulate, as observed. An additional important observation, however, is that a wide range of conjugated and larger structures formed by radical coupling were observed in DBK irreversible carbon-carbon bond cleavage reactions, and their abundances increased as the reaction progressed. The formation of conjugated structures is accompanied by elimination of water (the dehydration mentioned above) and also molecular hydrogen. Much of the molecular hydrogen is presumably consumed to generate the large quantities of fragmentation product (e.g., toluene) to maintain a hydrogen balance within the organic system. At longer reaction times it is clear that large conjugated structures with multiple benzene rings become the major product type, structures that are reminiscent of kerogen and coal structures rather than alkanes and carboxylic acids.

The results in the mineral experiments, however, point to large influences on chemical reactivity compared to water alone. Even on the timescales of the current experiments, which were designed to be short to identify primary products, the starting



material conversions and product distributions were found to be quite different in some cases. Extrapolation to longer timescales will amplify these differences, so that on geochemically relevant timescales the reactions in water alone could be essentially irrelevant. What is also learned from this work is that specific minerals or metal ions can promote bond cleavage reactions via surface catalysis, reduce organic structures with multiple bonds, and oxidize different functional groups in hydrothermal solutions. In other words, it will be necessary to take into account the mineral environment when considering geochemically relevant hydrothermal organic reactions. However, this does not mean that water alone studies are not important, because without them, the interpretation of organic reactivity in the presence of additives would be very difficult. Further investigations into organic-mineral/metal hydrothermal interactions are clearly needed to allow development of predictive models, as detailed in the next section.

### **6.3. Recommendation for future work**

The work described in this thesis contributes to an emerging area of organic geochemistry, characterized by the transition from surveys of reactions products to detailed studies of reaction mechanisms. A key to developing a comprehensive understanding of hydrothermal organic transformations is uncovering mechanisms that will allow reactions to become more predictable. The combination of model organic systems with mechanistic and physical organic chemistry methodologies appears to be a useful tool in this regard. Based on this thesis work, some suggested topics for future studies are summarized below.

(1) Dibenzylketone has served as a useful model compound to study hydrothermal chemistry of ketones. DBK, however, has a special structure with two benzylic carbons that facilitates bond-breaking. In natural systems, the mechanisms for ketone reactions may be more diverse than those discovered for DBK. More diverse ketone structures should be investigated in terms of relative hydrothermal reactivity and stability.

Aliphatic ketones such as dodecanone and cyclohexanone would be good candidates since they do not have reactive benzylic positions and should be amenable to the current analytical procedures.

(2) Carbon-carbon bond and carbon-hydrogen bond cleavage is clearly an important hydrothermal reaction pathway for the ketones included in this study. Iron oxide minerals have been found to exhibit surface-catalytic effects in promoting these reactions. From a mechanistic perspective, however, it is not clear exactly how the bonds are broken on the mineral surface. A very large number of organic reactions that undergo heterogeneous catalysis, such as C-H activation, have been described in the literature (e.g., Labinger and Bercaw, 2002; Gallezot, 2003). Review articles on heterogeneous catalysis, however, almost uniformly point to the difficulties in determining detailed mechanisms for reactions that occur on surfaces (e.g., Smith and Notheisz, 1999). A common simple approach suggested by the heterogeneous catalysis literature to quantify simple C-H bond breaking processes is to measure the rate of isotope exchange for reactions performed in deuterated water ( $D_2O$ ). An obvious starting point would be to compare the rates of exchange in structures with C-H bonds of differing strengths in hydrothermal  $D_2O$ , to see if this, or other structural features such as the ability to adsorb to the mineral surface are the critical factors controlling bond activation.

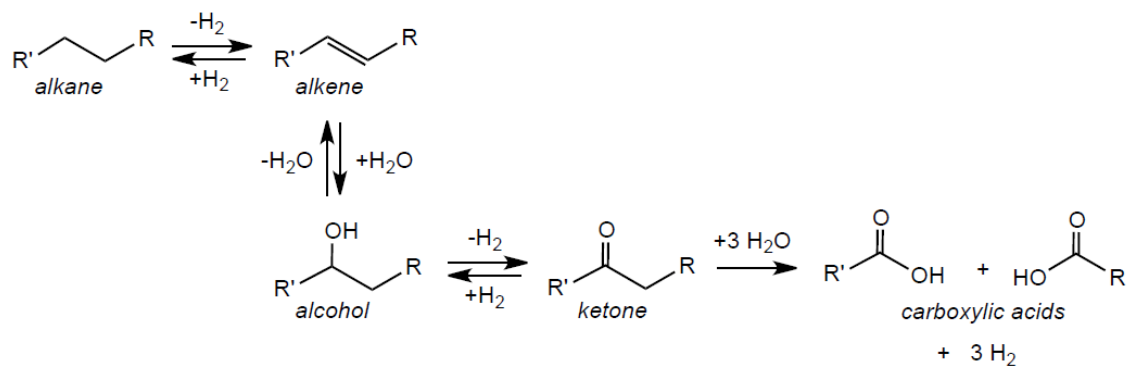
(3) Hydrothermal reduction of ketones to alkanes has been demonstrated for DBK in the presence of the sulfide mineral troilite. Other transition metal sulfide minerals, such as pyrite ( $\text{FeS}_2$ ), sphalerite ( $\text{ZnS}$ ), NiS, and CoS, may exhibit similar reducing abilities since they can presumably also produce dissolved sulfur species such as  $\text{H}_2\text{S}$  and  $\text{S}^{2-}$  that can act as reducing reagents. Heterogeneous catalysis using sulfide minerals of hydrothermal carboxylation and carbonyl insertion with alkylthiol compounds has been well documented (e.g., Huber and Wachtershauser, 1997; Cody et al., 2001, 2004). It would be interesting to systematically study these sulfide minerals as potential hydrothermal reducing agents for ketones, and to differentiate surface and solution phase effects by varying surface area to compare with existing data from this thesis and elsewhere.

(4) Hydrogenation of alkenes and dehydrogenation of alkanes are perhaps among the least understood hydrothermal reactions from a mechanistic perspective, compared to hydration of alkenes and dehydration of alcohols that are much better mechanistically studied under hydrothermal conditions. Hydrogenation of ketones and alkenes are of interests because they are expected to be widespread in reducing geological environments. Both reactions involve molecular hydrogen incorporation by breaking a  $\pi$ -bond and forming a new C-H  $\sigma$ -bond. Just as the iron oxides minerals can active C-C bond cleavage reactions (see Chapter 4), the minerals could potentially catalyze the addition of hydrogen to C=C and C=O bonds on the mineral surface. Similar to industrial hydrogenation of alkenes that uses common solid catalysts such as palladium and the Lindlar catalyst (Smith and March, 2007), minerals seem likely to form surface-H and surface-C bonds that will lower the activation energy for hydrogen addition across

the double bonds. So it would be worth exploring the catalytic effects of iron oxides minerals on hydrogenation of model alkene and ketone compounds, such as stilbene and cyclohexanone, in  $H_{2(aq)}$ -rich hydrothermal solutions.

(5) Copper (II) is found to be a surprisingly useful oxidizing reagent for organic structures under hydrothermal conditions, as described in Chapter 5, so further investigation on the scope and mechanisms of these reactions should be continued. Additional alcohol, aldehyde, and carboxylic acid structures (e.g., cyclohexanol, acetaldehyde, and hydrocinnamic acid) will be useful to explore copper (II) hydrothermal oxidations. More detailed kinetic measurements will also be useful to verify the mechanisms that are proposed in Chapter 5. Specifically, more accurate and systematic analyses of substituent effects by construction of Hammett plots for compounds with a benzene ring (Johnson, 1973) is a classic textbook mechanistic approach that has recently been applied to hydrothermal decarboxylations (Glein, 2012). The construction of Hammett plots requires absolute rate constant data for a series of related organic reactions with different electron withdrawing and donating groups, which will require more detailed kinetic studies of the copper-organic hydrothermal reactions. In addition to copper, other metal ions with similar redox potentials such as the ferric ion could also be good candidate for such hydrothermal organic redox transformations. The experiments described in Chapter 5 could serve as a basis for a systematic study of metal ions of varying redox potentials in hydrothermal organic transformations.

**Figure 1.** Schematic illustration of functional group interconversions that connect simple hydrocarbons and carboxylic acids, proposed by Seewald (2003) for hydrothermal organic reactions.



#### 6.4. References

- Akiya N. and Savage P. E. (2002) Roles of water for chemical reactions in high-temperature water. *Chem. Rev.* **102**, 2725-2750.
- Cody G. D., Boctor N. Z., Hazen R. M., Brandes J. A., Morowitz H. J., Yoder H. S. (2001) Geochemical roots of autotrophic carbon fixation: Hydrothermal experiments in the system citric acid, H<sub>2</sub>O-(±FeS)-(±NiS). *Geochim. Cosmochim. Acta* **65**, 3557-3576.
- Cody G. D. (2004) Transition metal sulfides and the origins of metabolism. *Annu. Rev. Earth Planet. Sci.* **32**, 569-599.
- Gallezot P. (2003) Hydrogenation – heterogeneous. In *Encyclopedia of Catalysis* (ed. Horvath I. T.). Volume 4. Wiley, New York.
- Glein C. R. (2012) *Theoretical and experimental studies of cryogenic and hydrothermal organic geochemistry*. Doctoral dissertation, Arizona State University. Ann Arbor: ProQuest/UMI. (Publication No. 3521607).
- Huber C. and Wächtershäuser G. (1997) Activated acetic acid by carbon fixation on (Fe,Ni) S under primordial conditions. *Science* **276**, 245-247.
- Johnson C. D. (1973) *The Hammett Equation*. Cambridge University Press, London.
- Labinger J. A. and Bercaw J. E. (2002) Understanding and exploiting C-H bond activation. *Nature* **417**, 507-514.
- Seewald J. S. (2003) Organic-inorganic interactions in petroleum producing sedimentary basins. *Nature* **426**, 327-333.
- Smith G. V. and Notheisz F. (1999) *Heterogeneous Catalysis in Organic Chemistry*. Academic Press, San Diego.
- Smith M. B. and March J. (2007) *March's Advanced Organic Chemistry: Reactions, Mechanisms, and Structure*. Wiley-Interscience, Hoboken, New Jersey.

## REFERENCES

- Adlhart C. and Uggerud E. (2007) Mechanisms for the dehydrogenation of alkanes on platinum: insights gained from the reactivity of gaseous cluster cations,  $\text{Pt}_n^+$   $n = 1-21$ . *Chem. Eur. J.* **13**, 6883-6890.
- Akiya N. and Savage P. E. (1998) Role of water in formic acid decomposition. *AICHE J.* **44**, 405-415.
- Akiya N. and Savage P. E. (2001) Kinetics and mechanism of cyclohexanol dehydration in high-temperature water. *Ind. Eng. Chem. Res.* **40**, 1822-1831.
- Akiya N. and Savage P. E. (2002) Roles of water for chemical reactions in high-temperature water. *Chem. Rev.* **102**, 2725-2750.
- Allen S. E., Walvoord R. R., Padilla-Salinas R. and Kozlowski M. C. (2013) Aerobic copper-catalyzed organic reactions. *Chem. Rev.* **113**, 6234-6458.
- Amarnath V. and Amarnath K. (1995) Intermediates in the Paal-Knorr synthesis of furans. *J. Org. Chem.* **60**, 301-307.
- Amend J. P. and Helgeson H. C. (1997) Calculation of the standard molal thermodynamic properties of aqueous biomolecules at elevated temperatures and pressures. Part I. L- $\alpha$ -amino acids. *J. Chem. Soc., Faraday Trans.* **93**, 1927-1941.
- Amend J. P. and Helgeson H. C. (2000) Calculation of the standard molal thermodynamic properties of aqueous biomolecules at elevated temperatures and pressures. Part II. Unfolded proteins. *Biophys. Chem.* **84**, 105-136.
- Amend, J. P. and Shock, E. L. (1998) Energetics of amino acid synthesis in hydrothermal ecosystems. *Science* **281**, 1659-1662.
- An J., Bagnell L., Cablewski T., Strauss C. R. and Trainor R. W. (1997) Applications of high-temperature aqueous media for synthetic organic reactions. *J. Org. Chem.* **62**, 2505-2511.
- Andersson E. and Holm N. G. (2000) The stability of some selected amino acids under attempted redox constrained hydrothermal conditions. *Origins Life Evol. Bios.* **30**, 9-23.
- Anikeev V. and Ermakova A. (2003) The influence of the density of supercritical water on the rate constant for the dehydration of isopropanol. *Russ. J. Phys. Chem.* **77**, 211-214.

- Anslyn E. and Dougherty D. (2005) *Modern Physical Organic Chemistry*. University Science Books, Sausalito, CA.
- Antal M. J., Brittain A., DeAlmeida C., Ramayya S., Roy J. C. (1987) Heterolysis and hemolysis in supercritical water. *ACS Sym. Ser.* **329**, 77-86.
- Antal M. J., Carlsson M., Xu X. and Anderson D. G. M. (1998) Mechanism and kinetics of the acid-catalyzed dehydration of 1- and 2-propanol in hot compressed liquid water. *Ind. Eng. Chem. Res.* **37**, 3820-3829.
- Arbour C. and Atkinson G. H. (1989) Picosecond photodissociation of dibenzyl ketone. *Chem. Phys. Letts.* **159**, 520-525.
- Archibald S. M., Migdisov A. A. and Williams-Jones A. E. (2002) An experimental study of the stability of copper chloride complexes in water vapor at elevated temperatures and pressures. *Geochim. Cosmochim. Acta* **66**, 1611-1619.
- Avola S., Guillot M., da Silva-Perez D., Pellet-Rostaing S. and Kunz W.; Goettmann F. (2013) Organic chemistry under hydrothermal conditions. *Pure Appl. Chem.* **85**, 89-103.
- Barnes H. L. (1979) Solubility of ore minerals. *Geochemistry of Hydrothermal Ore Deposits* (ed. H. L. Barnes). John Wiley & Sons, New York.
- Becke A. D. (1993) Density functional thermochemistry. III. The role of exact exchange. *J. Chem. Phys.* **98**, 5648-5652.
- Bell J. L. S. and Palmer D. A. (1994) Experimental studies of organic acid decomposition. *Organic Acids in Geological Processes* (eds. E. D. Pittman and M. D. Lewan). Springer-Verlag, New York. pp. 226-269.
- Bell J. L. S., Palmer D. A., Barnes H. L., and Drummond S. E. (1994) Thermal decomposition of acetate. 3. Catalysis by mineral surfaces. *Geochim. Cosmochim. Acta* **58**, 4155-4177.
- Belsky A. J., Maiella P. G. and Brill T. B. (1999) Spectroscopy of hydrothermal reactions – 13. Kinetics and mechanisms of decarboxylation of acetic acid derivatives at 100-260°C under 275 bar. *J. Phys. Chem. A* **103**, 4253-4260.
- Blanksby S. J. and Ellison G. B. (2003) Bond dissociation energies of organic molecules. *Acc. Chem. Res.* **36** (4), 255-263.



- Bordwell F. G. and Harrelson J. A. (1990) Acidities and homolytic bond dissociation energies of the  $\alpha$ C-H bonds in ketones in DMSO. *Can. J. Chem.* **68**, 1714-1718.
- Bruice P. Y. (2006) *Organic Chemistry* (5th Edition). Prentice Hall.
- Burdige D. J. (2006) *Geochemistry of Marine Sediments*. Princeton University Press: Princeton, NJ.
- Candela P. and Holland H. D. (1986) A mass transfer model for copper and molybdenum in magmatic hydrothermal systems; the origin of porphyry-type ore deposits. *Econ. Geol.* **81**, 1-19.
- Chen J.-X., Kim C. K., Lee H. W., Xue Y. and Kim C. K. (2011) Reexamination of the  $\pi$ -bond strengths within  $H_2C_5XH_n$  systems: A theoretical study. *J. Comput. Chem.* **32**, 1361–1367.
- Chen X. and Tong M. (2007) Solvothermal in situ metal/ligand reactions: A new bridge between coordination chemistry and organic synthetic chemistry. *Acc. Chem. Res.* **40**, 162-170.
- Coan S. B. and Becker E. I. (1954) Synthesis of unsymmetrical 1,3-diphenyl-2-propanes. *J. Am. Chem. Soc.* **76**, 501-503.
- Coan S. B. and Becker E. I. (1963) *Organic Synthesis*, Wiley, New York, Volume **4**, 174-177.
- Cody G. D. (2004) Transition metal sulfides and the origins of metabolism. *Annu. Rev. Earth Planet. Sci.* **32**, 569-599.
- Cody G. D., Boctor N. Z., Filley T. R., Hazen R. M., Scott J. H., Sharma A. and Yoder H. S. (2000) Primordial carbonylated iron-sulfur compounds and the synthesis of pyruvate. *Science* **289**, 1337-1340.
- Cody G. D., Boctor N. Z., Hazen R. M., Brandes J. A., Morowitz H. J., Yoder H. S. (2001) Geochemical roots of autotrophic carbon fixation: Hydrothermal experiments in the system citric acid,  $H_2O-(\pm FeS)-(\pm NiS)$ . *Geochim. Cosmochim. Acta* **65**, 3557-3576.
- Crerar D. A. and Barnes H. L. (1976) Ore solution chemistry. V. Solubilities of chalcopyrite and chalcocite assemblages in hydrothermal solution at 200 to 350°C. *Econ. Geol.* **71**, 772-794.
- D'Hondt S., Jørgensen B. B., Miller D. J., Batzke A., Blake R., Cragg B. A., Cypionka H., Dickens G. R., Ferdelman T., Hinrichs K.-U., Holm N. G., Mitterer R., Spivak A., Wang G., Bekins B., Engelen B., Ford K., Gettemy G., Rutherford W. D., Sass

- H., Skilbeck C. G., Aiello I. W., Guèrin G., House C. H., Inagaki F., Meister P., Naehr T., Niituma S., Parkes R. J., Schippers A., Smith D. C., Teske A., Wiegel J., Padilla C. N. and Acosta J. L. S. (2004) Distributions of microbial activities in deep subseafloor sediments. *Science* **306**, 2216-2221.
- Dasgupta, R. (2013) Ingassing, storage, and outgassing of terrestrial carbon through geologic time. *Rev. Mineral. Geochem.* **75**, 183-229.
- Davidson E. R. (1996) Comment on "Comment on Dunning's correlation-consistent basis sets". *Chem. Phys. Lett.* **260**, 514-518.
- Dick J. M., LaRowe D. E., and Helgeson H. C. (2006) Group additivity calculation of the standard molal thermodynamic properties of aqueous amino acids, polypeptides, and unfolded proteins as a function of temperature, pressure and ionization state. *Biogeosciences* **3**, 311-336.
- Drobner E., Huber H., Wachtershauser G., Rose D. and Stetter K. O. (1990) Pyrite formation linked with hydrogen evolution under anaerobic conditions. *Nature* **346**, 742-744.
- Dunning T. H. (1989) Gaussian basis sets for use in correlated molecular calculations. I. The atoms boron through neon and hydrogen. *J. Chem. Phys.* **90**, 1007-1023.
- Dust J. M. and Arnold D. R. (1983) Substituent effects on benzyl radical ESR hyperfine coupling constants. The .sigma..alpha..cntdot. scale based upon spin delocalization. *J. Am. Chem. Soc.* **105**, 1221-1227.
- Eberson L. (1988) *Electron Transfer Reactions in Organic Chemistry*. Springer-Verlag, New York.
- Espitalie J., Madec M. and Tissot B. (1980) Role of mineral matrix in kerogen pyrolysis – influence on petroleum generation and migration. *AAPG Bulletin-American Association of Petroleum Geologists.* **64**, 59-66.
- Falkowski P., Scholes R. J., Boyle E., Canadell J., Canfield D., Elser J., Gruber N., Hibbard K., Hogberg P., Linder S., Mackenzie F. T., Moore B., Pedersen T., Rosenthal Y., Seitzinger S., Smetacek V. and Steffen W. (2000) The global carbon cycle: A test of our knowledge of earth as a system. *Science* **290**, 291-296.

- Fernandez-Ramos A., Miller J. A., Klippenstein S. J. and Truhlar D. G. (2006) Modeling the kinetics of bimolecular reactions. *Chem. Rev.* **106**, 4518–4584.
- Foustoukos D. I. and Seyfried Jr. W. E. (2004) Hydrocarbons in hydrothermal vent fluids: the role of chromium-bearing catalysts. *Science* **304**, 1002-1005.
- Frisch M. J. et al. (2009) Gaussian 09, revision A.02. Gaussian, Inc., Wallingford, CT.
- Frisch M. J. et al. (2010) Gaussian 09, revision C.01. Gaussian, Inc., Wallingford, CT.
- Fu Q., Foustoukos D. I., Seyfried Jr. W. E. (2008) Mineral catalyzed organic synthesis in hydrothermal systems: An experimental study using time-of-flight secondary ion mass spectrometry. *Geophys. Res. Lett.* **35**, L07612.
- Gallezot P. (2003) Hydrogenation – heterogeneous. In *Encyclopedia of Catalysis* (ed. Horvath I. T.). Volume 4. Wiley, New York.
- Gamez P., Arends I., Reedijk J. and Sheldon R. A. (2003) Copper (II)-catalysed aerobic oxidation of primary alcohols to aldehydes. *Chem. Comm.* **19**, 2014-2015.
- Gamez P., Aibel P. G., Driessen W. L. and Reedijk R. (2001) Homogeneous bio-inspired copper-catalyzed oxidation reactions. *Chem. Soc. Rev.* **30**, 376-385.
- GarciaGaribay M. A., Zhang Z. and Turro N. J. (1991) Diffusion and percolation of radical pairs in zeolite media – A product analysis study. *J. Am. Chem. Soc.* **113**, 6212-6218.
- Glein C. R. (2012) *Theoretical and experimental studies of cryogenic and hydrothermal organic geochemistry*. Doctoral dissertation, Arizona State University. Ann Arbor: ProQuest/UMI. (Publication No. 3521607).
- Gould I. R., Baretz B. H. and Turro N. J. (1987) Primary processes in the Type I photocleavage of dibenzyl ketones - A pulsed laser and photochemically induced dynamic nuclear-polarization study. *J. Phys. Chem.* **91**, 925-929.
- Gould I. R., Turro N. J. and Zimmt M. B. (1984) In *Advances in Physical Organic Chemistry* (eds: Gold V. and Bethell D.). Academic Press, New York. Vol. 20, 1-51.
- Greenwood N. N. and Earnshaw A. (1997) *Chemistry of the Elements*, 2nd ed., Butterworth-Heinemann, Oxford, UK.

- Harvey A. H. and Friend D. G. (2004) In *Aqueous Systems at Elevated Temperatures and Pressures* (eds: Palmer D. A., Fernandez-Prini R. and Harvey A. H.). Elsevier, San Diego, CA.
- Haynes D. W. and Bloom M. (1987) Stratiform copper deposits hosted by low-energy sediments: III. Aspects of metal transport. *Econ. Geol.* **82**, 635-648.
- Hazen R. M. and Deamer D. (2007) Hydrothermal reactions of pyruvic acid: synthesis, selection, and self-assembly of amphiphilic molecules. *Origins of Life and Evolution of Biospheres* **37**, 143-152.
- Head I. M., Jones D. M. and Larter S. R. (2003) Biological activity in the deep subsurface and the origin of heavy oil. *Nature* **426**, 344-352.
- Heinrich C. A., Henley R. W. and Seward T. M. (1989) *Hydrothermal Systems*. Australian Mineral Foundation, Adelaide.
- Helgeson H. C., Knox A. M., Owens C. E. and Shock E. L. (1993) Petroleum, oil field waters and authigenic mineral assemblages: Are they in metastable equilibrium in hydrocarbon reservoirs? *Geochim. Cosmochim. Acta* **57**, 3295-3339.
- Helgeson H. C., Owens C. E., Knox A. M. and Richard L. (1998) Calculation of the standard molal thermodynamic properties of crystalline, liquid, and gas organic molecules at high temperatures and pressures. *Geochim. Cosmochim. Acta* **62**, 985-1081.
- Helgeson H. C., Richard L., McKenzie W. F., Norton D. L. and Schmitt A. (2009) A chemical and thermodynamic model of oil generation in hydrocarbon source rocks. *Geochim. Cosmochim. Acta* **73**, 594-695.
- Hemley J. J., Cygan G. L., Fein J. B., Robinson G. R., and D'Angelo W. M. (1992) Hydrothermal ore-forming process in the light of studies in rock-buffered systems, I. Iron-copper-zinc-lead sulfide solubility relations. *Econ. Geol.* **87**, 1-22.
- Hertwig R. H. and Koch W. (1997) On the parameterization of the local correlation functional. What is Becke-3-LYP? *Chem. Phys. Lett.* **268**, 345-351.
- Hilborn J. W. and Pincock J. A. (1991) Rates of decarboxylation of acyloxy radicals formed in the photocleavage of substituted 1-naphthylmethyl alkanoates. *J. Am. Chem. Soc.* **113**, 2683-2686.
- Hinrichs K.-U., Hayes J. M., Bach W., Spivak A. J., Hmelo L. R., Holm N. G., Johnson C. G. and Sylva S. P. (2006) Biological formation of ethane and propane in the deep marine subsurface. *Proc. Natl. Acad. Sci. USA* **103**, 14684-14689.

- Hoering T. C. (1984) Thermal reactions of kerogen with added water, heavy water and pure organic substances. *Org. Geochem.* **5**, 267-278.
- Holm N. G. (ed.) (1992) *Marine Hydrothermal Systems and the Origin of Life*. Kluwer Academic Publishers, Dordrecht, Netherlands.
- Horsfield B., Schenk H. J., Zink K., Ondrak R., Dieckmann V., Kallmeyer J., Mangelsdorf K., di Primo R., Wilkes H., Parkes R. J., Fry J. and Cragg B. (2006) Living microbial ecosystems within the active zone of catagenesis: Implications for feeding the deep biosphere. *Earth Planet. Sci. Lett.* **246**, 55-69.
- Howell J. O., Goncalves J. M., Amatore C., Klasinc L., Wightman R. and Kochi J. K. (1984) Electron transfer from aromatic hydrocarbons and their  $\pi$ -complexes with metals. Comparison of the standard oxidation potentials and vertical ionization potentials. *J. Am. Chem. Soc.* **106**, 3968-3976.
- Huber C. and Wächtershäuser G. (1997) Activated acetic acid by carbon fixation on (Fe,Ni) S under primordial conditions. *Science* **276**, 245-247.
- Hunter S. E. and Savage P. E. (2004) Recent advances in acid- and base-catalyzed organic synthesis in high-temperature liquid water. *Chem. Eng. Sci.* **59**, 4903-4909.
- Hurd D. D., Christ R. and Thomas R. L. (1933) Preparation and pyrolysis of dibenzyl ketone, phenylacetic anhydride and diphenylacetic anhydride. *J. Am. Chem. Soc.* **55**, 2589-2592.
- Isegawa M., Fiedler L., Leverentz H. R., Wang Y., Nachimuthu S., Gao J. and Truhlar D. G. (2013) Polarized molecular orbital model chemistry. 3. The PMO method extended to organic chemistry. *J. Chem. Theory Comput.* **9**, 33-45.
- James B. R. and Williams R. J. P. (1961) The oxidation-reduction potentials of some copper complexes. *J. Chem. Soc.* 2007-2019.
- Johnson C. D. (1973) *The Hammett Equation*. Cambridge University Press, London.
- Johnson J. W. and Norton D. (1991) Critical phenomena in hydrothermal systems: State, thermodynamic, electrostatic, and transport properties of H<sub>2</sub>O in the critical region. *Am. J. Sci.* **291**, 541-648.
- Johnson J. W., Oelkers E. H. and Helgeson H. C. (1992) SUPCRT92: A software package for calculating the standard molal thermodynamic properties of minerals, gases, aqueous species, and reactions from 1 to 5000 bar and 0 to 1000°C. *Comput. Geosci.* **18**, 899-947.

- Jones D. M., Head I. M., Gray N. D., Adams J. J., Rwan A. K., Aitken C. M., Bennett B., Huang H., Brown A., Bowler B. F. J., Oldenburg T., Erdmann M. and Larter S. R. (2008) Crude-oil biodegradation via methanogenesis in subsurface petroleum reservoirs. *Nature* **451**, 176-180.
- Jurg J. W. and Eisma E. (1964) Petroleum hydrocarbons: generation from fatty acid. *Science* **19**, 1451-1452.
- Katritzky A. R., Nichols D. A., Siskin M., Murugan R. and Balasubramanian M. (2001) Reactions in high-temperature aqueous media. *Chem. Rev.* **101**, 837-892.
- Kendall R. A., Dunning T. H. and Harrison R. J. (1992) Electron affinities of the first-row atoms revisited. Systematic basis sets and wave functions. *J. Chem. Phys.* **96**, 6796-6806.
- Kesler S. E. and Wilkinson B. H. (2008) Earth's copper resources estimated from tectonic diffusion of porphyry copper deposits. *Geology*. **36**, 255-258.
- Kochi J. K. (1967) Mechanisms of organic oxidation and reduction by metal complexes. *Science* **155**, 415-424.
- Kochi J. K. (1974) Electron-transfer mechanisms for organometallic intermediates in catalytic reactions. *Accts. Chem. Res.* **7**, 351-360.
- Kuck, D. (2004) Mass spectrometry and gas-phase ion chemistry of phenols. The Chemistry of Phenols (ed. Z. Rappoport). Wiley, New York. p. 259.
- Kuhlmann B., Arnett E. M. and Siskin M. (1994) Classical organic reactions in pure superheated water. *J. Org. Chem.* **59**, 3098-3101.
- Labinger J. A. and Bercaw J. E. (2002) Understanding and exploiting C-H bond activation. *Nature* **417**, 507-514.
- Lang S. Q., Butterfield D. A., Schulte M. D., Kelley D. S. and Lilley M. D. (2010) Elevated concentrations of formate, acetate and dissolved organic carbon found at the Lost City hydrothermal field. *Geochim. Cosmochim. Acta* **74**, 941-952.
- LaRowe D. E. and Dick J. M. (2012) Calculation of the standard molal properties of crystalline peptides. *Geochim. Cosmochim. Acta* **80**, 70-91.
- LaRowe D. E. and Helgeson H. C. (2006a) Biomolecules in hydrothermal systems: Calculation of the standard molal thermodynamic properties of nucleic-acid bases,

nucleosides, and nucleotides at elevated temperatures and pressures. *Geochim. Cosmochim. Acta* **70**, 4680-4724.

LaRowe D. E. and Helgeson H. C. (2006b) The energetics of metabolism in hydrothermal systems: Calculation of the standard molal thermodynamic properties of magnesium complexed adenosine nucleotides and NAD and NADP at elevated temperatures and pressures. *Thermochim. Acta* **448**, 82-106.

LaRowe D. E. and Van Cappellen P. (2011) Degradation of natural organic matter: A thermodynamic analysis. *Geochim. Cosmochim. Acta* **77**, 2030-2042.

Larter S. R., Wilhelms A., Head I., Koopmans M., Aplin A., Di P. R., Zwach C., Erdmann M. and Telnaes N. (2003) The controls on the composition of biodegraded oils in the deep subsurface: Part I - Biodegradation rates in petroleum reservoirs. *Org. Geochem.* **34**, 601-613.

Lehr G. F. and Turro N. J. (1981) Measurement of rate processes of free radicals in homogeneous and micellar solutions by cidnp. *Tetrahedron* **37**, 3411-3420.

Leif R. N. and Simoneit B. R. T. (1995) Ketones in hydrothermal petroleum and sediment extract from Guaymas Basins, Gulf of California. *Org. Geochem.* **23**, 889-904.

Leif R. N. and Simoneit B. R. T. (2000) The role of alkenes produced during hydrous pyrolysis of a shale. *Org. Geochem.* **31**, 1189-1208.

Li J. and Brill T. B. (2001) Spectroscopy of hydrothermal solutions 18: pH-dependent kinetics of itaconic acid reactions in real time. *J. Phys. Chem. A* **105**, 10839-10845.

Liang, L.; Rao, G.; Sun, H.-L.; Zhang, J.-L. (2010) Aerobic oxidation of primary alcohols catalyzed by copper salts and catalytically active  $\mu$ -hydroxyl-bridged trinuclear copper intermediate. *Adv. Synth. Catal.* **352**, 2371-2377.

Liu W., McPhail D. C. and Brugger J. (2001) An experimental study of copper (I)-chloride and copper (I)-acetate complexing in hydrothermal solutions between 50°C and 250°C and vapor-saturated pressure. *Geochim. Cosmochim. Acta* **17**, 2937-2948.

Lu J. Y. (2003) Crystal engineering of Cu-containing metal-organic coordination polymers under hydrothermal conditions. *Coord. Chem. Rev.* **246**, 327-347.

Luo Y-R. (2007) *Comprehensive Handbook of Chemical Bond Energies*. CRC Press: Boca Raton, FL.

- March J. (1985) *Advanced Organic Chemistry: Reactions, Mechanisms, and Structure* (third edition). Wiley, New York.
- Marcus R. A. and Sutin N. (1985) Electron transfers in chemistry and biology. *Biochim. Biophys. Acta* **811**, 265-322.
- Marshall C. P. and Fairbridge R. W. (1999) *Encyclopedia of Geochemistry*. Kluwer Academic Publishers, The Netherlands.
- Mason O. U., Nakagawa T., Rosner M., Van Nostrand J. D., Zhou J., Maruyama A., Fisk M. R. and Giovannoni S. J. (2010) First investigation of the microbiology of the deepest layer of ocean crust. *PLoS ONE*. **5**, 1-11.
- Mayer J. M. (2010) Understanding hydrogen atom transfer: From bond strengths to Marcus theory. *Acc. Chem. Res.* **44**, 36-46.
- McCollom T. M. (2013) The influence of minerals on decomposition of the n-alkyl-alpha-amino acid norvaline under hydrothermal conditions. *Geochim. Cosmochim. Acta* **104**, 330-357.
- McCollom T. M. and Seewald J. S. (2003a) Experimental constraints on the hydrothermal reactivity of organic acids and acid anions: I. Formic acid and formate. *Geochim. Cosmochim. Acta* **67**, 3625-3644.
- McCollom T. M. and Seewald J. S. (2003b) Experimental study of the hydrothermal reactivity of organic acids and acid anions: II. Acetic acid, acetate, and valeric acid. *Geochim. Cosmochim. Acta* **67**, 3645-3664.
- McCollom T. M. and Seewald J. S. (2007) Abiotic synthesis of organic compounds in deep-sea hydrothermal environments. *Chem. Rev.* **107**, 382-401.
- McCollom T. M., Lollar B. S., Lacrampe-Couloume G. and Seewald J. S. (2010) The influence of carbon source on abiotic organic synthesis and carbon isotope fractionation under hydrothermal conditions. *Geochim. Cosmochim. Acta* **74**, 2717-2740.
- McCollom T. M., Ritter G. and Simoneit B. R. T (1999) Lipidsynthesis under hydrothermal conditions by Fischer-Tropsch-type reactions. *Orig. Life Evol. Bios.* **29**, 153-166.
- McMillen D. F., Golden D. M. (1982) Hydrocarbon bond dissociation energies. *Ann. Rev. Phys. Chem.* **33**, 493-532.



- McSween H., Richardson S. and Uhle M. (2003) *Geochemistry: Pathways and Processes* (Second Edition). Columbia University Press, New York.
- Michl J. and Bonacic-Koutecky V. (1990) *Electronic Aspects of Organic Photochemistry*. Wiley-Interscience, New York.
- Migdisov A. A., Bychkov A. Y., Williams-Jones A. E. and Hinsberg V (2014) A predictive model for the transport of copper by HCl-bearing water vapour in ore-forming magmatic-hydrothermal systems: Implications for copper porphyry ore formation. *Geochim. Cosmochim. Acta* **129**, 33-53.
- Morooka S., Matubayasi N. and Nakahara M. (2007) Kinetic study on disproportionations of C1 aldehydes in supercritical water: Methanol from formaldehyde and formic acid. *J. Phys. Chem. A* **111**, 2697-2705.
- Murov S. L., Carmichael I. and Hug G. L. (1993) *The Handbook of Photochemistry, 2nd Edition*. CRC Press, Boca Raton.
- Nicholas A. and Arnold D. (1982) Thermochemical parameters for organic radicals and radical ions. I. The estimation of the pK<sub>a</sub> of radical cations based on thermochemical calculations. *Can. J. Chem.* **60**, 2165-2179.
- Nigh W. G. (1973) Oxidation by cupric ion. In *Oxidation in Organic Chemistry* (ed. Trahanovsky W. S.). Vol. 5-B. Academic Press, New York.
- Noh T. H., Step E. and Turro N. J. (1993) Singlet-state photochemistry of dibenzyl ketone and its o-tolyl derivatives. *J. Photochem. Photobiol.* **72**, 133-145.
- Ott L., Bicker M. and Vogel H. (2006) Catalytic dehydration of glycerol in sub- and supercritical water: A new chemical process for acrolein production. *Green Chem.* **8**, 214-220.
- Palmer D. A. and Drummond S. E. (1986) Thermal decarboxylation of acetate. 1. The kinetics and mechanism of reaction in aqueous solution. *Geochim. Cosmochim. Acta* **50**, 813-823.
- Patnaik P. (2003) *Handbook of Inorganic Chemicals*. McGraw-Hill, New York.
- Pedley J. B., Naylor R. D. and Kirby S. P. (1986) *Thermochemical Data of Organic Compounds*. 2nd Ed., Chapman and Hill: New York.

- Pittman E. D. and Lewan M. D. (1994) *Organic Acids in Geological Processes*. Springer-Verlag, Berlin.
- Plyasunov A. V. and Shock E. L. (2000) Standard state Gibbs energies of hydration of hydrocarbons at elevated temperatures as evaluated from experimental phase equilibria studies. *Geochim. Cosmochim. Acta* **64**, 2811-2833.
- Plyasunov A. V. and Shock E. L. (2003) Prediction of the vapor-liquid distribution constants for volatile nonelectrolytes in H<sub>2</sub>O up to the critical temperature of water. *Geochim. Cosmochim. Acta* **67**, 4981-5009.
- Plyasunova N. V., Plyasunov A. V. and Shock E. L. (2004) Database of thermodynamic properties for aqueous organic compounds. *Int. J. Thermophys.* **25**, 351-360.
- Ragtop R. A., Ellis J., Crisp. P. T., Ekstrom A. and Fookes C. J. R. (1985) Pyrolysis of model compounds on spent oil shales, minerals and charcoal – Implications for shale oil composition. *Fuel*. **64**, 1640-1646.
- Reeves E. P., Seewald J. S. and Sylva S. (2012) Hydrogen isotope exchange between n-alkanes and water under hydrothermal conditions. *Geochim. Cosmochim. Acta* **77**, 582-599.
- Richard L. (2001) Calculation of the standard molal thermodynamic properties as a function of temperature and pressure of some geochemically important organic sulfur compounds. *Geochim. Cosmochim. Acta* **65**, 3827-3877.
- Richard L. and Helgeson H. C. (1998) Calculation of the thermodynamic properties at elevated temperatures and pressures of saturated and aromatic high molecular weight solid and liquid hydrocarbons in kerogen, bitumen, petroleum, and other organic matter of biogeochemical interest. *Geochim. Cosmochim. Acta* **62**, 3591-3636.
- Robbins W. K. and Eastman R. H. (1970a) Photodecarbonylation in solution. I. Quantum yields and quenching results with dibenzyl ketones. *J. Am. Chem. Soc.* **92**, 6076-6077.
- Robbins W. K. and Eastman R. H. (1970b) Photodecarbonylation in solution. II. Trapping of intermediates in the photolysis of dibenzyl ketone. *J. Am. Chem. Soc.* **92**, 6077-6079.
- Russell M. J. and Hall A. J. (1997) The emergence of life from iron monosulfide bubbles at a submarine hydrothermal redox and pH front. *J. Geol. Soc. London* **154**, 377-402.

- Rylander P. N. (1967) *Catalytic Hydrogenation over Platinum Metals*. Academic Press, New York.
- Savage P. E. (1999) Organic chemical reactions in supercritical water. *Chem. Rev.* **99**, 603-621.
- Scalmani G. and Frisch M. J. (2010) Continuous surface charge polarizable continuum models of solvation. I. General formalism. *J. Chem. Phys.* **132**, 114110.
- Schulte M. and Shock E. L. (2004) Coupled organic synthesis and mineral alteration on meteorite parent bodies. *Meteorit. Planet. Sci.* **39**, 1577-1590.
- Scuseria G. E. and Staroverov V. N. (2005) In *Theory and Applications of Computational Chemistry: The First 40 Years (A Volume of Technical and Historical Perspectives)* (eds: Dykstra C. E., Frenking G. and Kim K. S.). Elsevier, Amsterdam.
- Seewald J. S. (1994) Evidence for metastable equilibrium between hydrocarbons under hydrothermal conditions. *Nature* **370**, 285-287.
- Seewald J. S. (2001) Aqueous geochemistry of low molecular weight hydrocarbons at elevated temperatures and pressures: constraints from mineral buffered laboratory experiments. *Geochim. Cosmochim. Acta* **65**, 1641-1664.
- Seewald J. S. (2003) Organic-inorganic interactions in petroleum producing sedimentary basins. *Nature* **426**, 327-333.
- Seewald J. S., Zolotov M. Y. and McCollom T. (2006) Experimental investigation of single carbon compounds under hydrothermal conditions. *Geochim. Cosmochim. Acta* **70**, 446-460.
- Seyfried Jr. W. E. and Ding K. (1993) The effect of redox on the relative solubility of copper and iron in Cl-bearing aqueous fluid at elevated temperature and pressures: An experimental study with application to subseafloor hydrothermal systems. *Geochim. Cosmochim. Acta* **57**, 1905-1918.
- Shanab K., Neudorfer C., Schirmer E. and Spreitzer H. (2013) Green solvents in organic synthesis: An overview. *Curr. Org. Chem.* **17**, 1179-1187.
- Sheldon R. A. and Kochi J. K. (1981) *Metal-catalysed Oxidations of Organic Compounds*, Academic Press, New York.

- Shen Z., Zhang Y., Jin F., Zhou X., Kishita A. and Tohji K. (2010) Hydrogen-transfer reduction of ketones into corresponding alcohols using formic acid as a hydrogen donor without a metal catalyst in high-temperature water. *Ind. Eng. Chem. Res.* **49**, 6255-6259.
- Shimoyam A. and Johns W. D. (1971) Catalytic conversion of fatty acids to petroleum-like paraffins and their maturation. *Nat. Phys. Sci.* **232**, 140-144.
- Shipp J., Gould I., Herckes P., Shock E., Williams L., and Hartnett H. (2013) Organic functional group transformations in water at elevated temperature and pressure: Reversibility, reactivity, and mechanisms. *Geochim. Cosmochim. Acta* **104**, 194-209.
- Shock E. L. (1988) Organic acid metastability in sedimentary basins. *Geology* **16**, 886-890.
- Shock E. L. (1989) Calculation of the thermodynamic and transport properties of aqueous species at high pressures and temperatures: Standard partial molal properties of inorganic neutral species. *Geochim. Cosmochim. Acta* **53**, 2157-2183.
- Shock E. L. (1994) Catalysing methane production. *Nature* **368**, 499-500.
- Shock E. L. (1995) Organic acids in hydrothermal solutions: Standard molal thermodynamic properties of carboxylic acids, and estimates of dissociation constants at high temperatures and pressures. *Am. J. Sci.* **295**, 496-580.
- Shock E. L. (2000) Thermodynamic response of organic compounds in geochemical processes of sedimentary basins. *Reviews in Economic Geology*, Vol. **9** (eds: T. H. Giordano, R. M. Kettler, S. A. Wood). Society of Economic Geologists, Inc., Littleton, CO., pp. 105-117.
- Shock E. L. and Canovas P. C. (2010) The potential for abiotic organic synthesis and biosynthesis at seafloor hydrothermal systems. *Geofluids* **10**, 161-192.
- Shock E. L. and Helgeson H. C. (1990) Calculation of the thermodynamic and transport properties of aqueous species at high pressures and temperatures: Standard partial molal properties of organic species. *Geochim. Cosmochim. Acta* **54**, 915-945.
- Shock E. L. and Koretsky C. M. (1993) Metal-organic complexes in geochemical processes: Calculations of standard partial molal thermodynamic properties of aqueous acetate complexes at high pressures and temperatures. *Geochim. Cosmochim. Acta* **57**, 4899-4922.

- Shock E. L. and Schulte M. D. (1998) Organic synthesis during fluid mixing in hydrothermal systems. *J. Geophys. Res.* **103**, 28513-28527.
- Shock E. L., Canovas P., Yang Z., Boyer G., Johnson K., Robinson K., Fecteau K., Windman T., and Cox A. (2013) Thermodynamics of organic transformations in hydrothermal fluids. *Rev. Mineral. Geochem.* **76**, 311-350.
- Simoneit, B. R. T. (1992) Aqueous organic geochemistry at high temperature/high pressure. In *Marine Hydrothermal Systems and the Origin of Life*, Holm N.G. Ed., Kluwer, Dordrecht, Netherlands, Chapter 4.
- Simoneit, B. R. T., Lein, A. Y. Peresykin, V. I., Osipov, G. A. (2004) Composition and origin of hydrothermal petroleum and associated lipids in the sulfide deposits of the Rainbow field (Mid-Atlantic Ridge at 36°N). *Geochim. Cosmochim. Acta* **68**, 2275-2294.
- Siskin M. and Katritzky A. R. (1991) Reactivity of organic compounds in hot water – Geochemical and technological implications. *Science* **254**, 231-237.
- Siskin M. and Katritzky A. R. (2001) Reactivity of organic compounds in superheated water: general background. *Chem. Rev.* **101**, 826-835.
- Siskin M., Katritzky A. R. and Balasubramanian M. (1995) Aqueous organic chemistry. 9. Reactivity of 1,5-, 1,6-, 1,7- and 2,6-dihydroxynaphthalenes, dibenzofuran, 2-hydroxydibenzofuran, carbazole, 2-hydroxycarbazole, acridine and 4-hydroxyacridine. *Fuel* **74**, 1509-1511.
- Smith G. V. and Notheisz F. (1999) *Heterogeneous Catalysis in Organic Chemistry*. Academic Press, San Diego.
- Smith M. B. and March J. (2007) *March's Advanced Organic Chemistry: Reactions, Mechanisms, and Structure*. Wiley-Interscience, Hoboken, New Jersey.
- Stephens P. J., Devlin F. J., Chabalowski C. F. and Frisch M. J. (1994) Ab initio calculation of vibrational absorption and circular dichroism spectra using density functional force fields. *J. Phys. Chem.* **98**, 11623-11810.
- Stewart J. J. P. (2007) Optimization of parameters for semiempirical methods V: Modification of NDDO approximations and application to 70 elements. *J. Mol. Model.* **13**, 1173-1213.
- Stewart R. (1964) *Oxidation Mechanisms*. Benjamin Press, New York. p. 49.

- Sverjensky D. A. (1987) The role of migrating oil field brines in the formation of sediment-hosted Cu-rich deposits. *Econ. Geol.* **82**, 1130-1141.
- Sverjensky D. A., Harrison B. and Azzolini D. (2014) Water in the deep Earth: The dielectric constant and the solubilities of quartz and corundum to 60 kb and 1200 degrees C. *Geochim. Cosmochim. Acta* **129**, 125-145.
- Tassi F., Vaselli O., Capaccioni B., Montegrossi G., Barahona F. and Caprai A. (2007) Scrubbing process and chemical equilibria controlling the composition of light hydrocarbons in natural gas discharges: An example from the geothermal fields of El Salvador. *Geochim. Geophys. Geosys.* **8**, doi:10.1029/2006GC001487.
- Tivey M. K. (1995) The influence of hydrothermal fluid composition and advection rates on black smoker chimney mineralogy: Insights from modeling transport and reaction. *Geochim. Cosmochim. Acta* **59**, 1933-1949.
- Turro N. J. (1982) Laser flash spectrometric investigations of biradicals and caged radical pairs. *Tetrahedron* **38**, 809-917.
- Turro N. J. (1991) *Modern Molecular Photochemistry*. University Science Books, Sausalito, CA.
- Turro N. J. (2000) From boiling stones to smart crystals: Supramolecular and magnetic isotope control of radical-radical reactions in zeolites. *Acc. Chem. Res.* **33**, 637-646.
- Turro N. J. and Weed G. C. (1983) Micellar systems as "supercages" for reactions of geminate radical pairs - Magnetic effects. *J. Am. Chem. Soc.* **105**, 1861-1868.
- Turro N. J., Chow M-F., Chung C-J., Tanimoto Y. and Weed G. (1981) Time-resolved laser flash spectroscopic study of benayl radical pairs in micelle cages. *J. Am. Chem. Soc.* **103**, 4574-4576.
- Turro N. J., Gould I. R. and Baretz B. H. (1983) Absolute rate constants for decarbonylation of phenylacetyl and related radicals. *J. Phys. Chem.* **87**, 531-532.
- Turro N. J., Ramamurthy V. and Scaiano J. C. (2010) *Modern Molecular Photochemistry of Organic Molecules*. University Science Books, Sausalito, CA.

- Uematsu M. and Franck E. U. (1980) Static dielectric constant of water and steam. *J. Phys. Chem. Ref. Data* **9**, 1291-1306.
- Var'yash L. N. (1992) Cu (I) complexing in NaCl solutions at 300 and 350°C. *Geochem. Intl.* **29**, 84-92.
- Vijh A. K. and Conway B. E. (1967) Electrode kinetic aspects of the Kolbe reaction. *Chem. Rev.* **67**, 623-664.
- Watanabe M., Sato T., Inomata H., Smith Jr. R. L., Arai K., Kruse A. and Dinjus E. (2004) Chemical reactions of C<sub>1</sub> compounds in near-critical and supercritical water. *Chem Rev.* **104**, 5803-5821.
- Wayner D. and Griller D. (1985) Oxidation and reduction potentials of transient free-radicals. *J. Am. Chem. Soc.* **107**, 7764-7765.
- Wiberg K. B. and Richardson W. H. (1961) The chromic acid oxidation of aromatic aldehydes. Some observations concerning the oxidation by the chromium species of intermediate valence. *J. Am. Chem. Soc.* **84**, 2800-2807.
- Williams L. B., Hervig R. L., Holloway J. R. and Hutcheon I. (2001) Boron isotope geochemistry during diagenesis. Part 1. Experimental determination of fractionation during illitization of smectite. *Geochim. Cosmochim. Acta* **65**, 1769-1782.
- Williams L. B., Holloway J. R., Canfield B., Glein C., Dick J., Hartnett H. and Shock E. L. (2010) Birth of biomolecules from the warm wet sheets of clays near spreading centers. In *Earliest Life on Earth* (eds. Golding S. and Glikson M.). Springer Publishing. Chapter 4.
- Windman T., Zolotova N., Schwandner F. and Shock, E. L. (2007) Formate as an energy source for microbial metabolism in chemosynthetic zones of hydrothermal ecosystems. *Astrobiology* **7**, 873-890.
- Xiao Z., Gammons C. H. and Williams-Jones A. E. (1998) Experimental study of copper (I) chloride complexing in hydrothermal solutions at 40 to 300°C and saturated water vapor pressure. *Geochim. Cosmochim. Acta* **62**, 2949-2964.
- Xu X., Antal M. J. and Anderson D. G. M. (1997) Mechanism and temperature-dependent kinetics of the dehydration of tert-butyl alcohol in hot compressed liquid water. *Ind. Eng. Chem. Res.* **36**, 23-41.
- Yaghi O. M. and Li H. (1995) Hydrothermal synthesis of a metal-organic framework containing large rectangular channels. *J. Am. Chem. Soc.* **117**, 10401-10402.

- Yamamoto M., Yokota Y., Oshima K. and Matsubara S. (2004) H-D exchange reaction on benzene ring of polystyrene in hydrothermal deuterium oxide with platinum (IV) oxide catalyst. *Chem. Comm.* **15**, 1714-1715.
- Yang Z., Gould I. R., Williams L. B., Hartnett H. E., and Shock E. L. (2012) The central role of ketones in reversible and irreversible hydrothermal organic functional group transformations. *Geochim. Cosmochim. Acta* **98**, 48-65.
- Yu J. and Savage P. E. (1998) Decomposition of formic acid under hydrothermal conditions. *Ind. Eng. Chem. Res.* **37**, 2-10.
- Zhang X. (2005) Hydro(solvo)thermal in situ ligand syntheses. *Coord. Chem. Rev.* **249**, 1201-1219.